Scholars' Mine

Spring 2013

Scaleup and hydrodynamics study of gas-solid spouted beds

Shreekanta Basavaraj Aradhya

SCALEUP AND HYDRODYNAMICS STUDY OF GAS-SOLID SPOUTED BEDS

by

SHREEKANTA BASAVARAJ ARADHYA

A DISSERTATION

Presented to the Faculty of the Graduate School of the

MISSOURI UNIVERSITY OF SCIENCE AND TECHNOLOGY

In Partial Fulfillment of the Requirements for the Degree

DOCTOR OF PHILOSOPHY

in

CHEMICAL ENGINEERING

2013

Approved by:

Dr. Muthanna Al-Dahhan, Advisor
Dr. Parthasakha Neogi
Dr. Serhat Hosder
Dr. Shoaib Usman
Dr. Xinhua Liang

ABSTRACT

A thorough understanding of the complex flow structure of gas-solid spouted bed is crucial for design, scale-up and performance. Advanced gas-solid optical probes were developed and used to evaluate different hydrodynamic parameters of spouted beds. These optical probes measure solids concentration, velocity and their time series fluctuations. Since solids concentration needs to be converted to solids holdup through calibration, for meaningful interpretation of results, a novel calibration method was proposed (which is inexpensive and reliable compared to the current reported methods) and validated in the present study. The reported dimensionless groups approach of spouted bed scale-up was assessed and was found that the two different spouted beds were not hydrodynamically similar. Hence, a new scale-up methodology based on maintaining similar or close radial profiles of gas holdup was proposed, assessed and validated. CFD was used after it was validated as an enabling tool to facilitate the implementation of the newly developed scale-up methodology by identifying the new conditions for maintaining radial profiles of gas holdup while scaling up. It can also be implemented to quantify the effect of various variables on their hydrodynamic parameters. Gamma Ray Densitometry (GRD), a non-invasive radioisotope based technique, was developed and demonstrated to montior on-line the conditions for the scale-up, flow regime and spouted beds operation. The solids holdup in spout region increases with axial height due to movement of solids from the annulus region. However, solids velocity in the spout region decreases with axial height. In the annulus region the solids move downward as a loose packed bed and the solids velocity and holdup do not change with axial height. Using factorial design of experiments it was found that solids density, static bed height, particle diameter, superficial gas velocity and gas inlet diameter had significant effect on the identification of spout diameter. Flow regimes in spouted bed were determined with the help of optical probes, pressure transducers and GRD. It was found that the range of stable spouting regime is higher in 0.152 m beds and the range of stable spouting decreases in the 0.076 m beds. The newly developed non-invasive radioisotope technique (GRD) was able to successfully identify different flow regimes and their transition velocities besides scale-up conditions and operation.

ACKNOWLEDGMENTS

Throughout my stay here at Missouri University of Science and Technology, several people have supported me both academically and personally and inspired me. I owe my deepest gratitude to Dr. Muthanna Al-Dahhan, who gave me an opportunity to conduct research under his supervision. Dr. Muthanna has continuously conveyed a passion for research work and has been a constant source of knowledge, guidance, encouragement and support. Without his guidance and valuable inputs this dissertation would not have been possible.

I would also like to thank my committee members Dr. Parthasakha Neogi, Dr. Serhat Hosder, Dr. Shoaib Usman, and Dr. Xinhua Liang, who have been a source of inspiration and guidance during my graduate stay at Missouri University of Science and Technology. In addition, I want to thank Dr. Palghat Ramachandran from Washington University in St Louis, and Dr. Xingying Lan from China University of Petroleum, Beijing for their guidance and numerable inputs during the course of my research work.

I want to take this opportunity to also thank Department of Energy – Nuclear Energy Research Initiative (DOE-NERI) grant (NERI DEFC07-07ID14822) for the financial support that made this work possible.

I would like to express my deep sense of gratitude to my parents S.N Basavaraj and K. Geetha Basavaraj, for their faith, support and belief in me. My mother is my strength, and I forever will be indebted to her unconditional love and also for the sacrifices she has made, without which I would not have made it this far in my life. A special thanks to my brother Vishwanath Aradhya, who has been supporting me throughout my life. I would like to also thank my close friends Gautham, Kiran, Anoop, Anurag, Arvind, Vaibhav, Anjana and many others for the wonderful times and memories, which will be cherished for a long time. Last but not the least; I would like to thank the almighty god, who has been my source of inspiration for all these years and for helping me in successfully completing one of the biggest endeavors in my life. Finally I would like to finish it off with one of the famous mantras of lord Ganesha:"Vakra Tunda Mahakaya Surya Koti Samaprabha, Nirvighnam Kurmu Me Deva, Sarva Karyessu Sarvada".

TABLE OF CONTENTS

LIST OF ILLUSTRATIONS

LIST OF TABLES

NOMENCLATURE

Symbol	Description

Ar $\quad Ar = \dfrac{d_p^{\ 3}(\rho_s - \rho_f)\rho_f g}{\mu^2}$, Archimedes Number

C_μ , $C_{1\varepsilon}$, $C_{2\varepsilon}$ Co-efficient's in turbulence model

C_D Drage co-efficient

D_c Column diameter, m

D_i Inlet diameter, m

D_0 Diameter of inlet gas, m

D_s Mean spout diameter, m

d_p Particle diameter, m

e_{ss} Co-efficient of restitution of particle

e_w Particle-wall restitution co-efficient

$G_{k,g}$ Production of turbulence kinetic energy

g Gravitational constant, m/s^2

$g_{0,ss}$ Radial distribution function

H Static Bed Height, m

H_F Fountain height, m

h Bed height, m

I_{2D} The second invariant of the deviatoric stress tensor

I Unit tensor

k_g Turbulence quantities of gas phase, m^2/s^2

L Column height, m

m, m_0 Parameters for solids velocity equation

P Bed pressure, N/m^2

$P_{dimensionless}$ Dimensionless pressure

ΔP Overall pressure drop, N/m^2

Re_s $Re = d_p v \rho / \mu$, Particle reynolds number

r Radial co-ordinate, m

r_s	Radius of spout at a given z level, m
T	Temperature, K
t	Time, sec
U	Superficial gas velocity, m/s
U_{ms}	Minimum spouting velocity, m/s
U_{mf}	Minimum fluidization velocity, m/s
v_z	Central solids velocity, m/s
v_0	Solids velocity in the central spout, m/s
v_s	Particle velocity, m/s
$v_{s,w}$	Tangential velocity at wall, m/s
z	Height of measurement, m

Greek letters

α_g	Gas volume fraction
α_s	Solids volume fraction
$\alpha_{s,max}$	Maximum packing limit of solids
β	Fluid–particle interaction coefficient, $kg/m^3 s$
ε_g	Turbulence dissipation of gas phase, m2 s-3
ε_0	Loose packed voidage
φ	Internal friction angle of particle, º
φ_s	Particle sphericity
ϕ	Specularity coefficient
$\Gamma_{\Theta s}$	Diffusion coefficient, J/kg
$\gamma_{\Theta s}$	Energy dissipation, $kg/m^3 s$
τ_g	Stress tensor for gas phase, N/m^2
τ_s	Stress tensor for solid phase, N m-2
λ_s	Solid bulk viscosity, Pa s
μ_g	Gas effective viscosity, Pa s
$\mu_{l,g}$	Gas molecular viscosity, Pa s
μ_s	Solid shear viscosity, Pa s
$\mu_{s,col}$	Solid collisional viscosity, Pa s

$\mu_{s,fr}$	Solid frictional viscosity, Pa s
$\mu_{s,kin}$	Solid kinetic viscosity, Pa s
$\mu_{t,g}$	Turbulent viscosity, Pa s
$\Pi_{k,g}$, $\Pi_{\varepsilon,g}$	Influence of the dispersed phases on the continuous phase
Θ_s	Granular temperature, m^2/s^2
Θ_w	Granular temperature at the wall, m^2/s^2
ρ_f	Fluid density, kg/m^3
ρ_g	Gas density, kg/m^3
ρ_s	Solid density, kg/m^3
σ_k, σ_ε	Prandtl number

Subscripts

g	gas phase
s	solid phase

1. INTRODUCTION

Spouted beds are two-phase gas-solid systems where the gas phase is injected as a jet through a small opening at the bottom of the bed to spout the particles that are charged in the column above. Under proper conditions, the gas phase penetrates the bed of particles as a jet, creating a central spout zone, a fountain above the spout, and an annulus moving downward surrounding the spout. Particles entrained in the gas spout move upward and form a fountain of particles above the bed surface that disengage from the gases and fall back to the bed surface, thus, inducing bed circulation. Hence, three distinct regions are created in the spouted bed namely: spout (which is dominated by the gas phase and characterizes by carrying the solid particles upward), fountain (which is also dominated by the gas phase where the solid particles that are carried from the spout form fountain at the top surface of the bed and then fall back again to the bed surface) and the annulus (which is dominated by solids phase and is characterized by the slow downward movement of solids). Due to their efficiency in contacting gases and coarser particles, spouted fluidized beds have been successfully applied to a wide variety of processes, such as coating, granulation, drying, coal gasification, catalytic reactions, etc. (Ishkura et al., 2004; Freitas et al., 2004 a, b; Pina et al., 2006). Different spouted bed configurations have been used and studied, such as conical, cylindrical with cone base, cone-based, and slot-rectangular spouted beds (Freitas et al., 2004 a,b; Zanoelo et al., 2004). The schematic of a cylindrical with cone base and conical spouted beds are shown in Figure 1.1. Spouted bed has been recently used in the manufacture of TRISO (Tri-Isotropic) nuclear fuel particles which is the core fuel material for the fourth generation nuclear reactors (GEN IV). Nuclear energy is one of the alternate sources of energy

which is being used widely in recent times. The increase in global economy, energy demand and coupled with depletion of natural resources of energy (fossil fuels, oil, etc.) have forced to draw the attention to nuclear energy. Nuclear energy is currently responsible for about one-fifth of all global energy demands. From 1980 to 2004 the total world primary energy demand grew by 54%, and to 2030 it is projected to grow at the same rate (average 1.6% per year, from 469 EJ to 716 EJ). Due to fast growing economies (OECD/IEA World Energy Outlook, 2004), the electricity demand is increasing much more rapidly than overall energy use and is likely to almost double from 2004 to 2030 (growing at an average of 2.6% per year from 17408 TWh to 33750 TWh). Due to the aforementioned reasons nuclear energy renaissance (Figure 1.2) was bound to happen, as nuclear power is the most environmentally benign way to produce electricity on a large scale (OECD/IEA World Energy Outlook, 2004).
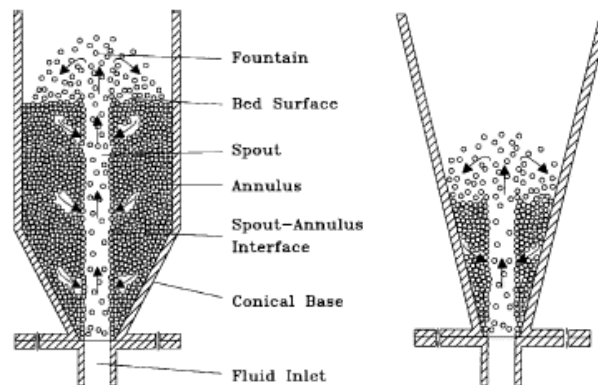
Figure 1.1. Schematic of cylindrical with cone based and conical spouted beds (Olzar et al., 2003)

Therefore the increasing importance of nuclear power in meeting energy needs while achieving security of supply and minimizing carbon-dioxide emissions cannot be overlooked. Today there are 439 nuclear reactors operating in 30 different countries, with a combined capacity of about 370 GWe. In 2006 these provided about 2658 billion kWh, which is about 16% of the world's electricity (coal 40%, oil 10%, natural gas 15% and hydro and others 19%). Nuclear energy production by some countries around the world is shown in Figure 1.3 (OECD/IEA Energy Information 2005).
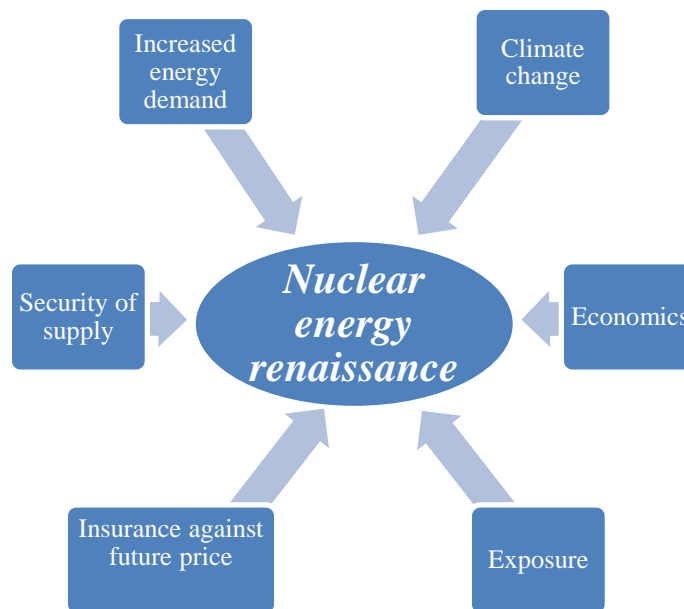
Figure 1.2. Schematic showing the reasons of Nuclear Energy Renaissance (OECD/IEA Energy Information 2005)

Generation IV reactors (Gen IV) are nuclear reactor designs currently being researched around the world (Figure 1.4 depicts the evolution of nuclear power from GEN I to GEN IV). Current reactors in operation around the world are generally considered second or third-generation systems, with most of the first-generation systems having been retired or revamped to second or third generation reactors some time ago. Research into these reactor types was officially started by the Generation IV International Forum (GIF) based on eight technology goals that include improving nuclear safety, improving proliferation resistance, minimizing waste (radioactive for few centuries instead of millennia) and natural resource utilization (more energy from the same amount of nuclear fuel), and decreasing the cost to build and run such plants.
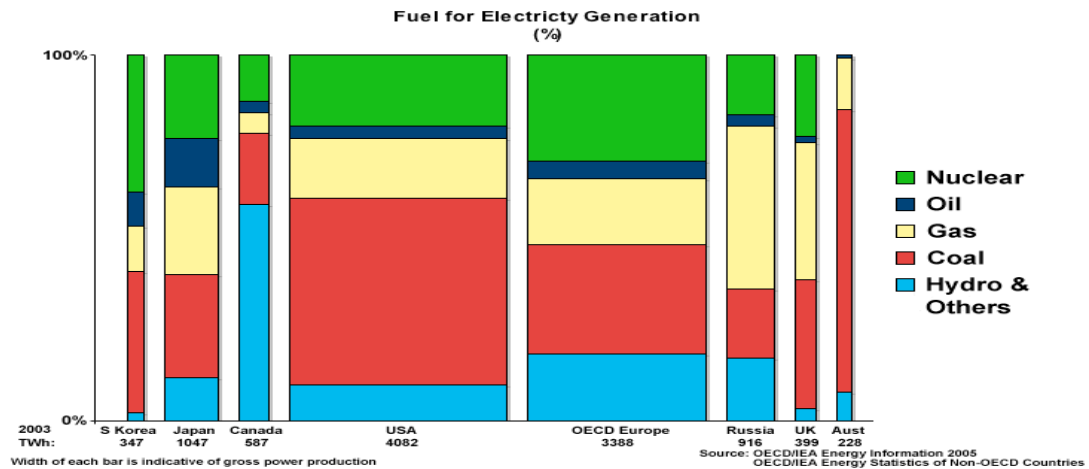
Figure 1.3. Fuel for electricity generation in few countries around the world (OECD/IEA Energy Information 2005)

Many reactor types were considered initially; however, the list was downsized to focus on the most promising technologies and those that could most likely meet the goals of the Gen IV initiative. Three systems are nominally thermal reactors and three are fast reactors. The Very High Temperature Reactor (VHTR) is also being researched for potentially providing high quality process heat and hydrogen production. The fast reactors offer the possibility of burning actinides to further reduce waste and of being able to "breed more fuel" than they consume. These systems offer significant advances in sustainability, safety and reliability, economics, proliferation resistance and physical protection.
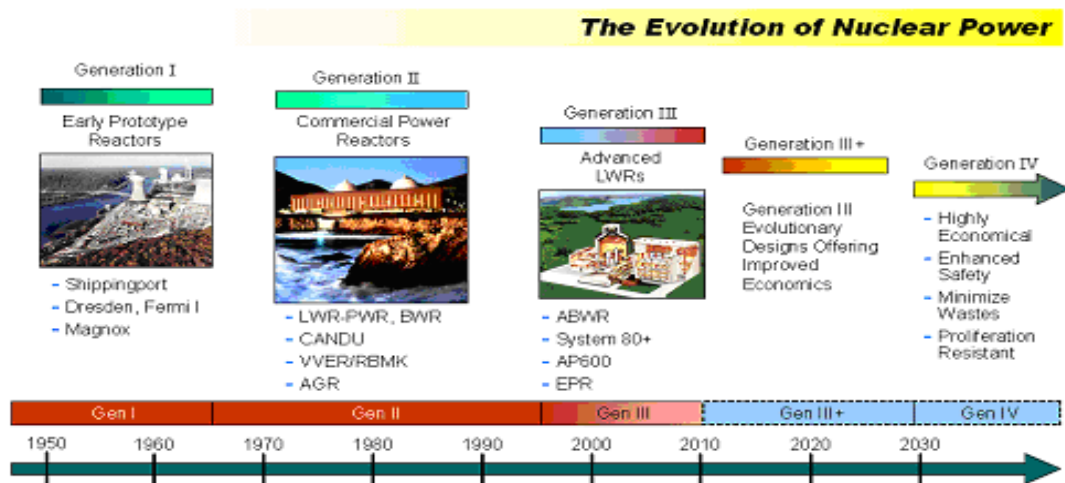
Figure 1.4. Evolution of Nuclear Power over the years (US Department of Energy annual report for Gen IV reactors, 2011)

The very high temperature reactor (VHTR), or high temperature gas-cooled reactor (HTGR), is a Generation IV reactor concept that uses a graphite-moderated nuclear reactor with a circulating uranium fuel cycle. The VHTR is a type of high temperature reactor (HTR) that can conceptually have an outlet temperature of 900°-1000°C. The reactor core can be either a "prismatic block" or a "pebble-bed" core. The high temperatures enable applications such as process heat or hydrogen production via the thermochemical sulfur-iodine cycle. However, in practice the term "VHTR" is usually thought of as a gas-cooled reactor, and commonly used interchangeably with "HTGR" (high temperature gas-cooled reactor). There are two main types of HTGR's (which both use TRISO fuel particles): pebble bed reactors (PBR) and prismatic block reactors (PMR). The prismatic block reactor refers to a prismatic block core configuration, in which hexagonal graphite blocks are stacked to fit in a cylindrical pressure vessel. The pebble bed reactor (PBR) design consists of fuel in the form of pebbles, stacked together in a cylindrical pressure vessel, like a gum-ball machine. Both reactors may have the fuel stacked in an annulus region with a graphite center spire, depending on the design and desired reactor power.

The pebble bed reactor (PBR) is a graphite-moderated, gas-cooled, nuclear reactor (Kadak, A. C, 2005). Like other VHTR designs, the PBR (Figure 1.5) uses TRISO fuel particles, which allows for high outlet temperatures and passive safety. Berkeley professor Richard A. Muller has called pebble bed reactors "in every way... safer than the present nuclear reactors and arguably safer than the global-warming danger posed by fossil fuels". The basic design of pebble bed reactors features spherical fuel elements called, naturally, pebbles (Figure 1.6).

These tennis ball-sized pebbles are made of pyrolytic graphite (which acts as the moderator), and they contain thousands of micro fuel particles called TRISO particles. These TRISO fuel particles consist of a fissile material (such as ^{235}U) surrounded by four layers of coating, as it will be discussed later, for structural integrity and fission product containment.
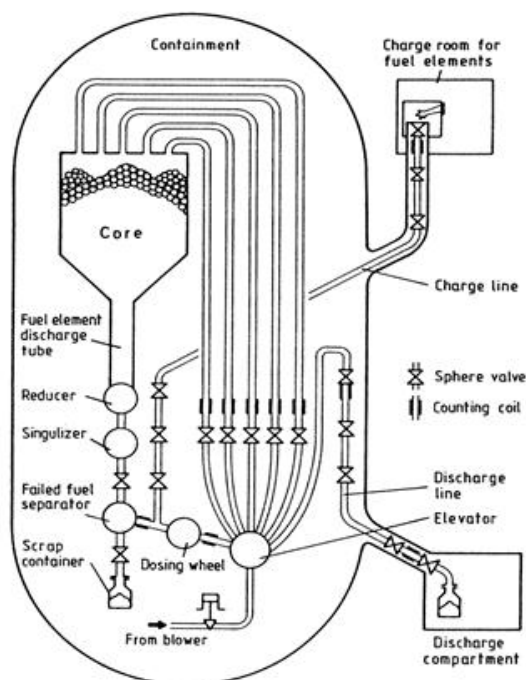
Figure 1.5. Schematic representation of Pebble Bed Reactor, PBR (Department of Nuclear Science and Engineering, Massachusetts Institute of Technology)

In the PBR, thousands of pebbles are amassed to create a reactor core, and are cooled by a gas, such as helium, nitrogen or carbon dioxide, which does not react chemically with the fuel elements. This type of reactor is claimed to be passively safe;

that is, it removes the need for redundant, active safety systems. Because the reactor is designed to handle high temperatures, it can cool by natural circulation and still survive in accident scenarios, which may raise the temperature of the reactor to 1,600 °C. Because of its design, its high temperatures allow higher thermal efficiencies than possible in traditional nuclear power plants (up to about or more than 50%) and has the additional feature that the gases do not dissolve contaminants or absorb neutrons as water does, so the core has less in the way of radioactive fluids. China is expecting to have pebble bed nuclear reactor in operation by 2013.
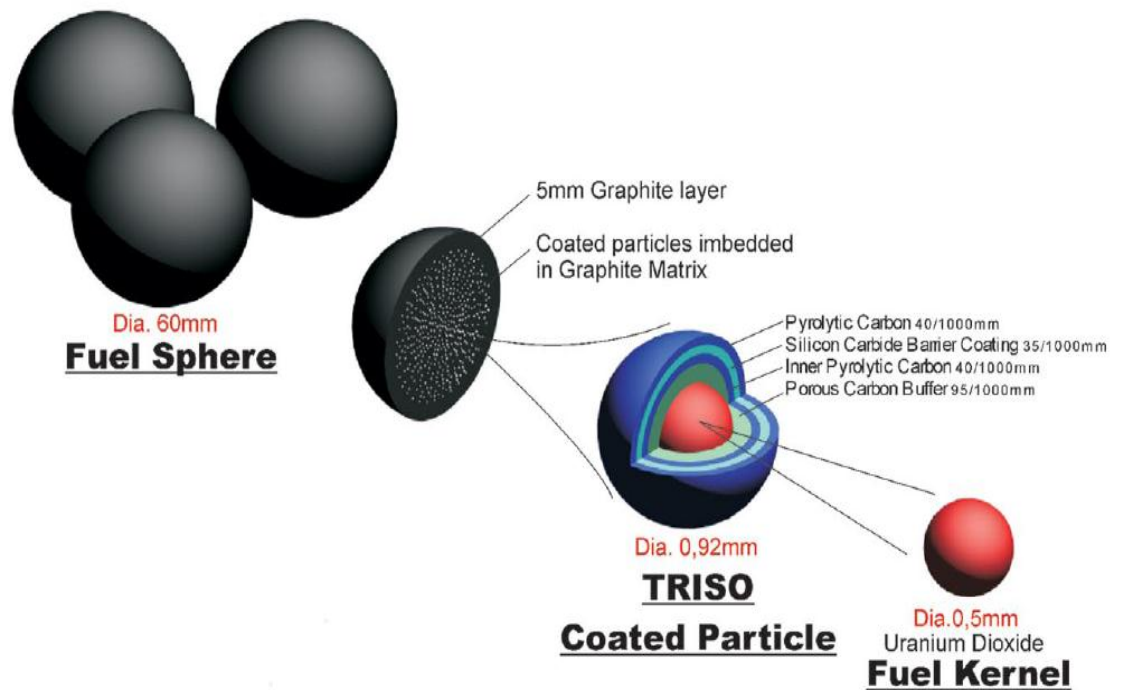
Figure 1.6. Pebbles charged as fuel into PBR, which is made up of numerous TRISO particles (Nuclear Power Industry News, 2009)

The prismatic block reactors (PMR), supports the development of high temperature process heat and closed cycle gas technology (Nuclear Power Industry News, 2009). PMR (Figure 1.7) uses prismatic fuel in the form of hexagonal blocks (Figure 1.8). The TRISO fuel particles are mixed with graphite and pressed to form cylindrical fuel pellets of about 2 inches long. The fuel pellets are then inserted into holes drilled into the hexagonal graphite fuel element blocks, which measure 14 inches wide by 31 inches high. The fuel blocks which also have helium coolant channels, are then stacked into the reactor core.
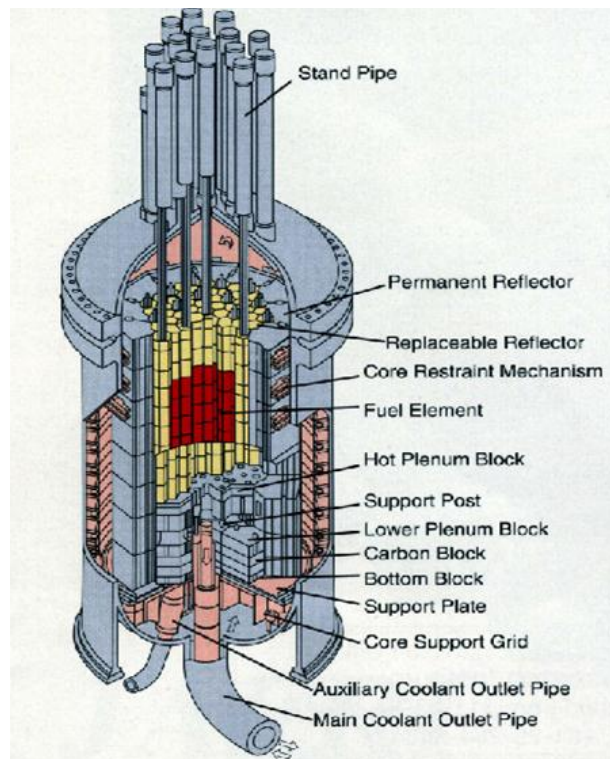
Figure 1.7. Schematic of Prismatic Block Reactor, PMR (Nuclear Power Industry News, 2009)

The initial development of PBR's was started in USA, it was then moved to Germany and then to South Africa. South Africa's developed Pebble Bed Modular reactor (PBMR) project was abandoned before commissioning due to lack of funds. China has an operating 10-megawatt HTR of the pebble bed design called HTR-10, with plans to construct a commercial 200-megawatt unit by the end of 2013 (South China Morning Post, 05/10/2004). General Atomics, based in San Diego, is developing the Gas Turbine Modular Helium Reactor (GT-MHR), which has a prismatic fuel rod design. Japan is operating a 30-megawatt high temperature test reactor, HTTR, of the prismatic design. Although the fuel configurations differ, both reactor types and other GEN IV reactors start with the same kind of fuel particles that will revolutionize electricity generation and industry throughout the world. Developed and improved over the past 50 years, these ceramic coated nuclear fuel particles, three-hundredths of an inch in diameter, make possible a high-temperature reactor that cannot melt down.

The successful development and commercial implementation of these nuclear reactors for energy production depends on the TRISO-coated fuel particles and their quality. Therefore, fuel-coating technology and processes are key in the future of nuclear power generators as alternative sources of energy production.
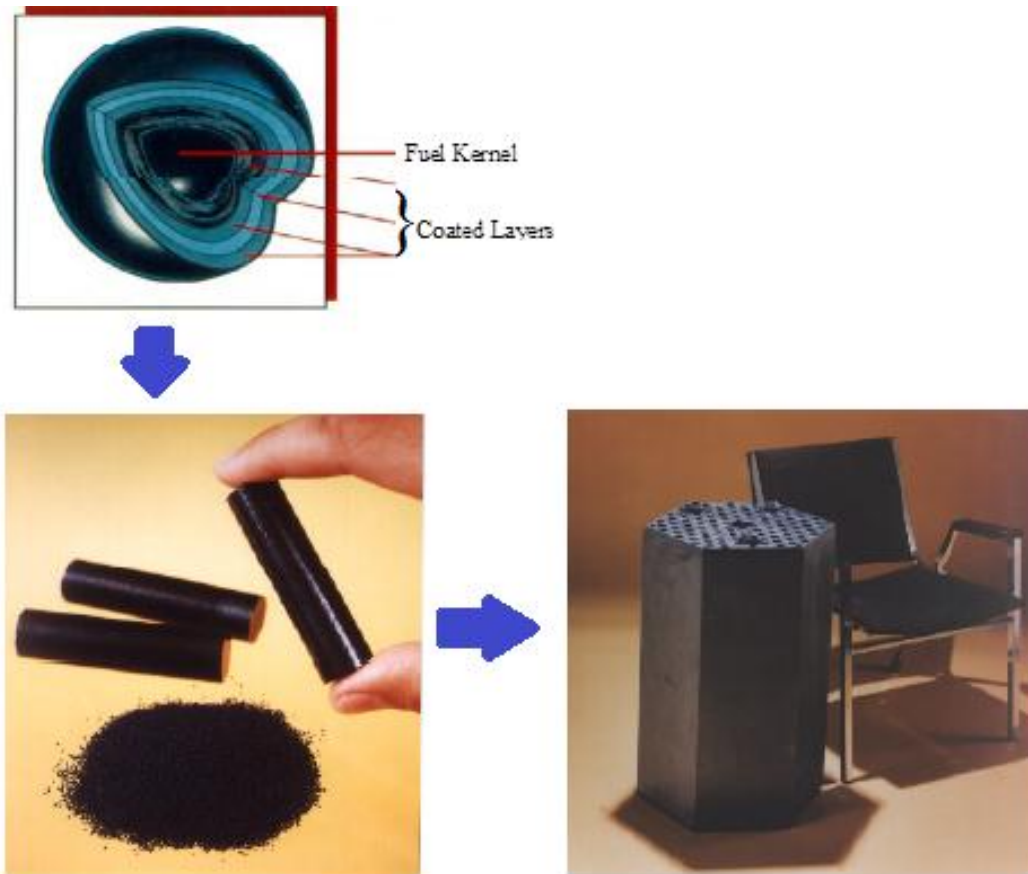
Figure 1.8. TRISO fuel particles charged into pellet forms to be arranged into the fuel rod assemblies for PMR core (Nuclear Power Industry News, 2009)

"The TRISO fuel particle consists of a kernel of fissile material surrounded by layers of carbon and ceramic material for protection and containment (Figure 1.9). The coated particle fuel has many attractive features, such as the ability to operate at high temperatures, to achieve high burn up, and to survive adverse conditions (World Nuclear Association report, Page. 5, 2009). Ranging in size from approximately 350 μm to 500 μm, the particles are durable and impervious to moisture for long periods of times, making them an attractive alternative to current metallic fuel containers. The TRISO

coating process is an engineering challenge to retain fuel and fusion products under normal operation ($\leq$1500° C), during accidental conditions up to 1600ºC, and potentially in permanent disposal. The excellent containment characteristics of TRISO particles provide the opportunity for the revival of nuclear power by addressing concerns of reactor safety and long-term disposal. The fissionable material is a ceramic bead or kernel that is the center of the particle (500µm). The first coating is a 60 - 100µm layer of low-density porous carbon, which attenuates fission product recoils from the kernel surface, provides a space for the fission gas released from the kernel, and accommodates kernel swelling without transmitting force to the outer layers. The next 30 - 40µm layer is high-density, isotropic pyrolytic carbon. The isotropic carbon traps the fission gases inside the particle and also protects the fuel kernel from chlorine generated during the deposition of the next coating, a silicon carbide layer. This carbon layer also protects the subsequent Silicon Carbide (SiC) layer from some fission products and carbon monoxide. This 35µm SiC layer is the strongest layer. Silicon carbide, a high-temperature ceramic, does not undergo appreciable dimensional changes during irradiation and is impervious to gaseous fission products, and thus it is the primary component in this miniature fission product containment vessel. It is an effective, but not perfect, barrier to metallic fission products, for SiC is susceptible to chemical reactions with certain noble metal and lanthanide fission products at elevated temperatures (thus the need for the underlying high-density carbon coating). Another 40µm layer of high-density isotropic carbon covers the SiC. This additional carbon coating protects the SiC from impurities in the reactor environment. The carbon also shrinks during irradiation and holds the SiC in compression. It can also provide protection during the handling and compaction

associated with pebble or fuel rod fabrication. The final size of the TRISO particles is around 1mm in diameter. Thus, the fuel kernel coating process consists of four stages on the base fuel kernel size of 500μm:

1. Fuel kernel with a low-density carbon buffer coating (porous carbon) of size 60-100μm.

2. Buffered layer over coated with a high-density inner pyrocarbon (IPyC) coating of size 30-40μm.

3. A silicon carbide layer coated on the pyrocarbon of the size 35μm.

4. An outer pyrocarbon (OPyC) layer of size 40μm, covers the SiC layer.

The TRISO coating is applied using chemical vapor deposition technique in a spouted bed (high temperature, ≤1500°C), a process by which gases are reacted or decomposed to produce solid layers in a high-temperature furnace (Beatty, 1967; Federer, 1977). Due to their efficiency in contacting gases and coarser particles, spouted beds have been successfully applied to a wide variety of processes, such as coating, granulation, drying, coal gasification, catalytic reactions, etc. (Ishkura et al., 2004; Freitas et al., 2004 a, b; Pina et al., 2006)" (Al-Dahhan, DOE Proposal DEFC07-07ID14822).
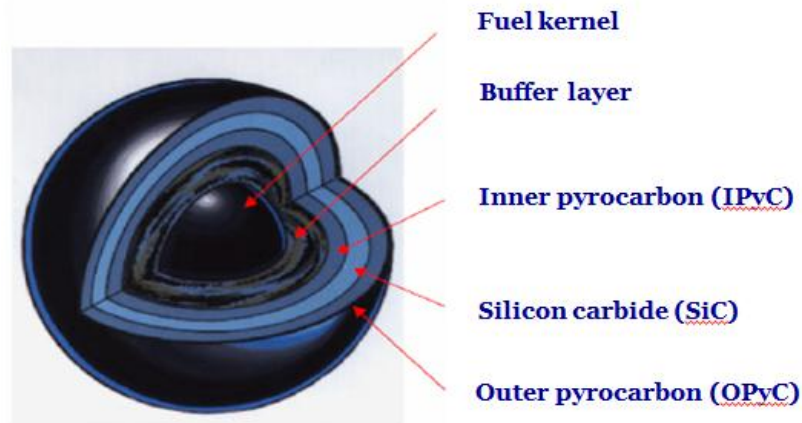
Figure 1.9. TRISO fuel particle used in GEN IV Nuclear Reactors (Nuclear Power Industry News, 2009)

1.1 MOTIVATION

The proposal of Al-Dahhan, DOEFC07-07ID14822, stated that "In HTGRs, the acceptable level of defective/failed coated TRISO particles is essentially zero. This level requires processes that produce coated spherical particles with even coatings having extremely low defect fractions. Hence, a voluminous amount of experimental development and trial and error work has been conducted, and through over 40 years of improvements, failure rates on the order of 10^{-5} are typical (IAEA 1997). The successful coating of fuel particles is a complex problem, and it is surprising that much success has been achieved through empirical modifications of process parameters and careful control of process conditions to maintain precise control and smooth operation. Commonly identified coating problems include non-spherical "faceting" (GA 1984, 1985), uneven layers, connected porosity (GA 1984, 1985), circumferentially discontinuous layers (Minato et al. 1994), and defects are apparently due to collisions (GA 1984, 1985; IAEA

1997).   German operations have improved coating defect rates by automation (IAEA 1997). Additional improvements were achieved by avoiding mechanical shocks to the particles by applying all the layers in succession without unloading the particles from the reactor (Minato et al. 1994, IAEA 1997).   Further improvements were achieved by controlling fluidization conditions in the spouted beds. In German and Japanese efforts (Minato et al. 1994, IAEA 1997), fluidization was characterized by dimensionless parameters for particle buoyancy (Archimedes number), particle free fall (Beranek number), and gas velocity, and was roughly related to modes of particle fluidization (e.g., "no spouting", "normal spouting", and "violent spouting") by visual observation of the top surface of the bed.

This control of fluidization was aimed at producing conditions of "normal spouting" to (1) avoid violent spouting conditions, which cause excessive particle collisions and ejection of particles into cooler regions above the bed where undesirable SiC layers may be formed, and (2) avoid conditions of low particle circulation under "no spouting" conditions. As shown in Figure 1.10, the product particles exhibited a reduced variation of coating thickness and reduced faceting; in addition, it was reported that the microstructure was less varied (GA 1984). *This example (Figure 1.10) confirms that the quality of the coating applied to fuel kernels is impacted by the <u>hydrodynamics, flow field</u>, and <u>flow regime characteristics of the spouted bed</u>, which, in turn, are <u>influenced by the design parameters and operating variables</u>.* For example, the formation of a flat slug of particles above the gas inlet leads to fouling of the gas inlet and impaired bed circulation. This condition results in an unacceptably high occurrence of non-spherical particles, coating flaws, and missing coating layers.

<div align="center">
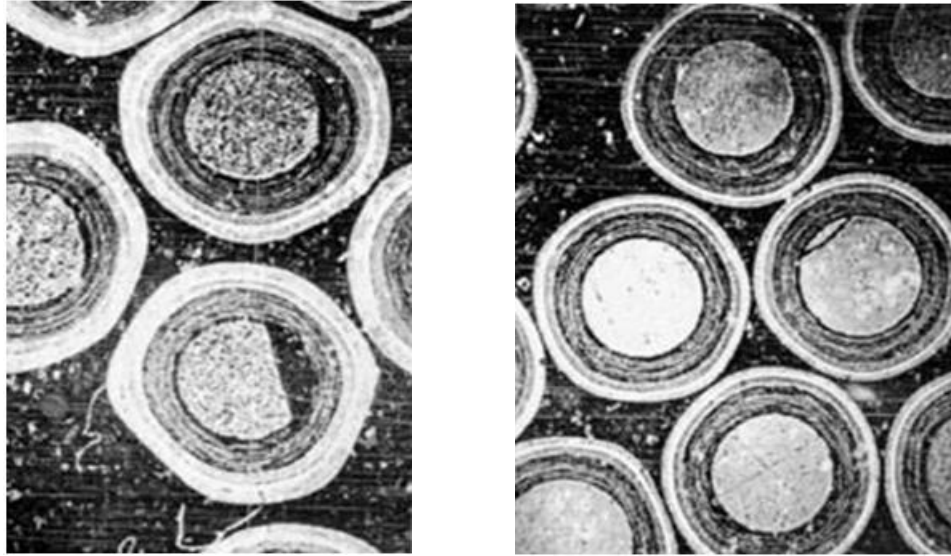
(a)   (b)

a) Faceted particles by low velocity fluidization
b) More Spherical particles by fast fluidization
Figure 1.10. Example of the potential for process improvements by control of fluidization
behavior (GA 1984)

</div>

Unfortunately, the current spouted bed coating technology is primarily based on empirical approaches to design and scale-up and is operated as a "black box". Moreover, the outlook for future fuel-coating technology and applications is further complicated by the fact that the variety of new concepts will involve fuel kernels of different sizes and with compositions of different densities. *Without fundamental understanding of the underlying phenomena of the spouted bed fluidization of the TRISO particle coater, empirical approaches will continue to be relied on, and hence, a significant effort will be required to produce each type of particle, with a significant risk of not meeting the specifications.* This difficulty will impact significantly and negatively the applications of

HGTRs for power generation and cause further challenges to them as alternative sources of commercial energy production. To overcome this difficulty, to accelerate process development, and to better control coater operations, we must properly understand the flow field, flow regime characteristics, and the detailed local hydrodynamic parameters (e.g., velocity, solids distribution, turbulent parameters, spouted bed diameter, fountain height, circulation-times, dead-zones, and many others) of the spouted bed coater and the effect of design and operating variables on these parameters. This understanding will significantly help in the development of reliable and safe scale-up methodology and design, and ensure desired performance and operation of TRISO fuel coaters" (Al-Dahhan, DOE Proposal DEFC07-07ID14822).

1.2 OBJECTIVES

The overall objectives of this work are to assess the current scale-up methodology based on matching dimensionless groups, develop a new scale-up methodology, develop an on-line monitoring technique to monitor the operation of spouted beds, flow pattern identification and to facilitate the implementation of the new scale-up methodology, study the effect of design and operating variables on the fluid dynamics of spouted beds and validate the computational fluid dynamics (CFD) simulation to be used as an enabling tool to implement the new scale-up methodology and to quantify the effects of the operating and design variables on the hydrodynamics of spouted beds. Such work should help in better understanding of the TRISO nuclear fuel particles coating process and other processes where gas-solid spouted beds find applications. These objectives will

be achieved by developing and implementing sophisticated measurement techniques. Based on the above objectives the work can be grouped as follows:

1.2.1 Developing a New Sophisticated Gas-Solid Optical Probe for Solids Dynamics Measurement and a New Methodology for Optical Probe Calibration.

- Developing a new optical probe technique that can measure simultaneously the solids holdup, solids velocity and their time series fluctuations, and developing a new simple and reliable methodology for calibrating gas-solid optical probes in general and the developed one in particular for the measured solids velocity and for correlating the voltage signal that is related to solids concentration in front of the probe to solids holdup.

1.2.2 Assessing the Current Scale-Up Methodology Based on Matching Dimensionless Groups and Developing A New Mechanistic Scale-Up Methodology for Spouted Beds.

- Evaluating the reported dimensionless groups as scaling parameters for hydrodynamics similarity via quantification of the local parameters in addition to the global ones by identifying conditions that give matching dimensionless groups and mismatch dimensionless groups. Such evaluation will be performed using the developed gas-solid optical probe and pressure transducers.

- Developing a new mechanistic scale-up methodology for gas-solid spouted bed by identifying and matching key parameters that dictate the spouted bed hydrodynamics for maintaining hydrodynamic similarity.

- Developing a non-invasive radioisotope based technique called Gamma ray densitometry to monitor on-line the conditions for the scale-up, flow regime and the spouted beds operation.

1.2.3   Investigating the Effect of Design and Operating Variables on Solids Velocity and Spout Diameter.

- Studying the effect of base angle (design variable) and gas velocity (operating conditions) on particles velocity in the three zones of the spouted bed: spout, annulus and fountain using optical probe and validated CFD.

- Developing a new correlation for spout diameter based on the new approach of design of experiments using fractional factorial analysis method. In this case, experiments with varying design and operating parameters will be conducted.

1.2.4 Developing Non-Invasive Measurement Technique Based on Gamma Ray Densitometry for On-line Monitoring, Flow Regime Identification and for Facilitating the Implementation of Newly Developed Scale-up Methodology in Spouted Beds.

- Developing Gamma Ray Densitometry (GRD) technique (based on industrially available and used Nuclear Gauge Densitometry, NGD) as non-invasive measurement technique for on-line monitoring, flow pattern and flow regime identification and for facilitating the implementation of the newly developed scale-up methodology.

- Comparing the results of GRD with those obtained by optical probe and pressure transducers.

1.2.5   Performing Computational Fluid Dynamics (CFD) Simulation for Facilitating the Implementation of the Newly Developed Scale-up Methodology and for Quantifying the Effects of Design and Operating Variables on the Hydrodynamics of Spouted Beds.

- Identifying and validating the key models and closures that describe the spouted bed hydrodynamics.

- Evaluating the reported dimensionless groups as scaling parameters for hydrodynamics similarity. Such evaluation will be performed using the Computational fluid dynamics and the results will be compared with the results from the developed gas-solid optical probe and pressure transducers.

- Demonstrating and assessing the use of CFD as an enabling tool to facilitate the implementation of the newly developed scale-up methodology.

1.3 THESIS ORGANIZATION

A general review of the available scale-up methodologies on spouted beds is discussed in Section2. A detailed review of some of the important parameters related to spouted beds and simulation techniques performed on spouted beds is discussed in this section. Section 3 gives an overview of all the optical probes used in the literature till date and the development of a new advanced gas-solid optical probe. The advanced

optical probe measures solids concentration, velocity and its time series fluctuations simultaneously. Solids concentration needs to be converted to solids holdup by calibration, for meaningful interpretation. This section discusses a new simple and reliable methodology for gas-solid optical probes calibration. Section 4 discusses the scale-up of spouted beds, which consists of two parts. First part addresses the assessment of the current approach of matching dimensionless groups for scale-up of spouted beds. The second part presents newly proposed and developed scale-up methodology for spouted beds. The development of non-invasive radioisotope technique called as Gamma ray densitometry (GRD) for on-line monitoring in spouted beds and for facilitating the implementation of the newly developed scale-up methodology. Section 5 discusses the effect of conical base angles (design variable) and gas velocity (operating variable) on the solids velocity in different parts of the spouted bed. Later part of the section discusses the use of Factorial Design of Experiments approach to find the influence of key parameters on spout diameter. Section 6 discusses the use of Gamma ray densitometry (GRD) for identifying different flow regimes in spouted beds and comparing the results with the pressure transducers and optical probes. Section 7 explains the different models and closures used to study and validate the spouted bed hydrodynamics by using Computational Fluid Dynamics (CFD) as enabling tool to facilitate the implementation of new scale-up methodology and to quantify the effect of design and operating conditions on the hydrodynamics of spouted beds. Section 8 summarizes the findings and implications of the dissertation and concludes with future research. Appendix A discusses in detail the analysis procedures followed for the gas-solids optical probes to obtain solids holdup and solids velocity. Appendix B lists the different MATLAB

programs used for the gas-solid optical probes for estimating different parameters. Appendix C discusses the grid convergence studies performed for CFD simulations and also gives a comparison of the 2D and 3D simulation performed for the spouted bed.

2. LITERATURE REVIEW

Although spouted beds have been studied for nearly 50 years, still there is a need to further advance their understanding and there is still considerable amount of uncertainty about reliable scale-up methods. Scale-up studies of spouted beds are therefore important. Many correlations are available based on small scale vessels ($D_c <$ 0.3 m) to predict hydrodynamics in spouted beds, but are still unreliable and also do not work well with large scale columns. Since most of the currently operated spouted beds are of large diameters, it's still surprising that the operation of these large columns is still based on unreliable empirical equations. The main objective of the present work is to address some of these issues to advance the understanding and knowledge of the gas-solid spouted beds in general and for efficient coating processes for TRISO particles, in particular. In this section, literature review of some of the parameters that are related to this work is discussed below.

2.1 SCALE-UP METHODOLOGY

The principle of similarity is often used in obtaining experimental data to represent large-scale complex flow phenomena, e.g. to calculate wind loads on buildings and to design ship hulls. The basic concept is that if two flow fields are geometrically similar and are operated with identical values of all important independent non-dimensional parameters, then the dependent non-dimensional variables must also be identical at corresponding locations (Bisio and Kabel, 1985). This simple hydrodynamic principle has been applied to multiphase flow systems in general and also to fluidized beds, in particular. Prescriptions of dimensionless groups to characterize the dynamics of

fluidized beds can be traced back at least as far as Romero and Johanson (1962). In order to develop proper scaling relationships between a cold model and a hot fluidized bed, four dimensionless similarity groups: a Froude number, a Reynolds number, the ratio of solid to fluid densities, and the ratio of particle to vessel diameters –were derived by Broadhurst and Becker (1973) based on the Buckingham Pi theorem. These groups were later tested experimentally by Fitzgerald et al. (1984). Theoretical analysis of the scaling relationships was subsequently reported by Glicksman (1984), and experimental evaluation of the scaling relationships has been investigated experimentally using global parameters by a number of research groups.

2.1.1 Glicksman (1984) Scaling Relationships for Gas-Solid Fluidized Beds Scale-Up. Glicksman (1984) was the first to propose a set of scaling relationships for fluidized beds based on dimensional analysis using two fluid equations of motion. When the equations governing a particular phenomenon can be written, the most insightful way to derive the scaling relationships is to non-dimensionalize the governing equations. Thus the equations reveal useful information, even though they cannot be solved in general. The equations of motion and conservation of mass for both particles and fluid can be represented as shown in equations 1-4 (Glicksman 1984). Inter-particle collisions, particle-particle collisions and electrostatic forces were not considered for simplicity.

The conservation of mass for fluid is

$$div(\varepsilon \bar{u}) = 0 \tag{1}$$

The conservation of mass for particles is

$$div[(1-\varepsilon)\bar{v}] = 0 \tag{2}$$

The equation of motion for fluid is

$$\rho_f \varepsilon \left[\frac{\partial \bar{u}}{\partial t} + \bar{u} * grad.\bar{u} \right] + \bar{i}\,\rho_f\, g\varepsilon + grad.p + \beta(\bar{u} - \bar{v}) = 0 \tag{3}$$

The equation of motion for particles is

$$\rho_s (1-\varepsilon)\left[\frac{\partial \bar{v}}{\partial t} + \bar{v} * grad.\bar{v} \right] + \bar{i}\,\rho_s\, g(1-\varepsilon) - \beta(\bar{u} - \bar{v}) = 0 \tag{4}$$

In order to non-dimensionalize the above equations, the following dimensionless quantities need to be used

$$\bar{U}' = \frac{\bar{U}}{U}, \bar{v}' = \frac{\bar{v}}{U}, \nabla' = d_p \nabla, t' = \frac{U}{d_p} t \tag{5}$$

The non-dimensional form of continuity equations and equations of motion for both fluid and particles is shown below from equations $6 - 9$.

$$div(\varepsilon \bar{U}') = 0 \tag{6}$$

$$div[(1-\varepsilon)\bar{v}'] = 0 \tag{7}$$

$$\frac{\rho_f}{\rho_s} \varepsilon \left[\frac{\partial \bar{U}'}{\partial t} + (\bar{U}'.\nabla')\bar{U}' \right] + \frac{\bar{i}\rho_f}{\rho_s} \frac{gd_p}{U^2} \varepsilon + \nabla'(\frac{p}{\rho_s U^2}) + \frac{\beta d_p}{\rho_s U} (\bar{U}' - \bar{v}') = 0 \tag{8}$$

$$(1-\varepsilon)\left[\frac{\partial \bar{v}'}{\partial t} + (\bar{v}'.\nabla')\bar{v}' \right] + \bar{i}\,\frac{gd_p}{U^2}(1-\varepsilon) - \frac{\beta d_p}{\rho_s U}(\bar{U}' - \bar{v}') = 0 \tag{9}$$

From the equations $6 - 9$ and based on bed geometric similarity, the controlling non-dimensionless parameters can be identified as

$$\frac{\beta d_p}{\rho_s U}, \frac{p}{\rho_s U^2}, \frac{gd_p}{U^2}, \frac{\rho_f}{\rho_s}, \frac{H}{d_p}, \frac{D_c}{d_p} \tag{10}$$

Along with the set of parameters obtained in equation 10, particle size distribution, bed geometry and sphericity (ϕ_s) for non-spherical particles needs to be considered. Glicksman et al. (1993) reworked the governing equations to consider

various drag relationships. However, those drag relationships are not valid for spouted beds. Hence, the simplified scaling relationships are therefore not discussed further in the present work.

2.1.2 Horio (1986) Similarity Rule for Gas-Solid Fluidized Beds Scale-Up. Horio (1986) developed a similarity rule for bubbling fluidized beds based on the governing equations of bubbles and interstitial gas dynamics developed by Horio et al. (1983). The study involves the following factors which are defined as below

$$m = \frac{H_1}{H_2} = \frac{D_{c1}}{D_{c2}} = \frac{d_{p1}}{d_{p2}}$$

(11)

The condition for geometrically similar bubble coalescence was derived as

$$U_1 - U_{mf1} = \sqrt{m}(U_2 - U_{mf2})$$

(12)

The developed similarity rule requires fewer controlling conditions than Glicksman's. However, Horio's similarity rule is valid only for bubbling fluidized beds. For turbulent beds, fast fluidized beds and spouted beds, etc., a new rule needs to be developed individually. Horio et al. (1989) developed a new set of scaling parameters for the circulating fluidized beds. But Glicksman (1988) showed his original parameters reduce to that of Horio (1986) when Re is low (<4), a condition which is highly unlikely to be encountered in spouted beds.

2.1.3 He et al. (1997) Scaling Relationships for Gas-Solid Spouted Bed. Although fluidized beds and spouted beds share many common features, there are also significant differences between them. Most notably, the annulus of a spouted bed constitutes a moving packed bed with countercurrent interstitial flow of fluid, while the solids in fluidized beds appear to be in more random motion fully supported and dictated

by the gas. There is substantial particle-particle contact in the annulus region of spouted beds, so that the rheological characteristics of the dense phase may play a more important role than in fluidized beds, where dense phase rheology is commonly ignored. Therefore, He et al. (1997) modified the set of scaling groups to be adopted for spouted beds. The equation of motion of fluid can be applied to spouted bed while the equation of motion of particle needs special consideration. More attention was given to the inter-particle stresses in the annulus region where the particles are in contact with each other. The continuity equations and the equations of motion for fluid and particles applicable in a spouted bed can be written as follows

The conservation of mass for fluid is

$$div(\varepsilon\bar{u}) = 0 \tag{13}$$

The conservation of mass for particles is

$$div[(1-\varepsilon)\bar{v}] = 0 \tag{14}$$

The equation of motion for fluid is

$$\rho_f \varepsilon \left[\frac{\partial \bar{u}}{\partial t} + \bar{u} * grad.\bar{u} \right] + \bar{i}\,\rho_f g\varepsilon + grad.p + \beta(\bar{u} - \bar{v}) = 0 \tag{15}$$

The equation of motion for particles is

$$\rho_s (1-\varepsilon) \left[\frac{\partial \bar{v}}{\partial t} + \bar{v} * grad.\bar{v} \right] + \bar{i}\,\rho_s g(1-\varepsilon) - \beta(\bar{u} - \bar{v}) - div.E_p = 0 \tag{16}$$

E_p is the effective stress tensor for the particle phase. The dimensionless quantities introduced are

$$\bar{U}' = \frac{\bar{U}}{U}, \bar{v}' = \frac{\bar{v}}{U}, \nabla' = d_p \nabla, t' = \frac{U}{d_p} t, E'_p = \frac{E_p}{g\rho_s d_p} \tag{17}$$

The non-dimensional form of continuity equations and equations of motion for both fluid and particles is shown below from equations $18 - 21$.

$$div(\varepsilon \overline{U}') = 0 \tag{18}$$

$$div[(1-\varepsilon)\overline{v}'] = 0 \tag{19}$$

$$\frac{\rho_f}{\rho_s}\varepsilon\left[\frac{\partial \overline{U}'}{\partial t} + (\overline{U}'.\nabla')\overline{U}'\right] + \frac{\overline{i}\rho_f}{\rho_s}\frac{gd_p}{U^2}\varepsilon + \nabla'(\frac{p}{\rho_s U^2}) + \frac{\beta d_p}{\rho_s U}(\overline{U}' - \overline{v}') = 0 \tag{20}$$

$$(1-\varepsilon)\left[\frac{\partial \overline{v}'}{\partial t} + (\overline{v}'.\nabla')\overline{v}'\right] + \overline{i}\frac{gd_p}{U^2}(1-\varepsilon) - \frac{\beta d_p}{\rho_s U}(\overline{U}' - \overline{v}') - \frac{gd_p}{U^2}(\nabla'.E_p') = 0 \tag{21}$$

From the equations $18 - 21$ and based on bed geometric similarity, the controlling non-dimensionless parameters for spouted bed can be identified as

$$\frac{gd_p}{U^2}, \frac{\rho_s d_p U}{\mu}, \frac{\rho_f}{\rho_s}, \frac{H}{d_p}, \frac{D_c}{d_p}, \phi_s, \varphi, \varepsilon_0 \tag{22}$$

Along with the above mentioned controlling dimensionless groups, dimensionless particle size distribution and dimensionless bed geometry needs to be considered. Based on this set of scaling parameters, He et al. (1997) studied two different size spouted beds at both ambient temperature and at elevated temperature. It was demonstrated in his work that this scaling groups were able to successfully scale-up when they were matched between the prototype and model spouted beds by maintaining similar dimensionless fountain heights, dimensionless pressure profiles and dimensionless spout diameters. By analysis of the force balance of the particles in the annulus region of a spouted bed, two additional non-dimensional parameters, the internal friction angle (φ) and the loose packed voidage (ε_o), have been added to the scaling relationships. It was also concluded that the successful scaling of spouted bed cannot be achieved by varying only bed and

particle dimensions. Particle internal friction angles and sphericity have significant influence on the maximum spoutable depth, fountain height and longitudinal pressure profiles while particle-particle interaction forces cannot be ignored in spouted bed scale-up.

2.1.4 Bao et al. (2007) Scaling Relationships for Gas-Solid Spouted Bed. By non-dimensionalizing the continuity and momentum equations for the fluid and solids phases along with the boundary conditions, together with the consideration of the stress tensor by using the kinetic theory of granular flow, Bao (2007) proposed modified set of the scaling parameters as follows.

$$\frac{gd_p}{U^2}, \frac{\rho_s d_p U}{\mu}, \frac{\rho_f}{\rho_s}, \frac{H}{d_p}, \frac{D_c}{d_p}, \phi_s, \varphi, \varepsilon_0, e_{ss} \tag{23}$$

Along with the above mentioned controlling dimensionless groups, dimensionless particle size distribution and dimensionless bed geometry needs to be considered. Comparing equation 23 with the scaling relationship of He et al. (1997) equation 22, shows that an additional parameter, the coefficient of restitution of particles, e_{ss}, was introduced in Bao's work. It is well known that e_{ss} is a measure of the elasticity of the collision between two particles, and relates to how much of the kinetic energy of the colliding particles before the collision remains after the collision. It was shown that the flow dynamics of gas-solids systems, such as the bed expansion ratio, particle velocities were sensitive to e_{ss} (Goldschmidt et al., 2001). Huilin et al. (2004) and Du et al. (2006) showed that e_{ss} could greatly affect the CFD simulation results of the spouted beds. However, in their validation experiments, the particles used in different cases by He et al. (1997) are same or have close e_{ss}, the possible effect of e_{ss} on the scaling of spouted bed is undetectable. The results of the experimental verification showed that the

hydrodynamic parameters such as the fountain height, spout diameter, and voidage profiles were closely related to the coefficients of restitution (Bao, 2007). When the coefficients of restitution of two systems did not match, their similarity could not be satisfied.

2.2 SPOUT DIAMETER

The longitudinal average spout diameter, D_s, is an important parameter for determining the flow distribution between spout and annulus. There are a number of correlations reported in the literature to estimate the average spout diameter.   The correlation of McNab (1972) is widely used, which is given below

$$D_s = 2.0 \left\{ \frac{(\rho_f U)^{0.5} D_c^{0.68}}{[\rho_s (1 - \varepsilon_s)]^{0.41}} \right\} \qquad (24)$$

Equation 24 was tested in large sector beds of 30^0 by Green and Bridgewater (1983). It was found that McNab (1972) correlation underestimated the average spout diameter by 15% - 30%. However, Lim and Grace (1987) established that a measured data in a 0.91m diameter column were in good agreement with equation 24, with average absolute deviation less than 10%.

By a force balance on the spout–annulus interface in the cylindrical part of the column in which axial variation of the spout diameter is relatively small, including both hydrodynamic forces and solid stresses based on hopper flow of solids, Bridgwater and Mathur (1972) derived the following equation for the spout diameter

$$\frac{32 f \rho Q_s^2}{\pi^2 (\frac{-d\sigma_a}{dz})(D - D_s) D_s^4} = 1 \qquad (25)$$

They then made the following simplifying assumptions:

1. The volumetric gas flow through the spout, Qs, above the cone but well below the bed surface, is typically about one-half the total volumetric flow through the bed, that is, $Qs \approx 0.5\pi D^2 G/4\rho$.

2. Flow through the spout is equivalent to flow of a dilute air-solids suspension through a rough pipe with an equivalent sand roughness of $d_p/2D_s$ and a Fanning friction factor $f \approx 0.08$.

3. The analysis is limited to air spouting at ambient conditions, so $\rho = 1.2$ Kg/m^3.

With these assumptions, equation 25 is reduced to

$$D_s = \frac{(Const.)G^{0.5}D^{0.75}}{(\rho_b g)^{0.25}}$$
(26)

For spout-fluid beds (combination of spouted and fluidized bed), Hadzisdmajlovic (1983) proposed the following equation for predicting the average spout diameter

$$\frac{D_{sf}}{D_s} = \frac{Q}{Q_{msf}}[1-(1-h)^3]^{1/2}$$
(27)

Where h=H/H$_m$. H is the static bed height and H$_m$ is the maximum spoutable bed height. The maximum spoutable bed height, H$_m$, is the maximum initial static bed height at which spouting can be obtained. Beyond this bed height there is no spouting.

2.3 MINIMUM SPOUTING VELOCITY

The minimum fluid velocity for which the spouting occurs in a spouted bed is called as minimum spouting velocity (U$_{ms}$). It is determined experimentally by reducing the fluid velocity until a point is reached after which further reduction in velocity will cause the spout to collapse and the bed pressure to increase suddenly. It is a known fact

that the minimum spouting velocity depends on solids and fluid properties, bed geometry and bed depth. Numerous researchers have studied this parameter, a list of these correlations and their applicability is listed in Table 2.1. Though, there have been numerous correlations predicting the minimum spouting velocity, still there is numerous differences between them and the prediction of these correlations remains questionable.

Table 2.1. Correlations for minimum spouting velocity

No	Correlations	Authors	Observation
1	$$U_{ms} = \left(\frac{d_p}{D_c}\right)\left(\frac{D_i}{D_c}\right)^{1/3}\sqrt{\frac{2gH(\rho_s - \rho_f)}{\rho_f}}$$	Mathur and Gishler 1955	$D_c < 0.6$m
2	$$U_{ms} = k(1-\varepsilon)^{1/2}\left(\frac{D_i}{D_c}\right)^2\sqrt{\frac{2gH_0(\rho_s - \rho_f)}{\rho_f}}$$	Madonna and Lama 1958	Theoretical
3	$$\frac{U_{ms}}{U_{mf}} = 1 - \left(\frac{1-H}{H_m}\right)^3$$	Grbavcic et al. 1976	
4	$$(\mathrm{Re}_i)_{ms} = 1.24\,\mathrm{Re}_i\left(\frac{H_0}{D_i}\right)^{0.82}\tan\left(\frac{\gamma}{2}\right)^{0.92}$$	Wan-Fyong et al. 1969	D_i=2.6-7.6cm H_0=7-30cm γ=10^0-70^0 D_c=11.2-20cm dp=0.35-4mm ρ_s=0.45-1.39g/cm^3
5	$$(\mathrm{Re}_i)^2{}_{ms}(1.75 + 150(1-\varepsilon_{ms})/(\mathrm{Re}_i)_{ms}) = \\ 31.31Ar(H_0/D_i)^{1.757}(D_i/D_c)^{0.029}(\tan(\gamma/2))^{2.07}\varepsilon_{ms}{}^3$$	Markwski and Kaminski 1983	D_i=15-82mm H_0/D_i=1.3-8.5 H_0=30-150mm γ=24^0-60^0
6	$$U_{ms} = 2.0D_c{}^n\left(\frac{d_p}{D_c}\right)\left(\frac{D_i}{D_c}\right)^{1/3}\sqrt{\frac{2gH(\rho_s - \rho_f)}{\rho_f}}$$	Fane and Mitchell 1984	$D_c > 0.4$m

Table 2.1. Correlations for minimum spouting velocity cont.

7	$U_{ms} = 18.5 \left(\dfrac{\rho_s - \rho_f}{\rho_f} \right)^{0.263} \left(\dfrac{H}{D_c} \right)^{-0.103} \left(\dfrac{d_p}{D_c} \right)^{1.19} \left(\dfrac{D_i}{D_c} \right)^{0.373} \sqrt{2gH}$	Choi and Meisen 1992	
8	$U_{ms} = 2.44 \left(\dfrac{2gH(\rho_s - \rho_f)}{\rho_f} \right)^{0.28} \left(\dfrac{H}{D_c} \right)^{0.5} \left(\dfrac{d_p}{D_c} \right)^{0.7} \left(\dfrac{D_o}{D_c} \right)^{0.58}$	Anabtawi et al. 1992	For square column
9	$U_{ms} = \left(\dfrac{d_p}{D_c} \right) \left(\dfrac{D_i}{D_c} \right)^{0.1} \sqrt{\dfrac{2gH(\rho_s - \rho_f)}{\rho_f}}$	Olzar 1994	
10	$U_{ms} = \left(\dfrac{d_p}{D_c} \right) \left(\dfrac{D_i}{D_c} \right)^{0.1} \sqrt{\dfrac{2gH(\rho_s - \rho_f)}{\rho_f}}$	Olzar 1994	
11	$U_{ms} = 1.63 U_t \left(\dfrac{d_p}{D_c} \right)^{0.414} \left(\dfrac{D_i}{D_c} \right)^{0.127} \left(\dfrac{H_m}{D_c} \right)^{0.452} \left(\dfrac{\rho_s - \rho_f}{\rho_f} \right)^{-0.149}$	Li et al. 1996	Based on high temperature data
12	$\dfrac{\varepsilon}{1-\varepsilon} (Re_i)_{ms} = \left(\dfrac{H_0}{D_c} \right)^{0.38} \left(\dfrac{d_p}{D_c} \right)^{2.54} \left(\dfrac{D_i}{D_c} \right)^{0.33} \left(\dfrac{\rho_f (\rho_s - \rho_f) g D_c^3}{\mu^2} \right)^{0.75} Re_z^{-0.6}$	Wang et al. 2001	D_c=19cm γ=60^0 D_i=2.1cm H_0=20-30cm dp=1.45-2.5mm ρ_s=0.836-2.4g/cm^3 13$\leq$Re$_s$$\leq$82 For spouted bed with auxiliary gas
13	$\dfrac{U_{ms}}{U_{mf}} = \left(\dfrac{H}{H_m} \right)^{\left(\frac{1-0.5H}{H_m} \right)}$	Bi et al. 2004	Exponent approaching 1 for small H/Hm and 0.5 for large H/H$_m$ for γ=60^0
14	$U_{ms} = 0.2^{0.5} U_{mf} \left(\dfrac{H}{0.2 H_m} \right)^{1 - \left(\frac{2.5H}{H_m} \right)}$	Du et al. 2009	0<(H/H$_m$)$\leq$ 0.2

2.4 MAXIMUM SPOUTABLE BED HEIGHT

The maximum spoutable height is the bed length scaling parameter in spouted beds and for this reason one of the most important parameter in the design and scale-up. The maximum spoutable bed height, H_m, is the maximum initial static bed height at which spouting can be obtained. Beyond this initial static bed height there is no spouting. It is directly related to the amount of materials/solids that can be processed in a spouted bed. A common equation for predicting maximum spoutable bed height is given in equation 28.

$$H_m = \left(\frac{D_c}{d_p}\right)\left(\frac{D_c}{D_i}\right)^{2/3}\left(\frac{568b^2}{Ar}\right)[\sqrt{1+35.9*10^{-6}Ar}-1]^2 \qquad (28)$$

where,

$$b = \frac{U_{ms}}{U_{mf}} = 1.0 \sim 1.5 \qquad (29)$$

$$Ar = \frac{d_p{}^3(\rho_s - \rho_f)\rho_f g}{\mu^2} \qquad (30)$$

Equation 28 was tested by McNab and Bridgwater (1977) for b=1.11 and it was found to give a good fit to most existing experimental data. Equation 28 needs to be differentiated with respect to Ar. Substituting for d_p from the equation 30 and setting dH_m/dAr equal to zero gives a critical value, which is shown in equation 31.

$$(d_p)_{critical} = 60.6\left[\frac{\mu^2}{g(\rho_s - \rho_f)\rho_f}\right]^{1/3} \qquad (31)$$

Any values below the d_p critical values, H_m increases with particle size (d_p) and above which H_m decreases when d_p increases. Littman et al. (1977) proposed an equation to predict H_m for spherical particles as follows.

$$\frac{H_m D_s}{(D_c{}^2 - D_s{}^2)} = 0.345 \left(\frac{D_s}{D_c}\right)^{-0.384} \tag{32}$$

Combining equation 32 with McNab correlation (equation 28) and assuming $1 \gg (D_s/D_c)^2$, equation 33 and 34 was obtained for spouting with gases.

$$H_m = 0.842 \left\{ \frac{D_c{}^{1.45} \rho_{bulk}{}^{0.569}}{d_p{}^{1.35} \varepsilon_{mf}{}^{2.03}} \left[\frac{(1 - \varepsilon_{mf})v}{\rho_s}\right]^{0.677} \right\} \quad \text{for } \mathrm{Re_{mf}} \leq 10 \tag{33}$$

$$H_m = 0.0741 \left[\frac{D_c{}^{1.45} \rho_{bulk}{}^{0.569}}{d_p{}^{1.35} \varepsilon_{mf}{}^{1.02}} \frac{1}{(\rho_s \rho_f)^{0.339}} \right] \quad \text{for } \mathrm{Re_{mf}} \geq 1000 \tag{34}$$

Grbavcic et al. (1976) developed a correlation (equation 35) which was based on spherical particles in water spouted beds.

$$\frac{H_m}{D_c} = 0.347 \left(\frac{D_c}{D_i}\right)^{0.41} \left(\frac{D_c}{d_p}\right)^{0.31} \tag{35}$$

Littman et al. (1976) reported that the maximum spoutable bed height for a spout-fluid bed (H_{msf}) and a spouted bed (H_m) is same for a given system. Since, maximum spoutable bed height for spout-fluid bed and spouted bed is not same even for a given system, Hadzisdmajlovic et al. (1983) realizing this reworked the correlation for predicting H_m, which was proposed by Littman et al. (1976). Since H_{msf} is an important parameter in spout-fluid bed and its knowledge is important in predicting minimum spout-fluid flow rate, Hadzisdmajlovic et al. (1983) developed a semi-theoretical correlation for H_{msf} which is shown in equation 36.

$$\frac{H_{msf} D_{sf}}{D_c{}^2 - D_{sf}{}^2} = \sum_{n=0}^{5} A_n \left[\frac{q_a / A_a}{U_{mf}}\right]^n + \left[1 - \frac{q_a}{U_{mf}}\right] \left[0.345 \left(\frac{D_s}{D_c}\right)^{-0.384} - 0.596\right] \tag{36}$$

Where, $A_0 = 0.5962$, $A_1 = -0.4316$, $A_2 = 0.05617$, $A_3 = -0.2972$, $A_4 = 0.5675$ and $A_5 = -0.425$. D_{sf} can be evaluated by equation 37.

$$\frac{D_{sf}}{D_s} = \left\{ 1 - \left[1 - \left(\frac{H_{msf}}{H_m} \right) \right]^3 \right\}^{1/2} \tag{37}$$

H_m in equation 37 is calculated using equation 32. It was observed that equation 36 had some discrepancies and hence, Rao et al. (1985) proposed a new correlation for predicting maximum spoutable bed height in a spout-fluid bed which is described in equation 38.

$$\frac{H_m - H_{msf}}{H_m} = 0.998 \frac{q_{amsf}}{Q_{mf}} - 1.087 \left(\frac{q_{amsf}}{Q_{mf}} \right)^2 + 1.01 \left(\frac{q_{amsf}}{Q_{mf}} \right)^3 \tag{38}$$

Even though H_m has been studied for years, there still lies lot of differences in exactly predicting this important parameter of spouted bed.

2.5 FLOW REGIME AND REGIME MAPS IN SPOUTED BEDS

Spouting, which is visually observable in a transparent column with a fully circular cross-section by virtue of the rapidly reversing motion of particles in the fountain and the relatively slow particle descent at the wall, occurs over a definite range of gas velocity for a given combination of gas, solids, vessel geometry, and configuration. With increasing inlet gas velocity, typically five flow regimes can be observed in the systems that can be spouted (Figure 2.1): packed bed, stable spouting, un-stable spouting, bubbling and slugging. The stable spouting is distinguished by the formation of the stable spout/fountain, while unstable spouting is characterized by swirling and pulsation of the spout with time. Bubbling regime is characterized by formation of large packets of air

and also is termed as poor quality aggregative fluidization. Slugging flow regimes is characterized by complete aeration of the spouted bed with huge packets of air. Recognition and characterization of flow regimes play an important role in the application of spouted beds. Figure 2.1 illustrates schematically the transition from a quiescent to a spouted bed, and hence often to a bubbling and a slugging bed, as the superficial gas velocity (gas volumetric flow rate/column cross-sectional area) is increased.

(a) STATIC BED (FIXED PACKED BED) (b) SPOUTED BED (c) BUBBLINGBED (POOR QUALITY AGGREGATIVE FLUIDIZATION) (d) SLUGGING BED
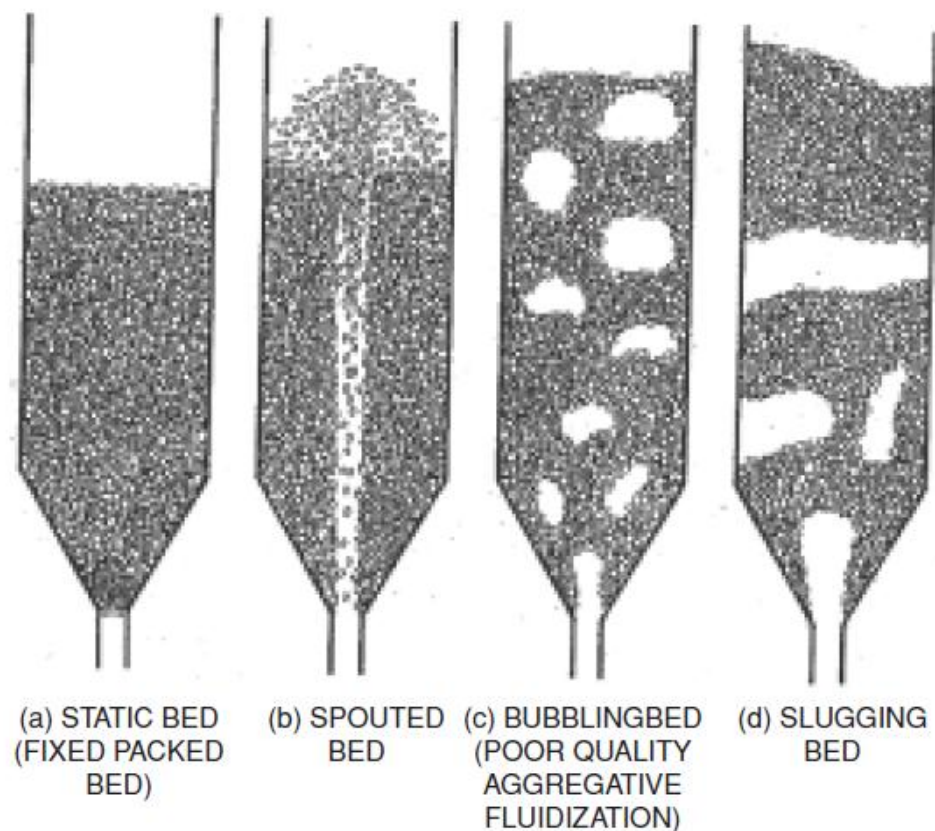
Figure 2.1. Regime transitions in a spouted bed with increasing gas flow (Epstein and Grace, "Spouted and Spout –Fluid beds" book, 2011)

Transitions can be represented quantitatively as plots of bed depth H versus superficial gas velocity U, or regime maps (sometimes referred to as "phase diagrams"), examples of which are shown in Figures 2.2 and 2.3. The line representing transition between a static and an agitated (spouted or bubbling-fluidized) bed is more reproducible in the direction of decreasing velocity than vice versa, the resulting static bed then being in the reproducible random loose packed condition (N. Epstein et al., 1969). Figure 2.2 shows that, for a given solids material contacted by a specific fluid (at a given temperature and pressure) in a vessel of fixed geometry, there exists a maximum spoutable bed depth (or height) H_m, beyond which spouting does not occur, being replaced by poor-quality fluidization. In Figure 2.2, H_m is represented by the horizontal lines at a bed depth of 0.76 m. The minimum spouting velocity, U_{ms}, is represented in the same figure by the inclined line that terminates at H_m, at which U_{ms} can be up to 50 percent greater (Pallai and N´emeth, 1969) than the corresponding minimum fluidization velocity, U_{mf}, although less difference between these two critical velocities has usually been found (Becker, 1961 and G. Lefroy et al., 1969). Figure 2.3 shows a gas inlet, particle, and column diameter combination for which spouting does not occur. For the same column and particles, but with a smaller gas inlet ($D_i = 12.5$ mm instead of 15.8 mm), coherent spouting could be obtained (Mathur and Gishler, 1955).

Becker (1961) attempted a more generalized regime diagram by plotting upward drag force (as measured by frictional pressure drop, $-\Delta P_f$) normalized with respect to downward gravitational weight of solids against U/U_m, with H/H_m as a parameter, whereas Pallai and N´emeth (1969) simply plotted $-\Delta P_f$ against U/U_{mf} with H as a parameter. The amount of information provided by these procedures for any given system

of fluid, solids, and column geometry is considerable, but the applicability to other systems is quite limited, given the complexity of the regime transitions.
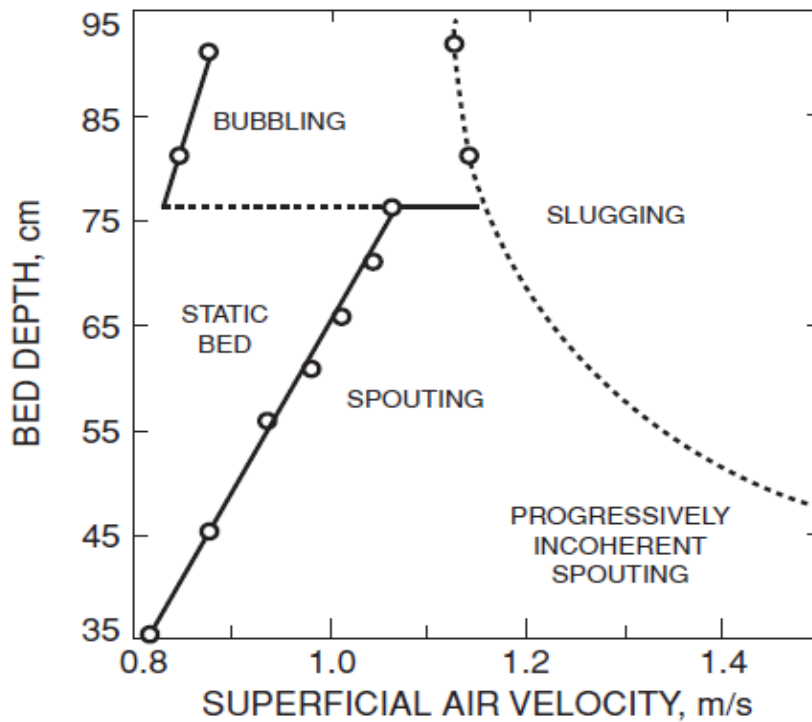
Figure 2.2. Flow regime map for wheat particles (prolate spheroids: 3.2 mm × 6.4 mm, ρ_s =1376 kg/m^3). Dc = 152 mm, D$_i$ = 12.5 mm. Fluid is ambient air (Mathur and Gishler, 1955)

A typical spouted bed in a cylindrical or conical-cylindrical vessel has a depth, measured from the fluid inlet orifice to the surface of the loose-packed static bed or the spouted bed annulus, of at least one-half the cylinder diameter. If the bed is much shallower, the system differs hydrodynamically from true spouting, and any generally formulated principles of spouted bed behavior would not be expected to apply. A

minimum spoutable bed depth has, however, not been precisely defined or investigated, except in the case of conical beds (M. Olzar et al., 1993), nor have any detailed studies been made about the maximum spouting velocity at which transition from coherent spouting to either bubbling fluidization or slugging occurs. For most practical purposes, however, there is usually sufficient latitude between the minimum and maximum spouting velocity that the fluid flow can be amply increased above the minimum without transition to fluidization.
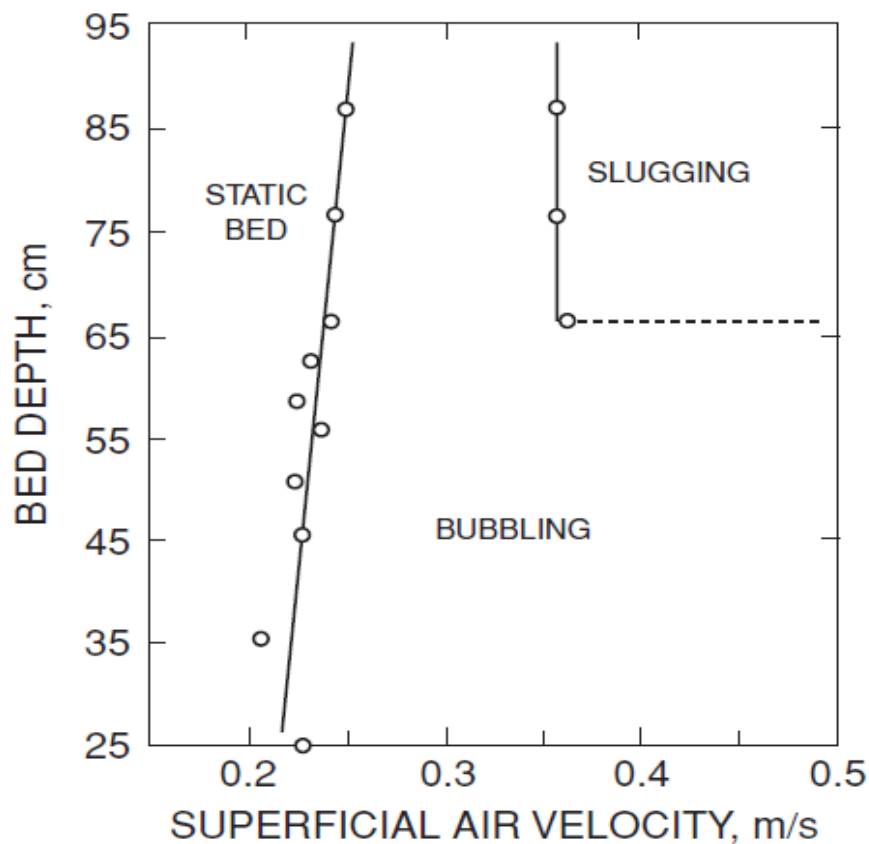
Figure 2.3. Regime map for Ottawa sand (dp = 0.589 mm). Dc = 152 mm, Di = 15.8 mm
(Mathur and Gishler, 1955)

2.6 SIMULATION OF SPOUTED BEDS

Numerous theoretical and experimental studies have been carried out in recent decades in an attempt to model the hydrodynamics of spouted beds. Most of the early models are one-dimensional, with spout and annulus considered separately by assuming that some parameters are constant. In addition, these models, though useful as first approximations, are complex, or require parameters to be determined by experiments.

Thanks to the explosion of computational power, the advance of numerical algorithms, and deeper understanding of multiphase flow phenomena, computational fluid dynamics (CFD) modeling has become a powerful tool for understanding dense gas–solid two phase flows in the recent past. The main advantage of CFD modeling is that a wide range of flow properties of the gas and solids may be predicted simultaneously without disturbing the flows. Currently, there are two main CFD approaches: the Eulerian-Eulerian approach (two fluid model, TFM), and the Eulerian-Lagrangian (discrete element method, DEM) approach.

In the Eulerian-Eulerian approach, the fluid and particulate phases are treated mathematically as interpenetrating continua. Several studies (listed in Table 2.2) have shown that this approach is capable of predicting gas-solids behavior in spouted beds. Because the volume of one phase cannot be occupied by the other, the concept of overlapping phases, each with its own volume fraction, is introduced. Volume fractions of the overlapping phases are assumed to be continuous functions of space and time, with their sum always equal to 1. The conservation equations have similar structure for each phase. Owing to the continuum description of the particle phase, two-fluid models require additional closure laws to describe particle–particle and particle–fluid interactions. The

Eulerian-Eulerian approach is often the first choice for simulation because of its lesser use of computational resources. The full Eulerian-Eulerian approach includes (1) conservation equations of mass and momentum for each phase, with an interphase momentum transfer term; (2) closure of the equations, which requires proper description of interfacial forces, solids stress, and turbulence of the two phases; and (3) meshing of domain, discretization of equations, and solution algorithms.

In the Eulerian-Lagrangian type (DEM approach), the fluid phase is treated as a continuum by solving the time-averaged Navier-Stokes equations, whereas the dispersed phase is solved by tracking a large number of individual particles through the computed flow field, not requiring additional closure equations. The dispersed phase can exchange momentum, mass, and energy with the fluid phase, and the two phases are coupled by interphase forces. The DEM approach offers a more natural way to simulate gas–solid flows, with each individual particle tracked. However, it is much more computationally demanding, especially as the number of particles simulated becomes large. Table 2.3 lists previous computations of this type of model for spouted bed hydrodynamics.

Table 2.2. Eulerian-Eulerian simulations on spouted bed

Investigators	Model Source	Software code	Contribution
Krzywanski et al. (1992)		Author developed code	Developed a multidimensional model to describe gas and particle dynamic behavior in a spouted bed.
Wang et al. (2006)	Kinetic theory of granular flow	FLUENT	Found that actual pressure gradient (APG term) in conical spouted beds significantly influences static pressure profiles.

Table 2.2. Eulerian-Eulerian simulations on spouted bed cont.

Lu et al. (2001, 2004, 2007)	Kinetic theory of granular flow; Gidaspow drag model with switch function	K-FIX; M-FIX	Viewed spout and annulus as interconnected regions. Incorporated kinetic-frictional constitutive model: kinetic theory of granular flow; friction stress was calculated by combining normal frictional stress model of Johnson et al. (1990) and modified frictional shear viscosity model proposed by Syamlal et al. (1993); behavior of agglomerates of nanoparticles in spouted bed systems was simulated numerically.
Du et al. (2006)	Kinetic theory of granular flow	FLUENT	Found that the descriptions of interfacial forces and solid stresses play important roles in determining the hydrodynamics for spouting both coarse and fine particles.
Shirvanian et al. (2006)	Kinetic theory of granular flow; Gidaspow drag model	FLUENT	Developed three-dimensional (3D) simulation model to describe isothermal liquid–solid two-phase flow in a rectangular spouted bed; it was able to predict experimentally observed "choking".
Wu and Mujumdar (2008)	Kinetic theory of granular flow; Gidaspow drag model with switch function	FLUENT	Described bubble formation and motion inside a 3D spout-fluid bed.
Gryczka et al. (2008)	Kinetic theory of granular flow	FLUENT	Compared drag models of Schiller and Naumann, Wen and Yu, Syamlal and O'Brien, Gidaspow et al., Koch and Hill, van der Hoef et al., and Beetstra et al. Better agreement with experiments was obtained by applying Schiller and Naumann model.

Table 2.2. Eulerian-Eulerian simulations on spouted bed cont.

Gryczka et al. (2009)	Kinetic theory of granular flow	FLUENT	Pointed out that an appropriate drag model alone is not sufficient to fit the simulation results to the experimental findings; other contributions such as particle rotation are also important.
Bettega et al. (2009)	Kinetic theory of granular flow	FLUENT	Obtained experimental data for a semi-cylindrical spouted bed; compared CFD simulations from a 3D simulation scheme; discussed influence of flat wall on solid behavior in semi-cylindrical vessel. Presented a numerical scale-up study of spouted beds. Verified that the scale-up relationships of He et al. produced good numerical results.
Santos et al. (2009)	Kinetic theory of granular flow	FLUENT	Simulated patterns of solids and gas flows in a spouted bed using 3D Eulerian multiphase model; 3D predictions showed better accuracy than 2D ones.
Duarte et al. (2009)	Kinetic theory of granular flow; Gidaspow drag model	FLUENT	Simulated spouted beds of conical and conical-cylindrical geometries. Predicted pressure drops and particle velocities agreed well with experimental values.
Lan et al. (2011)	Kinetic theory of granular flow; Gidaspow drag model	FLUENT	Simulated spouted beds of cone based cylindrical geometry and verified scale-up relationships of He et al. (1997).

Table 2.3. Eulerian-Lagrangian simulations on spouted bed

Investigators	Model Source	Software code	Contribution
Kawaguchi et al. (1998, 2000)	Newton's 3rd law for coupling between phases	Author developed	Proposed first Eulerian-Lagrangian approach for spouted beds; obtained typical spouted bed flow patterns.

Table 2.3. Eulerian-Lagrangian simulations on spouted bed cont.

Takeuchi et al. (2004,2005,2008)		Author developed	Simulated 3D cylindrical-conical spouted beds. Proposed new method for treating boundary conditions.
Swasdisevi et al. (2004)		Author developed	Simulated aerodynamics of particles and gas flow in slot-rectangular spouted bed with draft plates. Calculated Ums and pressure drop agreed well with correlations of Kalwar et al. (1993)
Limtrakul et al. (2004)		Author developed	By combining DEM and mass transfer models, investigated local mass transfer in gas–solid catalytic spouted bed reactor for decomposing ozone; results agreed well with the experimental results of Rovero et al. (1983)
Zhong et al. (2006)	k-ε turbulent model for gas motion	Author developed	Simulated turbulent motions of the gas and particles by treating the two phases separately. Particle motion modeled by DEM and gas motion by k-ε model.
Zhao et al. (2008)	Low Reynolds k− ε turbulence model for fluid phase	Author developed	Simulated flow of particles in 2D spouted bed with draft plates with a low Reynolds number k-ε turbulence model for the fluid phase.

The characteristic patterns of spouted beds can be reproduced well by both the Eulerian-Eulerian and the Eulerian-Lagrangian approaches. Parameters such as spout diameter, minimum spouting velocity and voidage profile all have been reported in literature to show reasonably good agreement with experimental data. This indicates that CFD modeling can serve as an important tool for predicting gas and solid behavior in spouted beds. The Eulerian-Eulerian approach is usually the first choice for simulation

because of its lesser use of computational resources and hence has been used in the present work, where the obtained data and results have been used to validate the models and simulation results. The successful application of this approach depends mainly on closure of the momentum equations, as the simulation is sensitive to the actual pressure gradient (APG), drag coefficient, interparticle coefficient of restitution and solid friction stresses. To describe the solid-phase stresses, the kinetic theory of granular flow has been widely adopted.

Although more computational capacity is required, the Eulerian-Lagrangian approach offers a more physically satisfying way to simulate gas–solid flows, with each individual particle tracked in the simulation. It can be applied readily for particle tracking – for example, for residence time and particle circulation studies.

In general, an important challenge in CFD studies of spouted beds is to describe properly the inherent turbulence for both the solids and gas phases, especially for the spout region. Further fundamental and experimental studies on the kinematic properties of the two phases are needed to improve the accuracy of the CFD models.

3. DEVELOPING A NEW SOPHISTICATED GAS-SOLID OPTICAL PROBE FOR SOLIDS DYNAMICS MEASUREMENT AND A NEW METHODOLOGY FOR OPTICAL PROBE CALIBRATION

3.1 INTRODUCTION

Various types of fiber optic probes have been developed and used to measure solids concentration, solids velocity and their fluctuations for gas-solid systems (e.g., fluidized beds: De Lasa et al., 1998; downer of circulating fluidized beds (CFBs): Rundqvist et al. 2004; riser of CFBs: Miao et al. 1992 etc.). The optical probe studies performed over previous decades use separate individual gas-solid probes for the measurement of solids velocity or solids concentration (Matsuno et al., 1983; Yang et al., 1993; Zhang et al., 1991; De Lasa et al. 1995; Zhu et al., 1995; etc.). Optical probes that can measure both solids concentration and solids velocity simultaneously, has not been developed and utilized. Additionally, these so called "older generation" gas-solid optical probes were plagued by the presence of blind regions and lesser measurement volumes, which affected their measurements. These drawbacks were addressed by the newer improved design probe systems. However, still separate probe systems were used for measurement of solids concentration and solids velocity. Thus, there is a need to measure simultaneously and at the same point the solids velocity, solids concentration and their time series fluctuations, where the solids concentration should be converted to solids holdup. Such need has been overcome by the development of advanced optical probe system that is used in the present study (PV-6 particle velocity analyzer). Institute of Process Engineering of the Chinese Academy of Sciences developed this new-sophisticated probe. This new probe can measure simultaneously solids velocity, solids concentration and their time series fluctuations. The measurement of solids concentration

needs to be converted to solids holdup (volume fraction of solids at the probe location) through reliable calibration. Also the measurement of the solids velocity must be validated before the probe is being used. Hence, gas-solid optical probes for the measurement of solids volume fraction and solids velocity must be calibrated properly with definite limits in order to obtain reliable measurements for gas-solid dynamic systems. The conversion of solids concentration to solids volume fraction is dependent on calibration, which in previous studies reported in the open literature involves an experimental set-up like a circulating fluidized bed, thereby increasing the cost of experimental procedures (Guigon et al., 1995 and Saberi et al., 1998). Therefore, simple and reliable calibration method for optical probe in general and the newly developed one for this study in particular is needed which has been addressed in this study.

In this section, first different gas-solid optical probes used to measure solids concentration and solids velocity till this date has been discussed. Later, the advanced optical probe used in the present study, its electronics and measurement is discussed in detail. Then, the developed new methodology for optical probe calibration and validation of optical probe solids velocity measurements using a high-speed camera are explained. The validation of the developed methodology using a non-invasive radioisotope based technique called as Gamma Ray Computed Tomography (CT) has been explained later.

3.2 OVERVIEW OF THE CURRENT REPORTED GAS-SOLID OPTICAL PROBES FOR MEASUREMENT OF SOLIDS CONCENTRATION AND SOLIDS VELOCITY

Optical fiber probes work based on either forward scattering or back scattering of light principle with emitting and receiving optical fibers. The back scattering probes have

found more applications in gas-solids systems because of simpler design and less intrusion (Chaouki et al. 2001) and hence will be discussed in this section. These probes can be further classified into two separate categories based on the type of measurements they are used for. The first can be classified as the probes, which measure solids concentration and the other as the probes, which measure solids velocity. The first part of this section will deal with the probes measuring solids concentration followed by the probes used for measuring solids velocity.

   3.2.1. Solids Concentration Probes. There have been several different probe designs developed over the years to measure solids concentration. Each type of probes having its own advantages and disadvantages over the others. The concentration probes use single channel signal processors. To summarize, a few of these probes is explained. The first type of probes consisted of a simple design (Louge, 1991), with two parallel single optical fibers, for light emitting and receiving light (Figure 3.1). The measurement region is the cross volume of two expected lights and depends on the medium concentration. Size of the light emitting fibers was bigger (800 μm in diameter) than the size of the receiving light fibers (200 μm in diameter). Hence, blind regions are evident in such probes. The overall probe size was in the order of 2-3 cm in diameter.
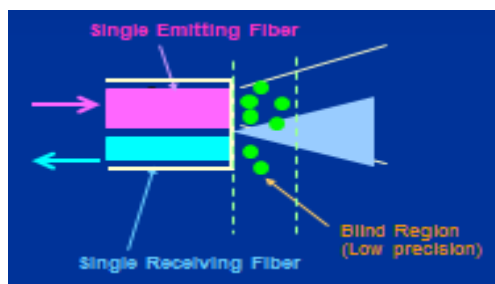
Figure 3.1. Single fiber optical probe with the presence of blind region (Lounge, 1991)

Parallel-optical fiber bundle probes were then developed to reduce the effect of blind region (Li et al., 1997). These were made by randomly arranging optical fibers in bundles. Half of the bundle consisted of light emitting fibers and the rest was light receiving fibers (Figure 3.2). The optical fibers used in this design were all of the same size (200 μm in diameter), thus making the overall probe size in the range of 2 cm in diameter. The measurement volume for this probe covered all the expected light crossings, but the blind region still existed (much smaller compared to previous design of probes).
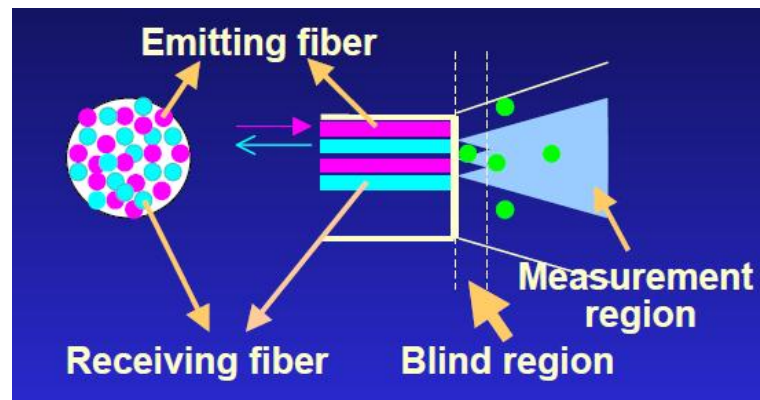
Figure 3.2. Parallel-optical fiber bundle with measurement volume and blind region (Li et al., 1997)

Cross-optical fiber probes were then (Johnston et al., 1998; Rundqvist et al., 2003) developed by using two cross-optical fibers (two single fibers placed in a predetermined angle) of each 0.8 mm in diameter (Figure 3.3) with a glass window at the tip of the probes. This probe effectively removed the blind region but maintained a small

measuring volume, which was one of its disadvantages. The overall size of these kinds of probes was 1.5 – 2 cm in diameter.
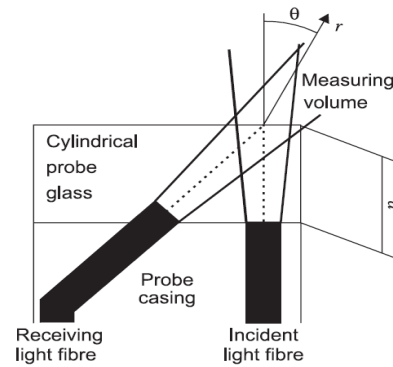
Figure 3.3. Cross-optical fiber probe with small measuring volume and glass window
(Rundqvist et al., 2004)

Due to the elimination of blind region, probes designed after the cross-optical fiber probes included the window at the tip of the probes. Parallel-optical bundle fibers with optical fibers arranged in a regular fashion were then developed. These probes were installed with quartz windows instead of glass windows; due to better refractive index (Jinzhong et al. 2003). These probes combined the increased measuring volume feature of parallel optical fiber bundle probe and elimination of blind region, a feature of cross-optical fiber probes. These were fabricated by arranging several bundles of light emitting and receiving light fibers (30 μm) alternatively to each other. The overall size of these probes was 1 – 1.5 cm in diameter.

The drawbacks of earlier probe systems were attributed to the design structure (Figure 3.1 and 3.2; Bi et al., 2004). Since the intensity of the reflected light by the solids

is maximum near the probe tips (Figure 3.4), the blind regions caused a major loss of such reflected light by the particles. With the arrangement of optical fibers in alternate fashion, the cross volumes of the expected lights increased and with the presence of quartz window the blind region was eliminated (Figure 3.5).
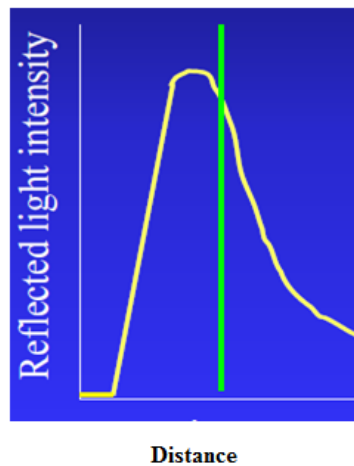
Figure 3.4. Reflected light intensity as a function of distance from the old generation probe tips
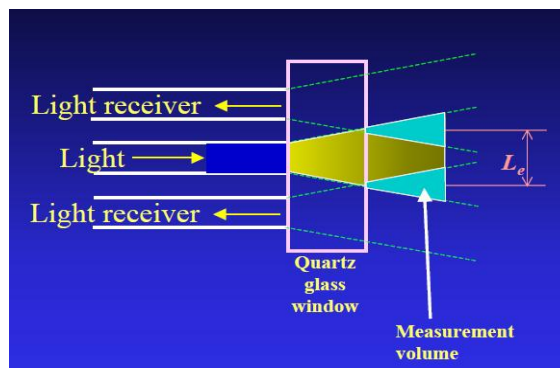
Figure 3.5. Small section of parallel optical fiber bundle probes showing the elimination of dead zone with the addition of quartz window

3.2.1.1. Solids concentration probes electronics and measurement. The reflected light from the solids captured by the optical probe system is converted into time series signals of voltage. The analysis of such signals is very important to extract meaningful parameters. The fibers first transmit the light to a photocell, which converts it into a voltage signal, and the data is then recorded on to a PC through A/D (analogue/digital) data acquisition card (Shakourzadeh et al., 1998; Almstedt et al., 2004). This is the general electronics used in all the probe systems used till date. With the improvement in the design of the probes, the electronics of the system has also been improved over the years. The probe systems available now have better response time and sensitivity, freedom from disturbance of electric and magnetic fields and insulation against high voltage (Zhu et al., 1998; Grace et al., 2003; Lim et al., 2009 etc.). All the concentration probes have single channel signal processors for the reflected light.

The gas-solid optical probes measure solids concentration in systems using the principle of reflection of light. Light reflected back to the optical probes contains the information of solids concentration, which refers to the amount of particles in the measuring volume. The intensity of the reflected light depends on the type, composition and size distribution of particles.

Once the signal is obtained, further analysis is required. Due to numerous studies over the years, there have been many findings reported in the open literature using these solids concentration probes. To represent their results, most of the studies talk about the conversion of solids concentration into solids holdup/volume fraction through calibration. The details of calibration and signal analysis that have been used in the literature are explained.

3.2.1.2. Current calibration methods of solids concentration of optical probes.

Calibration refers to the relation between the voltage signals generated by the optical probe to the solids volume fraction measured. Since, the measured voltage signals from the probes consists information about the solids concentration which needs to be represented in terms of solids holdup (volume fraction of solids), which is the common nomenclature used as a hydrodynamic parameter in the literature.

There have been several different calibration methods developed and reported in the literature. Some of these methods have been outlined in this section. Most of the methods listed in the literature can be classified into four different categories, namely: (a) Dropping/trapping technique, (b) Liquid-solid suspensions, (c) Circulating fluidized bed technique and (d) Polymer mixture technique. Each of the above categories is explained below.

3.2.1.2.1. **Dropping/trapping technique.** This method usually utilizes a

plexiglass column with constant feeder at the top of the system for the flow of solid particles. One of the many experimental set-ups used for such a purpose is shown in Figure 3.6. The system uses a vibrating feeder at the top to feed the solids to the column. This feeder helps to maintain a stable mass flow rate of solids and also to provide a range of mass flow rates (which will be encountered in the real experimental conditions). A small chamber is fabricated in the column at a sufficient distance from the top (and bottom of the downer). This ensures that the solid particles attain a fully developed state. Two slide valves are attached on either side of this chamber. The valves are closed simultaneously and the solid particles are trapped in the chamber. The mass of solids in the chamber and thus the solids holdup between them is determined. The optical probes

are located in this chamber in order to measure voltage signals. Zhu et al., 1998; Saberi et al., 1998; Grace et al., 2003 and several other researchers have reported such calibration methods for the use of fiber optical probes for solids concentration/holdup measurements. The solids used in such studies must be similar to the solids to be used in the actual experimentation process. Failure to adhere to this may result in errors in measurement.
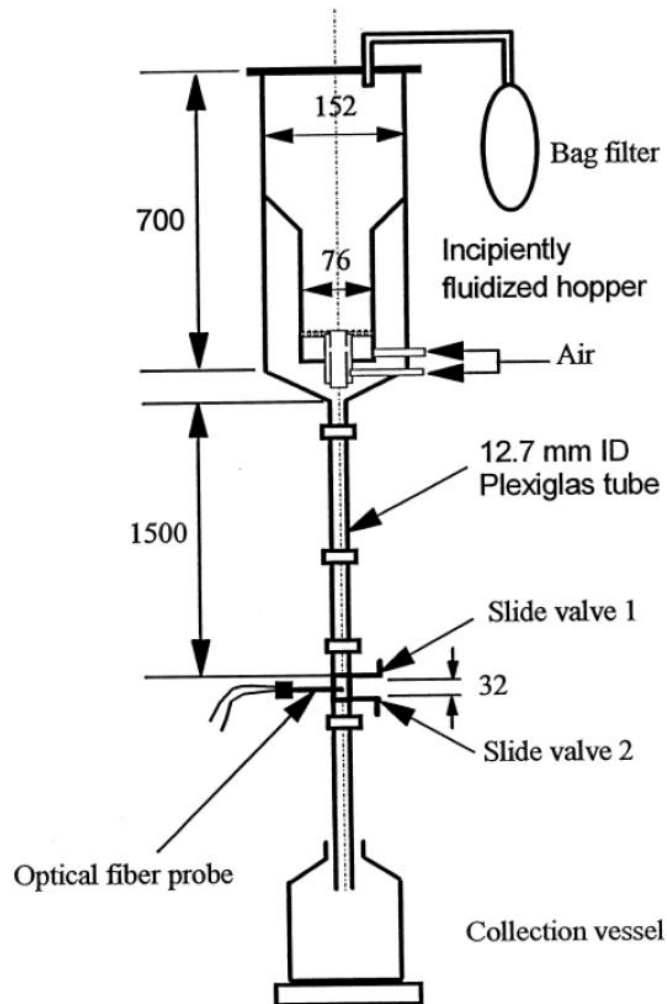
Figure 3.6. Dropping/trapping calibration technique for optical probes demonstrated in a downer set-up (Saberi et al., 1998)

3.2.1.2.2. <u>Liquid-solid suspensions.</u> This technique employs the use of water-particle suspension to generate the calibration equation for the optical probes. First a vessel filled with water is taken and then a stirrer is attached to the set-up. A known amount of solids is placed under this water suspension. The stirrer constantly stirs the suspension in order to obtain a uniform distribution of particles in the water. The probe is placed in the vessel to obtain the voltage signal. Figure 3.7 shows the commonly used set-up for such calibration methods. Since there is a known amount of particles present in the suspension, the solids holdup can be evaluated using this information. The particle quantity can be changed depending on the range of calibration required for the experimental conditions. The details of the procedure can be found in Qin et al., 1982; Grace et al., 1994 and Bi et al., 2009 who have reported such methods for calibration.
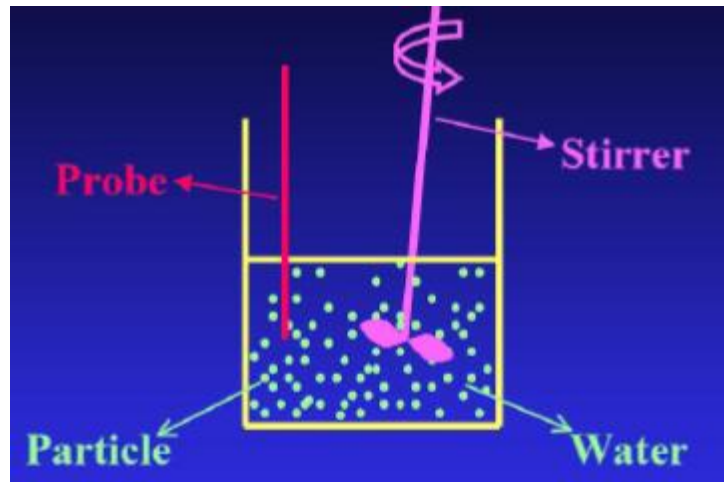
Figure 3.7. Liquid-solid suspension system used to calibrate optical fiber probes

3.2.1.2.3. <u>Circulating fluidized bed technique.</u> As the name suggests, this method uses a fluidized bed with a circulating feed system. Many researchers have developed their own circulating fluidized bed (CFB), for such purposes. One of the configurations of CFB used for calibration is shown in Figure 3.8. The system consists of a rectangular fluidized bed (riser) and a two-stage cyclone system with downer. The air enters the riser suspending and carrying the particles in the system. The particles are then carried over to the cyclone system and then again fed back to the bottom of the column through the downer. The riser has ports for pressure transducers and optical probes to aid measurement along its height. The solids flow rate is measured by means of a weighing hopper attached to the standpipes of the cyclones. Solid particles are returned to the lower part of the fluidized bed through an L-valve by using an injection of air at its bend. More details of the system can be found in Aguillon et al. (1995).

The solids are fluidized under different flow conditions to obtain a full range of calibration curve. The column was equipped with pressure taps related to water manometer on one side and the other side of the column was equipped with optical fiber probes for recording the voltage signals. The system was also equipped with velocity optical probes (discussed in later sections) to measure the solids velocity. Once a steady state of operation was reached for the system, the hopper measured the solids flow rate and voltage reading by the concentration optical probes was recorded. The solids volume fraction was determined by dividing the flow rate to the velocity of solids phase measured by the related velocity probe, thus generating the calibration curve. More details of the procedure can be found in Guigon et al. (1998), Aguillon et al. (1995), Fan et al. (1999) and Bi et al. (2003) who all have reported similar procedures for calibration.
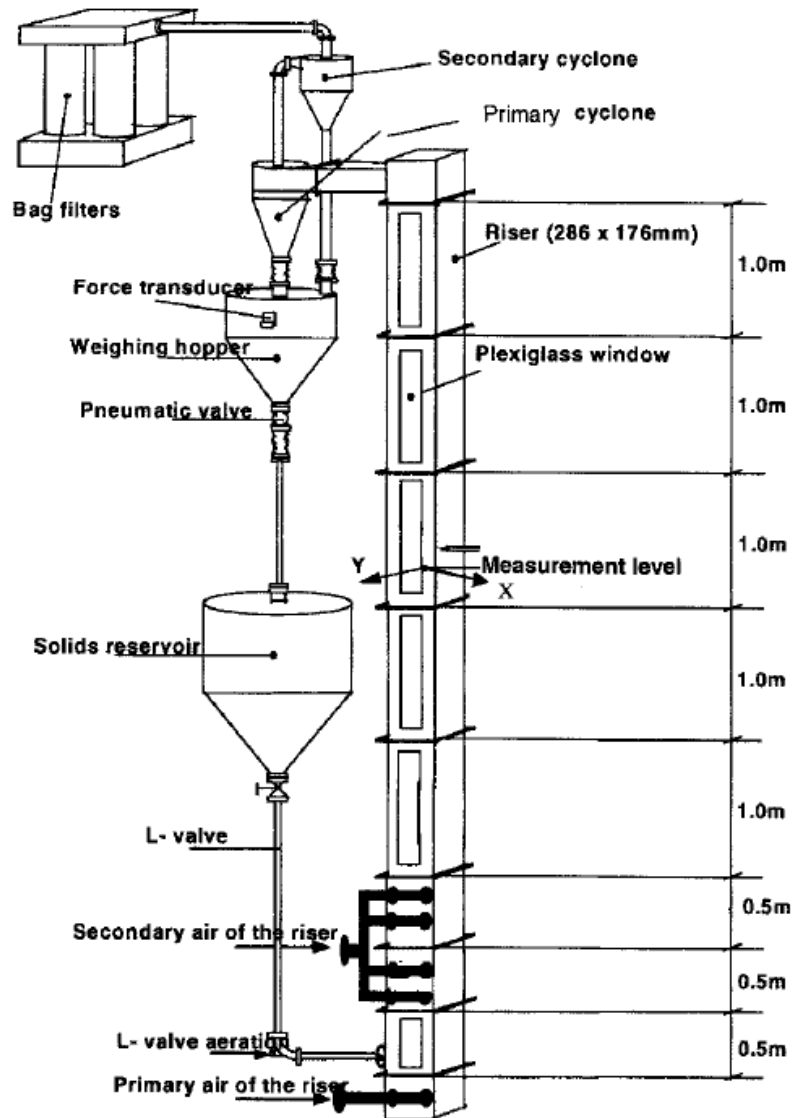
Figure 3.8. Circulating fluidized bed technique used for optical fiber probe calibration, Guigon et al., 1998

3.2.1.2.4. Polymer mixture technique. This is a new technique developed recently by Bi et al. (2011). The method involves infusing a predetermined amount of particles in a transparent polymer. The volume fraction of such particles ranges from 0 to 0.56 (using separate polymer for each value). The optical probe to be calibrated is then

subjected to these different polymers. The voltage signal generated from the probe is then related to the known volume fractions. The details of this technique can be found in Bi et al. (2011). The polymer particle used in such studies is shown in Figure 3.9.
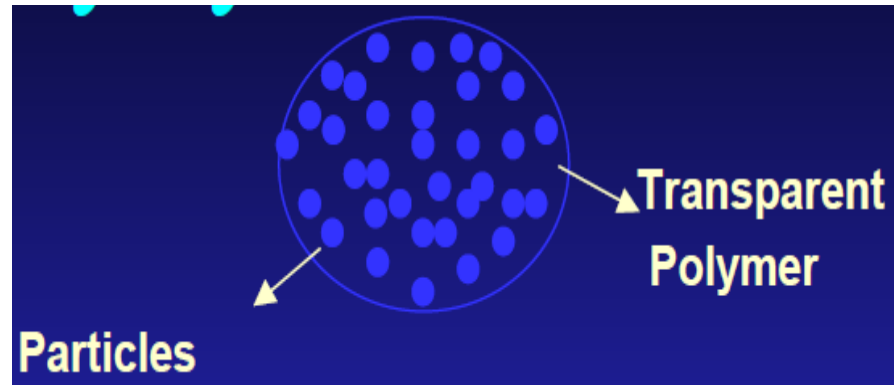
Figure 3.9. Particles infused in a transparent polymer for calibration

3.2.2. Solids Velocity Optical Probes. The solids velocity optical probes are designed differently as compared to the solids concentration probes. These probes employ the principle of cross-correlation analysis of signals to extract velocity information. A typical solids velocity probe consists of one light emitting fiber (80 μm) and two receiving light fibers (Figure 3.10). As the solids pass from one end of the probe to the other end, two signals are generated with a time shift. This time shift is due to the time taken by the particles to pass from one point to another. The two receiving light fibers have separate channels for processing the signals unlike concentration probes, which contains one channel for signal processing for the entire probe. By the method of cross-correlation analysis, the time delay between these two series of signals is estimated.

The distance between the light emitting and receiving light fiber is called the effective distance, L_e. To obtain the solids velocity the effective distance is divided by the time delay obtained through cross-correlation analysis. To obtain effective distance information, the velocity optical probes need to be calibrated first. The methods used for this calibration is explained in the following section.
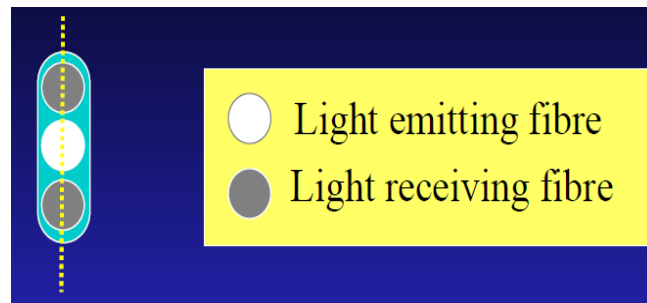
Figure 3.10. Solids velocity probe

The velocity optical probes also went through the design modifications over the years for better measurement purposes. Probes with different fiber arrangements have been established over the years, few of which are shown in Figure 3.11 (Olazar et al., 1995). These probes have several channels for signal processing depending on the design of the probe. Velocity optical probes have also been fitted with quartz window to eliminate the blind regions because it affected the measurements. The generation of signals in velocity optical probe is the same as concentration probes. The reflected light is passed through a photocell to convert them into voltage signals and through an A/D acquisition card the signals are recorded onto a PC.
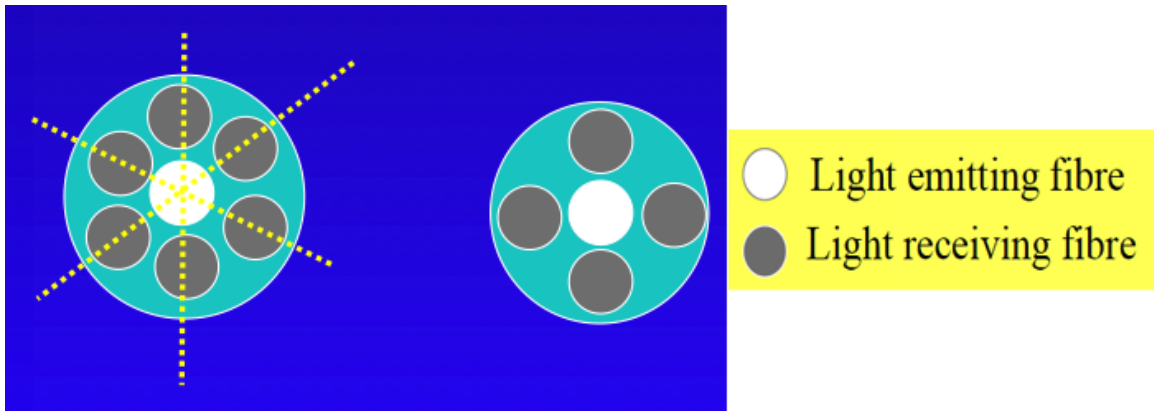
Figure 3.11. Different arrangement patterns of velocity optical probes

3.2.2.1. Calibration of solids velocity probes. Calibration for velocity probes is performed in order to find the effective distance between the light emitting fiber and receiving light fiber. The effective distance of a velocity probe was commonly determined using rotating disks (San Jose et al. 1998a) or rotating disks (or rod) with one or more particles attached (He, 1995). Wang et al. (2009) used rotating disks with different designs such as rotating disks with particles glued and rotating packed bed to determine the effective distance. One of the set-ups for a rotating disk is shown in Figure 3.12, which consists of a disk to hold the particles attached to a motor. The probe is placed face down onto the rotating disk at a certain distance from the top. The motor controls the speed of the rotating disk on which the particles under study are glued. The motor rotates the disk and the velocity optical probe records the signals. The velocity of the rotating disk is estimated or sometimes predetermined. The velocity optical probes record the signals when the glued particle passes the probe tip. The delay time is then estimated from the recorded signals. Since the velocity of the rotating disk is already

known, the effective distance of the velocity probe is calculated. More details of the calibration and the effect of different disks, particle size and particle properties on the effective distance can be found in Bi et al. (2009).
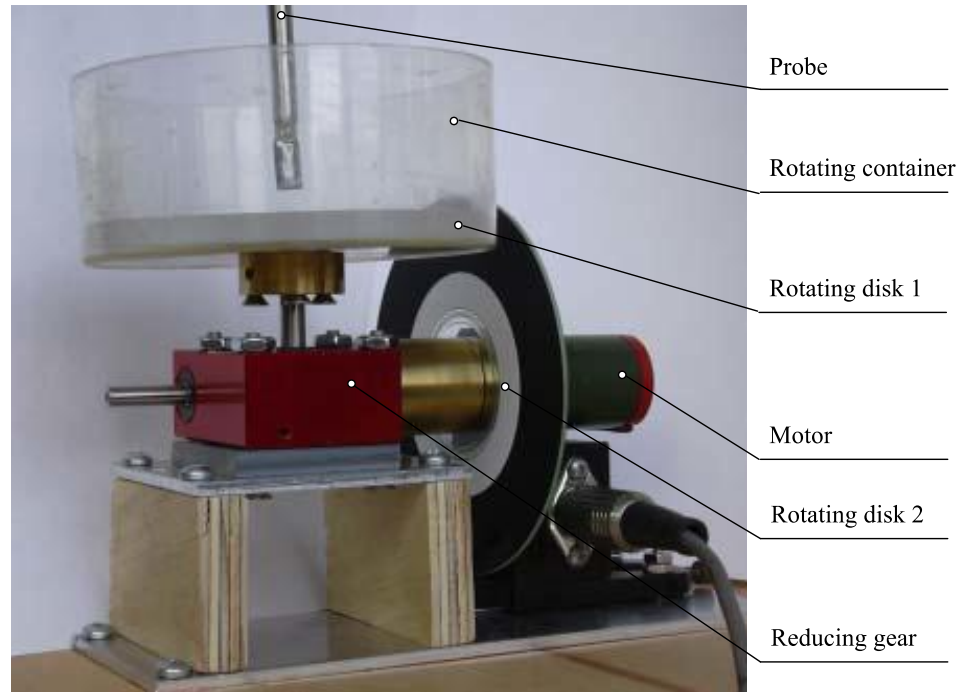
Figure 3.12. Rotating disk calibration device for velocity probes (Bi et al., 2009).

3.2.2.2. Cross correlation analysis for estimating solids velocity. As mentioned earlier, the velocity optical probe using cross correlation analysis measures solids velocity. The signals recorded from the two channels of the probes are analyzed by this method. The main objective of such analysis is to obtain the time delay between the two signals recorded by the probe. The equation used for the analysis is shown in equation 1.

$$\tau = \underset{T \to \infty}{Lim} \frac{1}{T - \tau} \int_{\tau}^{T} A(t)B(t - \tau) \tag{1}$$

The above equation gives the time delay between two signals. Since the velocity probe records time series signal, many data points are recorded. To pick the best data set among the series, cross correlation co-efficient must be estimated. If there are two discrete signals x_i and y_i, then the cross correlation co-efficient can be estimated by equation 2.

$$R_{xy} = \frac{\sum[(x_i - \bar{x})(y_i - \bar{y})]}{(N-1)S_x S_y} \tag{2}$$

Where, R_{xy} is the cross correlation co-efficient, $\bar{x}$ and $\bar{y}$ are the average values of x_i and y_i. N is the number of data points. S_x and S_y are the standard deviations of x_i and y_i.

$$\bar{x} = \frac{1}{N} \sum_{1}^{N} x_i \tag{3}$$

$$\bar{y} = \frac{1}{N} \sum_{1}^{N} y_i \tag{4}$$

$$S_x = \sqrt{\frac{1}{N-1} \sum_{1}^{N} (x_i - \bar{x})^2} \tag{5}$$

$$S_y = \sqrt{\frac{1}{N-1} \sum_{1}^{N} (y_i - \bar{y})^2} \tag{6}$$

The cross correlation co-efficient for the entire data set is estimated along with the corresponding time delays. Then a plot of cross correlation co-efficient versus time delay is plotted. The time delay with the maximum cross correlation co-efficient is then picked for estimating solids velocity (Wang, 2006; Liu et al., 2003 and Bi et al., 2009). After obtaining the time delay, effective distance (distance between light emitting and receiving light fiber) is divided by the time delay to get the solids velocity.

3.3 THE NEWLY DEVELOPED SOPHISTICATED GAS-SOLID OPTICAL PROBES

The different probes for measurement of solids volume fraction and solids velocity has been the norm for years. Concentration probes have large measurement volumes which makes it difficult for the probes to identify the individual particles for velocity measurement. In a typical situation, the concentration probe measures the amount of particles in the measuring volume. Due to the design of the concentration probes, two separate signals are impossible to achieve to cross correlate them in order to obtain velocity information. The electronics of concentration probes are all single channel signal processor making it difficult to use them as velocity probes. Velocity probes are designed in such a way that there is a fixed distance between the single light emitting fiber and two receiving light fibers, unlike concentration probes which are arranged in a tight fashion to increase the measuring volume. The electronics of the velocity probes consist of two signal processing channels. Due to all the above-mentioned reasons concentration probes could not be used to measure both solids volume fraction and solids velocity and vice versa.

Fortunately, the newly developed advanced optical probe that has been developed and manufactured by Institute of Process Engineering of the Chinese Academy of Sciences addressed this drawback. The developed optical probe is capable of measuring simultaneously solids concentration, solids velocity and their time series fluctuations. The design of the probe and the electronics were improved which have been discussed in detail below.

The first improvement was the addition of several layers of light emitting and receiving fibers in alternate fashion with small optical fibers of 15 μm in diameter. The probes were comparatively smaller in diameter to the probes available till date, making them less intrusive to the flow dynamics of the system. The entire probe is 5 mm in diameter, making it the smallest probe till now.

The new probe developed consists of two separate bundles of optical fibers. Each bundle consists of small optical fibers arranged in alternate fashion. The advanced probe had two small tips protruding from the face of the probe (which was lacking in the previous available probes). These tips are 1mm in diameter and at a distance of 1mm from each other. The schematic of the probe is shown in Figure 3.13. The two separate optical bundles have separate channels for signal processing. The design has defined measuring volume allowing for the measurement of solids concentration. The two probe tips provide two separate signals, which can be analyzed by cross correlation to obtain velocity measurements (Figure 3.14).
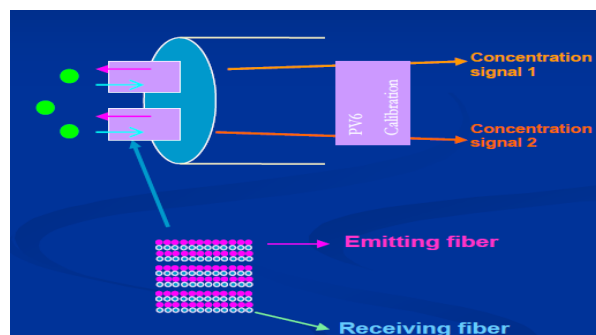
Figure 3.13. Design of advanced optical probe system

Since we have two tips separated by a very small distance, recording the time series signals, either of the signals can be analyzed to obtain solids volume fraction and

both the signals can be used to estimate velocity measurements. Both the tips of the probe are fitted with quartz window to remove the effects of blind regions.
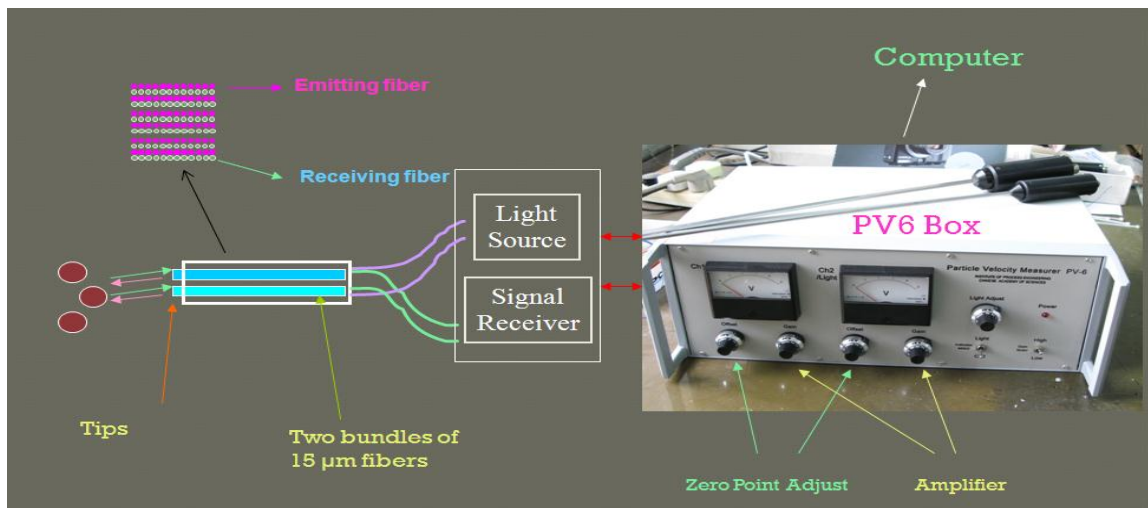
Figure 3.14. Electronics of the newly developed advanced optical probe showing two separate bundles of optical fibers for velocity and volume fraction measurements (Institute of Process Engineering of the Chinese Academy of Sciences)

As a result of new design changes to the optical probes system, the following advantages (Bi et al., 2011) can be noted as listed below

1. High sensitivity, fast response and high precision (due to removal of blind regions)

2. Least intrusive due to small tips and small diameter probe

3. Simultaneous measurement of solids velocity, solids concentration and its time series fluctuations

4. Light in weight and freedom from disturbance of electric and magnetic fields

The selection of probes (particle to probe ratio) is based on the size of particles to be studied for the experiment. At our laboratory, four optical probes have been acquired depending on the size of particles to be used. First probe which is 3 mm in diameter covers particle size range of 20 – 400 μm, the second probe which is 4 mm in diameter covers particle size range of 400 – 900 μm, third probe which is 5 mm in diameter covers particle size range of 1 mm – 3 mm and the fourth probe which is 7 mm in diameter covers particle size range of 3 mm – 4 mm. The particles used for experimentation should have good reflective properties, and should not be black or corrosive.

3.4 NEWLY DEVELOPED SIMPLE AND RELIABLE CALIBRATION METHOD FOR OPTICAL PROBES IN GENERAL AND FOR THE NEWLY DEVELOPED OPTICAL PROBE IN PARTICULAR

3.4.1. New Calibration Method for Solids Holdup (Solids Volume Fraction). As explained earlier, the voltage signals measured by probes contain information about solids concentration. This needs to be converted into solids volume fraction and hence calibration is needed. This section explains a new calibration method to estimate solids volume fraction using a simple, reliable and cost effective method.

The idea behind the proposed methodology is based on the principle of operation of optical probe. The optical probe works on back reflection of light and when there is movement of solid particles in front of the probe, the emitted light is reflected back and a signal corresponding to the intensity of the solids movement is produced. The peaks in the signal obtained correspond to the solids particle reflecting the light and the minima are by the void/air (which represents the empty bed). Hence, solids holdup can be said as the amount of time spent by the solids in the sampling time over the entire sampling time.

The time spent by the solids is evaluated for each signal by counting the number of peaks and the time span of each peak and vice versa for gas (void).

$$\varepsilon_s (Solids\_Holdup) = \frac{Time\_spent\_by\_Solids}{Overall\_Sampling\_Time} \qquad (7)$$

A programmable motor (KD Scientific, KDS410) which is capable of producing different flow rates, was used in order to obtain a solids holdup range from $0 - 0.6$. This range is chosen because the end application of such probes is in spouted beds. Spouted beds have a solids volume fraction range of 0 (at the center) $- 0.56$ (the annulus where downward moving bed exists). Hence, the current calibration covers the range of volume fraction that would be encountered in the actual experimentation. In our laboratory, all the four probes acquired have been calibrated using this procedure depending on the size of particles to be used. Since this work deals with particle size of 1 mm $-$ 3 mm range, the current section will discuss the detailed calibration procedure of 5 mm diameter probe and particle size of 2 mm in diameter. Glass beads of density 2450 Kg/m^3 was used for the evaluation. The experimental set-up including the motor and optical probe is shown in Figure 3.15.

The solid particles were passed under different flow rates into a funnel to cover the solids holdup range. The tube length of the funnel was 3 mm in diameter, which ensured that only one particle passed through at a time, thus forming a string of particles as they fall. The optical probe was placed at the end of the glass funnel tube to record the signals. The tip of the probe was placed vertically so that the particles pass both the tips. The raw signals obtained from the experiment are shown in Figure 3.16. The particles then fall down into a graduated cylinder. The entire setup is covered with a black cloth to stop any external interference of light.

Figure 3.15. Setup of programmable motor (KD Scientific, KDS410) to determine the voltage reading of optical probes at different flow rates

Experiments were conducted for 30 different flow rates and the number of data points for each flow rate was 5000 points. The entire time series signal was divided into 5 parts and analyzed separately. Each part consisted of 1000 data points for solids holdup calculation. This was performed to check the accuracy of the method and to ensure that same volume fraction would be obtained if different segments of the signals were to be analyzed. The entire sampling time for each flow rate was approximately 35 minutes. The signals recorded from both the tips were used in determining the solids holdup. The average voltage to be used is obtained by first normalizing the voltage signals obtained from measurement. The normalization of the voltage is done using the equation 8.

$$V_{avg} = \frac{V_i - V_{\min}}{V_{\max} - V_{\min}} \qquad (8)$$

The obtained voltage is then related to solids holdup. The time spent by the peaks in the signal were evaluated first and then all the times were added together to get the total time spent by the solids (peaks in the signal). Since the overall sampling time is already known (predetermined by the user), the solids volume fraction was estimated by dividing the time spent by solids to the overall sampling time. Once the solids volume fraction was estimated, the corresponding voltage signals were recorded. Thus a calibration equation relating the solids volume fraction to the voltage generated by the probe was estimated (Figure 3.17).

(a)   (b)
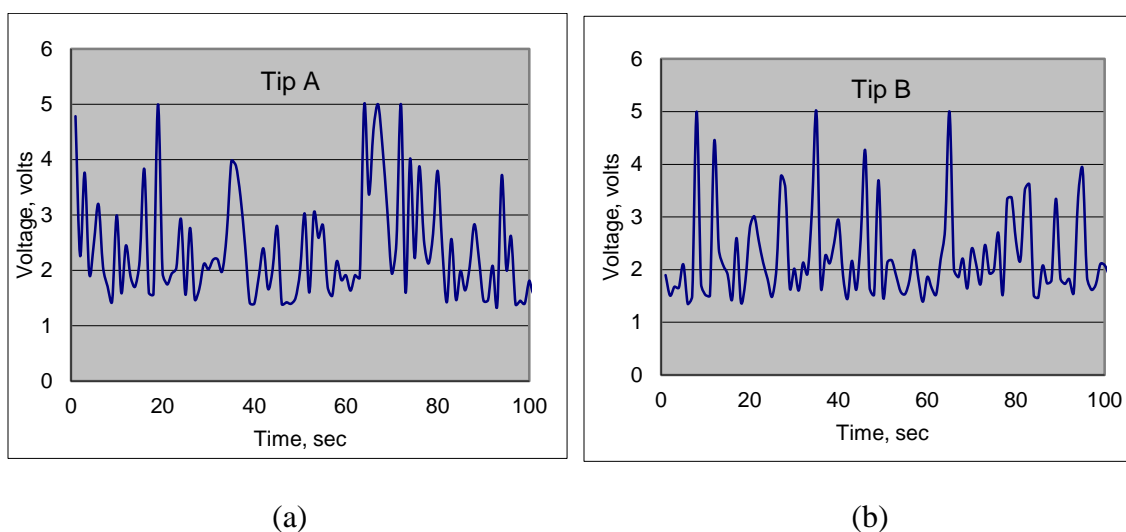
Figure 3.16. Raw signals obtained from optical probe; a. Tip A and b. Tip B.

The solids holdup was calculated for each tip of the optical probe at different flow rates. The relation obtained for tip A was y = 0.1519*x and for tip B was y = 0.1305*x. Where, y represents the solids volume fraction and x represents the voltage generated by the optical fiber probes. It would be very difficult to fabricate probes of such low diameter and high number optical fibers (5000), where both the probe tips would give

exact same values. However, the values from the two tips were found to be really close (absolute relative difference = 2.1%) and the slight deviation can be attributed to the fabrication process of the optical probes.
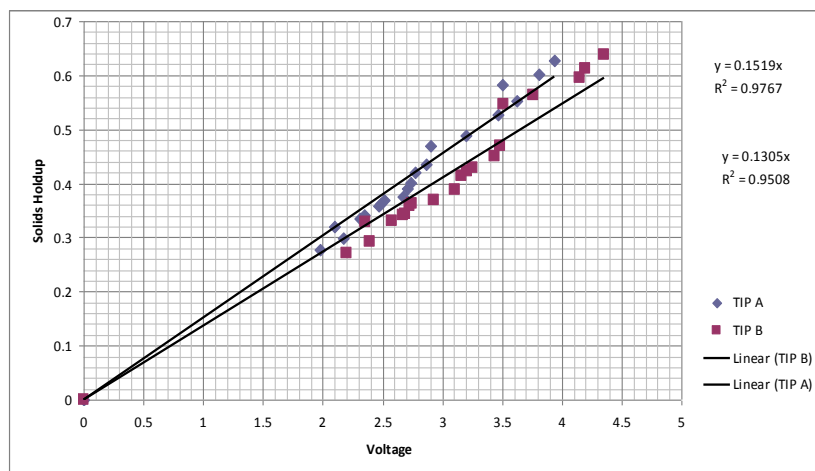
Figure 3.17. Calibration equation generated using optical probe based on new methodology

Once the calibration equation is obtained, the dynamic experiments can performed in spouted bed to implement this new optical probe. Same particles which were used for calibration were used to do experiments on spouted bed as well. In the actual experiments voltage fluctuations are recorded using the newly developed advanced optical probes. Then with the help of calibration, the solids holdup (volume fraction) is obtained for the corresponding voltage signals.

3.4.2. Calibration and Validation for Solids Velocity. Solids velocity using the newly developed advanced optical probe system is evaluated using cross-correlation

technique. The electronics involved and the analysis has been explained earlier. The main objective behind calibrating the probe for velocity measurements is to find the effective distance (distance between light emitting fibers and receiving light fiber) of the probe. In our case, the effective distance was provided to us by Institute of Process Engineering of the Chinese Academy of Sciences (who developed the advanced probe system). In order to make sure that the velocity measurements using these probes would be accurate, the velocity measurements were validated against a high speed camera. The details of this procedure are explained below.

The velocity measurements need to be validated to ensure the precision of the optical probe measurements. High speed camera was used to validate the results of the optical probe. The objective behind the present work was to record the velocity of solid particles at different flow rates using high speed camera and then compare it with the measurements of the optical probe. The experimental set-up (Figure 3.19) includes a programmable digital pump which can deliver solids at various flowrates. The solids were made to fall as a string of particles into a funnel, which would then discharge the solids into a graduated cylinder. The optical probe was placed at the end of the funnel to record the velocity of the solid particles. The set-up was covered by a black cloth to avoid any external interference of light (optical probes are sensitive to the external interference of light) and when the camera was used the cloth was removed. When the solids cross the probe tip, a signal is generated and another signal is generated when the same solids cross the second tip of the optical probe (Figure 3.18). Hence, two signals are generated with a certain phase shift in time. The delay in time by the passage of the solid particles from

one tip to another is calculated by cross-correlation analysis of two signals (equation 3.1). The effective distance is then divided by time delay to obtain solids velocity.
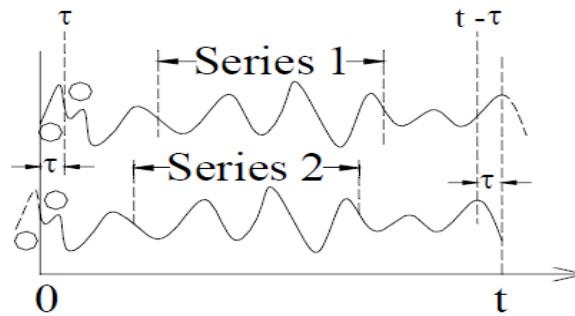
Figure 3.18. Signals generated by optical probes when solids cross two tips

The optical probe was then replaced with a high-speed camera (Figure 3.20). High speed camera used was FASTCAM Super 10KC. The camera was focused on a certain length of the funnel tube whose length was known. The two end points were marked on the tube for convenience (transparent tube through which camera could pick up the particles). The time taken for the solid particles to travel the known length on the funnel tube was calculated by the help of the high speed camera software at different flowrates. The velocity was then calculated by dividing the distance travelled by the solid particles with the time taken by them to travel. The results obtained by both the techniques at the same pump flowrates are compared in Figure 3.21. It is obvious the closeness of the velocity values by both the techniques, with a relative difference of 1.8% between the two methods. Hence, the optical probes can be relied on for proper measurement of solids velocities in real experimental conditions.
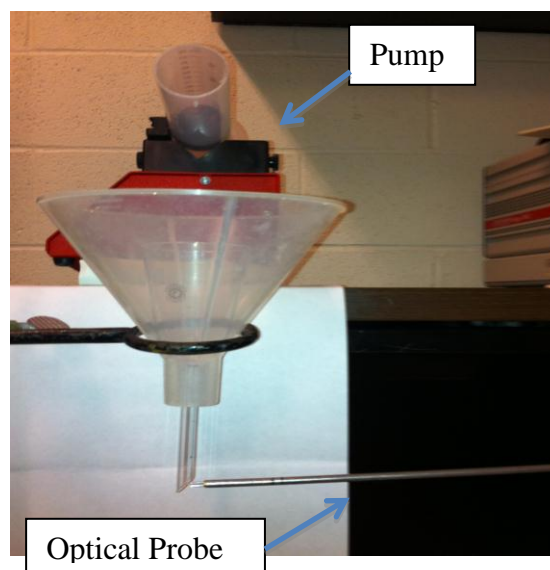
Figure 3.19. Experimental set-up with optical probes
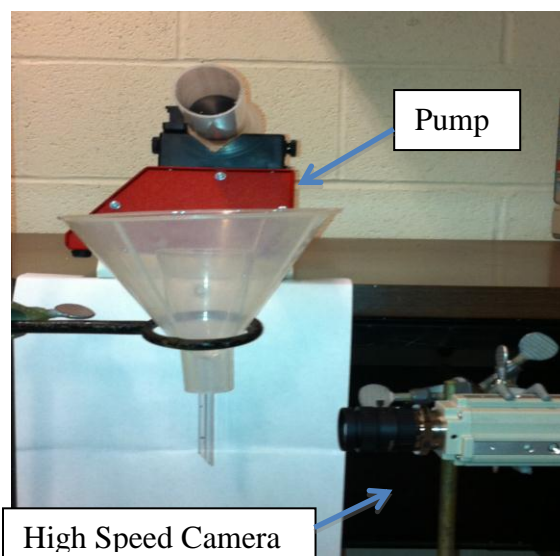
Figure 3.20. Experimental set-up with high speed camera
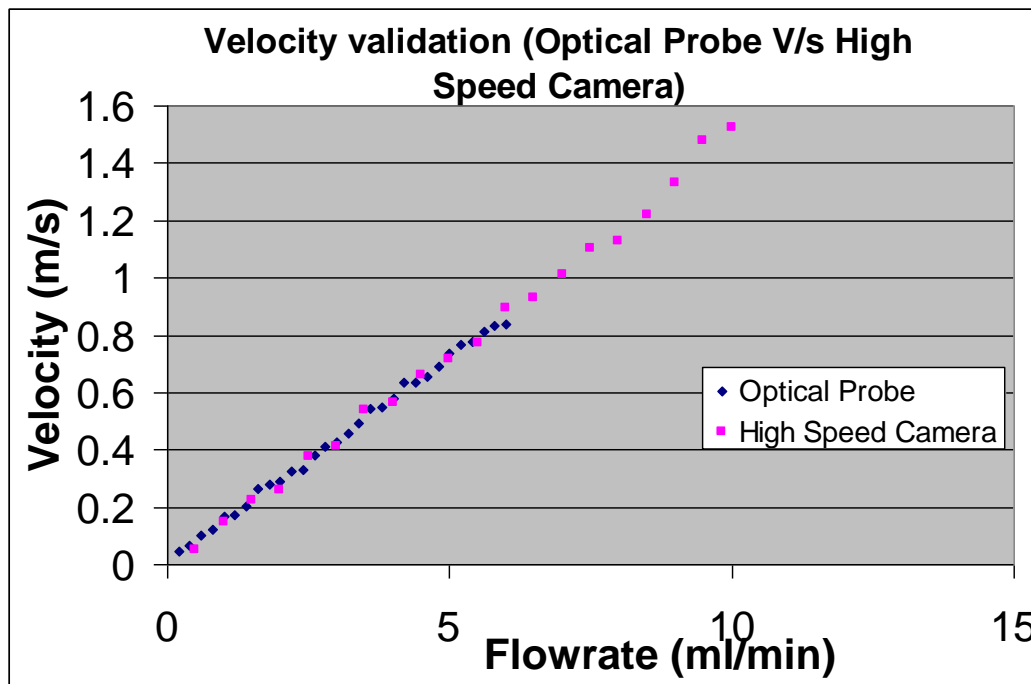
Figure 3.21. Comparison of solids velocity for optical probe and high speed camera at different flowrates

3.5 COMPARISON OF THE NEWLY DEVELOPED OPTICAL PROBE MEASUREMENTS FOR SOLIDS HOLDUP WITH GAMMA RAY COMPUTED TOMOGRAPHY (CT)

The calibrated optical probe needs to be tested and proved in real time experimental conditions. To test the accuracy of the new calibration method, optical fiber probes were used to estimate solids volume fraction in spouted bed at a specific condition. These results were then compared with the results obtained on the same spouted bed using non-invasive radioisotope based technique called as gamma ray computed tomography (CT) using single source.

The CT unit (Figure 3.22) is part of the dual source computed tomography which has been developed and implemented in our laboratory to measure the time averaged

cross-sectional phase holdup distribution (Varma et al., 2007 and Varma PhD thesis, 2007) of the phases in two or three phase systems. It has been designed to use a sealed point gamma ray source 137Cs (300 mCi) and Co-60. The sources are placed in a source collimator device (SCD) which is made of lead and tungsten respectively. A fan beam arrangement of source-detectors is used for measuring the transmission data of the gamma ray photons across the multiphase experimental setup. The detectors count the gamma ray photons that survive and pass through the multiphase experimental setup. The image re-construction carried out later is based on this data (Varma PhD thesis, 2007 and Varma et al., 2007). Quarterly report 14th of DEFC07-07ID14822 reported the use of this technique with Cs~137 source to study the solids/gas distribution in 0.152 m spouted bed. Since CT has been validated using phantom, it was chosen to compare the probe results in a real time spouted bed. In the present study, same experimentation was performed on spouted bed using this newly developed optical probe. The conditions used for the present study has been listed in Table 3.1. The detailed explanation of CT measurements and data analysis can be found in Varma, PhD thesis (2007) and Varma et al., 2007.

Usage of such sophisticated radioisotope technique is very intense both experimentally and in data processing. In addition, careful arrangement and preparation need to be made to ensure the desired accuracy; hence only one level of scan was used to validate the optical probe measurements in spouted bed.
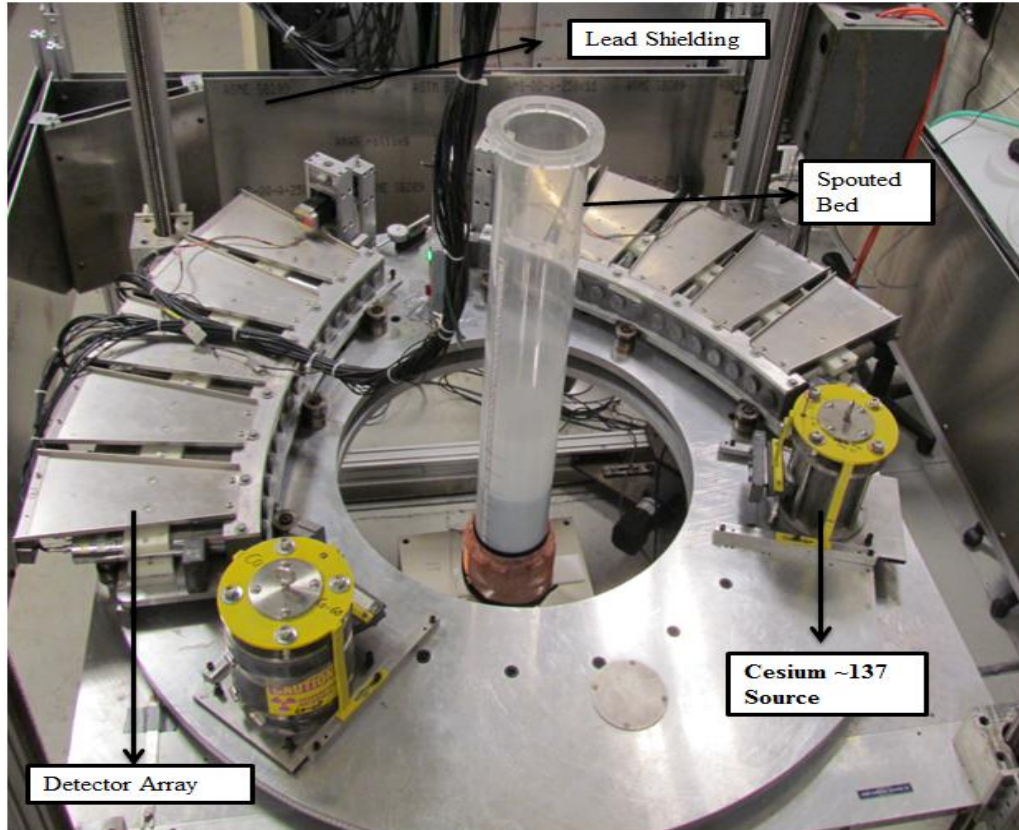
Figure 3.22. CT set-up (Varma et al., 2007) installed around the spouted bed reactor
(work done at Missouri S&T - Quarterly report 14th of DEFC07-07ID14822)

Table 3.1. Conditions used for experimentation on Spouted bed using optical probes and
CT set-up.

Case	0.152 m ID
D_c (m)	0.152
D_i (m)	0.019
L (m)	1.14
H (m)	0.323
T (K)	298
P (kPa)	101
d_p (m)	0.00218
ρ_p (kg/m^3)	2400
ρ_f (kg/m^3)	1.21
μ (10^{-5}) (Pa.s)	1.81
U (m/s)	1.08

Table 3.1. Conditions used for experimentation on Spouted bed using optical probes and CT set-up cont.

Case	0.152 m ID
H/D_c	2.1
D_c/D_i	8
D_c/d_p	69.9
ρ_p/ρ_f	1994
ε_o	0.41
ϕ_s	1
$\rho_f d_p U/\mu$	157
U^2/gd_p	54.5
$\rho_p d_p U/\mu$	3.13
U^2/gD_c	0.78

The obtained radial profiles of solids holdup was compared with the optical probe experiment. Both the tips from optical probe had very close values (absolute relative difference = 3.4%) to the CT experimental results (Figure 3.23). CT results were used to modify the calibration equation for optical probes using correction factor to bring the points of optical probe to that of the CT. The final calibration equation after comparing it with CT experimentation (Figure 3.24) is given below.

$$\text{Tip A: } y = 0.1519*x - 0.02514 \tag{9}$$

$$\text{Tip B: } y = 0.1305*x - 0.00374 \tag{10}$$
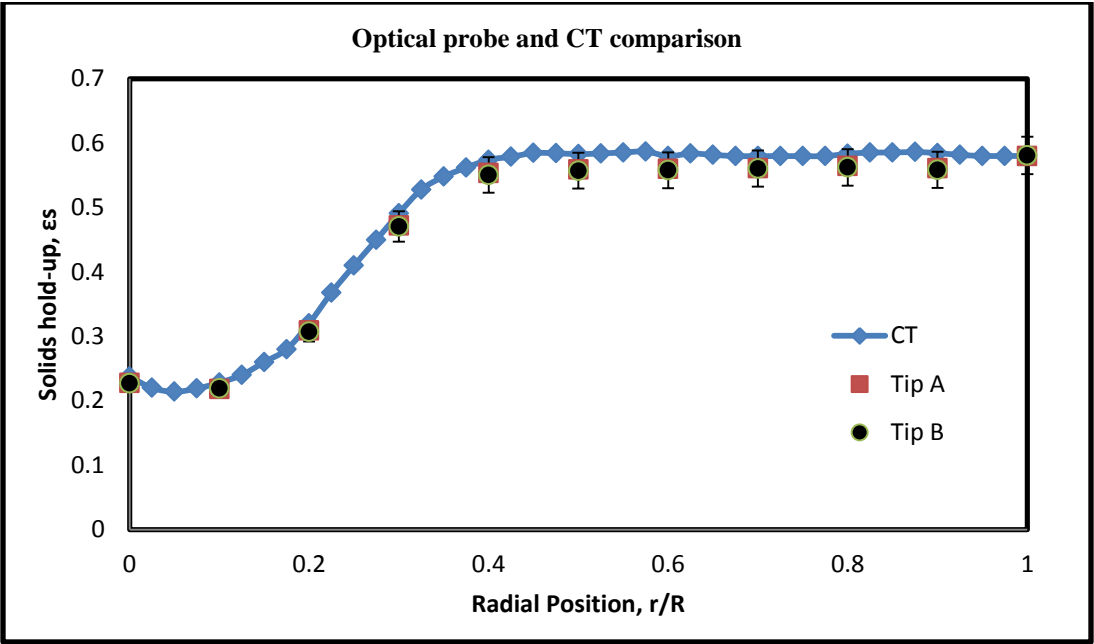
Figure 3.23. Graph comparing solids holdup from CT experimentation and optical probe
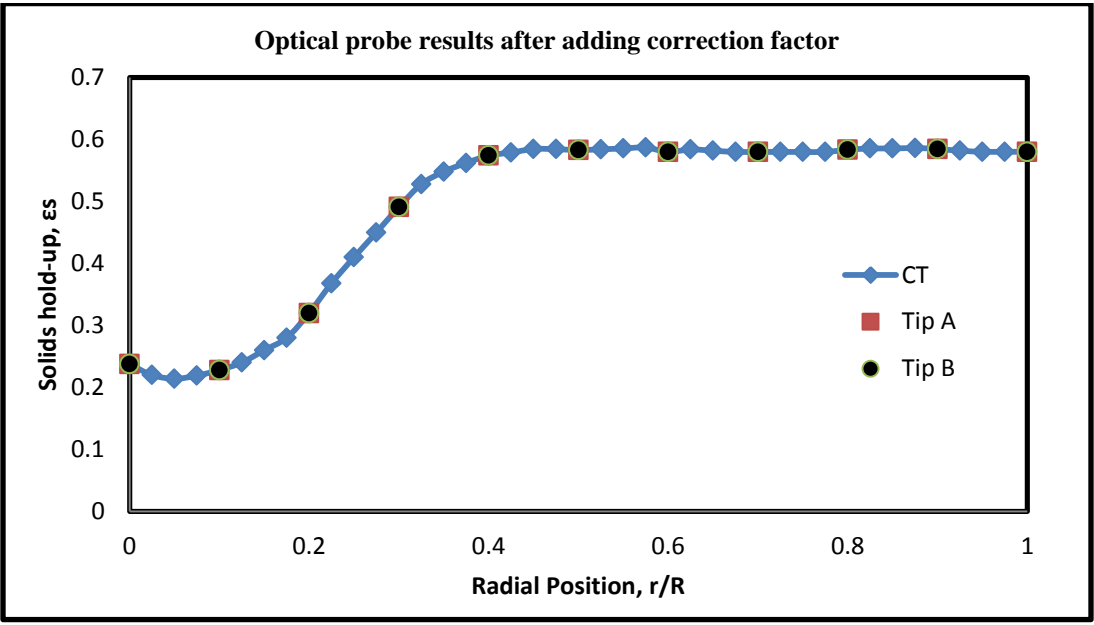
Figure 3.24. Graph comparing solids holdup from CT experimentation and optical probe after adding the correction factor

3.6 REMARKS

Optical fiber probes have been used over several decades to measure solids holdup (volume fraction) and solids velocity in multiphase systems. Optical probes can be divided into solids concentration and solids velocity probes depending parameter to be measured. The section provides a brief overview of the concentration probes and velocity probes developed over the years. The newly developed sophisticated gas-solid optical probes acquired from Institute of Process Engineering of the Chinese Academy of Sciences, which can measure simultaneously solids concentration, solids velocity and its time series fluctuations. The solids velocity measurement from the newly developed optical probe is based on cross-correlation analysis method. The velocity optical probes were validated using a high-speed camera. The results from the two techniques were in very good agreement, thus indicating the applicability of optical probes in real-time experimentation. The measured solids concentration needs to be converted to solids holdup (volume fraction) through calibration. Many methods have been reported in the literature for optical probe calibration, but includes high experimental cost and questionable accuracy. Hence, a new calibration methodology for optical probe was proposed in this work, which is simple, reliable and effective. The developed method was able to successfully predict solids volume fraction. The obtained calibration was implemented on 0.152 m ID spouted bed to evaluate solids holdup. To validate the proposed method, the experimental results obtained using the newly developed optical probe were compared with gamma ray computed tomography (CT) using single source. The solids holdup evaluated from the optical probe was in good agreement with the computed tomography results implemented on the same spouted bed. A correction factor

was added to the calibration equation in order to comply with the CT results, as CT is a non-invasive technique. The new calibration proposed method for the newly developed optical probe, can therefore be used to evaluate solids volume fraction and solids velocity in real time experimentation.

4. ASSESSING THE CURRENT SCALE-UP METHODOLOGY BASED ON MATCHING DIMENSIONLESS GROUPS AND DEVELOPING A NEW MECHANISTIC SCALE-UP METHODOLOGY FOR SPOUTED BEDS

4.1 INTRODUCTION

Due to their efficiency in contacting gases and coarser particles, spouted beds have been successfully applied to a wide variety of processes, such as coating, granulation, drying, coal gasification, catalytic reactions, etc. Under proper conditions, the jet penetrates the bed of particles, creating a central spout zone, a fountain above the spout, and an annulus surrounding the spout. Particles entrained in the gas spout form a fountain of particles above the bed surface that disengage from the gases and fall back to the bed surface, thus inducing bed circulation. Spouted beds have been used for manufacture of TRISO nuclear fuel particles for 4th generation nuclear reactors. In modern High Temperature Gas Reactors, the acceptable level of defective/failed coated particles is essentially zero. This level requires processes that produce coated spherical particles with even coatings having extremely low defect fractions. The quality of the coating applied to fuel kernels is impacted by the hydrodynamics, flow field, and flow regime characteristics of the spouted bed.

The reported studies in literature related to spouted beds used various techniques (such as visualization, light based techniques, pressure measurement at the wall, and various probes) to measure and investigate either global fluid dynamic parameters (e.g., overall solid and gas holdup, fountain height, spouted bed diameter, etc.) or used an invasive probe (e.g., an optical or capacitance probe) for local point measurement. Roy et al. (1994), Djeridane et al. (1998), and Cassanello et al. (1999) used an advanced non-invasive radioactive particle tracking technique with a limited number of detectors (only

8 detectors) to measure the flow field and some turbulent parameters (e.g., shear stress) at limited conditions (for example, Djeridane et al. (1998) used 3 mm diameter glass beads as particles and air as the gas phase in a Plexiglas spouted bed of 15.2 cm diameter). They concluded that more experimental investigation is needed to quantify specific influences of key parameters on the flow field, flow regime characteristics, and local hydrodynamics of spouted beds. These recommendations have been also confirmed by the most recent reported studies such as, for example, Link (2006), Abdul Salam and Bhattacharya (2006 a, b), Pina et al. (2006), and Zhong et al. (2006). Despite the fact that the influences of key parameters such as bed height, spouting velocity, and the size and density of particles on global behavior are quantitatively documented, there is still considerable uncertainty with respect to suitable scale-up methodologies or similarity behavior, even though some of these studies utilized advanced measurement techniques (He, et al., 1997; Glicksman et al., 1993; Nicastro and Glicksman, 1984, Djeridane et al., 1998; Schweitzer et al., 2001; Hilal and Gunn, 2002; Mabrouk et al., 2005; and many others). Hence, the reported dimensionless groups for spouted bed scale-up and hydrodynamic similarity need to be further evaluated. Although fluidized beds and spouted beds share many common features, there are also significant differences between them. Specifically, the annulus of a spouted bed constitutes a moving packed bed with countercurrent interstitial flow of fluid, while the solids in fluidized beds appear to be in more random motion, fully supported by the gas dynamics. Hence, particle-particle contacts and interaction forces cannot be ignored. Accordingly, He et al. (1997) modified the scaling factors for fluidized beds (or relationships), outlined earlier in Section 2, proposed by Glicksman (1984) and Glicksman et al. (1993) to provide a set of scaling

parameters for the similarity behavior of spouted beds by adding the internal friction angle and the loose packed voidage. He et al. (1997), as mentioned earlier in Section 2, proposed the following controlling non-dimensional parameters for a spouted bed: $\dfrac{gd_p}{u^2}$,

$\dfrac{\rho_s d_p u}{\mu}$, $\dfrac{\rho_f}{\rho_s}$, $\dfrac{H}{d_p}$, $\dfrac{D_c}{d_p}$, sphericity of particles (ϕ_s), interfacial angle of particle (φ), loose packed voidage (ε_0), dimensionless particle size distribution and dimensionless bed geometry.

Using different spouted bed conditions that cover ambient and high temperature and pressure conditions and different particle types and sizes, He et al. (1997) demonstrated that close hydrodynamic similarity was maintained in the beds when these scaling parameters were closely matched. Thus, scale-up of spouted beds is based on maintaining hydrodynamic similarity which is to be ensured by matching dimensionless groups between two scales or conditions. It is noteworthy that the hydrodynamic similarity was demonstrated in these beds based on measurements of global parameters such as dimensionless spout diameters, dimensionless fountain height, and pressure along the bed height. The measurements were made using a video camera (which can see the region close to the wall), a ruler attached to the column or to the window, and pressure transducers. Another point to note was that all these experiments were performed in a semi-cylindrical column. Accordingly, the present work focuses on evaluating the reported dimensionless groups as scaling parameters via quantification of their sensibility by identifying conditions that give match in hydrodynamic similarity and mismatch in hydrodynamic similarity based on matching and mismatching of these dimensionless groups. Furthermore, this work addresses the limitations reported in the current

dimensionless groups approach by measuring local parameters using the developed optical probe and proposes a new mechanistic scale-up approach for hydrodynamic similarity.

4.2 EXPERIMENTAL SET-UP AND MEASUREMENT TECHNIQUES

4.2.1 Experimental Set-up of Spouted Beds. Two spouted beds were used in the present study of inside diameter 0.152 m and 0.076 m. The schematic of spouted bed with detailed dimensions of 0.152 m and 0.076 m spouted bed is shown in Figure 4.1. The spouted bed columns are constructed from plexiglass and consist of one-piece column attached to a conical base. Having a one piece column will improve the symmetry of the column and help stabilize the fountain. The 0.152 m column is 1.016 m tall, with a total of thirty five measurement ports of 0.0127 m diameter spaced every 0.0508 m on both front and back so that axial measurements can be made at separations of 0.0254 m. To further measure the symmetry of the annulus, axial measurement ports are located on all sides of the column (90 degree separation) every 0.152 m from the bottom 0.3048 m of the column. This gives the ability to measure the dynamics of the spout and annulus without crossing and disrupting the spout with the probe. The column sits at the top of a plexiglass base, with two measurement ports in order to measure the dynamics and concentration of the spout near the air inlet. The cone is angled at 60 degrees and the gas inlet orifice for the gas jet is 0.019 m in diameter. A sliding distributor system is used, that will allow the use of multiple distributor designs for the gas jet to be created and also allow the assessment of the effects of different sizes of gas inlet jet on the spout and fountain. The 0.076 m diameter spouted bed very closely resembles the 0.152 m spouted

bed, only its overall height is 0.9144 m. The 0.076 m spouted bed also has axial measurement ports every 0.0508 m on both sides in order to take axial measurements at 0.0254 m increments along the whole column. Measurements to deduce symmetry is possible due to the inclusion of ports on all four sides of the column at 0.0762 m increments from the bottom 0.3048 m. The cone for the 0.076 m diameter spouted bed is also angled at 60 degrees and is fitted with a sliding distributor design like that of the 0.152 m diameter spouted bed.

Three criterion/conditions are essential to achieve stable spouting in spouted beds, listed in equations 1 - 3. The first criterion (equation 1) was proposed by Chandnani and Epstein (1986) based on the experimental data of small columns and fine particles, and was later extended to 0.91 m diameter column by Lim and Grace (1987). The second criterion (equation 2) was proposed by Mathur and Epstein (1974) based on the experimental evaluation of small columns. The third criterion (equation 3) was proposed by He et al. (1990).

$$D_i/d_p < 25\sim30 \tag{1}$$

$$D_c/D_i > 3\sim12 \tag{2}$$

$$H < H_m \tag{3}$$

Where, D_i is the gas inlet diameter, d_p is the particle diameter, D_c is the diameter of the column, H is the static bed height and H_m is the maximum spoutable bed height. The dimensions of the spouted bed used in the current study satisfy the three conditions necessary for stable spouting to be achieved. Both spouted beds were fitted with ports at different axial heights in order to aid in measurement. Compressed air was used as the gas phase, which was supplied by industrial scale high capacity air compressor. Various

solids type and sizes were used to assess the dimensionless group approach for scale-up in the current study which has been listed in Table 4.1.

(a)   (b)
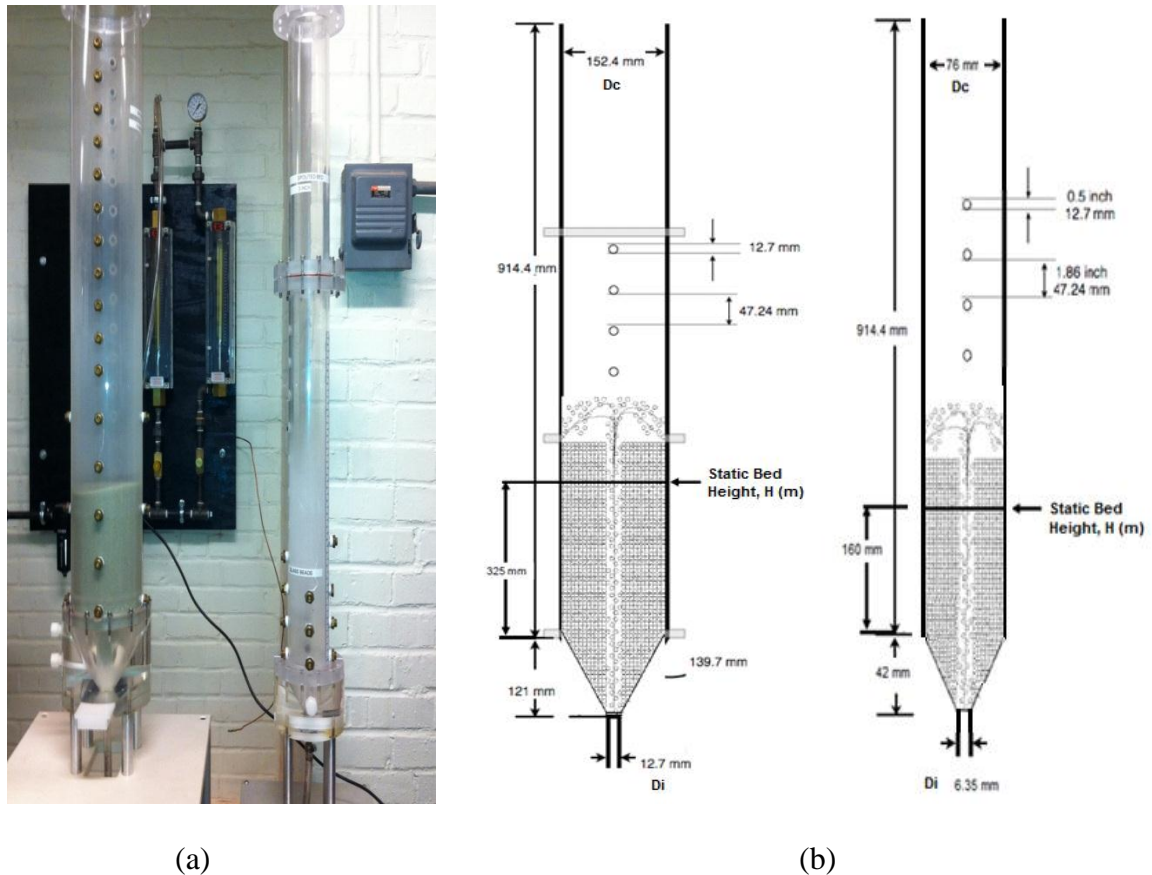
Figure 4.1. Schematic of spouted bed (a) 0.152 m and 0.076 m spouted bed used in the present work; (b) Detailed dimensions of 0.152 m and 0.076 m spouted bed.

The measurements for the current study were made using gas-solid optical probes (to measure solids holdup, solids velocity, their time series fluctuations and spout diameter) and pressure transducers (to measure overall pressure drop across the bed and pressure fluctuations at different axial planes). The local parameters measured were

solids holdup and solids velocity. The global parameters measured were overall pressure drop, spout diameter, fountain height and maximum spoutable bed height. Five experimental runs were performed for each parameter measured and the reproducibility of the results was in the error range of 3.2% - 4.1%.

4.2.2 Gas-Solids Optical Fiber Probes. Fiber optic probes have been used for measurements of local hydrodynamic parameters such as solids holdup, solids velocity and their time series fluctuations. Spout diameter was also evaluated using optical probes. As discussed in Section 3, advanced optical probes (Figure 4.2), which was acquired from Institute of Process Engineering of the Chinese Academy of Sciences, works on the principle of back reflection of light was used in the present study. The probes are capable of measuring solids holdup, solids velocity and their fluctuations all at the same time. The details of optical probe measurement and analysis can be found in Section 3.

(a)   (b)

Figure 4.2. Gas-solid optical probe (a) Fiber optic probe (PV6) used in the present work; (b) PV6 being used in 0.076 m ID spouted bed.

4.2.3 Pressure Transducers. Pressure transducer has been used to measure pressure and its time series at the wall region. Pressure is an expression of the force required to stop a fluid from expanding, and is usually stated in terms of force per unit area. Pressure transducer generates an electrical signal as a function of the pressure imposed. The pressure transducer used for the present study measures gauge pressure and is of the Model. No. PX309-002G5V purchased from Omega Dyne Inc. The pressure transducer used is a single ended pressure measurement device, which measures gauge pressure. The data acquisition for the pressure transducer consists of an A/D converter, which converts the pressure fluctuations into electrical signals.

Figure 4.3. Pressure transducer applied for measurement on 0.152 m ID spouted bed

The time series signals of pressure fluctuations obtained from the transducer are then analyzed to obtain important information about the hydrodynamics of the spouted bed under study. These help in understanding the flow pattern and flow dynamics of gas-

solid systems in particular and multiphase systems in general. The expansion of the gas and movement of solid particles in the bed cause pressure fluctuations. As a result these signals provide valuable information required for assessing the scale-up methods. Pressure fluctuations were analyzed for certain chosen cases proposed by He et al. (1997) and also for the proposed new mechanistic scale-up approach (discussed later in this Section).

4.3.   ASSESSMENT   OF   DIMENSIONLESS   GROUPS   (SCALING RELATIONSHIP) FOR SPOUTED BED SCALE-UP (He et al., 1997)

He et al. (1997) designed certain conditions of matching dimensionless groups and mismatching dimensionless groups experiments to verify their scaling parameters for spouted beds outlined in Table 4.1. Case A was the reference case and the rest of the cases were matched dimensionally or mismatched dimensionally with reference to Case A. Among these cases, Case B had the same value of dimensionless groups (matching dimensionless groups) with reference to Case A, which was designed to study the validity of the scaling relationships. Cases C to G had different values of dimensionless groups (mismatched dimensionless groups) with reference to Case A in order to study the influence of each dimensionless group on similarity. Here, the word match refers to maintaining the same value of dimensionless groups in the prototype spouted bed (Case A) and the model spouted bed (Case B). The word mismatch refers to the variation of the values of one or more dimensionless groups from cases C to G compared to the prototype case A. In this work, local and global hydrodynamic parameters were studied for the cases A, B, C and D mentioned in Table 4.1. Cases A and B were studied due to the matching dimensionless groups, as it evaluated the validity of the scaling relationships.

Cases C and D were selected due to the mismatch in dimensionless groups and also to study the influence of each of these groups on the scaling relationship. Cases E, F and G, were not selected under the present study as it was reported to have vast differences in the global parameters by He et al. (1997) and hence was selected not to be repeated again for studying local parameters. However, *Case E and Cases A, B, C, D have been evaluated using Computational fluid dynamics (CFD)*, which has been reported in detail in Section 7. *Cases A, B, C and D have been assessed experimentally.*

Table 4.1. Conditions for matching dimensionless groups and mismatching dimensionless groups identified by He et al. (1997)

Condition	A	B	C	D	E	F	G
D_c (m)	0.152	0.076	0.076	0.076	0.076	0.076	0.152
D_i (mm)	19.1	9.5	9.5	9.5	9.5	9.5	19.1
L (m)	1.14	1.14	1.14	1.14	1.14	1.14	1.14
H (m)	0.323	**0.16**	**0.16**	**0.16**	**0.16**	**0.16**	0.323
T (K)	298	298	298	298	298	298	298
P (kPa)	101	312	101	101	312	101	101
Particles	Glass	**Steel**	Glass	Glass	Glass	Glass	Sand
d_p (mm)	2.18	**1.09**	**1.09**	**1.09**	2.18	2.18	2.18
ρ_s (kg/m^3)	2450	**7400**	2450	2450	2450	2450	2490
ρ_f (kg/m^3)	1.21	**3.71**	1.21	1.21	**3.71**	1.21	1.21
μ (*10^5)(Pa s)	1.81	1.81	1.81	1.81	1.81	1.81	1.81
U (m/s)	1.08	0.75	0.74	2.15	1.06	1.12	1.11
ϕ_s	1	1	1	1	1	1	**0.88**
H/D_c	2.1	2.1	2.1	2.1	2.1	2.1	2.1
D_c/D_i	8	8	8	8	8	8	8
D_c/d_p	69.9	69.9	69.9	69.9	**35.0**	**35.0**	69.9
ρ_s/ρ_f	1994	1995	2029	2029	**648**	1994	**2068**
$\rho_f d_p U/\mu$	157	168	**54**	157	**474**	161	163
U^2/gd_p	54.5	52.6	51.2	**432**	52.5	57.6	58.7
$\rho_s d_p U/(\mu*10^{-3})$	313	334	**109**	317	307	324	333
U^2/gD_c	0.78	0.75	0.73	**6.18**	**1.50**	**1.65**	**1.84**

Optical probes were used to measure solids holdup, solids velocity and also to identify spout diameters. Due to the difference in the amount of solids in the annulus and spout region, the optical probes were able to differentiate these regions due to the nature of signals obtained. Hence, optical probes were helpful in identifying local spout diameters to a good accuracy. Pressure profiles using pressure transducers mounted at the wall, dimensionless fountain heights and maximum spoutable bed heights for the above mentioned cases were also measured. Fountain height was determined by attaching a ruler to the spouted bed column and noting the height at regular time intervals of the spouted bed experiments and taking the overall average. Dimensionless fountain height was obtained by dividing the fountain height by the column diameter. Maximum spoutable bed height refers to the initial static bed height beyond which spouting in the bed does not occur. This was measured by gradually loading solids until the spouting in the bed ceased. The initial static bed height which leads to this ceasing of spouting was noted as the maximum spoutable bed height. Time series of pressure signals were also analyzed for these cases to look into the nature of these signals and extract any meaningful information. The different measurement levels where the measurements were performed in the present work are shown in Figure 4.4. To assess the validity of scaling relationships using dimensionless groups, more focus has been given to the matching dimensionless groups conditions (Case A and B) in the present study. For convenience, only the first few figures are shown with error bars to show the reproducibility of the results. The rest of them are shown without error bars, since the reproducibility of the values are within acceptable range ($\leq$ 6-7%).
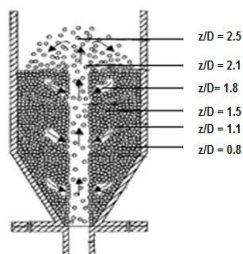
Figure 4.4 Schematic representation of different axial measurement levels measured in spouted bed.

4.3.1 Solids Holdup/ Solids Volume Fraction. Solids holdup is an important parameter in evaluating the hydrodynamics of spouted beds. The solids holdup varies from the center of the spouted bed (spout region) to the wall and along the axial height of the spouted bed. Gas enters the bottom of the spouted bed as a jet and penetrates the solids bed. As a result the amount of solids near the inlet of the spouted bed is low.
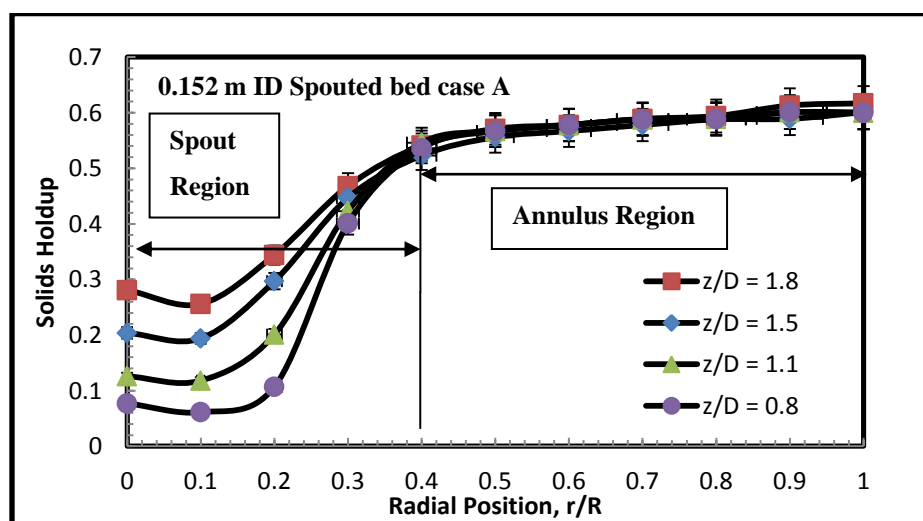
Figure 4.5. Radial profile of solids holdup in a 0.152 m spouted bed at different measuring planes (z/D) using conditions in Case A at Ug = 1.08 m/s listed in Table 4.1.

As the axial height increases in the spouted bed, the solids in the spout region increase. This is caused by the decrease in gas velocity at higher axial heights, due to the penetration of gas through the thick bed of solids. The maximum variation of solids holdup is in the spout region due to this effect. Figure 4.5 shows the radial profiles of the solids holdup in a 0.152 m ID spouted bed for conditions of Case A listed in Table 4.1. In the annulus, the particles move slowly downward as a loose packed bed. The maximum volume fraction of solids (ε_s = 0.6) is in the annulus region and this remains approximately the same throughout the height of the spouted bed. At the center, as the axial height increases from z/D 0.8 to 1.1 the percentage increase of solids is 30.76%, from z/D 1.1 to 1.5 is 35% and from z/D 1.5 to 1.8 is 35.48%. The deviation in the solids holdup decreases at different axial heights as the spout-annulus interface is reached. As the gas moves up the spouted bed and reaches the bed surface, a fountain region is formed. The solids then fall back onto the bed surface by gravity, thus feeding the annulus region with solids. This movement of solids creates a cyclic flow pattern of solid particles in the spouted beds. Figure 4.6 shows the solids holdup profile in the fountain region for conditions of Case A listed in Table 4.1. The movement of gas phase is also very important in the spouted bed. Since the hydrodynamics of the spouted bed is dictated by the gas phase dynamics, the measurement of gas holdup profiles was done for different cases. The maximum volume fraction of gas phase is in the spout region and the annulus region has the lowest volume fraction of gas phase. Due to the movement of solids and gas phase, the overall system becomes a composite of a centrally located gas phase (moving upward) surrounded by a dense-phase moving packed bed (moving downward). This systematic cycle movement of solids and gas leads to many industrial

applications. Figure 4.7 shows the radial profiles of gas holdup in 0.152 m ID spouted bed at different measurement levels. Figure 4.8 shows the radial profile of gas holdup in the fountain region.
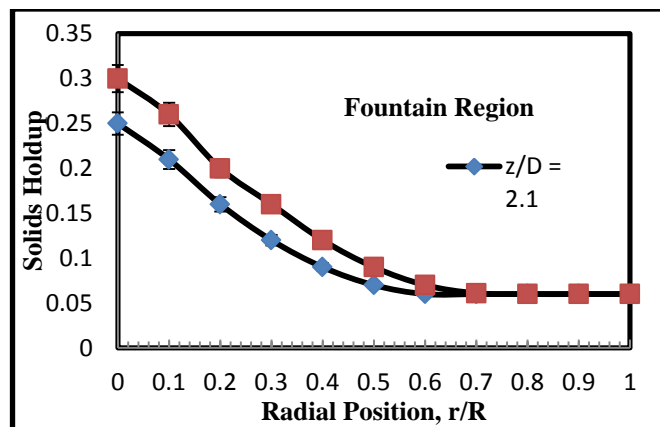
Figure 4.6. Radial profile of solids holdup in a 0.152 m spouted bed in the fountain region using conditions in Case A at Ug = 1.08 m/s listed in Table 4.1.
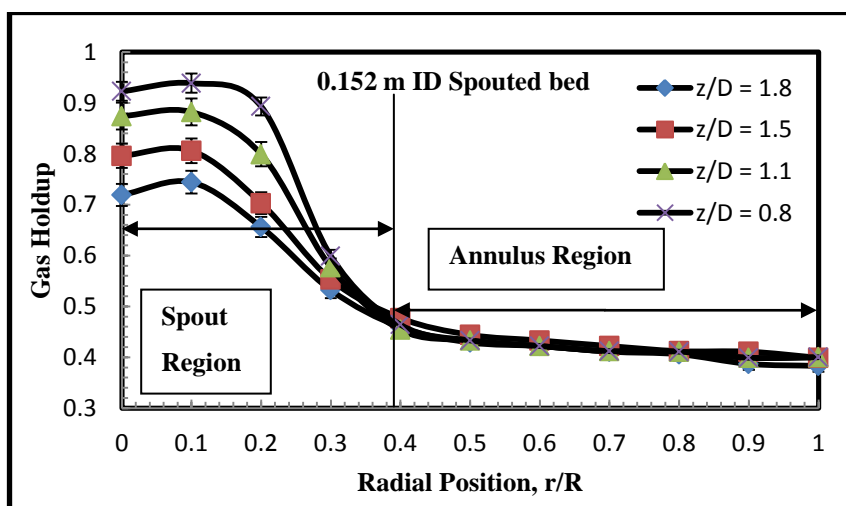
Figure 4.7. Radial profile of gas holdup in a 0.152 m spouted bed at different measuring planes (z/D) using conditions in Case A at Ug = 1.08 m/s listed in Table 4.1.
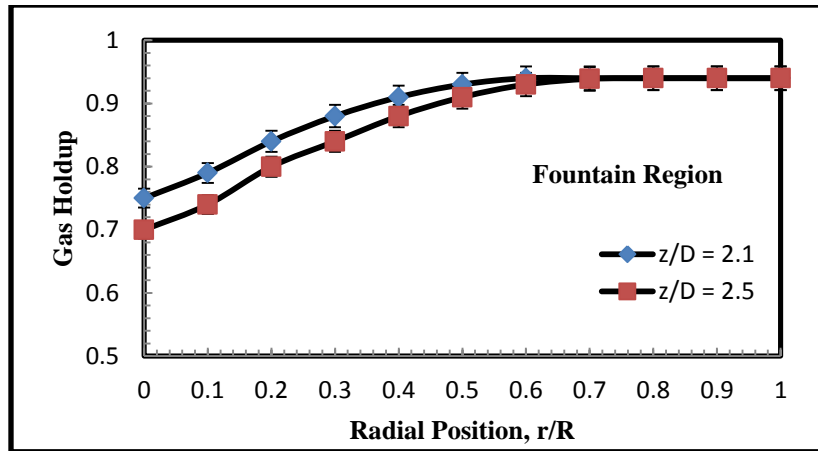
Figure 4.8. Radial profile of gas holdup in a 0.152 m spouted bed in the fountain region using conditions in Case A at Ug = 1.08 m/s listed in Table 4.1.

The validity of the current scaling relationships should be assessed, which is based on the dimensionless groups approach. The important case which is used to test this is Case A (reference model) and Case B (prototype model) listed in Table 4.1. The two cases are called conditions for matching dimensionless groups, since the values of the dimensionless groups are same in both the cases. The evaluation of solids holdup profiles and gas holdup profiles for these two cases should provide useful information regarding the validity of scaling relationships. The solids holdup and gas holdup profiles for Case A listed in Table 4.1 have been discussed earlier in this Section. The profiles for Case B have been shown in Figure 4.9, 4.10, 4.11 and 4.12. The solids holdup and gas holdup profile for Case B (0.076 m) shows the same trend seen in Case A (0.152 m) of spouted bed. The maximum variation in the radial profiles is observed in the spout region as expected (percentage variation from z/D 1.1 to 1.8 is 52.17%). The nature or profiles in the annulus region remains same which is equal to loose packed bed ($\varepsilon_s = 0.6$).
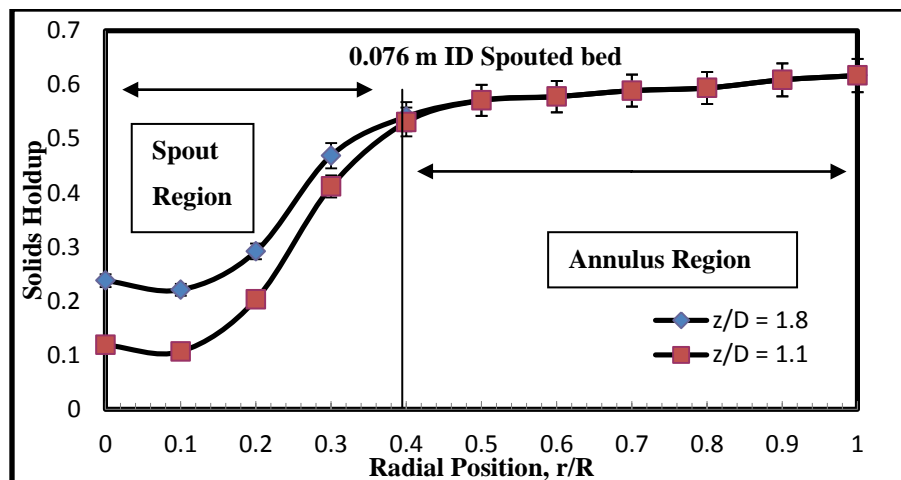
Figure 4.9. Radial profile of solids holdup in a 0.076 m spouted bed at different measuring planes (z/D) using conditions in Case B at Ug = 0.75 m/s listed in Table 4.1.
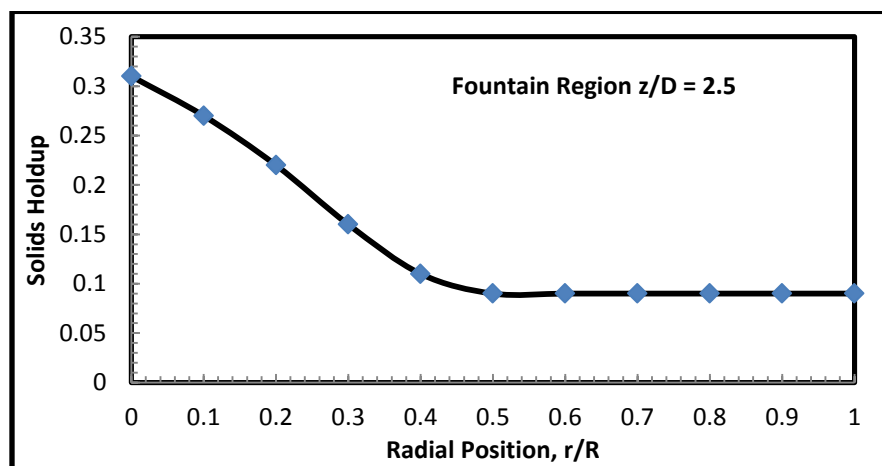
Figure 4.10. Radial profile of solids holdup in a 0.076 m spouted bed in the fountain region using conditions in Case B at Ug = 0.75 m/s listed in Table 4.1.

The gas holdup profiles for the 0.076 m ID spouted bed have been measured. As mentioned earlier, since gas phase dictates the hydrodynamics of spouted bed the measurement of gas holdup profiles is important. The percentage deviation in the center

of the column (spout region) from z/D 1.1 to 1.8 was found to be 15.90%. The value of gas holdup in the annulus was found to be constant at $\varepsilon_g = 0.4$.
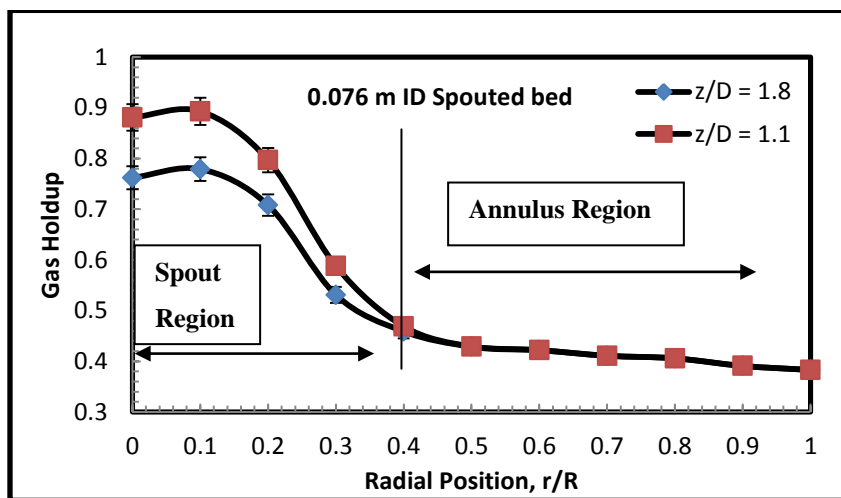
Figure 4.11. Radial profile of gas holdup in a 0.076 m spouted bed at different measuring planes (z/D) using conditions in Case B at Ug = 0.75 m/s listed in Table 4.1.
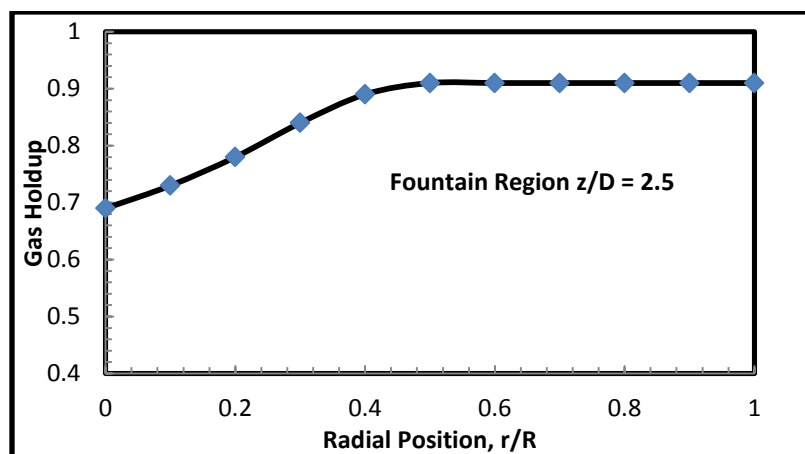
Figure 4.12. Radial profile of gas holdup in a 0.076 m spouted bed in the fountain region using conditions in Case B at Ug = 0.75 m/s listed in Table 4.1.

The two cases should now be compared to test the closeness of the holdup profiles of solids and gas. Comparison of such parameters gives an estimation of the closeness of hydrodynamics in the two different size spouted beds and also testifies for the dimensionless groups approach. The solids holdup profiles compared for both the matching dimensionless groups condition at different levels (z/D = 1.1, 1.8 and the fountain region) are shown in Figure 4.13, 4.14 and 4.15(a). Since the 0.076 m spouted bed has lesser static bed height, only three levels of axial measurements could be measured. The z/D levels of the 0.076 m and 0.152 m spouted bed for the basis of comparison were the same (z/D 1.1, 1.8 and the fountain region, 2.5).
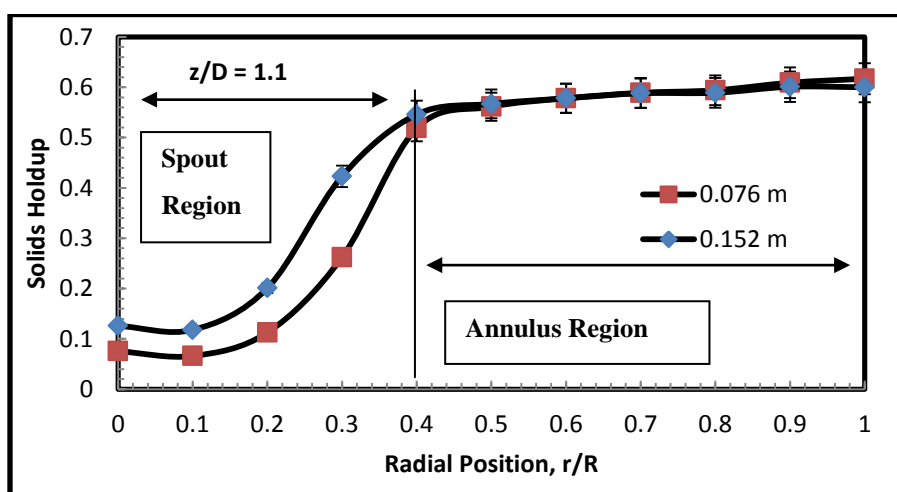
Figure 4.13. Comparison of radial profiles of solids holdup at z/D = 1.1 for Case A (0.152 m) and Case B (0.076 m) spouted bed.

It is observed that the solids holdup profiles in the two different size spouted beds differ in the spout region. The deviation in the solids holdup profiles is majorly in the

spout region. At r/R = 0 (which is the center of the spouted bed), the percentage of variation between the two beds was 21.46%, at r/R = 0.1 it was 22.6%, at r/R = 0.2 it was 28.71% and at r/R = 0.3 it was 34.61%. The comparison of the solids holdup profiles at z/D level 1.1 has an average percentage deviation of 26.5% between the two spouted beds. At r/R = 0.4, is the spout-annulus interface, beyond which the solids holdup is constant and equal to $\varepsilon_s = 0.6$. This is because the annulus acts as a loose packed bed and the volume fraction of solids is maximum in this region. The spout has varying degrees of solids volume fraction along the axial height of the spouted bed. The dimensionless groups, which control the hydrodynamics of the spouted bed, cannot predict the same solids phase holdup in the spout region when compared between the two spouted beds. The absolute percentage deviations for the compared three levels were evaluated. At level z/D 1.8 and r/R = 0 (which is the center of the spouted bed), the percentage of variation between the two beds was 15.30%, at r/R = 0.1 it was 13.67%, at r/R = 0.2 it was 15.11% and at r/R = 0.3 it was 8.33%. The average percentage deviation is 13.10%. This difference in the percentage deviation at the lower level is because of the higher chaotic nature caused by the gas phase near the inlet region.

The variation in gas holdup profiles between the two beds is observed (Figure 4.16 and 4.17). As the axial height increases, the differences between the two profiles reduce because the solids phase volume fraction increases. More solids cross into the spout region from the annulus at higher axial heights. The gas holdup remains low and constant in the annulus region due to high volume fraction of solids ($\varepsilon_g = 0.4$).
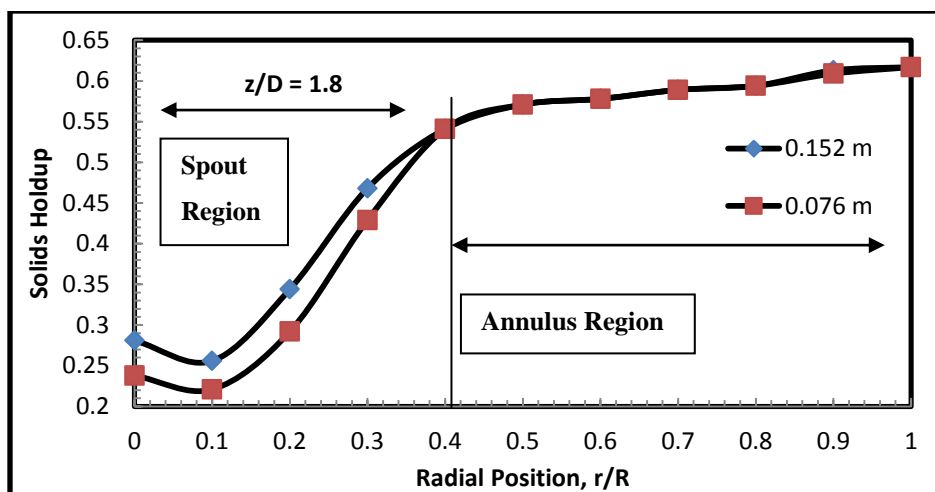
Figure 4.14. Comparison of radial profiles of solids holdup at z/D = 1.8 for Case A
(0.152 m) and Case B (0.076 m) spouted bed.

Fountain region is the third distinct region in the spouted bed, where the solids

after reaching a particular height fall back onto the bed surface due to gravity. When the

solids holdup profiles were compared in this region, the average deviation for the three

levels was found to be 23.71% for the two spouted beds. The amount of solids falling

back onto the bed surface depends on the incoming gas phase. The gas holdup profiles for

both the spouted beds are shown in Figures 4.15 (b), 4.16 and 4.17. Deviations in the

spout region for the compared spouted beds have been observed at all the three levels of

measurement. The gas holdup comparison at z/D = 1.1 and r/R = 0 (which is the center

of the spouted bed), the percentage of variation between the two beds was 21.46%, at r/R

= 0.1 it was 22.6%, at r/R = 0.2 it was 28.71% and at r/R = 0.3 it was 34.61%. The

average percentage deviation of 26.5% was found between the two spouted beds. At level

z/D 1.8 and r/R = 0 (which is the center of the spouted bed), the percentage of variation

between the two beds was 15.30%, at r/R = 0.1 it was 13.67%, at r/R = 0.2 it was 15.11% and at r/R = 0.3 it was 8.33%. The average percentage deviation is 13.10%.

(a)   (b)
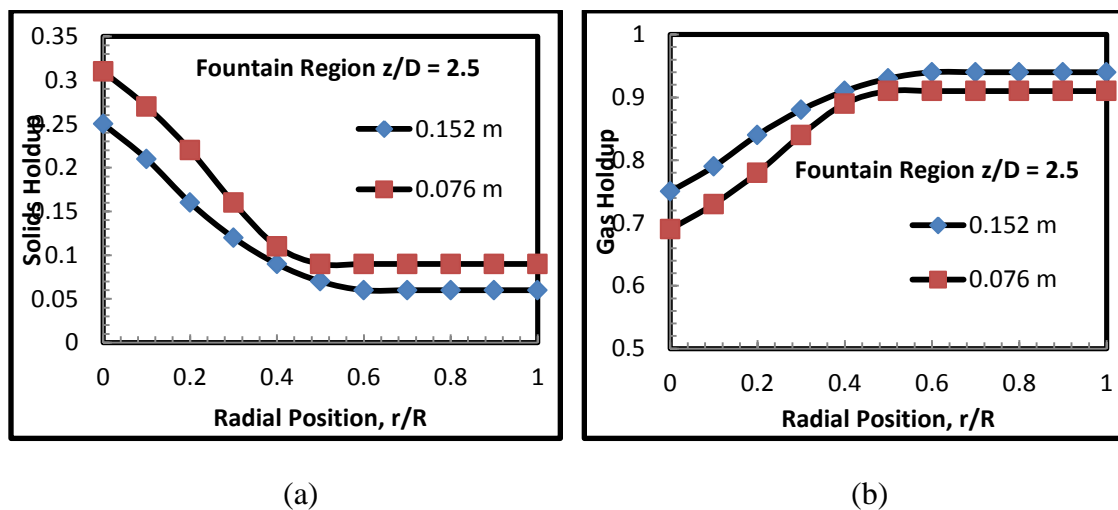
Figure 4.15. Comparison of radial profiles of: (a) solids holdup and (b) gas holdup in the fountain region for Case A (0.152 m) and Case B (0.076 m) spouted bed.
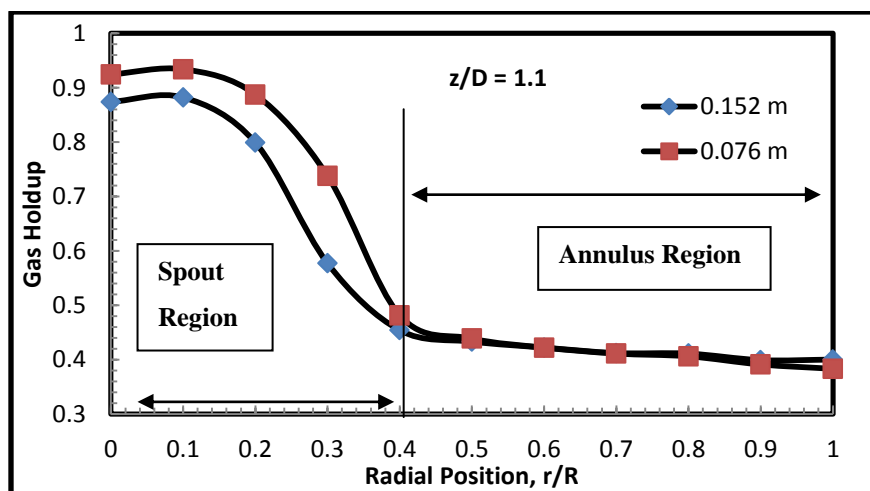
Figure 4.16. Comparison of radial profiles of gas holdup at z/D = 1.1 for Case A (0.152 m) and Case B (0.076 m) spouted bed.
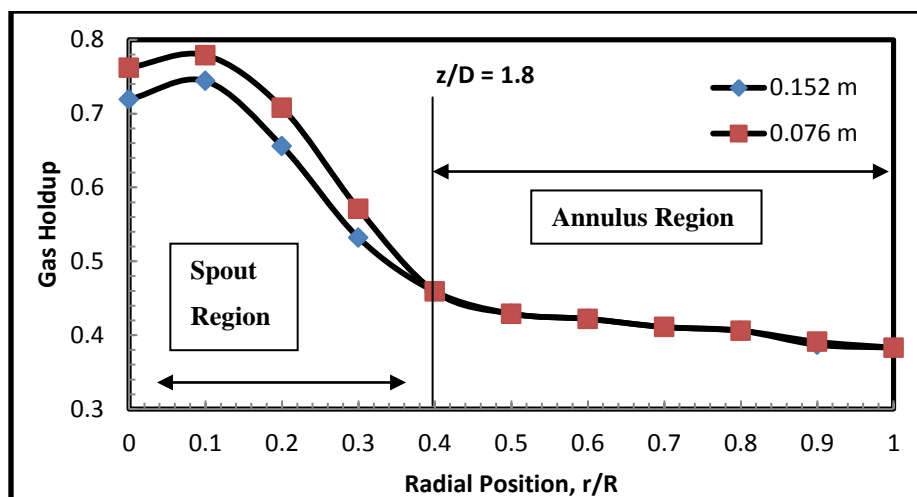
Figure 4.17. Comparison of radial profiles of gas holdup at z/D = 1.1 for Case A (0.152 m) and Case B (0.076 m) spouted bed.

The difference in the profiles can be attributed to the dimensionless groups, even though matched completely in both the spouted beds, these groups many not completely account for the entire hydrodynamics. Additional investigation and assessment is required to draw such a conclusion. Hence, solids velocity was selected to assess further the conditions for matching dimensionless groups.

4.3.2. Solids Velocity. The solids velocity profile for both the beds was measured using optical probe for matching dimensionless groups condition listed in Table 4.1. The details of measurement of solids velocity using optical probe can be found in Section 3. The solids velocity profile for Case A (0.152 m) at different measuring planes is shown in Figure 4.18. The solids velocity is high in the spout region as it is being picked up by the gas phase. The maximum velocity is in the center of the spout region and the velocity reduces as it reaches the spout-annulus interface. The particles velocity in the annulus is very low and is negative (downward). The solids move downwards in the annulus as a

loose moving packed bed, as a result the particles velocity tends to be low. At the center, as the axial height increases from z/D 0.8 to 1.1 the percentage decrease of solids velocity is 17.14%, from z/D 1.1 to 1.5 is 16.66% and from z/D 1.5 to 1.8 is 17.64%. The velocity is maximum at the inlet and as the axial height increases the particles velocity decreases.
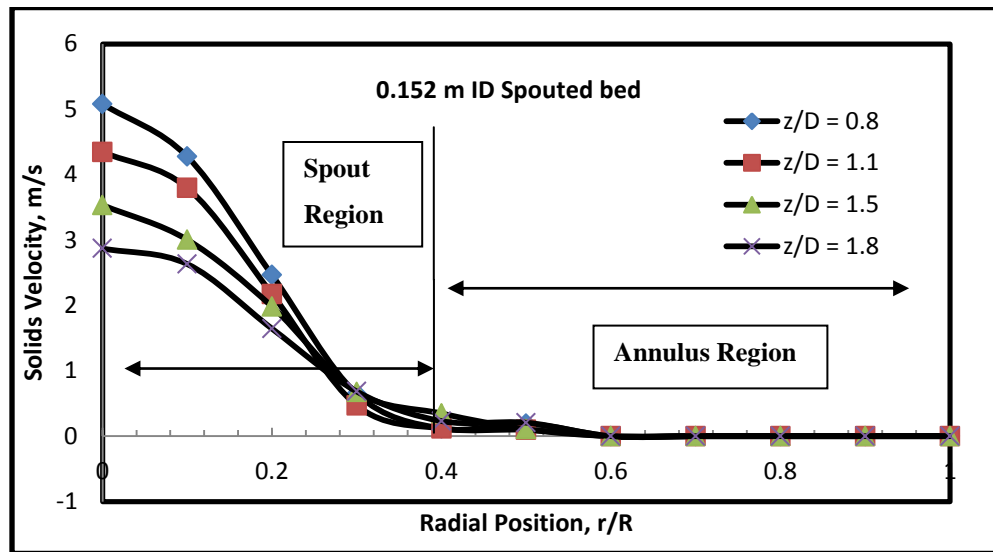
Figure 4.18. Radial profiles of solids velocity for 0.152 m ID spouted bed at different z/D measuring planes for Case A at Ug = 1.08 m/s.

The particles velocity first increase near the inlet and then decreases with the increase in height of the spouted bed as more solids are carried and more energy gets dissipated (Figure 4.18). The velocity also decreases with the increase of radial distance as shown in Figure 4.18. In the fountain region, the velocity of solids carried by the gas fall back onto the bed surface. The center of the fountain region has the maximum velocity (Figure 4.19) and as the radial distance increases, the velocity of the solids decreases. The solids velocity converts from positive to negative at about r/R 0.45-0.55

(Figure 4.19). Beyond this position in the fountain region particles move downwards and the velocity increases negatively as shown in Figure 4.19. The average percentage deviation in the velocity values from z/D 2.1 to 2.5 is 56.45%.

The radial profiles of solids velocity were also measured for 0.076 m spouted bed at different measuring planes. The same trend was observed in the spout, annulus and in the fountain regions. Figures 4.20 and 4.21 show the radial profiles for 0.076 m spouted bed.
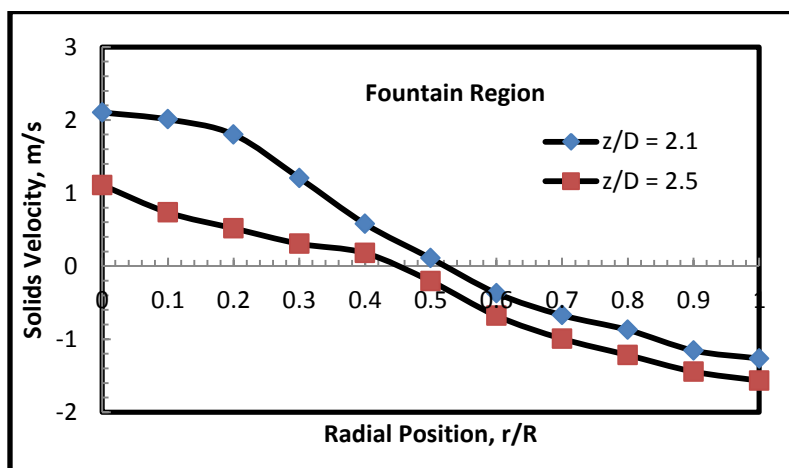
Figure 4.19. Radial profiles of solids velocity for 0.152 m ID spouted bed in the fountain region for Case A at Ug = 1.08 m/s.

In Figure 4.20, the average percentage deviation for the solids velocity from z/D 1.1 to 1.8 is 20.62%. At r/R = 0 (which is at the center of the column), the percentage deviation was found to be 27.5%, at r/R = 0.1 it was 30.13%, at r/R = 0.2 it was 20% and at r/R = 0.3 it was 5%. Beyond r/R = 0.4, the solids velocity increases negatively as the particles in the annulus region move downward as a loose moving packed bed.
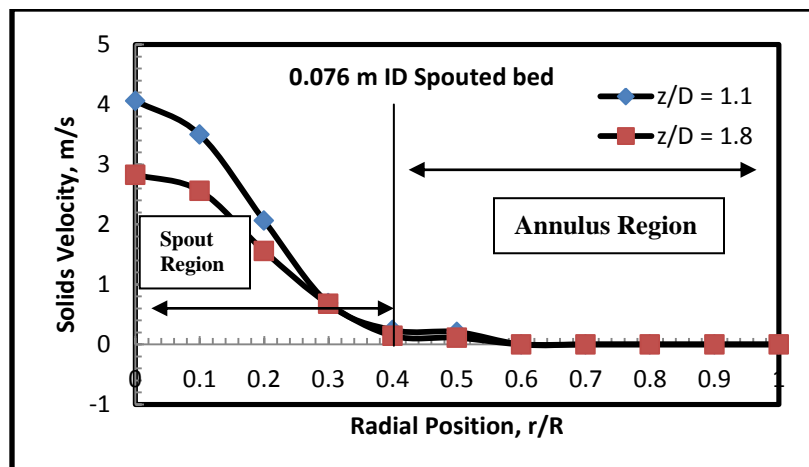
Figure 4.20. Radial profiles of solids velocity for 0.076 m ID spouted bed at different measuring planes for Case B at Ug = 0.75 m/s.
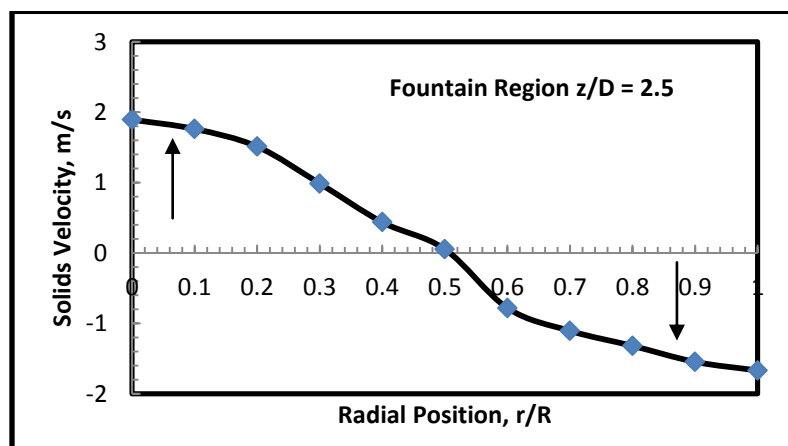
Figure 4.21. Radial profiles of solids velocity for 0.076 m ID spouted bed in the fountain region for Case B at Ug = 0.75 m/s

Since, the assessment of dimensionless groups is the main objective of the present section; the two spouted beds are compared with respect to the particles velocity. It is found that the velocity profiles in the two spouted beds are different (Figure 4.22). To

have a common basis for comparison and to examine if the velocity profiles and magnitudes get closer in the two beds, the radial profiles of the particles velocity in both spouted beds were dimensionalized by dividing with the minimum spouting velocity (U_{ms}). Minimum spouting velocity (measurement of this parameter is explained in Section 2.3) refers to the velocity at which the onset of spouting occurs and below this velocity there is no spouting in the bed. This was measured experimentally and evaluated using correlation predictions in both beds. The gas was introduced into the spouted bed in very small increments. The velocity at which spouting initiated was noted down. To confirm the identified U_{ms}, it was compared with the correlation predictions available in literature (Mathur and Gishler, 1955 and Bi, 2004; as the geometric dimensions and other criteria of the beds under study satisfy these correlations). Table 4.1 shows the comparison of U_{ms} measured experimentally and that predicted by correlations. It was found that the comparison of the values in Table 4.2 is in a good agreement. U_{ms} becomes a very important parameter and can be estimated by many means (experimentally and correlation predictions). Figures 4.23, 4.24 and 4.25 show the compared dimensionless radial profiles of velocity in both the beds. 6 inch represents the Case A and 3 inch represents the Case B listed in Table 4.1. The minimum spouting velocity for 0.152 m spouted bed was found to be 1.04 m/s and for 0.076 m spouted bed it was 0.69 m/s. The comparison of the different size spouted beds for the dimensionless radial profiles of solids velocity show that the profiles are not similar and the differences have increased. At z/D level of 1.1, the profiles had an average deviation of 31.03%. The variation is maximum in the center of the bed (spout region) and decreases as it reaches the spout annulus interface (Figure 4.23). This indicates that by dimensionalizing with respect to

U_{ms} does not help in producing closer particles velocity profiles that would be used as scaling up criterion from the base conditions to estimate the particles velocity profiles at other different conditions and scales using the measured profiles at the base conditions.

Table 4.2. Comparison between experimental values and correlation predictions of U_{ms}

Diameter of Spouted bed	Experimental Values	Correlation prediction of Mathur and Gishler, 1995	Correlation prediction of Bi et al., 2004
0.152 m	1.04 m/s	1.028 m/s	1.035 m/s
0.076 m	0.69 m/s	0.675 m/s	0.681 m/s
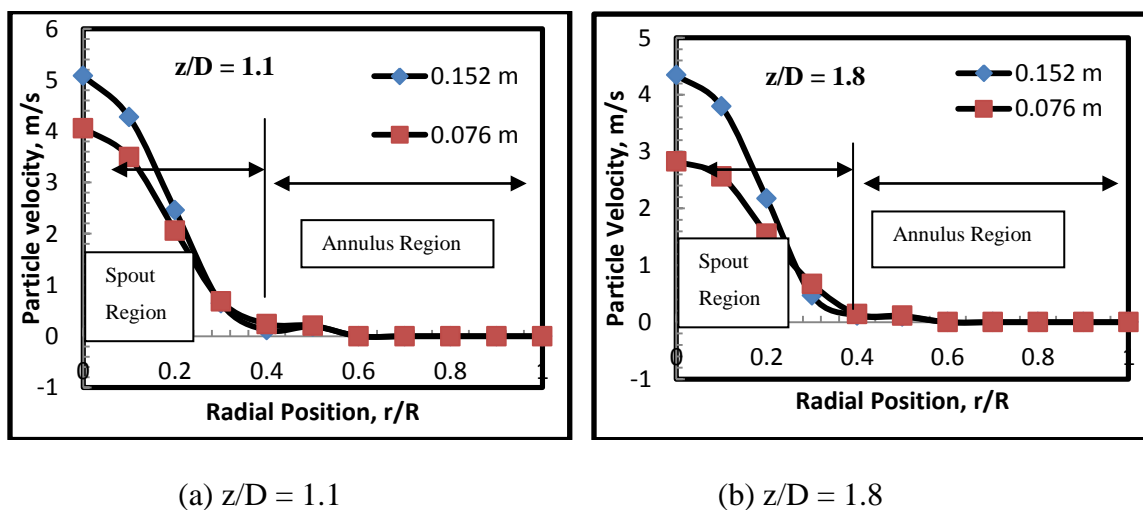
(a) z/D = 1.1   (b) z/D = 1.8

Figure 4.22. Comparison of radial profiles of particles velocity at z/D = 1.1, 1.8 and 2.5 for Case A (0.152 m) and Case B (0.076 m) spouted bed.
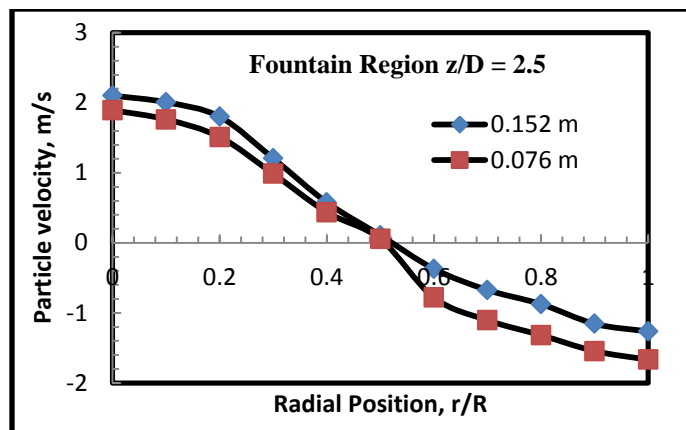
Figure 4.22. Comparison of radial profiles of particles velocity at z/D = 1.1, 1.8 and 2.5 for Case A (0.152 m) and Case B (0.076 m) spouted bed cont.
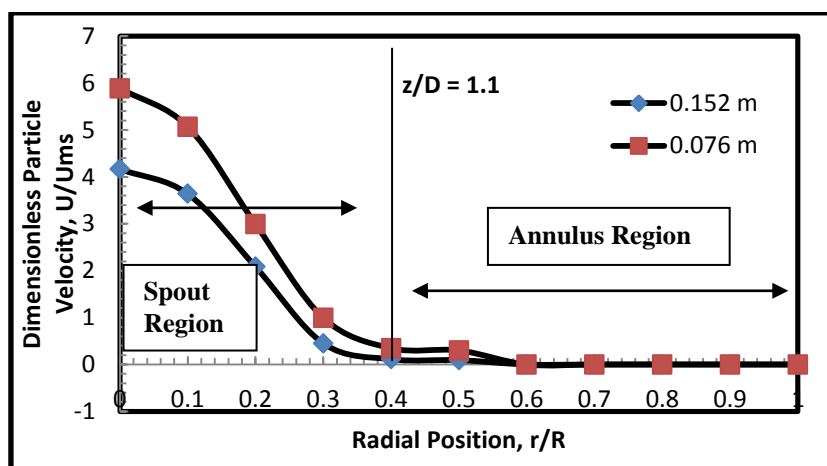
Figure 4.23. Comparison of radial profiles of dimensionless particles velocity at z/D = 1.1 for Case A (0.152 m) and Case B (0.076 m) spouted bed.

In the annulus region, the dimensionless solids velocity profiles are close to each other. This can be explained since the annulus moves down as a loose packed bed and the solids velocity is low. Comparison of dimensionless profiles at z/D level 1.8 (Figure

4.24), the average percentage deviation was found to be 35.16% in the center of the spout region and decreased as it reached the spout-annulus interface.
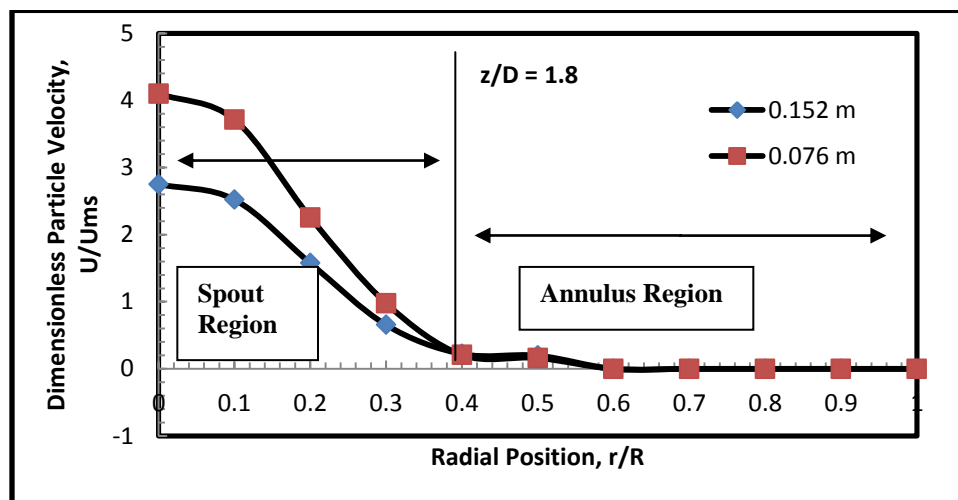
Figure 4.24. Comparison of radial profiles of dimensionless particles velocity at z/D = 1.8 for Case A (0.152 m) and Case B (0.076 m) spouted bed.

In the fountain region, the solids velocity is maximum at the center of the spout and decreases as it approaches the wall. Figure 4.24 shows the same trend and when the dimensionless velocity profiles are compared in this region, the non-similarity in the radial profiles were observed (average percentage deviation of 46%). The average percentage deviation was maximum at the center and decreased near the center of the column. From the center of the column, the average deviation increased until the wall was reached. The comparison of all the measurement planes showed the deviations between the profiles indicating the dissimilarity between the hydrodynamics of the two

spouted beds (Case A and Case B). The percentage of difference is more in the dimensionless radial profiles compared to the absolute particle velocity profiles.
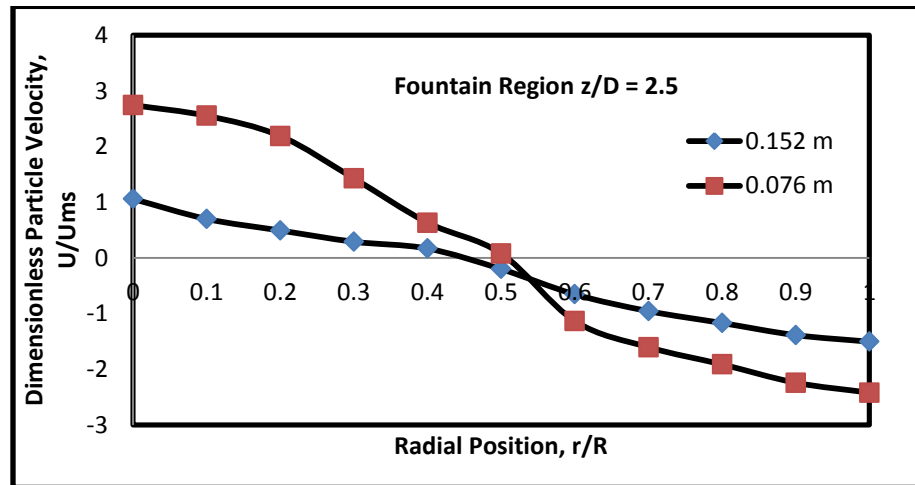
Figure 4.25. Comparison of radial profiles of dimensionless particles velocity in the fountain region for Case A (0.152 m) and Case B (0.076 m) spouted bed.

Additional investigation and assessment is required to draw conclusions on the applicability of the dimensionless groups for hydrodynamics similarity of spouted beds. Hence, pressure fluctuations were selected to assess further the conditions of matching dimensionless groups.

4.3.3. Pressure Fluctuation Analysis. The analysis of pressure signals is very important as it gives information about bed fluctuations. The pressure fluctuation signals were measured by mounting pressure transducers at the wall at different axial heights of the spouted bed. The pressure transducers used in the present study measures gauge pressure fluctuations. The details of the pressure transducers used for the current study is

explained in the earlier section (Section 4.2.3). The effect of axial height on the measurements of pressure fluctuation (intensity of the pressure fluctuations were measured) was analyzed (Section 6.3.2). It was found that the axial height did not have any drastic effect on the measurements in spouted bed. But the intensity (magnitude) of fluctuations in the conical region of the spouted bed was more and the intensity decreased as the axial height increased. The gas velocity in the spout region of the conical section (which is closer to the inlet of spouted bed) is high and this will cause the intensity of the pressure fluctuations to be high. The intensity of pressure fluctuations will decrease as the axial height of the bed increases because the gas velocity decreases with the increase of axial height. Comparison of the standard deviations of pressure fluctuation signals at different axial heights showed that the standard deviations in the conical region were larger than those measured at higher axial heights. This can be attributed to the turbulent motion of the gas near the spouted bed inlet (conical region). More details about the effect of axial height on pressure transducer measurements can be found in Section 6.2.3.

In the present study, the pressure transducers were mounted at z/D levels of 1.1, 1.8 and 2.5 for both the cases. Mean and variance were calculated for these signals. The signals from Case A (0.152 m) and Case B (0.076 m) were compared at z/D 1.1 for the two cases in Figure 4.26. The mean and variance for Case A (0.152 m) were 0.4276 and 0.040076, respectively. The mean and variance for Case B (0.076 m) at z/D 1.1 were 0.126 and 0.013309, respectively (average percentage deviation in the compared cases were 66.45%). The comparison shows that the fluctuations in the two compared cases are different and hence the gas-solid interaction will be different in the two cases. The fluctuations analyzed for the levels z/D 1.8 and 2.5 are shown in Figures 4.27 and 4.28,

respectively. The values of mean and variance for the two cases at z/D levels 1.8 and 2.5 were calculated. At z/D 1.8, the values of mean for Case A (0.152 m) and Case B (0.076 m) were 0.4181 and 0.1187, respectively.

(a)

(b)
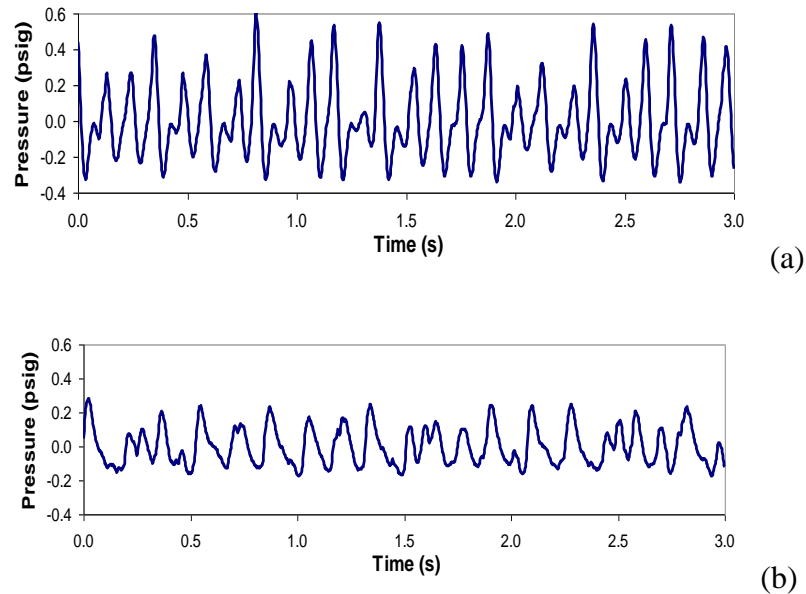
Figure 4.26. Gauge pressure fluctuations; a. Pressure fluctuation signal for Case A at height z/D = 1.1; b. Pressure fluctuation signal for Case B at height z/D = 1.1.

The values of variance for Case A (0.152 m) and Case B (0.076 m) were 0.039677 and 0.014236, respectively (percentage deviation in the compared cases were 64.47%). The comparison between the two cases at this level also showed differences. The nature of the signals also explains the behavior of the bed. The non-similarity in the magnitude and frequency of the fluctuations in case A and case B is obvious from the nature of the fluctuations (Figure 4.26, 4.27 and 4.28). However, in the fountain region

(z/D level 2.5), the pressure fluctuations were pretty close. The values of mean for Case A (0.152 m) and Case B (0.076 m) were 0.2686 and 0.2517, respectively. The values of variance for Case A (0.152 m) and Case B (0.076 m) were 0.02934 and 0.02331, respectively (percentage deviation was 20.55%). This is because the fountain region is made of solids falling back onto the bed surface due to gravity and solids volume fraction in this region is pretty close as explained in earlier section.

(a)

(b)
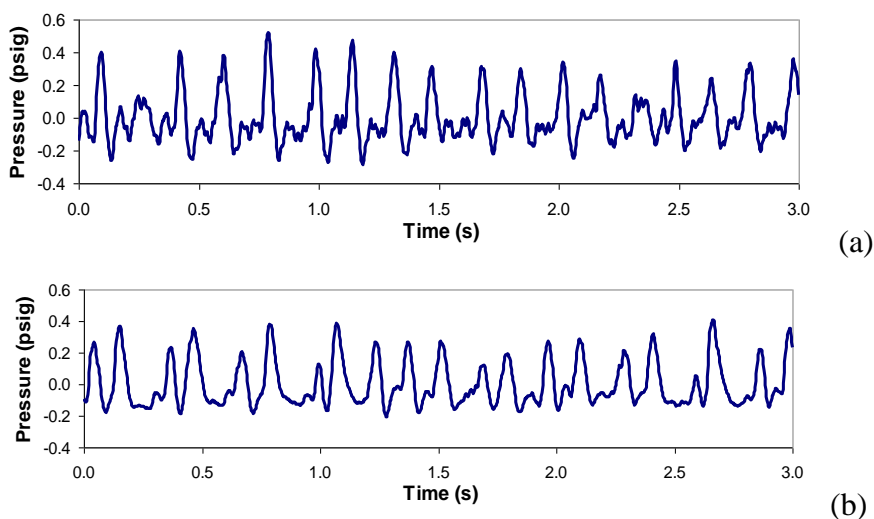
Figure 4.27. Gauge pressure fluctuations; a. Pressure fluctuation signal for Case A at height z/D = 1.8; b. Pressure fluctuation signal for Case B at height z/D = 1.8.
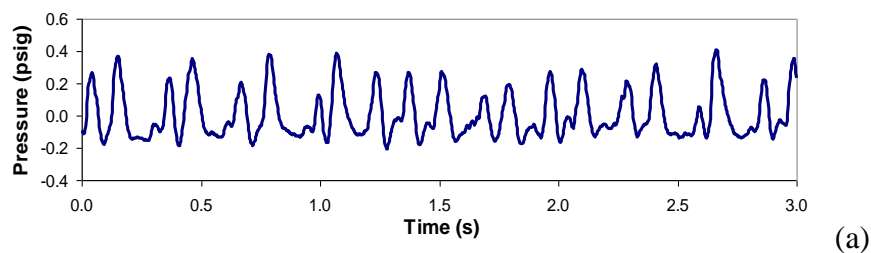
(a)

Figure 4.28. Gauge pressure fluctuations; a. Pressure fluctuation signal for Case A at height z/D = 2.5; b. Pressure fluctuation signal for Case B at height z/D = 2.5.
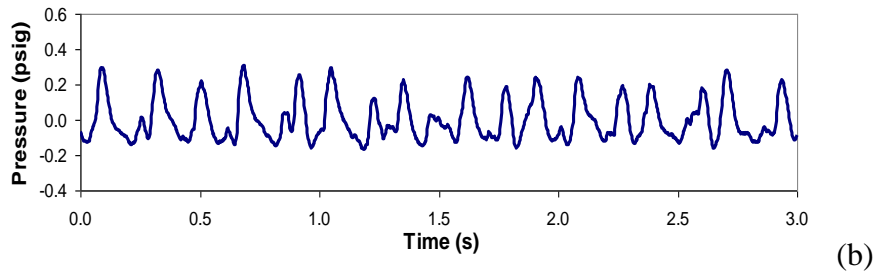
Figure 4.28. Gauge pressure fluctuations; a. Pressure fluctuation signal for Case A at height z/D = 2.5; b. Pressure fluctuation signal for Case B at height z/D = 2.5 cont.

4.3.4. Spout Diameter, Fountain Height And Maximum Spoutable Bed

Height. Spout diameters, fountain heights and maximum spoutable bed heights are among the key global parameters which are helpful in determining the hydrodynamics similarity of the different spouted beds. These are considered to be the global parameters and the similarity of these parameters also marks significance in scale-up methodology.

The spout diameters (D_s) were measured using optical probes. The probes work on back reflection of light, and the reflection of light is dependent on the number of particles in front of the probe. Since there is noticeable difference in the degree of solids in spout and annulus, distinct signals are obtained in these zones. The probe is first placed in the center of the bed and slowly moved towards the wall. The point where there is distinct change in the signal is marked and the distance is noted. Fountain height (H_F) is the maximum height of solids achieved in the spouted bed. The initial bed height is marked and then when the spouted bed is operated under the conditions of the experimentation, the maximum height reached by the solids is noted. Maximum spoutable bed height (H_m) refers to the maximum amount of solids that the spouted bed

can process, beyond which the spouting does not occur. It can also be termed as the amount of solids the spouted bed can process at a time. To measure this, the initial bed height of spouted bed was increased very gradually in small increments until the spouting in the bed did not occur. The bed height at that point was noted to be the maximum spoutable bed height. The spout diameters was measured for Cases A, B, C and D. To compare the above cases, the spout radius (R_s) was dimensionalized by dividing them with column diameter (D_c). Figure 4.29 represents the spout diameters for different cases studied. For convenience, one half of the complete diameter of the spout is shown in Figure 4.29. The spout diameter as a function of dimensionless height (z/H) is shown. Z refers to the height of the plane of actual measurement and H refers to the height of the bed.
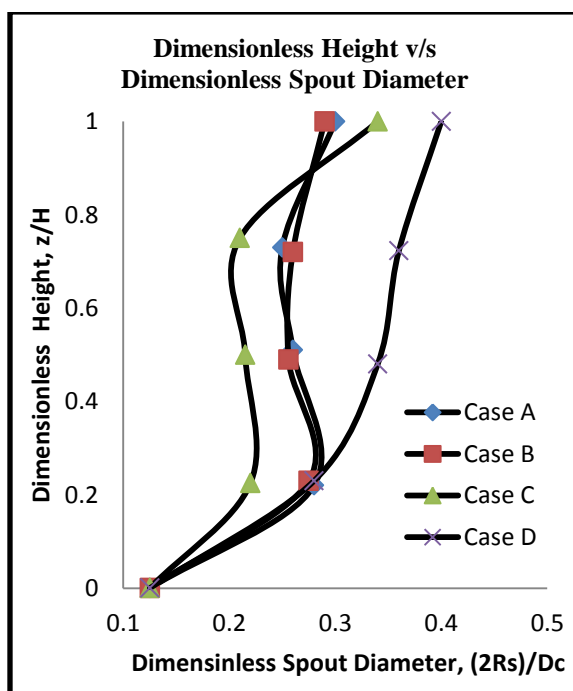
Figure 4.29. Dimensionless height versus dimensionless spout diameter for matching dimensionless groups and mismatch dimensionless groups conditions listed in Table 4.1.

The spout diameter for Cases A and B were close, however for Cases C and D were large from the reference Case A. The average deviation for Cases A and B was found to be 0.77% and for Cases C and D were 15.8% and 10.4% respectively. Table 4.3 gives the details of the parameters measured.

Same procedure to dimensionalize was followed for fountain height (H_F), which was dimensionalized by dividing with column diameter (D_c). The measured parameters were then compared with the reference case A. The deviation for Case B was 15%. However, for Cases C and D the deviation was 46% and 70%, respectively, which is too large. The deviations in Cases C and D show that the purposeful mismatching of the dimensionless groups gives large deviations in global parameters. Based on this the deviations in local parameters is an expected entity.

Table 4.3. Spout diameter and fountain heights for conditions of matching dimensionless groups (Case A and B) and mismatch dimensionless groups (Case A, C and D).

Case	A	B	C	D
Bed height, H(m)	0.323	0.16	0.16	0.16
D_c (m)	0.152	0.076	0.076	0.076
Spout diameter, D_s (m)	0.0395	0.0196	0.0205	0.0204
Fountain height, H_F(m)	0.131	0.057	0.045	0.248
Dimensionless spout diameter, Ds/Dc	0.259	0.257	0.299	0.285
Deviation (%)		0.77	15.8	10.4
Dimensionless fountain height, H_F/D_C	0.87	0.75	0.52	1.54
Deviation (%)	-	15	46	70

Maximum spoutable bed height was also dimensionalized by dividing it with column diameter. The dimensionalized parameters were compared in Table 4.4. Case B had less percentage of deviation when compared to the reference Case A (5.65%). Cases C and D had deviations of 20.4% and 10.4%, respectively. The analysis of all the above parameters, shows that the Case B was much closer to the reference Case A only in terms of these global parameters.

Table 4.4. Maximum spoutable bed height for conditions with matching dimensionless groups (Case A and B) and mismatch dimensionless groups (Case A, C and D) listed in Table 4.1.

Case	A	B	C	D
Bed Diameter, D_c (m)	0.152	0.076	0.076	0.076
Maximum Spoutable bed height, H_m (m)	0.390	0.184	0.235	0.235
H_m/D_c	2.56	2.42	3.09	3.09
Deviation (%)	-	5.65	20.4	10.4

Based on the analysis of the local and global parameters on the dimensionless group's methodology, it can be stated that the differences in the matching cases is large. Based on the experimental analysis performed in the present work the following limitations can be drawn:

1. Conditions for matching dimensionless groups (Case A and B) and mismatch dimensionless groups (case C and D) were identified to study the dimensionless groups approach in the present work. The focus was

based on the conditions for matching dimensionless groups due the wide use of the approach.

2. The local parameters (solids and gas holdup, solids velocity, pressure fluctuations) assessed for the matching dimensionless groups approach showed considerable percentage of deviations in the radial profiles.

3. Solids and gas holdup showed deviations in radial profiles when compared between two spouted beds using conditions of matching dimensionless groups in the spout region and the same trend was observed for the solids velocity profiles.

4. The deviations were prominent in the spout region, as the spout region is predominantly dominated by the gas phase. It is an important region where the gas interacts with the solids effectively. The inflow of solids into the spout region from the annulus varies along the height of the spout, thus leading to variation. The radial profiles compared in the annulus region had little or no deviations. Since annulus acts as a downward moving loose packed bed, the observed behavior is expected.

5. The statistical analysis of mean and variance for the pressure fluctuation signals performed for between the two spouted beds using conditions of matching dimensionless groups showed considerable deviations.

6. Global parameters (spout diameters, fountain height and maximum spoutable bed height) were in good agreement for the conditions of matching dimensionless groups. But in conditions of mismatch dimensionless groups (which were used to study the influence of the

dimensionless groups on the scaling relationships) there were considerable deviations observed.

It has been demonstrated experimentally, that there is non-similarity in local hydrodynamics for spouted beds when all dimensionless groups are matched. However, with the variation shown in the local parameter, this confirms that global parameters should not be used primarily to assess scale-up methodology. The assessment of the conditions for matching dimensionless groups suggests that current dimensionless groups are not sufficient to explain the complete hydrodynamics of the spouted bed system. Therefore, the scale-up methodology of dimensional analysis for spouted beds should be modified to establish a reliable scale-up methodology, not only considering the similarity in global hydrodynamics, but also considering the similarity in local hydrodynamics.

4.4 NEW METHOD FOR SCALE-UP OF SPOUTED BEDS

As mentioned earlier, spouted bed is a two-phase system consisting of gas and solids. The gas phase enters the spouted bed from the bottom as a jet and penetrates the bed of solid particles. As the gas phase penetrates the solids, the solids are being carried by the gas. The gas carrying the solids, reaches the top of the bed surface forming a fountain at the top. The solids then fall back on to the bed surface due to gravity. This nature of spouted bed creates three different zones namely: spout, annulus and the fountain. It is obvious that the gas phase dictates the flow dynamics of the spouted bed. Therefore as a hypothesis, if the radial profile or cross sectional distribution of gas holdup or the solids holdup is maintained the same particularly in the spout region, then the two spouted beds would be similar in the flow dynamics.

Accordingly, we propose a new hypothesis:

"*Radial profile or cross sectional distribution of gas holdup (or solids holdup) should be the same or closer particularly in the spout region for two beds to be hydrodynamically similar or closer*".

Hydrodynamics similarity means either the absolute values of hydrodynamic parameters (holdups, velocity, turbulent parameters etc.) are the same or the dimensionless representation of the hydrodynamic parameters is the same. In the later case, the dimensionless representation can be used as a scaling criterion to estimate the absolute values of hydrodynamic parameters at other different conditions or scales based on the dimensionless profiles measured at base conditions.

If the above-mentioned hypothesis were true, then the first step would be to identify conditions that provide us with closer radial profiles of gas or solids holdup particularly in the spout region. Finding such conditions experimentally would be very tedious and difficult. Hence, Computational Fluid Dynamics (CFD) needs to be used, once it is validated, as an enabling tool to search for these conditions. Conditions identified for hydrodynamics similarity then needs to be validated experimentally and the performance of the spouted bed for the developed new methodology should be monitored online. The later can be achieved by developing a non-invasive radioisotope based technique called Gamma ray densitometry (GRD). In the present section attempts to evaluate the proposed hypothesis experimentally using techniques like optical probes and pressure transducers, which is based on selecting conditions that provides similar and non-similar radial profiles of gas holdups in spouted beds, has been discussed. As demonstrated earlier, the current dimensionless groups are not enough to predict closely

the radial profiles of local parameters (holdups and velocity) in two different spouted beds. The conditions for non-similar radial profiles of gas holdup are required to demonstrate that even though the two spouted beds are geometrically similar, the radial profiles of gas holdup can be different leading to different flow dynamics in the system.

First trail simulations were done using validated CFD (as an enabling tool) to identify the conditions providing similar and non-similar radial profiles of gas holdup in two spouted beds. Optical probes and pressure transducers were used for experimental validation of the conditions selected from the CFD simulations. Computational fluid dynamics (CFD) was used as another tool to help further assess these conditions from computational point of view (discussed in Section 7).

The procedure for experimental evaluation of the proposed hypothesis is as follows:

1. Prototype/reference spouted bed is the 0.152 m (6 inch) spouted bed, which has the same conditions of Case A listed in Table 4.1.

2. 0.076 m (3 inch) spouted bed will be used to perform CFD simulation studies as an enabling tool to identify conditions for similar and non-similar hydrodynamics.

3. Once the two conditions are identified, a comprehensive evaluation (radial profiles of gas and solids holdup, solids velocity, pressure fluctuations, spout diameters and fountain heights) will be performed on the identified conditions using optical probes and pressure transducers to validate the proposed hypothesis.

4.   Perform computational fluid dynamics (CFD) simulations to assess the hypothesis from computational point of view.

5.   If the hypothesis is validated, then this will motivate the development of Gamma ray densitometry (GRD), a non-invasive radioisotope based technique, to be used for on-line monitoring of the scale-up conditions identified and flow regime or pattern identification.

Table 4.5 shows the similarity and non-similarity conditions identified during this study. The emphasis here is to show that if one maintains similar or closer radial profiles of gas holdup, the flow dynamics of the two systems will be the same or closer. Such a similarity in the flow dynamics of the system is the ultimate goal of any scale-up procedure to maintain the desired conversion and process performance.

Table 4.5 Conditions for similar and non-similar gas holdup radial profiles $(\varepsilon_g)_r$ for the hydrodynamics similarity approach.

Case	Reference Case Case A	Conditions For Similar $(\varepsilon_g)_r$	Conditions For Non-Similar $(\varepsilon_g)_r$
D_c (m)	0.152	0.076	0.076
D_i (m)	0.019	0.0095	0.0095
L (m)	1.14	1.14	1.14
H (m)	0.323	0.16	0.16
T (K)	298	298	298
P (kPa)	101	**364**	101
Particles	**Glass Beads**	**Steel**	**Glass**
d_p (m)	0.00218	0.00109	0.00109
ρ_p (kg/m^3)	2450	**7400**	2450
ρ_f (kg/m^3)	**1.21**	**3.71**	**1.21**
μ ($*10^{-5}$) (Pa.s)	1.81	1.81	1.81
U (m/s)	**1.08**	**0.64**	**0.74**
H /D_c	2.1	2.1	2.1
D_c /D_i	8	8	8
D_c/ d_p	69.9	69.9	69.9

Table 4.5 Conditions for similar and non-similar gas holdup radial profiles $(\varepsilon_g)_r$ for the hydrodynamics similarity approach cont.

	1994	1995	2029
ρ_p / ρ_f			
ε_{mf}	0.41	0.42	0.42
$\rho_f\, d_p\, U/\mu$	157	297	54
U^2/gd_p	54.5	38.3	51.2
$\rho_p d_p U/\mu$	3.13	1.39	1.09
U^2/gD_c	0.78	0.549	0.73

4.5. RESULTS

The statistical difference between parameters evaluated for the conditions are represented in terms of the average relative difference which is defined as follows

$$\text{Absolute Relative Difference} = \frac{1}{N}\sum_1^N \left[\frac{x(r) - y(r)}{x(r)} \right] \qquad (4)$$

Where, x and y can be local or global parameters at corresponding radial locations and N is the corresponding total number of data points. Since several parameters are evaluated for the conditions of similar and non-similar $\varepsilon_{g,r}$ identified in Table 4.5, each of them is discussed in separate sections below.

4.5.1. Gas Holdup and Solids Holdup Profiles. Gas holdup profiles measured for the two different size spouted beds using conditions for similar radial profile of gas holdup are shown in Figure 4.30. The measurement levels compared are at z/D 1.1, 1.8 and 2.5 (fountain region). First the solids holdup was measured using optical fiber probes and then the gas holdup was calculated ($\varepsilon_g = 1-\varepsilon_s$). The comparison of radial profiles of gas holdup in both 0.152 m and 0.076 m spouted beds show the profiles were very close to each other. The absolute relative difference between the two radial profiles was 4.1%.

This represents a close agreement of the newly utilized conditions which are successfully able to match the radial profiles. In the scale-up approach of He et al. (1997), the voidage in the annulus region was almost same, but differed drastically in the spout and in the founatin regions. Using the new conditions listed in Table 4.5, the profiles in the spout and annulus region were matched after numerous trials performed using CFD.

Gas holdup profiles were also measured for the conditions for non-similar radial profile of gas holdup to check the percentage of deviation between the two radial profiles. Figure 4.31 shows the radial profiles of gas holdup at z/D levels of 1.1, 1.8 and 2.5. It is observed that the deviations between the radial profiles were large in the spout region. In the annulus region, the deviations were very small as expected due to the downward movement of particles as a loose packed bed. The absolute relative difference between the profiles was found to be 55.8% in the spout region.
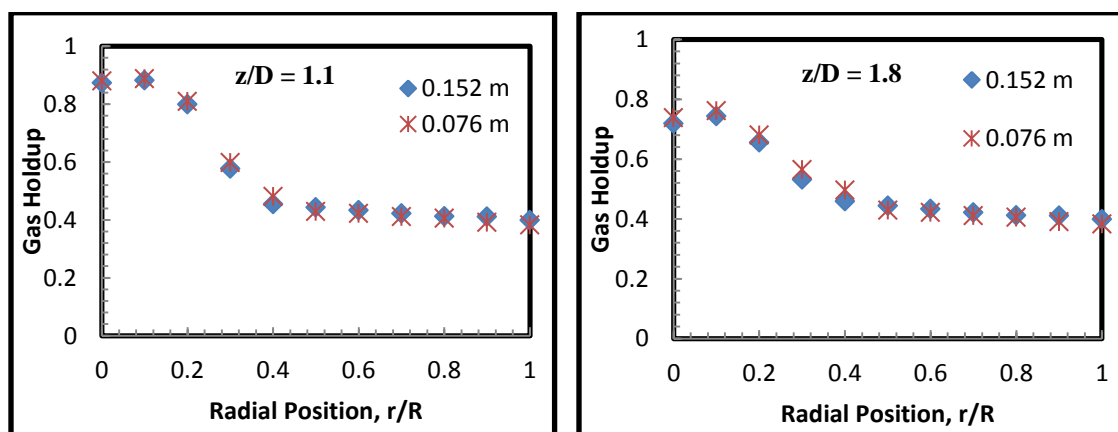
Figure 4.30. Gas holdup profiles for the conditions for similar radial profile of gas holdup in 0.152 m and 0.076 m spouted bed at different z/D measurement levels.
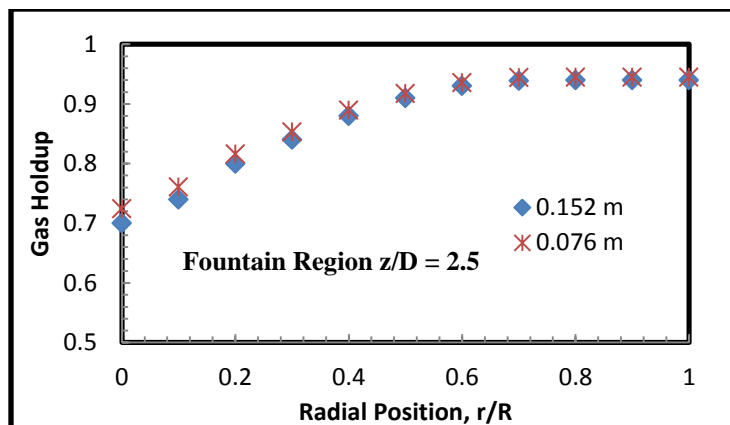
Figure 4.30. Gas holdup profiles for the conditions for similar radial profile of gas holdup in 0.152 m and 0.076 m spouted bed at different z/D measurement levels cont.
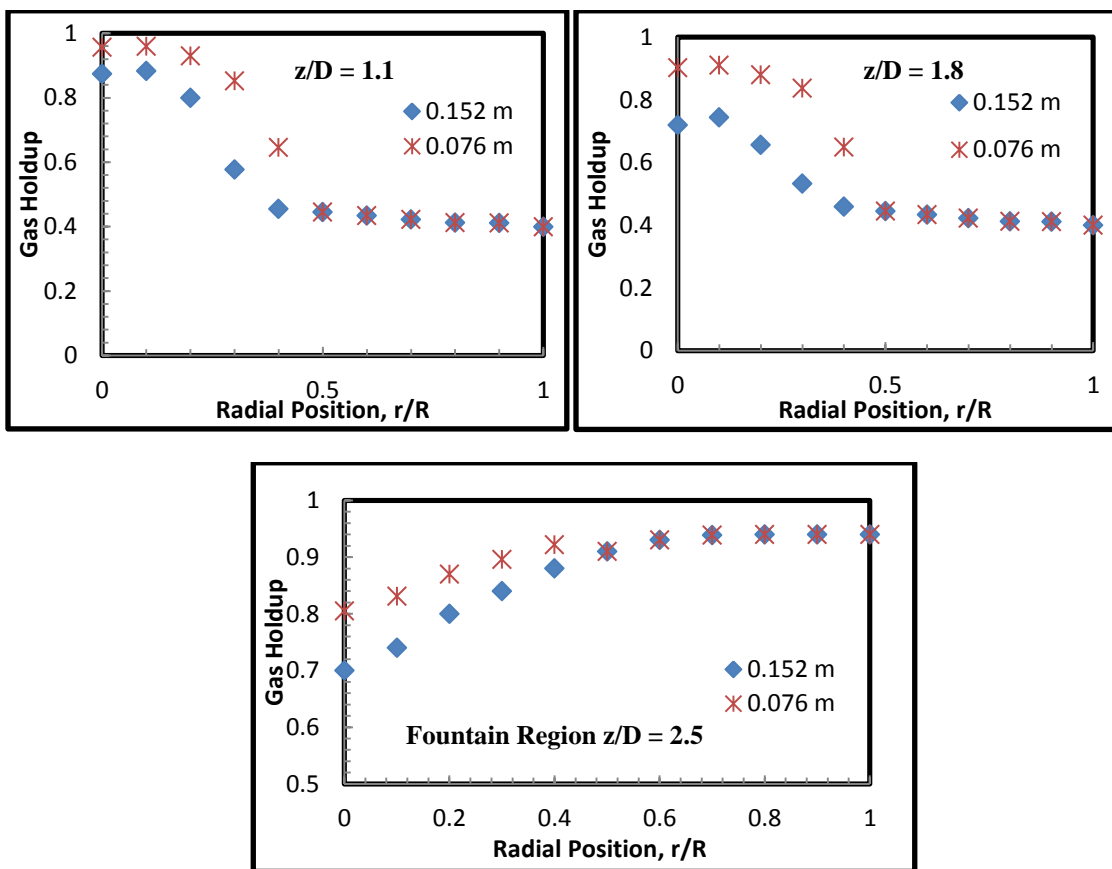
Figure 4.31. Gas holdup profiles for the conditions for non-similar radial profile of gas holdup in 0.152 m and 0.076 m spouted bed at different z/D measurement levels.

Solid holdup profiles for the conditions of similar radial profile of gas holdup are shown in Figure 4.32. The radial profiles were in close agreement with each other and the absolute relative difference between the profiles was 4.1%. The conditions for non-similar radial profile of gas holdup (Figure 4.33) gave noticeable difference in the radial profiles of the solids holdup with the absolute relative difference being about 55.8%. The differences were again mainly in the spout region, where as the annulus region showed negligible difference between the profiles. Since the spout is dominated by the gas phase, maximum variation can be found in this region. The dimensionless groups identified for the conditions for non-similar radial profile of gas holdup cannot predict the flow dynamics completely, which ultimately leads to the differences in the radial profiles.
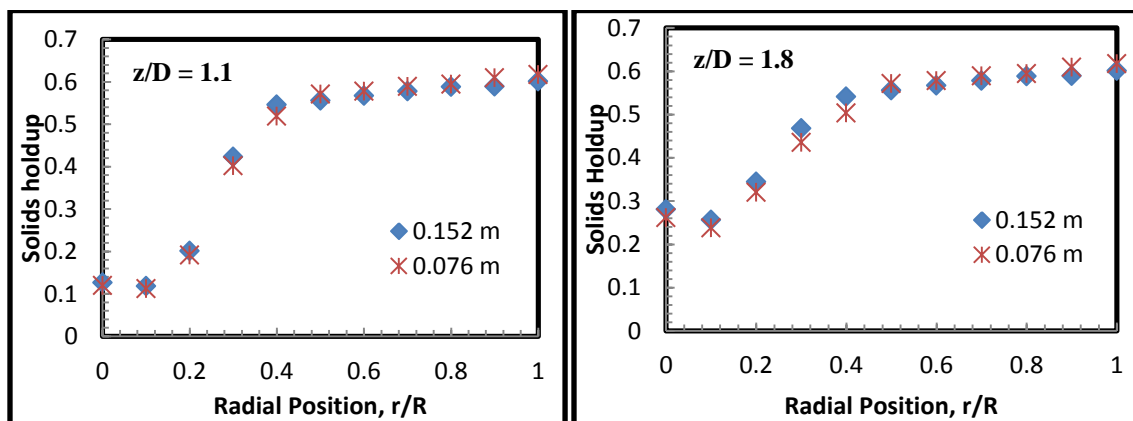
Figure 4.32. Solids holdup profiles for the conditions for similar radial profile of gas holdup in 0.152 m and 0.076 m spouted bed at different z/D measurement levels.
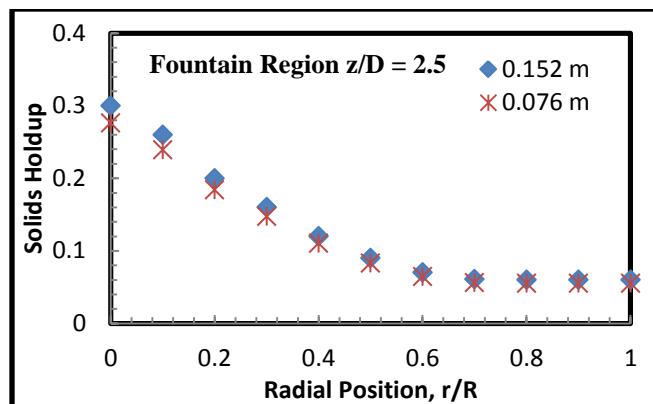
Figure 4.32. Solids holdup profiles for the conditions for similar radial profile of gas holdup in 0.152 m and 0.076 m spouted bed at different z/D measurement levels cont.
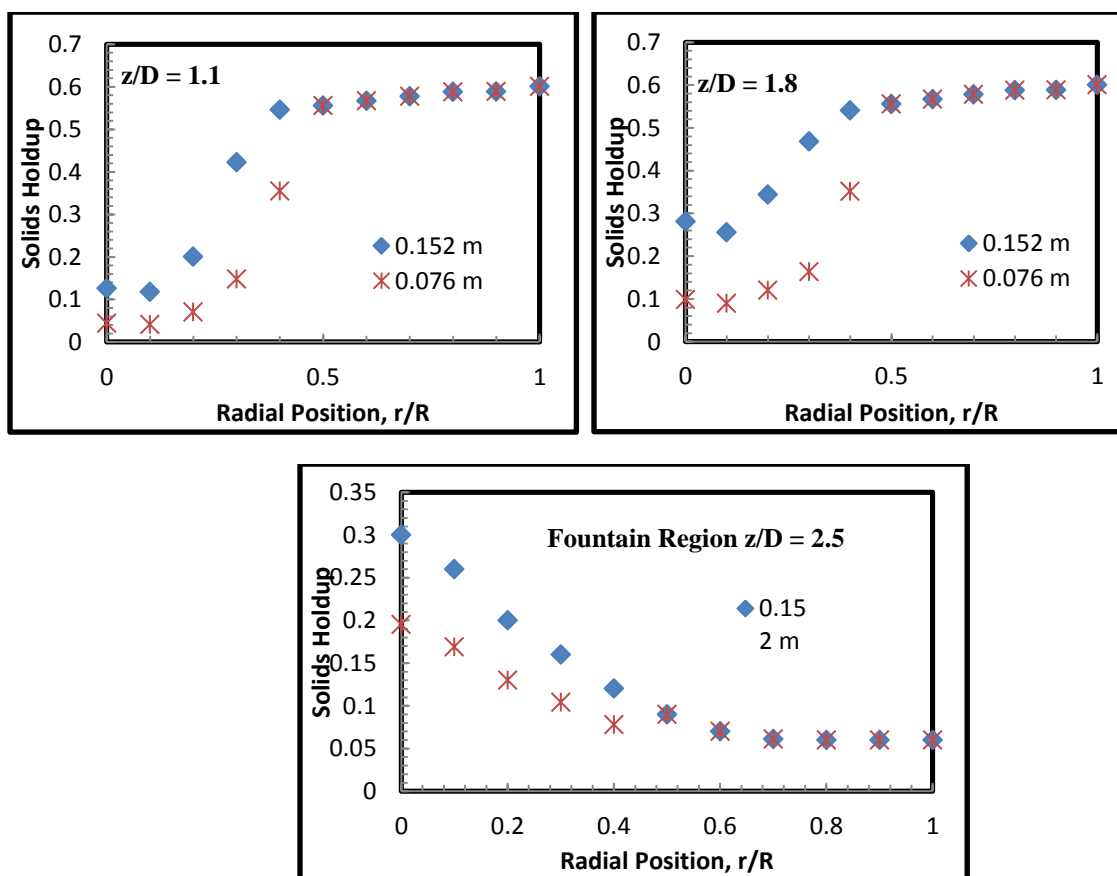
Figure 4.33. Solids holdup profiles for the conditions for non-similar radial profile of gas holdup in 0.152 m and 0.076 m spouted bed at different z/D measurement levels.

4.5.2. Solids Velocity. The solids velocity profile of both the beds was also measured for the conditions of similarity and non-similarity in radial profiles of gas holdup listed in Table 4.5, with the use of optical probe. The details of measurement of solids velocity using optical probe can be found in Section 3.

The solids velocity is high in the spout region as it is being picked up by the gas phase. The maximum velocity can be found in the center of spout region and the velocity reduces as it reaches the spout-annulus interface. The velocity in the annulus is very low and is negative. The solids move downwards in the annulus as a loose packed bed, as a result the velocity tends to be low. The particle velocity first increases near the inlet and then decreases as the height of the spouted bed increases (momentum imparted by the gas phase reduces as the height increases). In the fountain region, the center has the maximum velocity and as the radial distance increases, the velocity of the solids decreases (Figure 4.34 and 4.35).

The comparison of the particles velocity profiles at different z/D measurement levels for the two conditions is shown in Figure 4.34 and 4.35. Figure 4.34 shows the particles velocity profiles for the conditions of similar radial profile of gas holdup. The difference between the particles velocity profiles is maximum at the center of the spout and it decreases as it reaches the spout-annulus interface. The average percentage deviation for the particles velocity profiles for the conditions of similar radial gas holdup profile at z/D 1.1 is 22.38%. At r/R = 0 (which is at the center of the column), the percentage deviation was found to be 47.61%, at r/R = 0.1 it was 33.36%, at r/R = 0.2 it was 28.57% and at r/R = 0.3 it was 5%. The average percentage deviation for the particles velocity profiles at z/D 1.8 is 19.54%. At r/R = 0 it was 35.82%, at r/R = 0.1 it

was 30.06%, at r/R = 0.2 it was 23.33% and at r/R = 0.3 it was 8.5%. In the fountain region, the difference between the two profiles decreases until it reaches to r/R of about 0.47-0.53 and then the differences increases again. The average percentage deviation for the particles velocity profiles at z/D 1.8 is 20.77%.

Figure 4.35 shows the particles velocity profiles for the conditions of non-similar radial profile of gas holdup. The difference between the particles velocity profiles is lesser compared to the conditions of similar radial profiles of gas holdup. The average percentage deviation for the particles velocity profiles for the conditions of non-similar radial gas holdup at z/D 1.1 is 14.48%. At r/R = 0 (which is at the center of the column), the percentage deviation was found to be 34.21%, at r/R = 0.1 it was 20.21%, at r/R = 0.2 it was 11.18% and at r/R = 0.3 it was 3.8%. The average percentage deviation for the particles velocity profiles at z/D 1.8 is 16.11%. At r/R = 0 it was 30.05%, at r/R = 0.1 it was 28.34%, at r/R = 0.2 it was 19.02% and at r/R = 0.3 it was 3.31%. In the fountain region, the difference between the two profiles decreases until it reaches to r/R of about 0.51-0.57 and then the differences increases again. The average percentage deviation for the particles velocity profiles at z/D 1.8 is 15.85%. The explanation of these findings is explained in the following discussions.
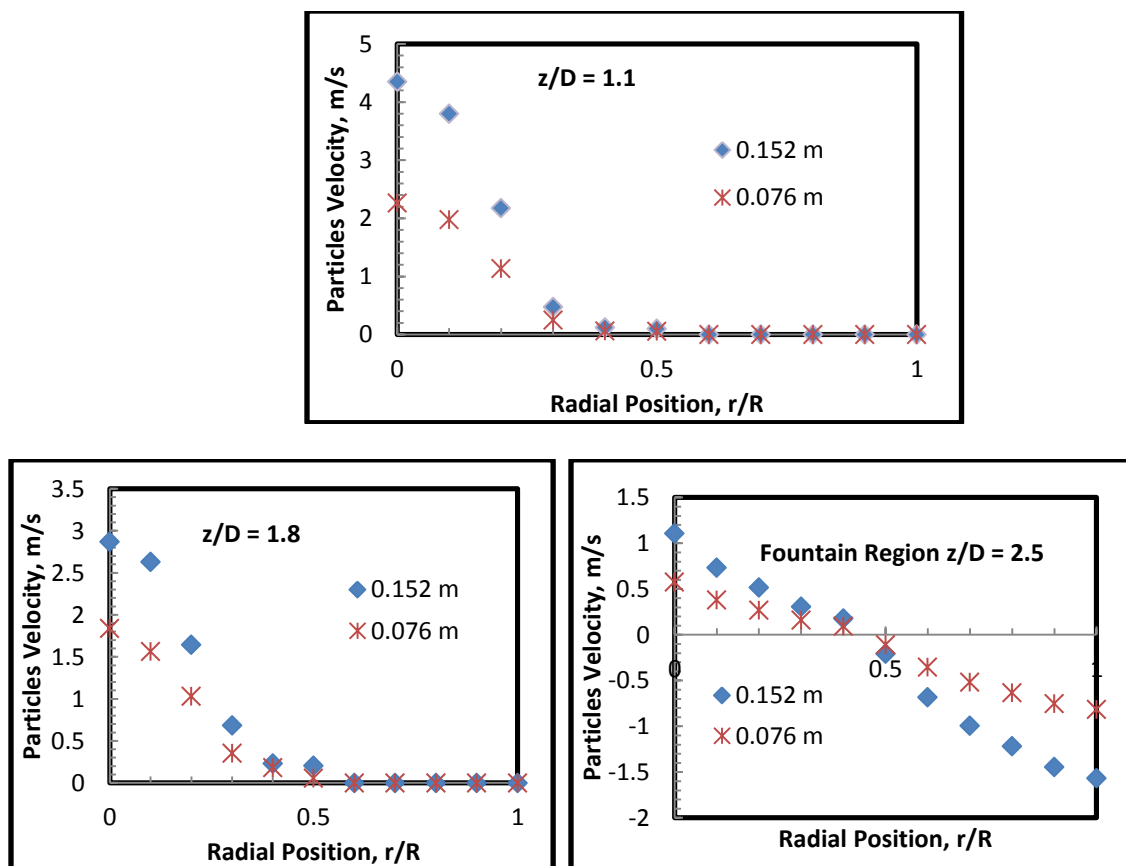
Figure 4.34. Particles velocity profiles for the conditions for similar radial profile of gas holdup in 0.152 m and 0.076 m spouted bed at different z/D levels.
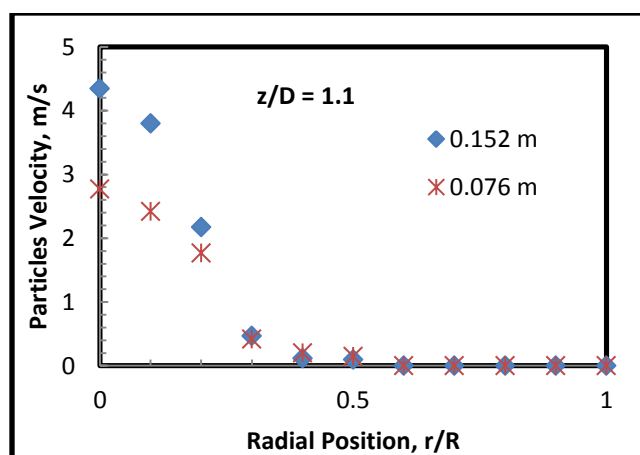
Figure 4.35. Particles velocity profiles for the conditions for non-similar radial profile of gas holdup in 0.152 m and 0.076 m spouted bed at different z/D levels.
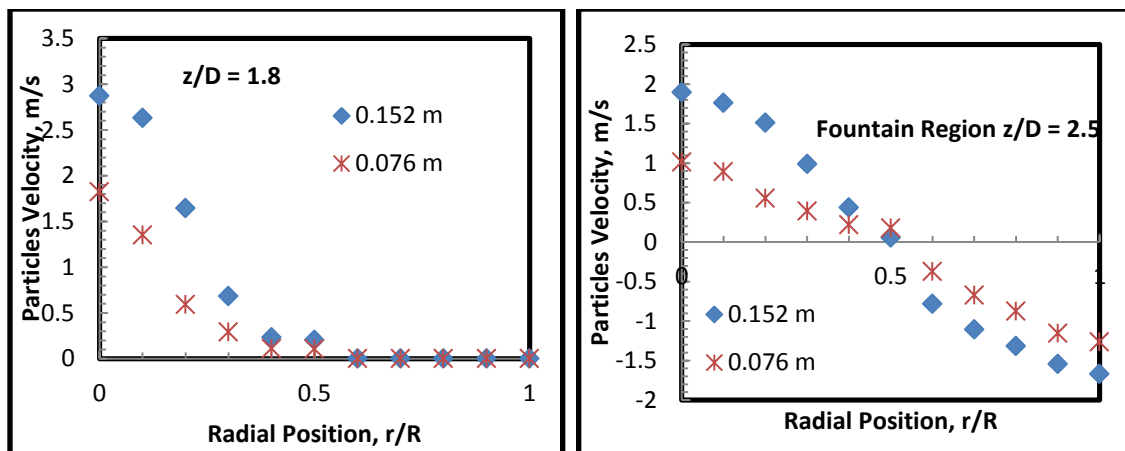
Figure 4.35. Particles velocity profiles for the conditions for non-similar radial profile of gas holdup in 0.152 m and 0.076 m spouted bed at different z/D levels cont.

To have a common basis for comparison, the radial profiles were dimensionalized for both the spouted beds by dividing with minimum spouting velocity (U_{ms}). Minimum spouting velocity refers to the velocity at which the onset of spouting occurs and below this velocity there is no spouting in the bed. This was measured experimentally in both the beds (Table 4.4). The gas was introduced into the spouted bed with very small increments. The velocity at which the spouting occurred was noted down as the minimum spouting velocity. The minimum spouting velocity for 0.152 m spouted bed was 1.04 m/s and for 0.076 m spouted bed was 0.52 m/s. To confirm the identified U_{ms}, it was compared with the correlation predictions available in literature (Mathur and Gishler, 1955 and Bi et al., 2004; Section 2.3 explains the details of correlations). Figure 4.36 shows the dimensionless particle velocity profiles for the two spouted beds at measurement levels of z/D 1.1, 1.8 and 2.5. The absolute relative difference between the radial profiles was found to be 3.5%. The closeness in the profiles was seen in all the

three measured levels. The dimensionless particle velocity profiles for the conditions of non-similar radial profiles of gas holdup were estimated and the results are shown in Figure 4.37. The absolute relative difference in the profiles at the center was found to be 47.9%. The observed deviations were in the spout region and the deviations in the annulus region were found to be very low or negligible. The velocity in the annulus is very low and is negative because solids move downwards in the annulus as a loose packed bed, as a result the velocity tends to be low.
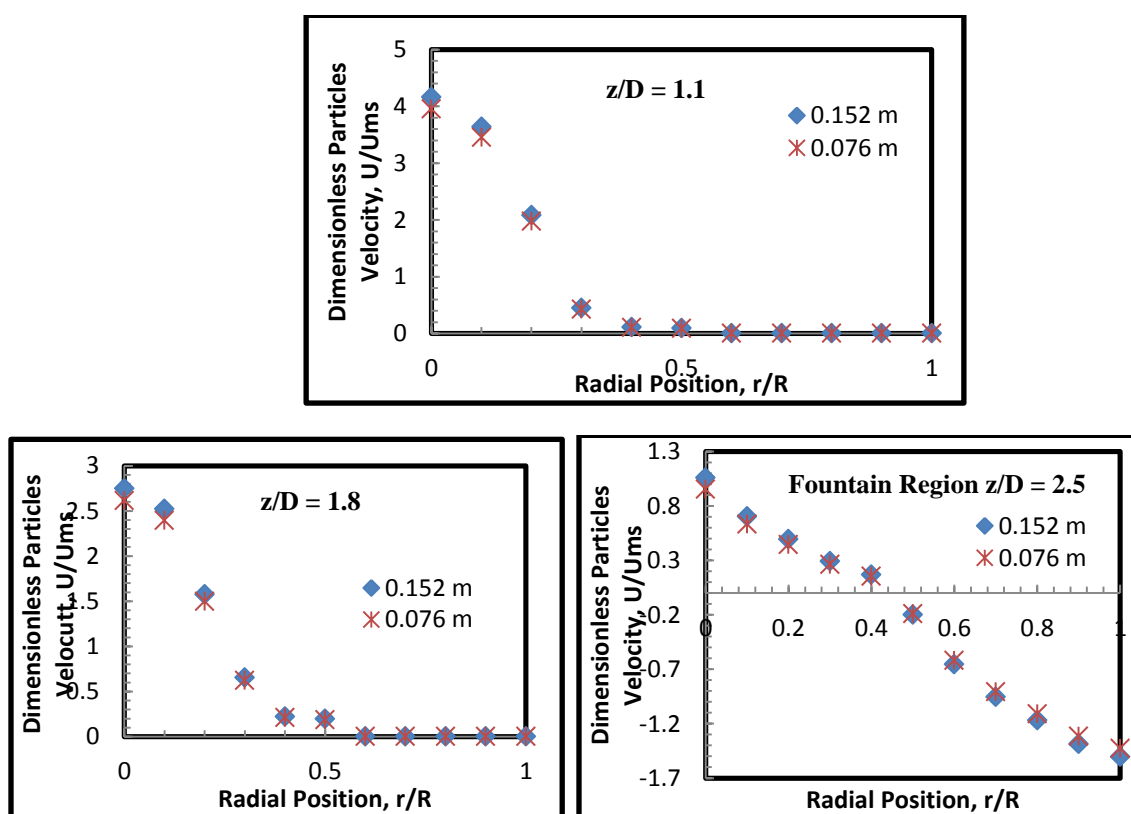
Figure 4.36. Dimensionless particles velocity profiles for the conditions for similar radial profile of gas holdup in 0.152 m and 0.076 m spouted bed at different z/D levels.
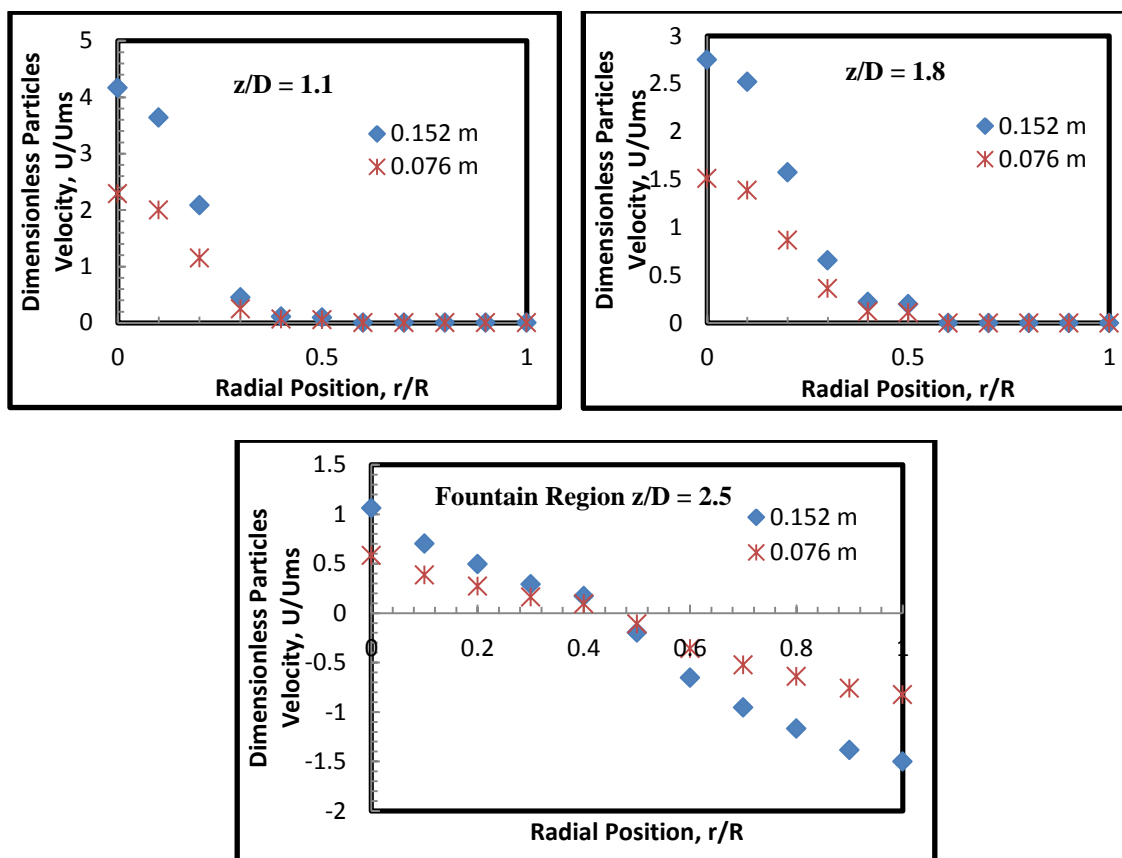
Figure 4.37. Dimensionless particles velocity profiles for the conditions for non-similar radial profile of gas holdup in 0.152 m and 0.076 m spouted bed at different z/D levels.

The difference in the absolute values of particles velocity profiles between the reference case and the case of similar radial profile of gas holdup was high. The reference case (0.152 m) uses glass beads (2450 Kg/m^3) as the solids phase. In this case, the cross sectional area of the spout region, gas velocity and the solids holdup is high. Hence, the cross sectional area for solids to flow in the spout region is higher in the reference case. In the case of similar radial profile of gas holdup, in another bed of 0.076 m, the solids phase is steel shots (7500 Kg/m^3). In this case, the cross sectional area of spout is lower, solids holdup is equal to that of the reference case and gas velocity is lower. As a result,

the cross sectional area for solids to flow is lower. To understand the difference between the particles velocity profiles in the two beds even though the solids holdup values are the same needs more insight. Hence, drag force was evaluated from CFD for both the conditions to see its effect on the particles velocity. In the spout region, the reference case (0.152 m) has a higher drag force on the particles compared to the case of similar radial profile of gas holdup which has lower drag force acting on the particles (Figure 4.38.a and b). The gas phase is the driving force in the spouted bed and thus dictates the hydrodynamics. The momentum from the gas phase is imparted to the solids phase. The imparted momentum from the gas phase is transferred to the mean particles velocity and its fluctuations. Hence, the mean and variance of the time series signal (fluctuations) of the particles velocity were measured using optical probes for both the reference case and the case of similar radial profile of gas holdup. Figure 4.39 shows the time series signal of particles velocity. The reference case has a mean of 3.3 and variance of 0.31. However, the case of similar radial profile of gas holdup has a mean of 2.31 and variance of 1.3. Since the value of the mean of the signal for the case of similar radial profile of gas holdup is lower and the value of the variance is higher compared to that of the reference case, the particles velocity of the case of similar radial profile of gas holdup is lower as shown in Figure 4.34.

The difference in the absolute values of particles velocity profiles between the reference case and the case of non-similar radial profile of gas holdup was less compared to that between the reference case and the case of similar radial profile of gas holdup. The case of non-similar radial profile of gas holdup uses glass beads (2450 Kg/m^3) as the solids phase. The cross sectional area of the spout region is much lesser compared to the

reference case and to the case of similar radial profile of gas holdup, gas velocity is higher compared to the case of similar radial profile of gas holdup and the solids holdup is lower compared to the reference case and the case of similar radial profile of gas holdup. Hence, the cross sectional area for the solids to flow in the case of non-similar radial profile of gas holdup is much lesser compared to that of the reference case and the case of similar radial profile of gas holdup. The drag force in the case of non-similar radial profile of gas holdup acting on the particles in the spout region was found to be much lesser compared to the other two beds (Figure 4.38.a and b). The mean and variance of the time series signal (fluctuations) of the particles velocity for the case of non-similar radial profile of gas holdup was found to be 1.72 and 0.98, respectively (Figure 4.40). The mean and variance of the time series signal of the particles velocity are lower compared to the reference case and hence, the particles velocity is lower. Since, both the cases of similar and non-similar radial profiles of gas holdup use different solids (steel shots versus glass beads), different gas velocities (0.64 m/s versus 0.74 m/s), same bed height and different gas density (higher pressure versus atmospheric pressure, Table 4.5), the drag forces acting on particles are different (Figure 4.38), which is lower in the case of non-similar radial profile of gas holdup. However, the spout diameter in the case of non-similar radial profile of gas holdup is lower than that of the case of similar radial profile of gas holdup and hence, the cross sectional area for the solids to flow is lower in the former case. All these cause the mean and variance of the time series signal of the particles velocity measurement of the case of non-similar radial profile of gas holdup to be lower than those of the case of similar radial profile of gas holdup. Since higher fluctuations encountered in the velocity measurements in the case of similar radial profile

of gas holdup, the particles velocity of this case is expected to be lower than that of the case of non-similar radial profile of gas holdup. This is supported in measurements of particles velocity demonstrated in Figure 4.34 and 4.35. Spouted bed system is a highly non-linear system and hence, more detailed investigation into the difference of particles velocity profiles when the gas or solids holdup profiles are similar and non-similar, needs to be further assessed using CFD and advanced measurement techniques like radioactive particle tracking (RPT), which will be able to provide more insight.

Minimum spouting velocity (U_{ms}) was used for dimensionless representation of the particles velocity for both cases. Different values of U_{ms} have been found in the (dimensionless representation) studied spouted beds and reported in Table 4.2 due to different conditions used (Table 4.5). It was observed that there was very little or less difference between the reference case and the case of similar radial profiles of gas holdup. But, for the case of non-similar radial profiles of gas holdup, the deviation with respect to the reference case increases and the deviation were found to be much more than that observed when the absolute particles velocity profiles were compared.

Therefore, minimum spouting velocity (U_{ms}) becomes an important parameter because of the closeness obtained between the profile of the reference case and the case of similar radial profiles of gas holdup profile. Based on this, U/U_{ms} ratio can be used as a scaling criterion to estimate the absolute particles velocity profiles in different spouted beds using the measured or computed dimensionless particles velocity profiles of a reference case provided that they have similar or closer gas holdup radial profiles. This confirms the similarity in the hydrodynamics between various spouted beds using the proposed methodology.
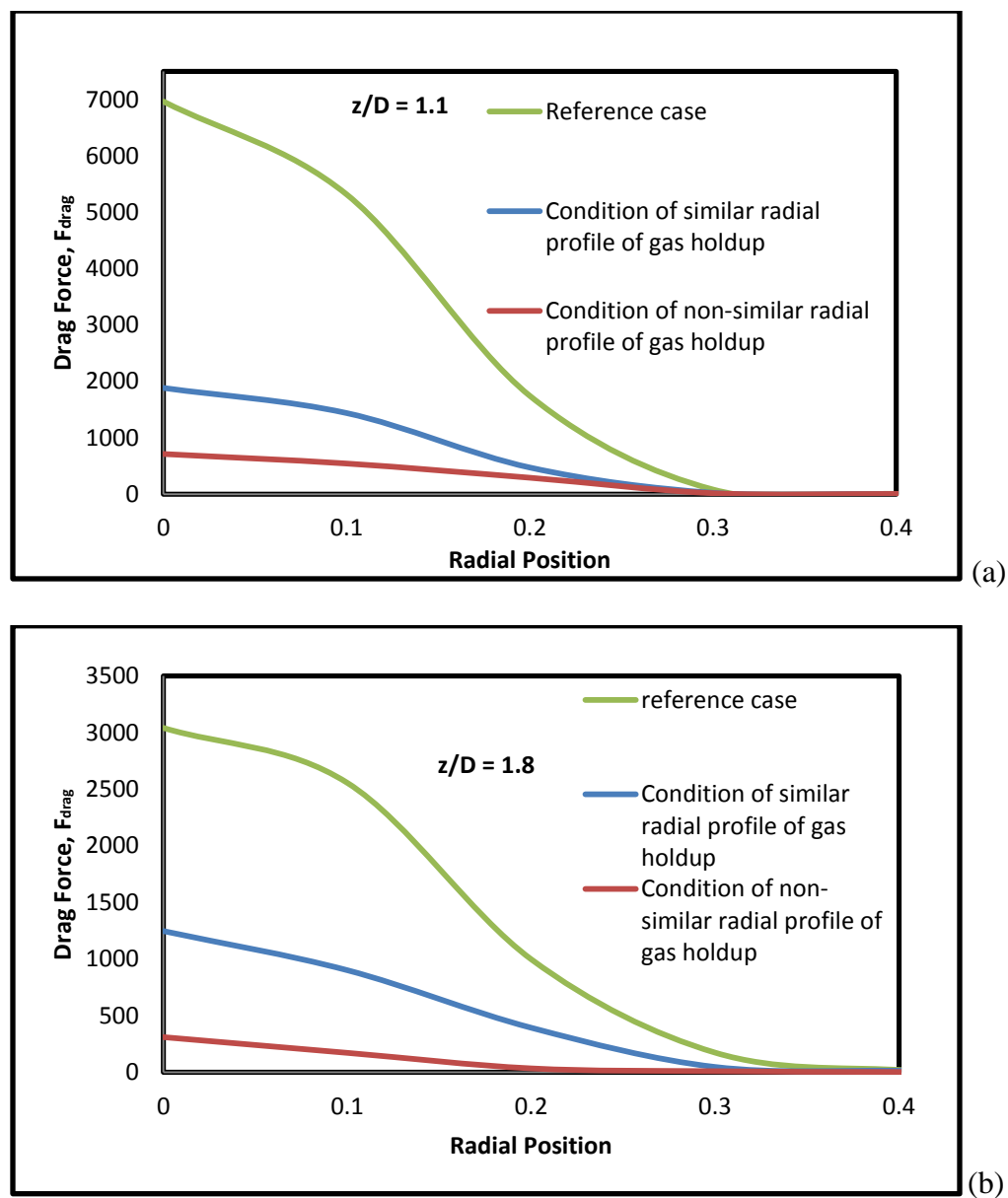
Figure 4.38. Drag force in the spout region evaluated from CFD; a. Drag force for reference case, conditions for similar and non-similar radial profiles of gas holdup at z/D = 1.1; b. Drag force for reference case, conditions for similar and non-similar radial profiles of gas holdup at z/D = 1.8.
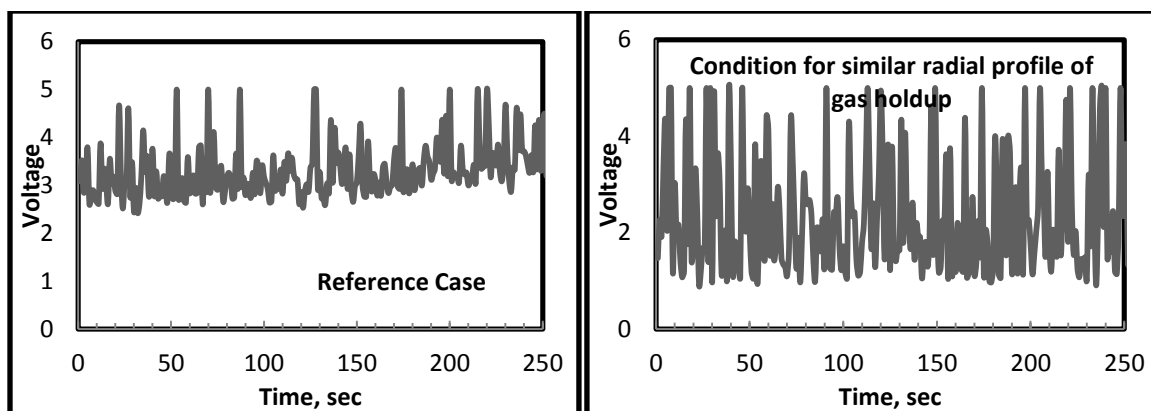
(a)   (b)

Figure 4.39. Time series fluctuations of particles velocity; a. For the reference case at z/D 1.1 with mean = 3.3 and variance = 0.31; b. For conditions of similar radial profile of gas holdup at z/D 1.1 with mean =2.31 and variance =1.3.
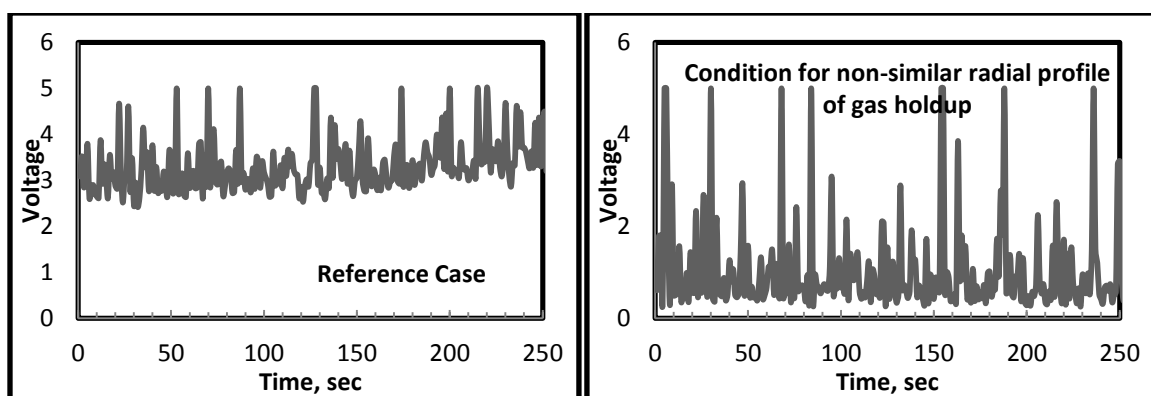
(a)   (b)

Figure 4.40. Time series fluctuations of particles velocity; a. For the reference case at z/D 1.1 with mean = 3.3 and variance = 0.31; b. For conditions of non-similar radial profile of gas holdup at z/D 1.1 with mean =1.72 and variance =0.98.

.

4.5.3. Pressure Fluctuations. The pressure fluctuations were measured using pressure transducers. The details of the pressure transducer used for the current study is explained in the earlier sections. In the present study, the pressure transducers were

attached at z/D levels of 1.1, 1.8 and 2.5 for all spouted beds. The signals were analyzed

by calculating their mean and variance. The signals from 0.152 m and 0.076 m spouted

bed were compared at z/D 1.1(Figure 4.41).

The mean and variance for 0.152 m spouted bed were 0.4276 and 0.040076,

respectively. The mean and variance for 0.076 m spouted bed at z/D 1.1 were 0.3961 and

0.03423 respectively (% deviation was 14.58%). The comparison shows that the

fluctuations in the two beds are close and the flow dynamics are also close. The

fluctuations analyzed for the levels z/D 1.8 and 2.5 are shown in Figures 4.42 and 4.43,

respectively.

(a)

(b)
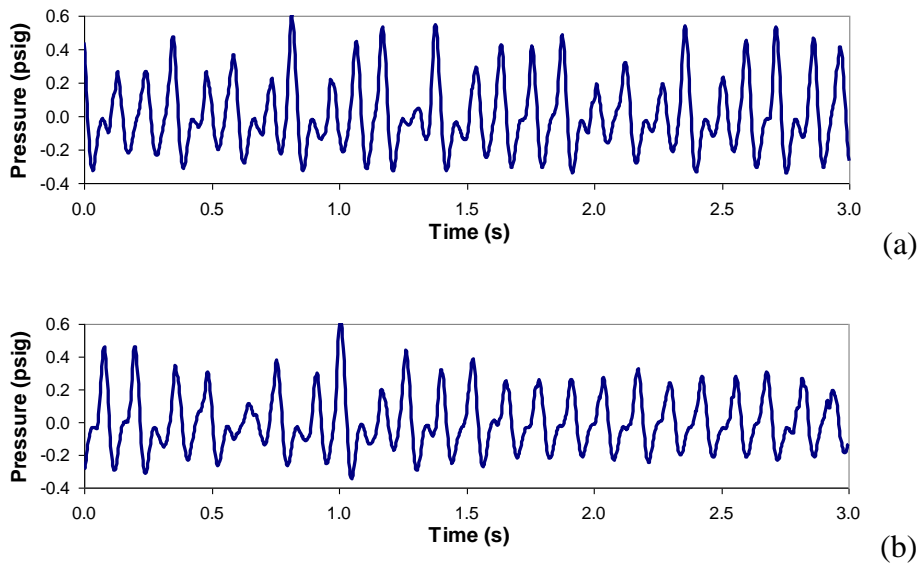
Figure 4.41. Gauge pressure fluctuations; a. Pressure fluctuation signals in 0.152 m
spouted bed at z/D = 1.1; b. Pressure fluctuation signals in 0.076 m spouted bed
at z/D = 1.1

.
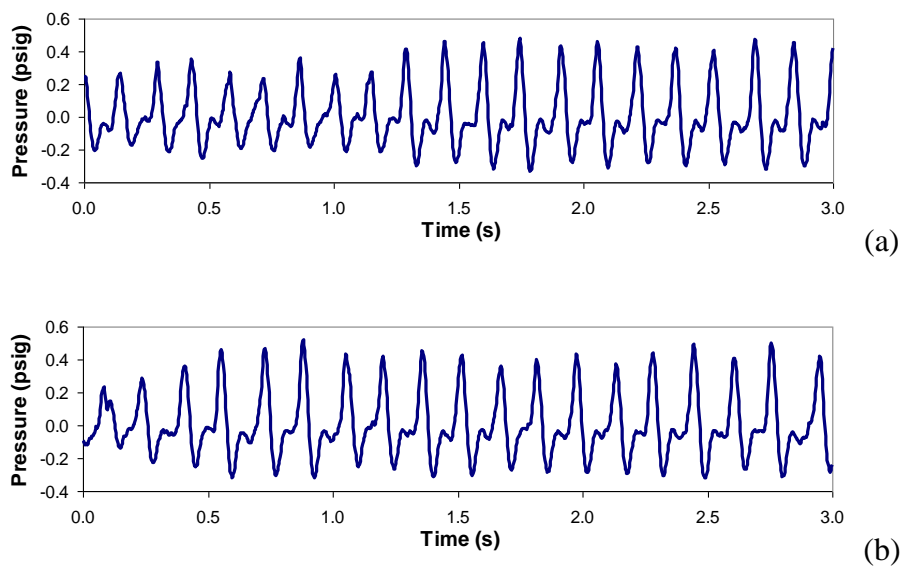
Figure 4.42. Gauge pressure fluctuations; a. Pressure fluctuation signals in 0.152 m spouted bed at z/D = 1.8; b. Pressure fluctuation signals in 0.076 m spouted bed at z/D = 1.8.
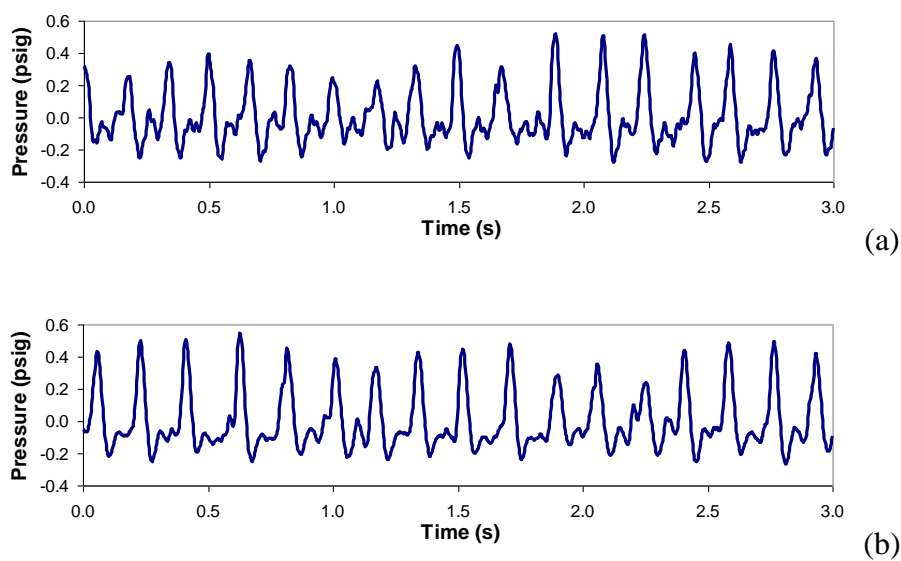
Figure 4.43. Gauge pressure fluctuations; a. Pressure fluctuation signals in 0.152 m spouted bed at z/D = 2.5; b. Pressure fluctuation signals in 0.076 m spouted bed at z/D = 2.5

The analysis of mean and variance for the two spouted beds at z/D levels 1.8 and 2.5 were performed. At z/D 1.8 the mean for 0.152 m and 0.076 m spouted beds were 0.4181 and 0.3887, respectively. The variance was 0.039677 in 0.152 m spouted bed and 0.02909 in 0.076 m spouted bed (% deviation was 13.72%). The comparison between the two beds at this level also showed closeness in pressure fluctuation profiles using the conditions for similar radial profile of gas holdup. The nature of the signals also explains the behavior of the bed. The similarity in the magnitude and frequency of the fluctuations in 0.076 m and 0.152 m spouted is obvious from the nature of the fluctuations. In the fountain region (z/D level 2.5), the pressure fluctuations were pretty close. The mean for 0.152 m and 0.076 m spouted bed was 0.2686 and 0.2577, respectively. The variance for 0.152 m and 0.076 m spouted bed was found to be 0.02934 and 0.02531, respectively (% deviation was 13.73%). This is because the fountain region is made of solids falling back onto the bed surface due to gravity and solids volume fraction in this region is pretty close. The analysis of conditions for non-similar radial profile of gas holdup had huge difference in the fluctuations and accounted for an absolute relative difference of 29.1%.

Pressure profiles were measured for the two spouted beds for both the conditions. The pressure transducers were attached to the spouted bed at different heights and the pressure measurement was measured. The overall bed pressure drop was also measured using the pressure transducer by taking readings before the gas inlet and at the outlet of the spouted bed. In order to compare the profiles, they were dimensionalized by dividing the pressure values at each measurement plane by the overall pressure drop of the bed. Figure 4.44 shows the profile, which shows that the conditions for similar radial profile of gas holdup had a close profile to the reference case and the absolute relative difference

was 13.4%. For the conditions for non-similar radial profile of gas holdup the difference

was 26.4%.
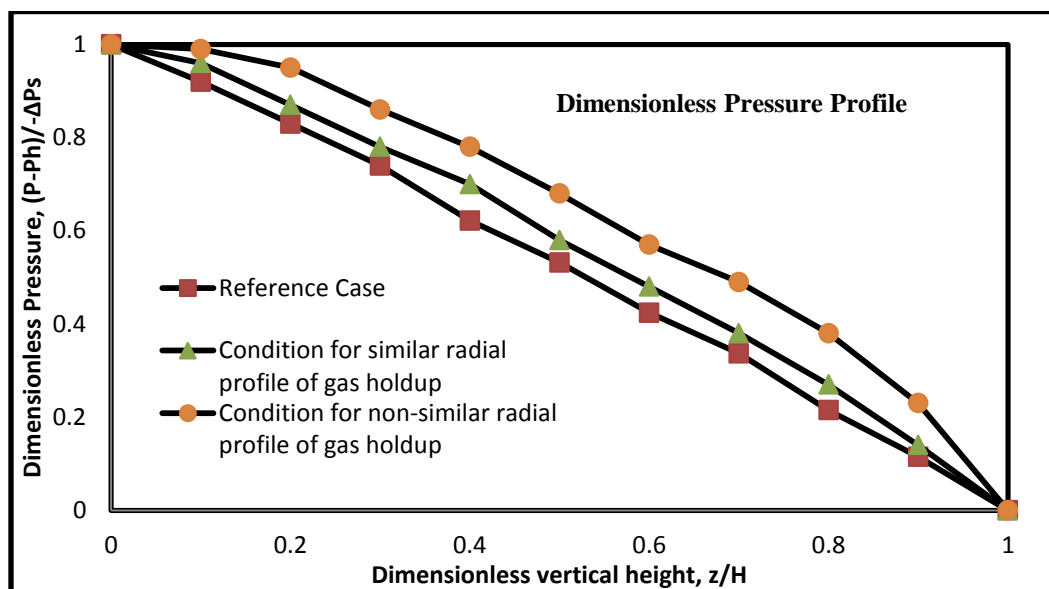
Figure 4.44. Dimensionless pressure profile for the conditions of similar and non-similar
radial profiles of gas holdup measured experimentally using pressure transducers.

4.5.4. Spout Diameter, Fountain Height and Maximum Spoutable Bed Height. Global parameters such as dimensionless fountain height, dimensionless spout diameter, and maximum spoutable bed height was measured for the conditions of similar and non-similar radial profile of gas holdup. The spout diameters (D_s) were measured using optical probes (Figure 4.45). The probes work on back reflection of light, and the reflection of light is dependent on the number of particles in front of the probe. Since there is large or significant difference in the degree of solids in spout and annulus, distinct signals are obtained in these zones. The probe is first placed in the center of the

bed and slowly moved towards the wall. The point where there is distinct change in the signal that point is marked and the distance was noted. Fountain height (H_F) is the maximum height of solids achieved in the spouted bed. The initial bed height is marked and then when the spouted bed is operated under the conditions of the experimentation, the maximum height reached by them is noted. Thus fountain height is measured. Maximum spoutable bed height (H_m) refers to the maximum amount of solids that a bed can accommodate beyond which the spouting does not occur. It can also be termed as the amount of solids the spouted bed can process at a time. To measure this, the initial bed height of spouted bed was increased very gradually in small increments until the spouting in bed did not occur. The bed height at that point was noted to be the maximum spoutable bed height.

All the above parameters were also in close agreement with each other for the condition of similar radial profile of gas holdup. For the conditions of non-similar radial profile of gas holdup the deviations were found to large. Table 4.6 gives the detail list of the dimensionless parameters and their corresponding deviations with the reference case.
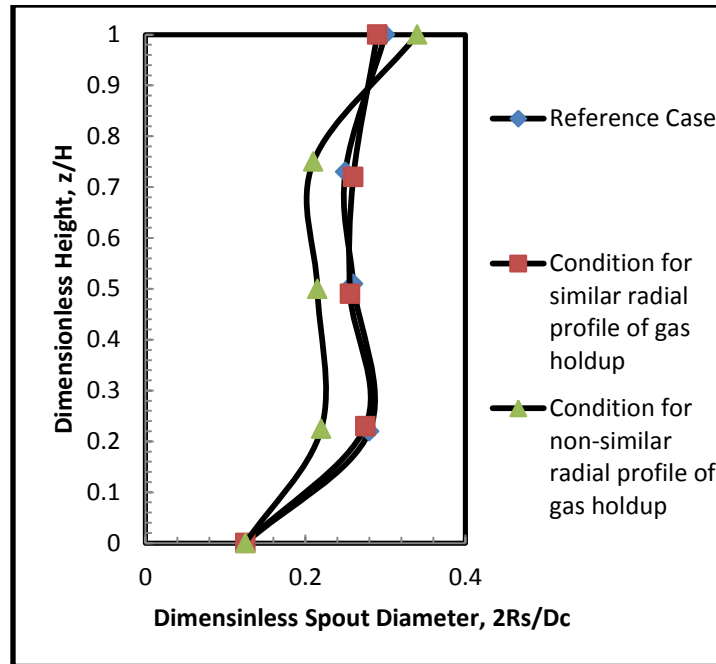
Figure 4.45. Dimensionless spout diameter versus dimensionless height.

Table 4.6. Dimensionless spout diameter and fountain height for the conditions of similar and non-similar radial profile of gas holdup.

Case	Reference Case	Conditions For Similar $(\varepsilon_g)_r$	Conditions For Non-Similar $(\varepsilon_g)_r$
Column diameter, D_c (m)	0.152	0.076	0.076
Mean Spout diameter, D_s (m)	0.045	0.024	0.0211
Fountain Height, H_F (m)	0.135	0.059	0.044
Dimensionless Spout diameter, D_s/D_c	0.27	0.28	0.277
Deviation %	-	+3.5	+6.5
Dimensionless Fountain Height, H_f/D_c	0.89	0.78	0.58
Deviation %	-	-12.3	-34.8
Maximum spoutable bed height, H_m (m)	396	195	240
H_m/D_c	2.6	2.56	3.15
Deviation (%)	-	-1.5	-21.2

The analysis of local and global parameters for the two spouted beds using the conditions of similar and non-similar radial profile of gas holdup has been reported. It is observed that the radial profiles of gas holdup in the two spouted beds were maintained close using the newly identified conditions of similar radial profile of gas holdup. The condition of non-similar radial profile of gas holdup was assessed to demonstrate that even though there is geometrical similarity in the compared spouted beds, the radial profiles of gas holdups could not be maintained close or similar. The hypothesis "*Radial profile or cross sectional distribution of gas holdup or solids holdup should be the same or close for two beds particularly in the spout region to be hydrodynamically similar or close*", can be said to be true in the present study.

The analysis of the absolute particles velocity profiles for both the conditions were not similar. But when the radial profiles were dimensionally represented (U/U_{ms}) the velocity profiles were close for condition of similar radial profile of gas holdup and had large deviations for condition of non-similar radial profile of gas holdup. Based on this, U/U_{ms} ratio can be used as a scaling criterion to predict the absolute velocity profiles in different spouted beds, provided the base conditions is maintained. The dimensionless group approach of He et al. (1997) is based on maintaining the same values of different dimensionless group in the two different spouted beds, poses a practical challenge. It is very hard to match all the dimensionless groups experimentally in different spouted beds, where the U/U_{ms} criterion should be helpful. Since there are many correlations available in open literature to predict U_{ms} depending on the spouted bed geometry, the absolute particle velocity profiles can be determined using the U/U_{ms} scaling criterion and thereby predicting the spouted bed hydrodynamics.

4.6. GAMMA RAY DENSITOMETRY (GRD) FOR ON-LINE MONITORING

Gamma ray densitometry (GRD), a non-invasive radioisotope based technique, was developed for on-line monitoring of the developed scale-up methodology and flow regime identification. This section deals with the use of GRD for monitoring on-line the gas/solids holdup profiles in the spouted beds. GRD consists of a sealed source (Cesium 137 of 250 mCi) in a source holder and a NaI scintillation detector in front of the source. The source holder is mounted on one side of a column, with the detector on the opposite side. A focused beam of radiation is transmitted from the source, through the column and process material, to the detector. As the density of the material in the column changes, the amount of radiation reaching the detector changes accordingly. It is generally believed that the amount of radiation that reaches the detector through the process material is reflective of its flow behavior and properties. Figure 4.46 shows the GRD with a source and a detector in front of it. The beam of γ-rays coming from the sealed source is made such that it provides a point beam, which was custom made for the requirements of measurement by Tracer Co Company (El Paso, Texas). The details of development, electronics and operation of GRD are discussed in Section 6.

The first step in obtaining holdup distribution profile is to obtain the attenuation profile from the raw scanned data. The attenuation (μ) profile of any object is quantified by the Beer Lambert's Law as follows.

$$I = I_0 . \exp(-\mu \rho l) \tag{5}$$

$$\ln \frac{I}{I_0} = -\mu \rho l = -A \tag{6}$$

$$A = \mu \rho l \tag{7}$$
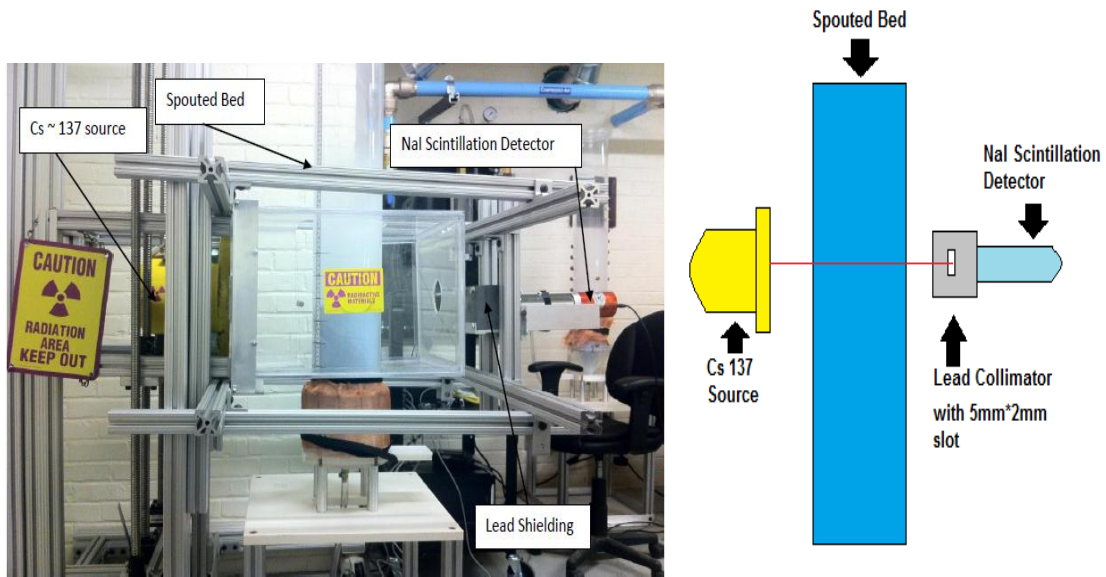
(a)   (b)

Figure 4.46. GRD technique; a. Applied on 0.152 m spouted bed and b. Schematic representation of GRD

Where, I_o is the intensity of incident radiation, I is the intensity of detected radiation, μ is the mass attenuation coefficient, ρ is the medium density and l is the path length through the medium. If the medium is made of two materials (such as solids and gas in this case) with mass attenuation coefficients μ_s for solids and μ_g for gas, ρ_s for solids density and ρ_g for gas density, and l_s for solids thickness and l_g for gas, then the total attenuation parameter A is

$$A = \rho_s \mu_s l_s + \rho_g \mu_g l_g \tag{8}$$

Since $l_s = \varepsilon_s L$ and $l_g = \varepsilon_g L$, where $L = l_s + l_g$ then

$$A = \left[\rho_s \mu_s \varepsilon_s + \rho_g \mu_g \varepsilon_g\right] L \tag{9}$$

The summation of the holdups is equal to unity (i.e. $\varepsilon_g = 1 - \varepsilon_s$). Hence equation 13 becomes

$$A = \left[\rho_s \mu_s \varepsilon_s + \rho_g \mu_g \left(1 - \varepsilon_s\right)\right] L \tag{10}$$

Accordingly,

$$\ln \frac{I}{I_0} = -A = -\left[\rho_s \mu_s \varepsilon_s + \rho_g \mu_g \left(1 - \varepsilon_s\right)\right] L \tag{11}$$

The measured quantity $\ln$ *(I/Io)* is equal to the integral sum of the attenuation through the material along the beam path. The total line attenuation $A_{s\text{-}g}$, can be written as

$$A_{s-g} = \left[\rho_s \mu_s \varepsilon_s + \rho_g \mu_g \left(1 - \varepsilon_s\right)\right] L \tag{12}$$

Where ε_s and ε_g are the holdups (volumetric fractions) of the solid and gas phases respectively, and L is the length along which a particular gamma ray beam passes through the column.

Since $\rho_g \ll \rho_s$, the attenuation caused by the gas phase is negligible compared to solids and L is common for all A's. Hence, solids holdup for the line averaged measurement can be written as follows

$$\varepsilon_s = A_{s-g} / L \rho_s \mu_s \tag{13}$$

Where,

$$A_s = \rho_s \mu_s \varepsilon_s L \tag{14}$$

The linear attenuation coefficient of solids (μ_s) was determined by using standard tables (such as NIST Physical Data) since the material composition of solids was known. Conditions listed for Case A were used to measure the radial profile of gas and solids holdup shown in Figure 4.47 and 4.48 respectively. The measurements were performed for z/D level of 1.8. Since GRD measurements are very extensive both experimentally

and for holdup measurement, one level of measurement was performed to demonstrate the capability of GRD technique for use of on-line monitoring. The measurements of the GRD were compared with the measurements performed by the optical probe (Figure 4.49). The comparison of the two techniques showed good agreement with each other. Hence, GRD becomes a more powerful and reliable technique for online measurement and monitoring.
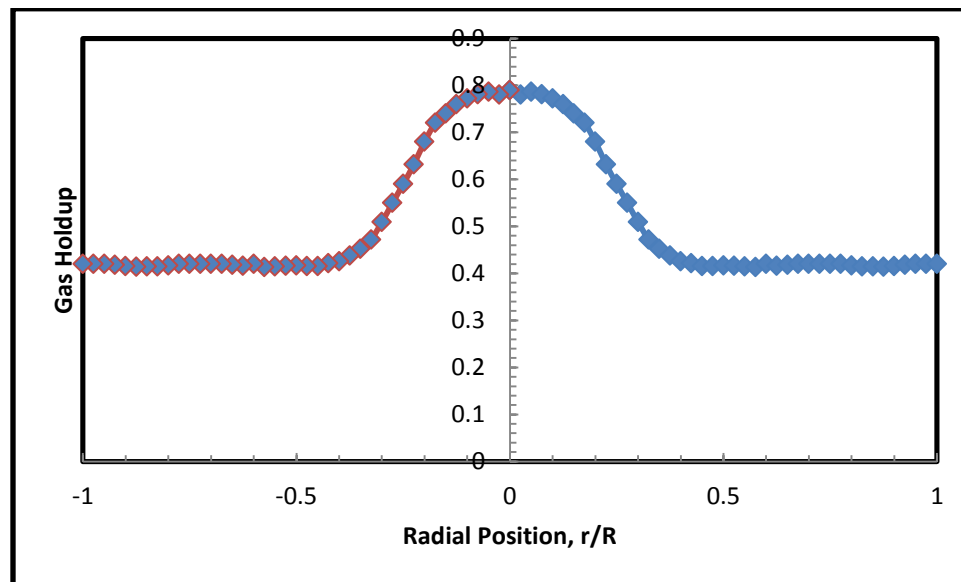
Figure 4.47. Radial profile of gas holdup measured using GRD technique for the conditions of reference case listed in Table 4.5 at z/D level 1.8.
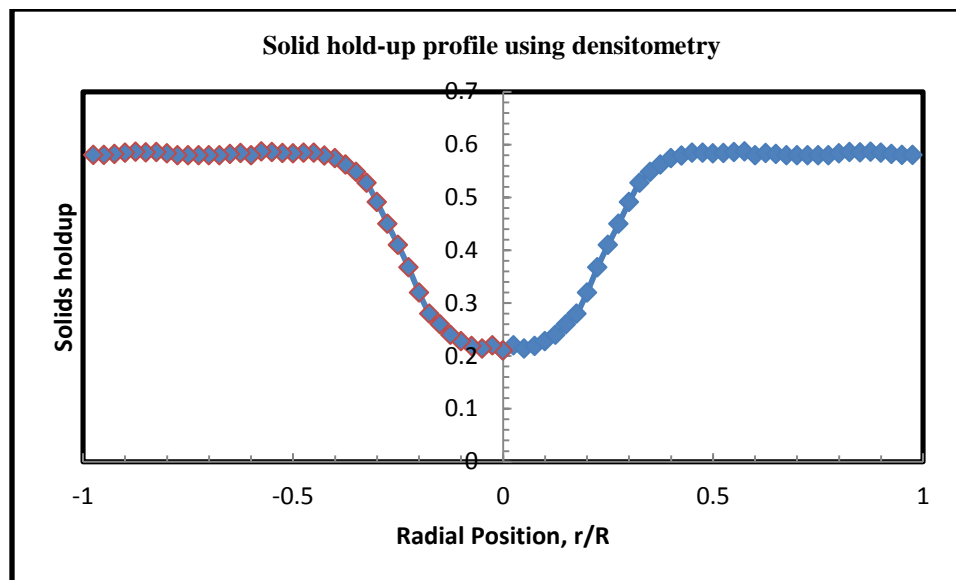
Figure 4.48. Radial profile of solids holdup measured using GRD technique for the conditions of reference case listed in Table 4.5 at z/D level 1.8.
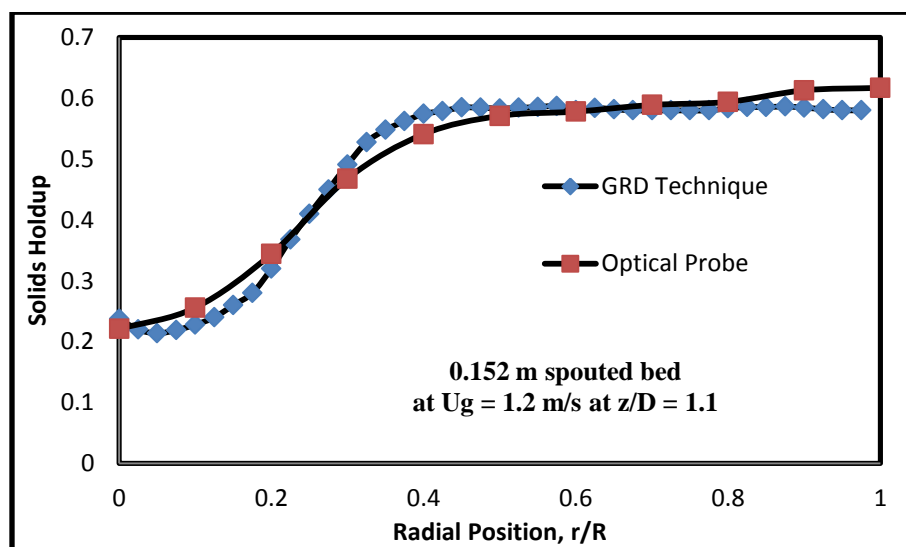
Figure 4.49. Comparison of radial profile of solids holdup for GRD and optical probe technique in a 0.152 m ID spouted bed at Ug = 1.2 m/s using glass beads of 2 mm diameter (2450 Kg/m^3) as solids phase at z/D 1.8.

4.7. REMARKS

Based on a comprehensive review of reported scale-up procedures in literature, the current work proposes a successful new hypothesis for similarity in flow dynamics of two different spouted beds by maintaining the radial profiles of gas holdup similar. The dimensionless groups approach was first assessed for local (solids and gas holdup, solids velocity and solids mass flow) and global (pressure fluctuations, spout diameters, fountain height and maximum spoutable bed height) parameters for the match and mismatch conditions reported by He et al. (1997). It was observed that the global parameters were in close agreement with each other for the studied match conditions, but the local parameters were different in the two spouted beds.

Limitations of the dimensionless groups approach motivated the proposal of a new hypothesis based on maintaining same or close radial profiles or cross sectional distribution of gas holdup or solids holdup in the two spouted beds. Two conditions were identified with respect to a reference case, conditions for similar and non-similar radial profiles of gas holdup. CFD was used as an enabling tool to identify these conditions initially. The condition for non-similar radial profiles of gas holdup was identified to demonstrate the deviation in radial profiles even if the geometric similarity is held similar in both the beds. The condition for similar radial profiles of gas holdup identified had the same or close radial profiles of gas holdup in the two different spouted beds, which proved the hypothesis of hydrodynamics similarity proposed by maintaining similar radial profiles. The assessed global and local parameters were in close agreement with each other. Based on the discussion of results, it was found that U_{ms} plays an important role, especially when the

radial profiles are dimensionally represented. Hence, U/U_{ms} can be used as a scaling criterion to predict the hydrodynamics of different spouted beds, if U_{ms} is estimated.

The validation of the new methodology motivated the development of Gamma ray densitometry (GRD), a non-invasive radio-isotope based technique, to monitor on-line the radial profiles of gas holdup. It was demonstrated that GRD had the capability to monitor on-line such profiles. Industrial reactors often vary from the laboratory scale reactors; hence the applicability of the proposed hypothesis needs to be checked in such systems.

5. INVESTIGATING THE EFFECT OF DESIGN AND OPERATING VARIABLES ON SOLIDS VELOCITY AND SPOUT DIAMETER

The work presented in this section can be divided into two parts based on the parameters investigated. The first part deals with studying the effect of different conical base angles and gas velocities on solids velocity in three different parts of the spouted bed (spout, annulus and fountain regions) using optical probes and validated computational fluid dynamics (CFD, Section 7). The second part focuses on studying the effect of solids density, static bed height, particle diameter, gas inlet diameter, superficial gas velocity and various combination of these on spout diameter. Factorial design of experiments was used in order to find the key parameters, among the above mentioned ones, which have a significant influence on the spout diameter. Based on the results of the factorial design of experiments approach, a new correlation was developed to identify the spout diameter in spouted beds.

5.1 SOLIDS VELOCITY IN SPOUT, ANNULUS AND FOUNTAIN REGIONS

Understanding of the solids flow pattern in spouted beds is of great interest for the design, scale-up and operation of spouted beds, because solids trajectories and residence time should fit the requirements of the process carried out. Solids flow investigation has been performed in different bed zones by many researchers using mainly optical probes and limited attempts using wire mesh tomography, radioactive particle tracking etc. (Huilian et al., 2004; Wang et al., 2009; Dan .S et al., 2010; Chaouki et al., 1994; Ricardo et al., 1995; Maria et al., 1998; Olzar et al., 2001). It has been confirmed that the particles

in annulus move downwards and radially inwards, describing approximately parabolic paths (He et al., 1992) as shown in Figure 5.1. It has also been reported that the spout region is straight and the movement of solids from the annulus region to the spout region occurs along the height of the spout (Esptein and Grace, 2011). However, further study of solids velocity is needed to advance the understanding of spouted beds. In the current study, the vertical and horizontal components of solids velocity has been studied using optical probes and CFD, for different conical bases and gas velocity in cylindrical spouted beds and the flow pattern in different regions of the bed.
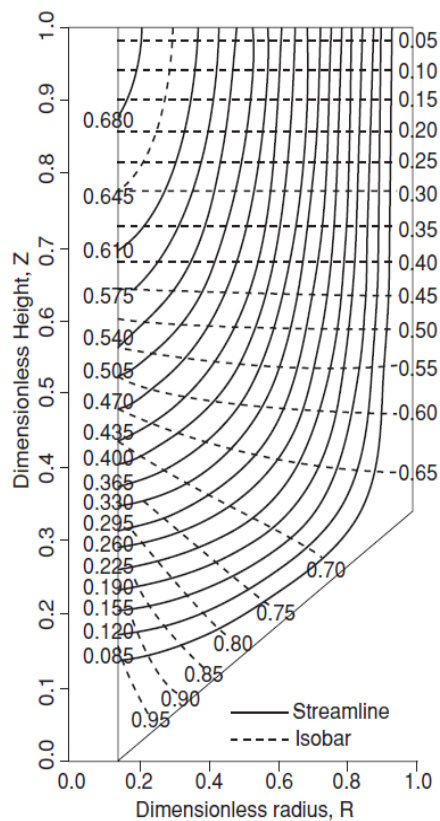
Figure 5.1. Fluid flow distribution in a spouted bed (He et al., 1992)

In the current study, 0.152 m ID spouted bed was used for experimentation purposes. Keeping in mind the experimental and computational time, only one configuration of bed geometry was studied. The detailed dimensions of the bed are discussed in Section 4. Three different conical angles (30^0, 45^0 and 60^0) were used in this study. The solids phase used was glass beads of 1mm in diameter. Three different gas velocities (1.1 U_{ms}, 1.2 U_{ms} and 1.3 U_{ms}) were used and the gas phase used was compressed air. Optical probes were used to measure vertical component of the solids velocity experimentally and Computational Fluid Dynamics (CFD) was used after it has been validated (Section 7) to estimate the vertical and horizontal components of the solids velocity. To measure horizontal component of solids velocity, the placement of optical probe would have been such that it would affect the flow dynamics of the spouted bed, and hence was not used. The CFD simulation results were compared with the vertical component of solids velocity obtained by the optical probe. The details of the optical probe and solids velocity calculation are discussed in Section 3. The details of the CFD simulation models and procedures will be discussed later in Section 7.

5.1.1 Vertical Component of Solids Velocity.

5.1.1.1. Experimental data and correlation predictions. The general correlation used to calculate the vertical component of the solids velocity was proposed by Mathur and Epstein (1978) and is given by equation 1.

$$v_z = v_0 \left[1 - \left(\frac{r}{r_s} \right)^2 \right] \tag{1}$$

Where, v_z is the vertical component of solids velocity, v_0 is the solids velocity at the spout axis (center of the bed), r is the radial coordinates and r_s is the radius of the

spout at a given level of measurement. Due to deviations in the prediction of the solids velocity, Epstein and Grace (1984) came up with a more generalized form shown in equation 2.

$$v_z = v_0 \left[1 - \left(\frac{r}{r_s} \right)^m \right]$$ (2)

Where, m is based on the bed geometry and has a value between 1.3 and 2.2.

Olzar et al. (2001) modified the above equation by suggesting a value for "m" using non-linear regression analysis performed in a cone based cylindrical spouted bed with different conical base angles ranging from 30^0 to 120^0. This was proposed due to the observed variations between the experimental and correlation results. The proposed equation is given by equation 3.

$$m = 2.0 + (m_0 - 2) \exp(-100z^2)$$ (3)

$$m_0 = 13.3 \left(\frac{d_p}{D_c} \right)^{0.20} \left(\frac{H_0}{D_c} \right)^{-0.16} \left(\frac{U}{U_{ms}} \right)^{0.45} \gamma_b^{-0.09} \exp\left(\frac{-5.11D_0}{D_c} \right)$$ (4)

Where, z is the level of measurement in the spouted bed.

v_0 is the solids velocity at the spout axis (center of the bed). There are no correlations that predict the solids velocity in the spout axis. Hence, it is difficult to estimate the vertical component of solids velocity using equation 2 without knowing v_0. In the present study, the value of v_0 was obtained from CFD simulations and then equation 2 was used to estimate the solids velocity and compared with that measured by optical probe. Figure 5.2 shows the vertical component of solids velocity measured by optical probe and that predicted by equation 2. The predictions of equation 2 had the same trend for solids velocity of those obtained by optical probe in the spout region, but

had deviations of 20.5% overall. In this work, non-linear regression was performed to fit the experimental data obtained using 0.152 m ID spouted bed to the equations 3 and 4 (Figure 5.3). The new set of correlations obtained in this work is as follows

$$v_z = v_0 \left[1 - \left(\frac{r}{r_s} \right)^m \right] \tag{5}$$

$$m = 1.86 + (m_0 - 1.57) \exp(-89z^2) \tag{6}$$

$$m_0 = 7.15 \left(\frac{d_p}{D_c} \right)^{0.34} \left(\frac{H_0}{D_c} \right)^{-0.52} \left(\frac{U}{U_{ms}} \right)^{1.03} \gamma_b^{-0.14} \exp\left(\frac{-1.45D_0}{D_c} \right) \tag{7}$$

The regression gave an $r^2 = 0.94$ with an error $< 8\%$. Although the predictions of the modified correlations are much better than those of Olzar et al. (2001), there are still differences between the predicted and the measured values particularly on the bottom sections of the spouted bed. Again in this case validated CFD has been used to estimate the center line velocity, v_0. Due to such difference in prediction and since CFD has been used to estimate v_0, in the following section validated CFD will be used along with experimental data to study the effect of conical base angle and gas velocity on vertical and horizontal components of solids velocity.

5.1.1.2. Experimental data and cfd predictions. In the present study, vertical components of solids velocity was measured in a 0.152 m spouted bed with one height of conical section ($H_0 = 0.121$ m). Measurements were taken at six different axial locations using optical probes. Experiments were done to confirm the closeness of CFD simulations. The measured solids velocity for 30^0, 45^0 and 60^0 conical bases at different axial heights and at $1.1U_{ms}$ is shown in Figures 5.4, 5.5 and 5.6 respectively. With the results presented later it is obvious that using CFD provide more reliable estimation.
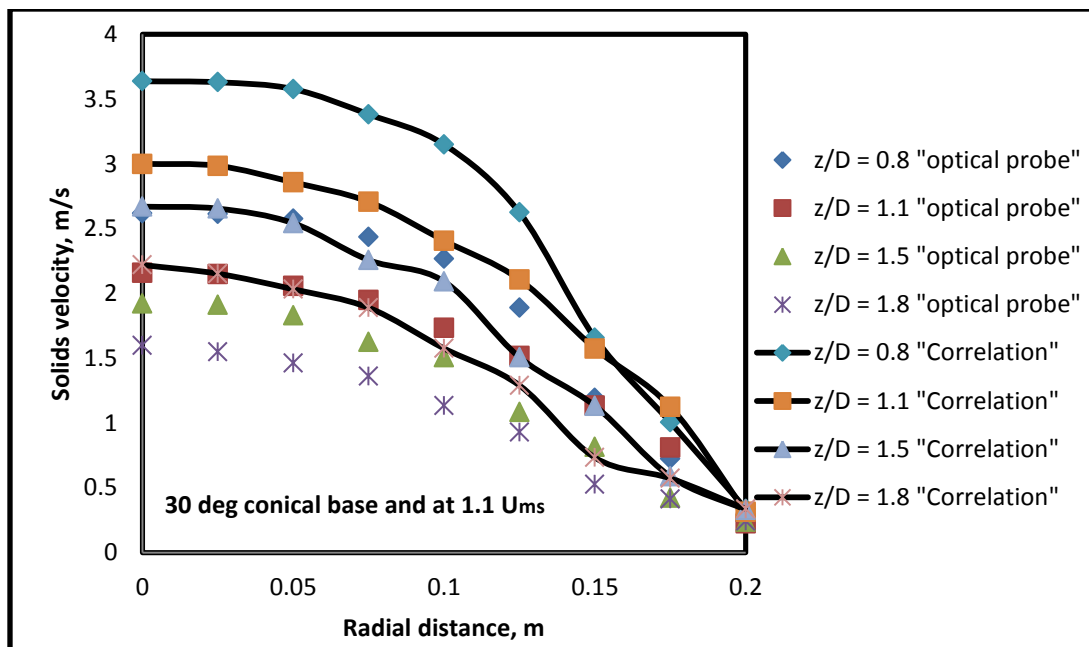
Figure 5.2. Vertical component of solids velocities measured by optical probe and those predicted by Olzar et al. (2001) correlation.
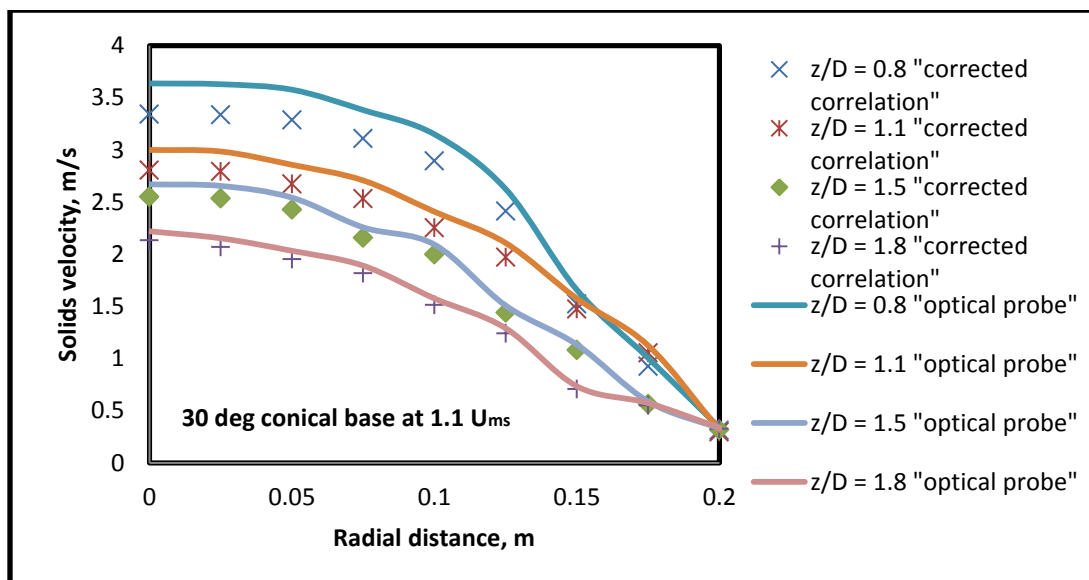
Figure 5.3. Vertical component of solids velocities measured by optical probe and those predicted by the modified correlation of this work.

The velocity of solids follow the same trend as reported in the literature and in Section 4 of this thesis. The velocity is maximum at the center of the spout as the solids are being carried by the jet of gas. The velocity then decreases to zero near the spout-annulus interface. With the increase of the gas velocity (1.2 U_{ms} and 1.3 U_{ms}), the magnitude of the velocity profiles at different heights increased, but the trend remains the same. The solids velocity is maximum at the inlet of the spouted bed and reduces as the axial height in the spouted bed increases. The gas entering the bed from the bottom has very high velocity and hence the solids are carried with high velocities at this point. As the gas penetrates the bed of particles in the higher regions of the bed, the velocity of the gas reduces and hence the solids velocity decreases. Such variation is observed in the spout region of the spouted bed.
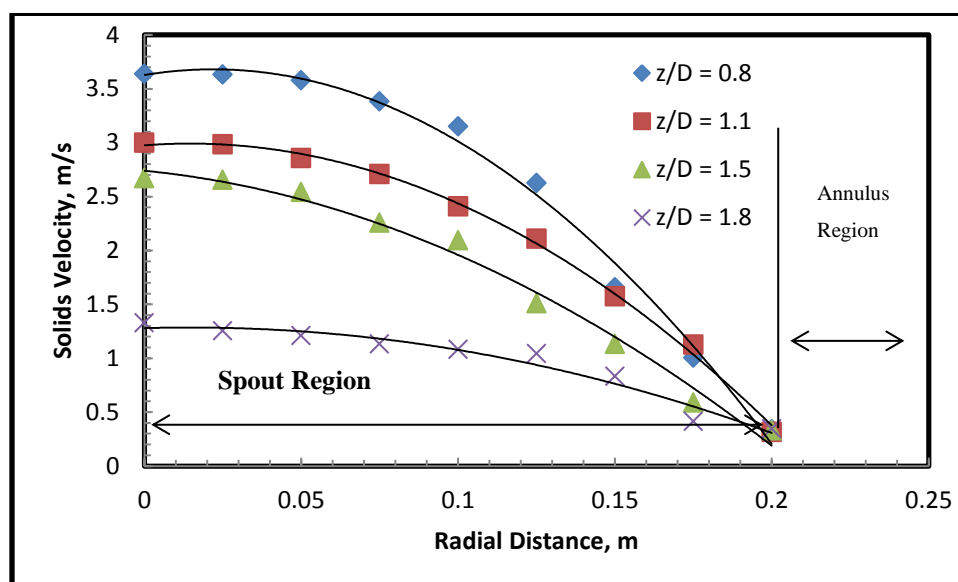
Figure 5.4. Optical probes (points) versus CFD simulation (lines) for vertical component of solids velocity in spout region at 1.1 U_{ms} for a 30^0 conical base angle for glass beads of 1 mm in diameter at different z/D levels.
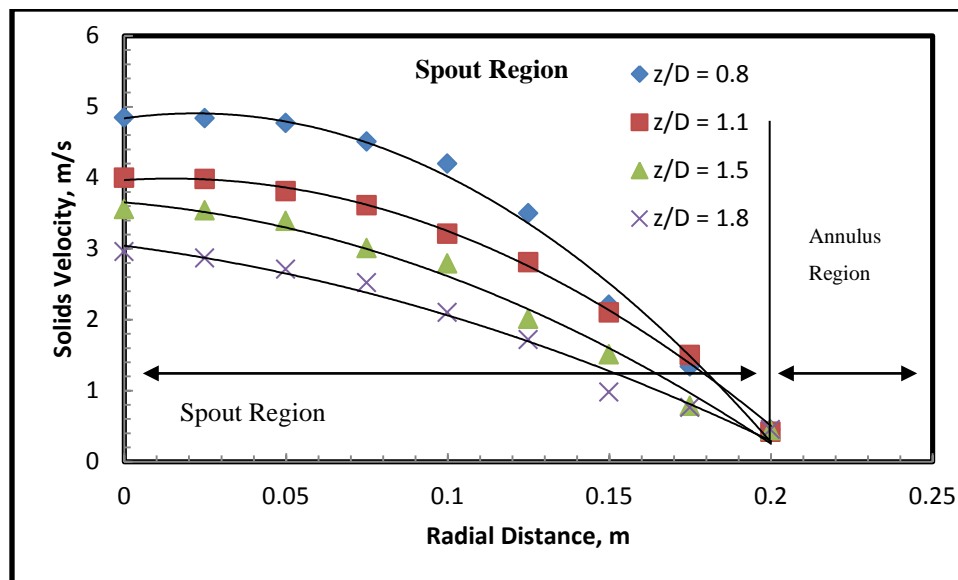
Figure 5.5. Optical probes (points) versus CFD simulation (lines) for vertical component of solids velocity in spout region at 1.1 U_{ms} for a 45^0 conical base angle for glass beads of 1 mm in diameter at different z/D levels.
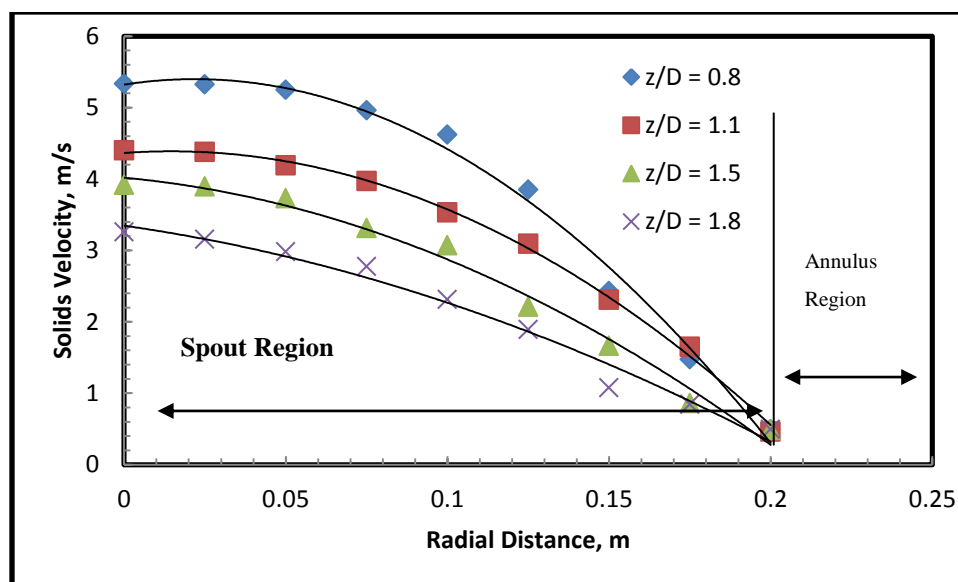
Figure 5.6. Optical probes (points) versus CFD simulation (lines) for vertical component of solids velocity in spout region at 1.1 U_{ms} for a 60^0 conical base angle for glass beads of 1 mm in diameter at different z/D levels.

The comparison of the simulated solids velocity with the experimental results was close. The average difference between the profiles of the experimental and simulated results was 9.15%. This showed that the optical probe used for experimental measurement and CFD simulations had close agreement to predict the flow behavior in the spouted bed. Conical base angle of spouted bed has great influence on the hydrodynamics of the bed. To study the influence of the conical base angle three different base angles were studied in the present work. It was observed that the solids velocity increased when the conical base angle increased from 30^0 to 45^0, but decreased when it was increased from 45^0 to 60^0 (Figures 5.7 and 5.8). This trend remains the same all along the height of the spouted bed and even when the gas velocity is increased, thus indicating the influence of conical base angle. For convenience, results of z/D level of 1.5 at different gas velocities have been shown here.
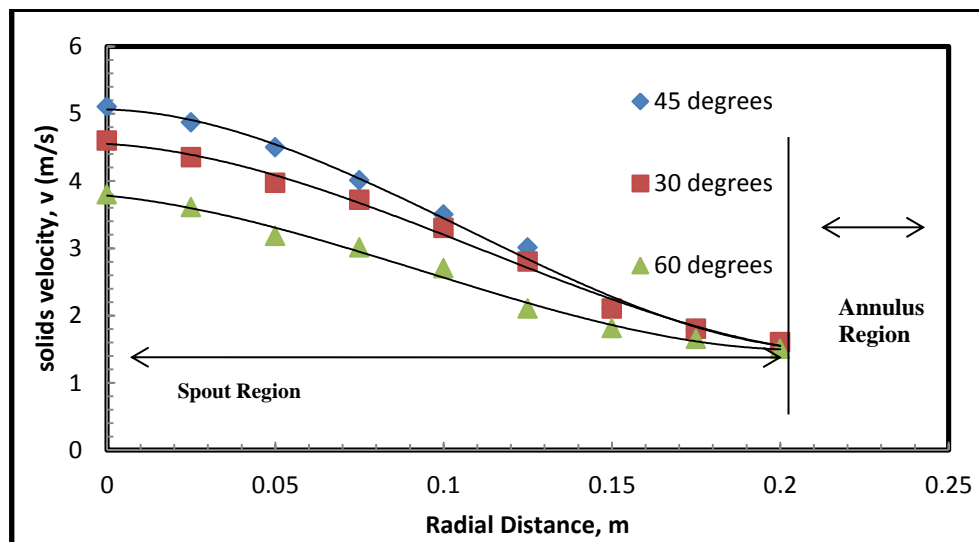
Figure 5.7. Vertical component of solids velocity for different conical base angles at 1.1 U_{ms} for glass beads of 1 mm in diameter at z/D = 1.5 using optical probe (points) and CFD (lines).
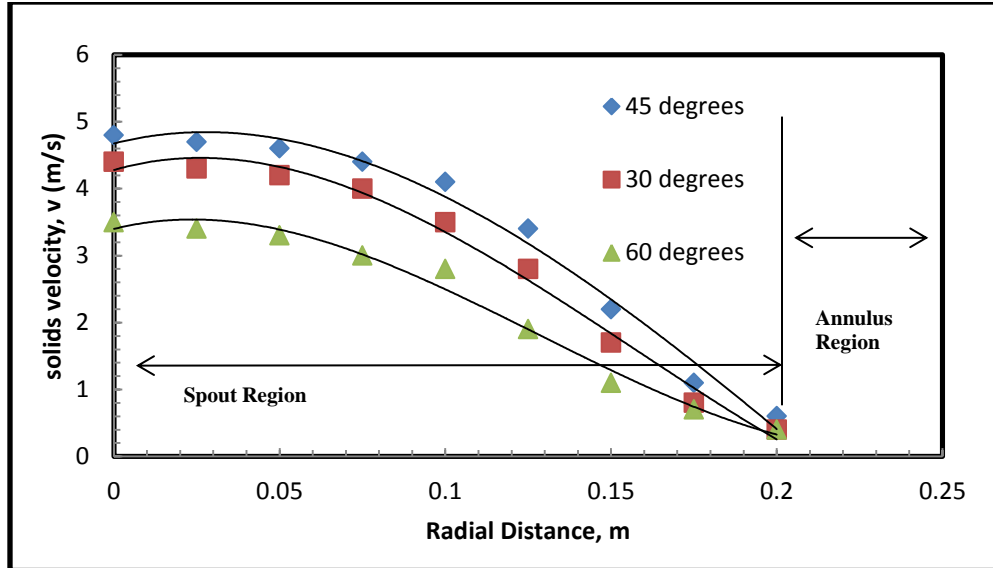
Figure 5.8. Vertical component of solids velocity for different conical base angles at 1.2 U_{ms} for glass beads of 1 mm in diameter at z/D = 1.5 using optical probe (points) and CFD (lines).

The solids velocity in the annulus and fountain regions needs to be measured as well to determine the solids movement in the spouted bed. In the center of the spout region the solids velocity starts at a maximum and then decreases until it reaches the spout-annulus interface. In the annulus, the solids are moving down as a loose packed bed slowly and slightly inward. The velocity is negative because the solids are moving down and into the spout region (Figure 5.9). The velocity in the annulus negatively increases to a higher value and then decreases negatively near the wall. This trend is seen in all the three different conical base angles. This decrease in solids velocity near the spout-annulus interface can be attributed to the solids influx into the spout region from the annulus. Simulated results had an overall deviation of 15.4% from the experimental values.
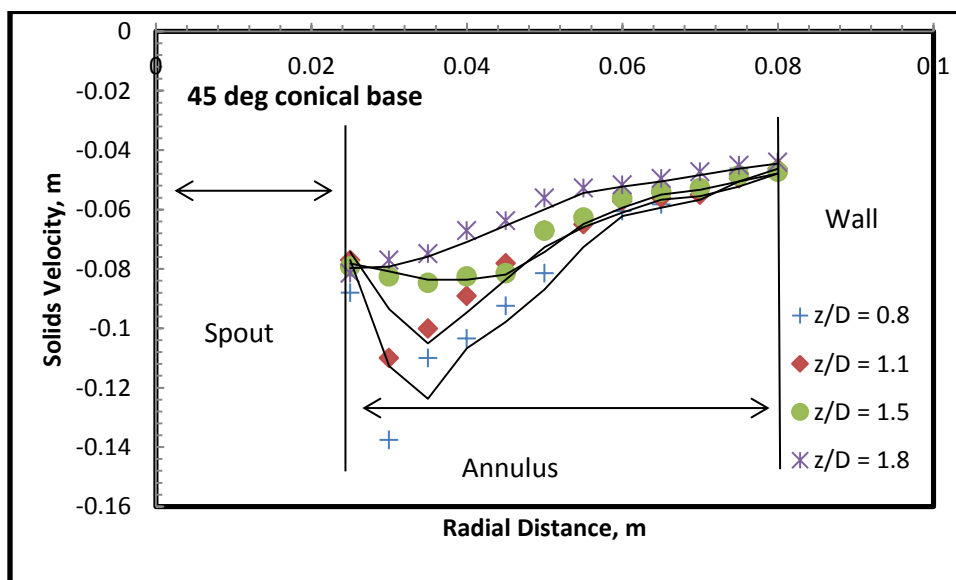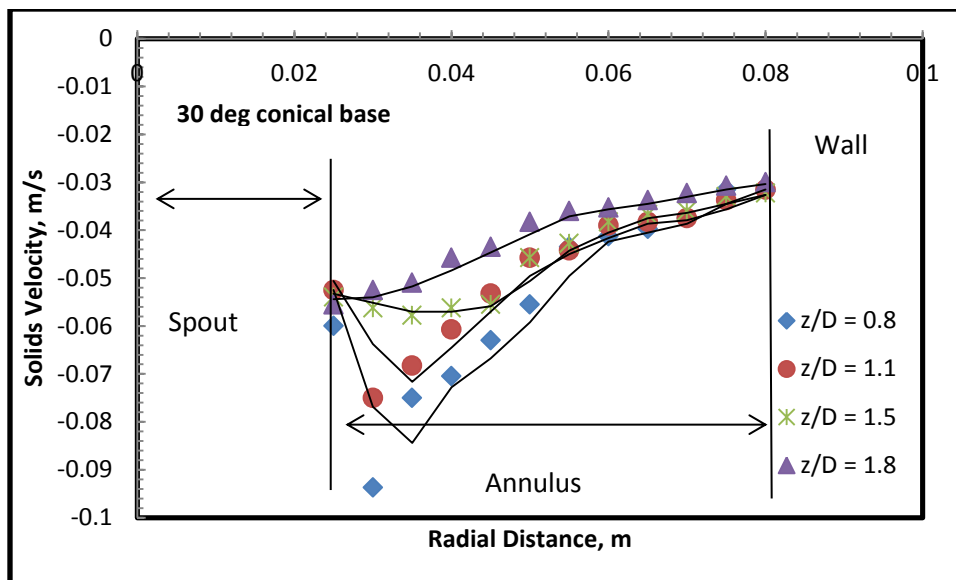
Figure 5.9. Optical probe (points) versus CFD simulation (lines) for vertical component of solids velocity in annulus region at 1.1 U_{ms} for a 30^0, 45^0 and 60^0 conical base angles for glass beads of 1 mm in diameter at different z/D levels.
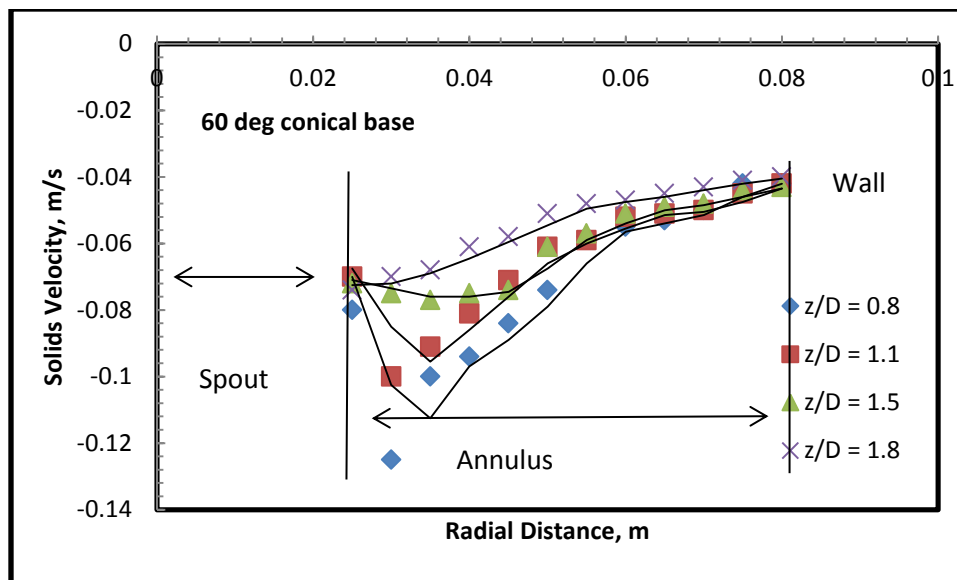
Figure 5.9. Optical probe (points) versus CFD simulation (lines) for vertical component of solids velocity in annulus region at 1.1 U_{ms} for a 30^0, 45^0 and 60^0 conical base angles for glass beads of 1 mm in diameter at different z/D levels, cont.

In the fountain region, the solids picked up by the incoming gas reached the top of the spouted bed and forms the fountain. The solids then fall back onto the bed surface due to gravity. The solids velocity has a maximum value at the center of the bed and then gradually reduces as it reaches the wall (Figure 5.10). This trend was seen in all the three different conical angles. The comparison of experimental (optical probe) and CFD simulation results showed an overall deviation of 15.3%. From the results analyzed for the three regions of spouted bed, it is observed that the conical base angel has an influence on the solids velocity. The general trend shows that the magnitude of velocity increases with the increase of base angel from 30^0 to 45^0 and then decreases when increased from 45^0 to 60^0.
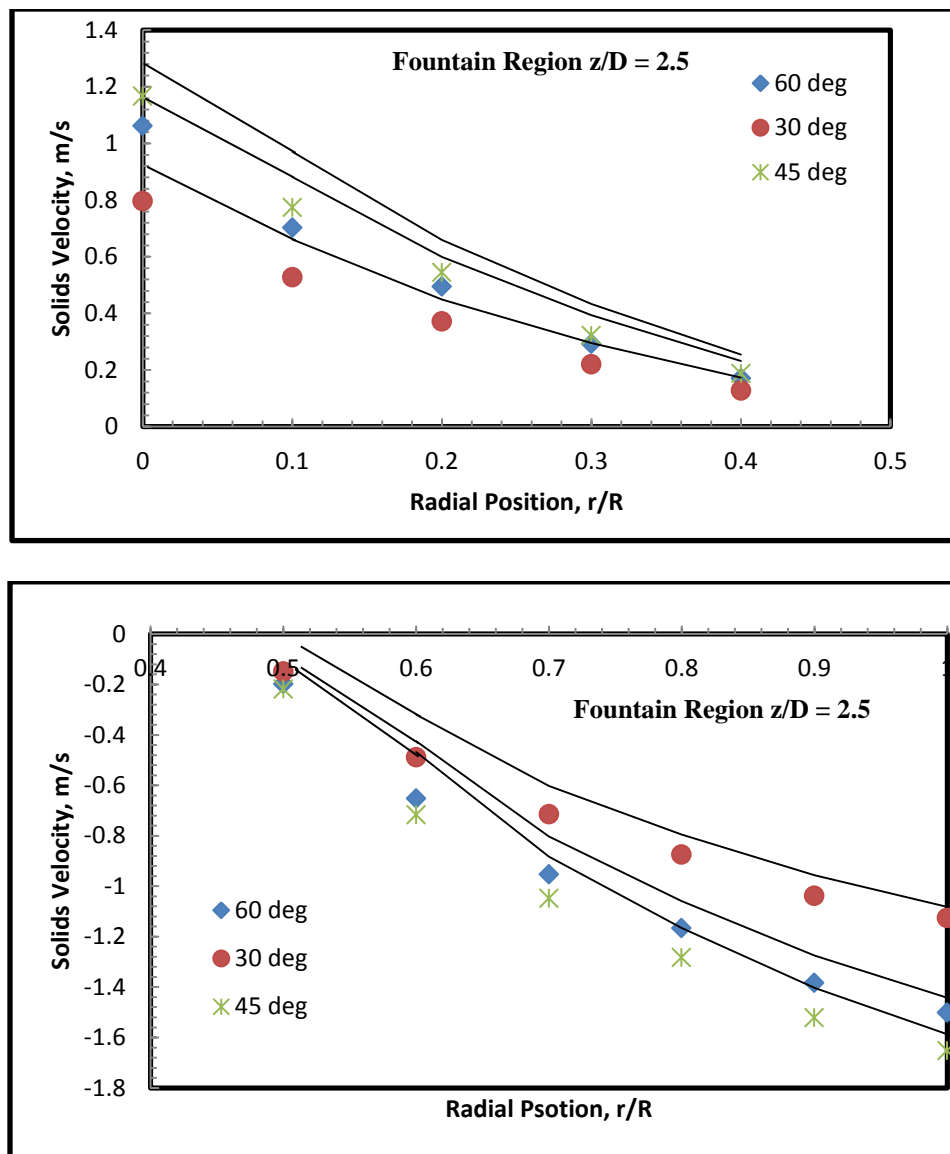
Figure 5.10. Optical probe (points) versus CFD simulation (lines) for vertical component of solids velocity in fountain region at 1.1 U_{ms} for a 30^0, 45^0 and 60^0 conical base angles for glass beads of 1 mm in diameter at a level of z/D 2.5.

5.1.2 Horizontal Component of Solids Velocity. The optical probe could not be used to measure horizontal component of solids velocity because the orientation of the probe would disrupt the flow dynamics in the bed. CFD simulation and correlation

reported in literature have been used in the present study to estimate the horizontal component of solids velocity. The only available correlation to predict the horizontal component of solid velocity was proposed by Kuthluoglu et al. (1983) given by equation 8.

$$v_r = \left[\frac{gr_f^{\,2}}{2(H_f - z_f)} \right]^{0.5} \tag{8}$$

Where, v_r is the horizontal component of solids velocity, r_f is radius of the fountain, H_f is the height of the fountain from the initial bed height and z_f is the longitudinal position in the fountain measured from the bed surface. The correlation prediction was used in this section, just to make sure that CFD is reliable for the estimation of horizontal component of solids velocity parameter.

The horizontal components were simulated by CFD, after its validation (details in Section 7) and then compared with the above correlation predictions (Equation 8). The radial profiles of the velocity in the spout region (Figure 5.11 and 5.12) show a parabolic profile, with the maximum value at the center of the column and at the spout-annulus interface. The same trend was obtained using the correlation predictions and by CFD simulation. The parabolic profile of solids velocity was same for all the three conical base angles. In annulus region (Figure 5.13 and 5.14), the radial profiles of solids velocity had similar range of values reported in the spout region, but the magnitude of the velocity was much lower. The solids velocity was negatively lower at the wall and increases negatively as it moves towards the spout region. The same trend was seen in all the three conical base angles and along the height of the spouted bed.
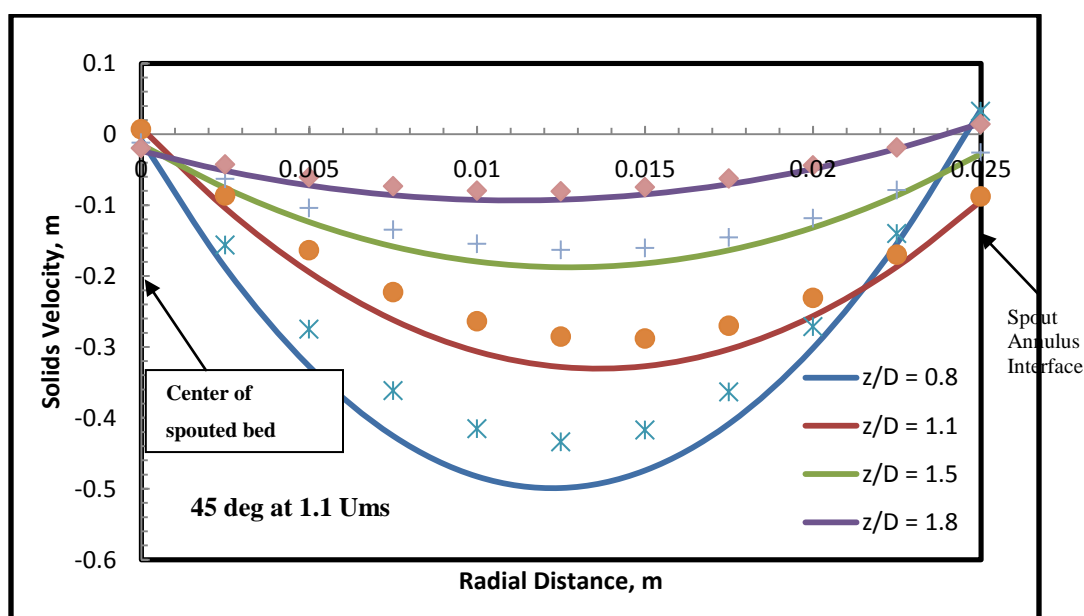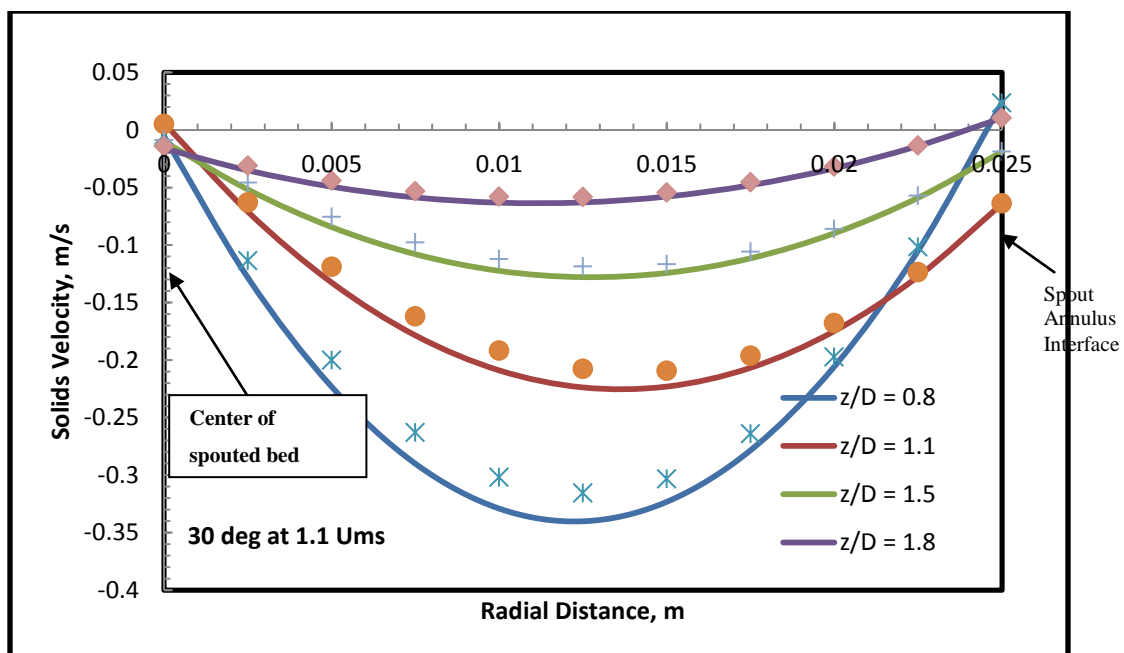
Figure 5.11. CFD simulation (line) versus correlation predictions (points) for horizontal component of solids velocity in spout region at 1.1 U_{ms} for a 30^0 and 45^0 conical base angle for glass beads of 1 mm in diameter at different z/D levels.
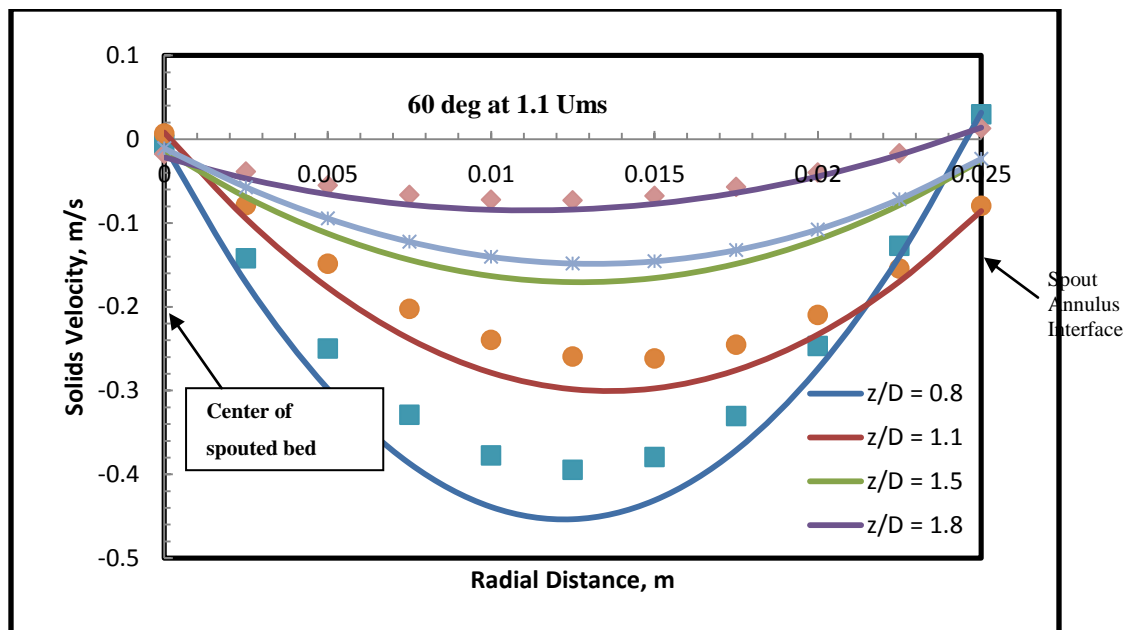
Figure 5.12. CFD simulation (line) versus correlation predictions (points) for horizontal component of solids velocity in spout region at 1.1 U_{ms} for a 60^0 conical base angle for glass beads of 1 mm in diameter at different z/D levels.
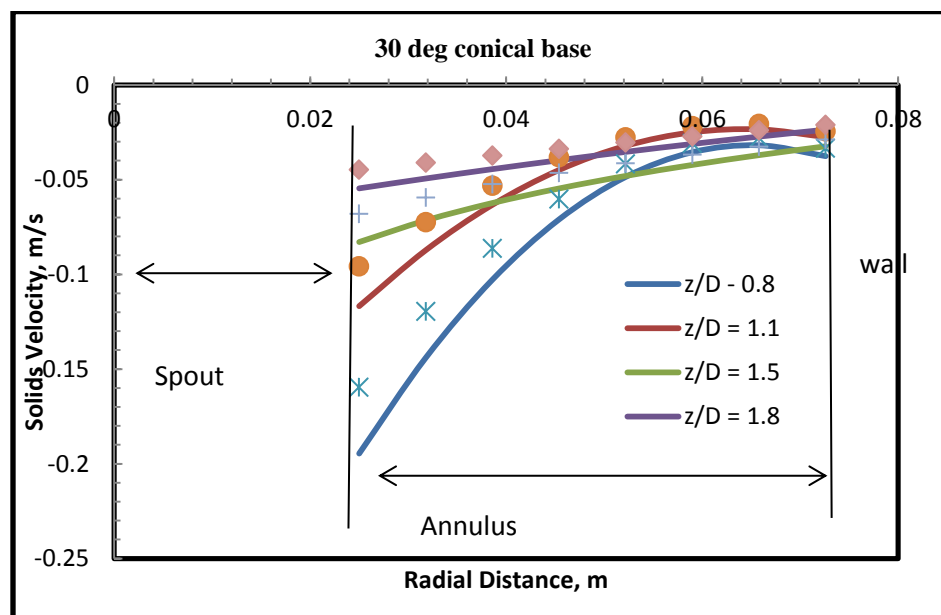
Figure 5.13. CFD simulation (line) versus correlation predictions (points) for horizontal component of solids velocity in annulus region at 1.1 U_{ms} for a 30^0 conical base angle for glass beads of 1 mm in diameter at different z/D levels.
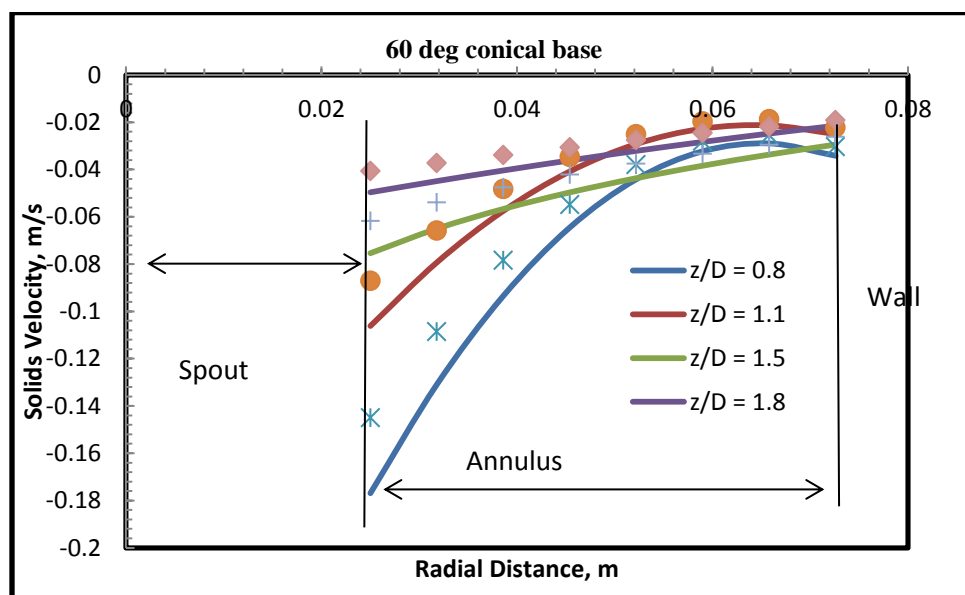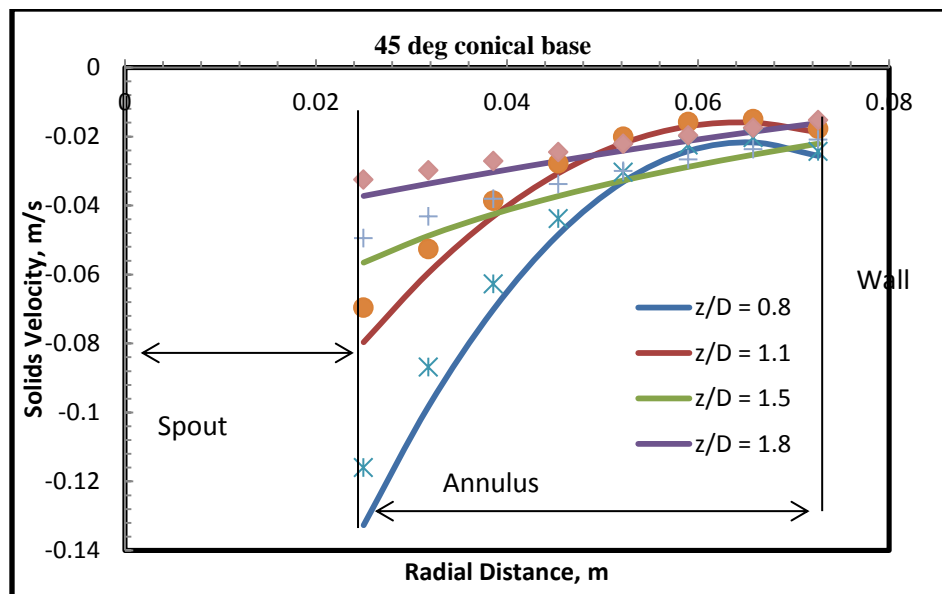
Figure 5.14. CFD simulation (line) versus correlation predictions (points) for horizontal component of solids velocity in annulus region at 1.1 U_{ms} for a 45^0 and 60^0 conical base angle for glass beads of 1 mm in diameter at different z/D levels.

The vertical and horizontal compnents of solids velocity and the velocity vectors were obtaiend using CFD simulation in the spout, annulus and fountain regions of spouted bed. The normal assumption in the literature is that the spout is straight along the height of the spouted bed and the solids flow into the spout region from the annulus region all along the length of the spout. Based on the CFD analysis in the present work, the spout was found to form a neck at the top protion of the bed. In the spout region it is observed that the particles are moving towards the axis at any level (Figure 5.15). In the neck region, the spout velocity vector is vertical except at the interface, where the particles tend to be pulled by the fountain region. It is observed that solids flow into the spout does not take place at all the axial positions along the spout-annulus interface. The direction of velocity vector indicates that there is a preferential zone of flow near the inlet of the spouted bed and another important zone of flow at the neck of the spout. The flow of solids into the spout apart from these two zones seems to be small. The same trend was observed in all the three conical angles, only the magnitude of velocity vector was different and the rest of the phenomena remaining the same. The formation of the neck in the spout region of the spouted bed was studied for one configuration of bed geometry only. The presence of neck in the spout region needs to be studied for different configurations of spouted bed geometry, before a general assumption can be made that the neck region exists in all the spouted beds. The above conclusions drawn are based solely on the interpretation of CFD simulations and needs to be validated with advanced experimental techniques.

(a)   (b)
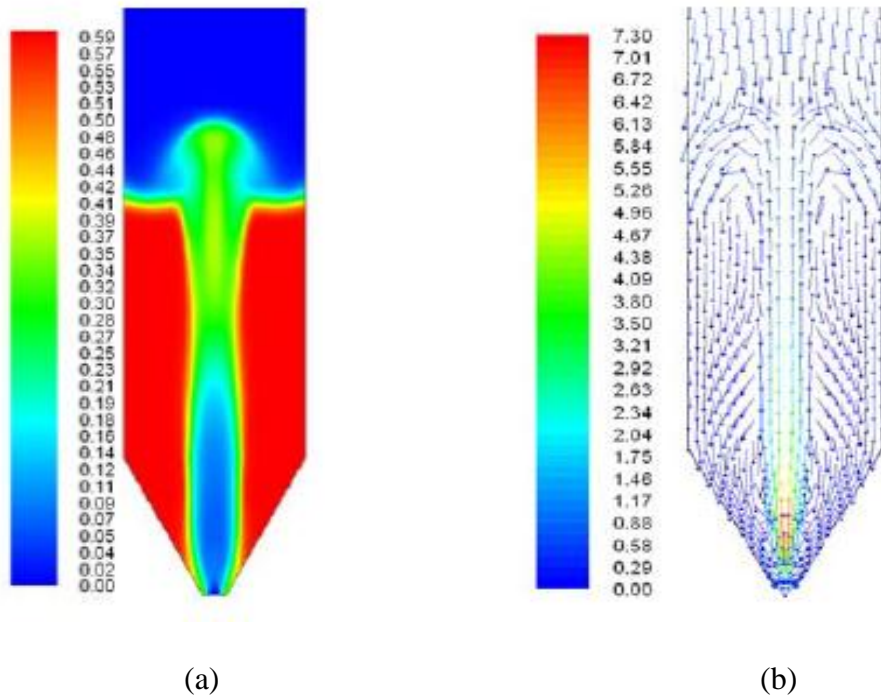
Figure 5.15. Contour and vector plot using CFD, (a) CFD simulation of 0.152 m spouted bed showing the neck formation in the spout region; (b) Velocity vectors obtained using CFD simulation showing the prefferential solids flow zones.

5.2 EFFECT OF DESIGN VARIABLES AND OPERATING PARAMETERS ON SPOUT DIAMETER

Numerous researchers have performed studies on determining average spout diameter and also the influence of different solids and fluid properties on them. Spout diameter is an important parameter in spouted beds as it dictates the hydrodynamics of the bed. Complete knowledge of this parameter is essential in modeling the design of spouted bed, as the bed characteristics is driven by the spout region. MacNab (1972), Bridgwater and Mathur (1972), Green and Bridgewater (1983) and Lim and Grace (1987) have all reported correlations for predicting average spout diameter, but most of them are still bound by large percentage of deviations. In the present work, factorial design of

experiments has been proposed to predict the average spout diameter. The motivation for the present work was the successful implementation of factorial design in predicting average spout diameter in a two-dimensional spouted bed by Zanoelo et al. (2004).

Factorial design of experiments is employed in order to analyze the influence of key design and operating parameters on the mean spout diameter in a spouted bed. Factorial design of experiments is a statistical procedure to determine the influence of one or several parameters on the spout diameter. Of the selected parameters, a single parameter or a combination of several parameters may affect the spout diameter. With the help factorial design of experiments, the influence of such parameters on the spout diameter can be identified. The present study attempts at such a way of experimentation to identify the key parameters or the combination of them which influence the spout diameter.

The effects of solids density, static bed height, particle diameter, superficial gas velocity and inlet jet diameter on mean spout diameter is studied in this section. The above-mentioned parameters are called the factors in the factorial design of experiments. These were selected in the present study, as these parameters appear in most of the correlations available in literature to predict mean spout diameter in spouted beds. A set of experiments has been carried out using 0.152 m conical based cylindrical spouted bed. The spouted bed consists of a transparent column of cylindrical cross-section made of plexiglass. The bed has ten axial ports for the sake of measurements. The air was provided by a high capacity industrial air compressor which has a capacity of 200 psi.

A 2^5 factorial design of experiments has been employed in order to investigate the influence of key operating parameters on the spout diameter. A 2^n factorial experiment is

an experiment whose design consists of two levels for each factor (n) considered. 2 here refer to the number of levels for each factor considered and the "n" represents the number of factors considered for a given experimental study. Each factor has discrete possible values or "levels", and the experimental units take on all possible combinations of these levels across all such factors. Such an experiment allows studying the effect of each factor on the response variable (in this case mean spout diameter), as well as the effects of interactions between factors on the response variable. For the 2^n factorial experiments, each factor has only two levels. For example, a 2^2 factorial design has two factors each taking two levels, a factorial experiment would have four treatment combinations in total, and is usually called a 2x2 factorial design. A 2^3 factorial design has three factors taking two levels and would have eight treatment combinations in total. A 2^4 factorial design has four factors taking two levels and would have sixteen treatment combinations in total. The 2^k design is particularly useful in the early stages of experimental work, when it is desired to investigate the effects of a large number of variables (Montgomery, 2001). The two levels must usually have an upper end and a lower end value. The levels of a factor are commonly coded as +1 for high level, and -1 for lower level. A factorial experiment allows for the estimation of experimental error by replication of experimental runs.

The experiments were run in a completely randomized (CR) design. By randomization, that is to say that the run sequence of experimental units is determined randomly. This randomization is done in order to control the effects of extraneous variables. The experimenter assumes that, on average, extraneous factors will affect treatment conditions equally; so any significant differences between conditions can fairly be attributed to the independent variable. Although randomization helps to ensure that

treatment groups are as similar as possible, the results of a single experiment, applied to a small number of objects or subjects, should not be accepted without question. Randomly selecting two individuals from a group of four and applying a treatment with "great success" generally will not impress the public or convince anyone of the effectiveness of the treatment. To improve the significance of an experimental result, replication, the repetition of an experiment on a large group of subjects, is required. Replication reduces variability in experimental results, increasing their significance and the confidence level with which a researcher can draw conclusions about an experimental factor.

Since, 5 factors with each having two levels have been identified to be used in the present study, it's a 2x5 (2^5) factorial design. This design yields thirty two treatment combinations in total. Hence, the experiment involved a total of 32 experimental measurements of mean spout diameter. Each factor had 2 levels of measurement (one high and one low). Two experimental runs (replication) were performed in order to estimate the experimental error. A total of 64 experimental measurements were performed. Each of the identified 5 factors in the study had two levels. Glass beads and steel shots of densities 2450 (coded unit: -1) and 7400 (coded unit: +1) Kg/m^3, respectively, were used as solid particles. Two particle sizes of 1 mm (coded unit: -1) and 2 mm (coded unit: +1) in diameter were considered for the experiment. The gas velocity used was 0.74 m/s (coded unit: -1) and 1.00 m/s (coded unit: +1). The static bed height used in the experiments was 0.250 m (coded unit: -1) and 0.300 m (coded unit: +1). The inlet diameter sizes used was 0.006 m (coded unit: -1) and 0.012 m (coded unit: +1).

The five factors analyzed in this work were solid density, static bed height, particle diameter, superficial gas velocity and inlet diameter. These were chosen based on

the following criteria: the factor appears in correlations found in the literature to calculate the average spout diameter of conventional spouted beds. At each operating condition, the spout width profile was obtained by optical fiber probes. The optical probe works on the principle of back reflection of light. The spout and annulus have completely different degrees of solids. Hence, the reflected light by the solid particles in these two regions are completely different and thus helps in determining the spout diameter. More details on the estimation of spout diameter using optical probes are discussed in Section 4. MINITAB software was used to perform the factorial analysis and to generate the random design structure for randomization of experimental runs. The factorial design was performed in coded units for simplification of usage in the software. The main objective of the present work is to propose the use of factorial design of experiments in order to analyze the influence of operating parameters (solid density, static bed height, particle diameter, superficial gas velocity and inlet diameter) on the mean spout diameter.

5.2.1. Factorial Design Structure. Factorial design structure refers to the structure of experimentation used to determine the influence of key parameters on spout diameter. The structure is generated by the statistical software based on the levels and number of parameters involved. The levels refer to higher and lower limit of the parameters involved in the study. The levels are coded for use of statistical software. The high level was denoted as +1 and the lower level was denoted as -1. The factorial design was generated in MINITAB software. The randomization of the design structure was performed using MINITAB. The factorial design is shown in Table 5.1. Table 5.1 shows all the experimental runs consisting of 64 experimental measurements ($2^5 = 32$ runs; with two replications) of spout diameter.

Table 5.1. Factorial design for completely randomized design

Solids Density	Static Bed Height	Particle Diameter	Gas Velocity	Inlet Diameter	Spout Diameter Ds, cm	
					Run 1	Run 2
-1	-1	-1	-1	-1	3.65	3.64
1	-1	-1	-1	-1	3.58	3.58
-1	1	-1	-1	-1	3.52	3.51
1	1	-1	-1	-1	3.47	3.46
-1	-1	1	-1	-1	3.43	3.43
1	-1	1	-1	-1	3.39	3.38
-1	1	1	-1	-1	3.31	3.31
1	1	1	-1	-1	3.38	3.36
-1	-1	-1	1	-1	4.05	4.04
1	-1	-1	1	-1	4.13	4.13
-1	1	-1	1	-1	3.93	3.93
1	1	-1	1	-1	3.84	3.81
-1	-1	1	1	-1	3.82	3.83
1	-1	1	1	-1	3.76	3.75
-1	1	1	1	-1	3.74	3.74
1	1	1	1	-1	3.69	3.68
-1	-1	-1	-1	1	5.91	5.90
1	-1	-1	-1	1	5.84	5.82
-1	1	-1	-1	1	5.70	5.72
1	1	-1	-1	1	5.72	5.71
-1	-1	1	-1	1	5.48	5.49
1	-1	1	-1	1	5.50	5.50
-1	1	1	-1	1	5.43	5.44
1	1	1	-1	1	5.42	5.43
-1	-1	-1	1	1	6.71	6.73
1	-1	-1	1	1	6.69	6.68
-1	1	-1	1	1	6.61	6.62
1	1	-1	1	1	6.59	6.59
-1	-1	1	1	1	6.30	6.30
1	-1	1	1	1	6.31	6.33
-1	1	1	1	1	6.11	6.12
1	1	1	1	1	6.21	6.22

It is necessary to remember that a statistical analysis for a 2^5 factorial design involves 5 main effects, 10 two-variable interactions, 10 three-variable interactions, 5 four-variable interactions and 1 five-variable interactions. The significance level in order to analyze the results was set $\alpha = 0.05$. MINITAB performs the ANOVA analysis for the factorial design structure.

5.2.2. Analysis of Variance (ANOVA) Table for Identifying the Influence of Each Operating Parameter. ANOVA is a collection of statistical models, and their associated procedures, in which the observed variance in a particular variable is partitioned into components attributable to different sources of variation. In its simplest form, ANOVA provides a statistical test of whether or not the means of several groups are all equal. Through ANOVA, the operating factors and the interaction between them, which will influence the mean spout diameter, can be identified. First the interpretation of the ANOVA table is necessary to understand and analyze the results.

Suppose we have "a" treatments and each treatment is applied to "n" experimental units in a CR design. We now measure the responses Y_{ij} (in this case mean spout diameter) of experimental units to treatments. Suppose an appropriate model to describe the Y_{ij} is:

$$Y_{ij} = \mu + \tau_i + \varepsilon_{ij} \tag{9}$$

Where, i = 1, 2, 3… a; j = 1, 2… n and $\varepsilon_j \overset{iid}{\sim} N(0, \sigma^2)$. The τ_i are called the treatment effects and is considered a fixed effect (i.e. the treatment levels are specifically chosen by the experimenter and can be replicated exactly any number of times). $\mu_i = \mu + \tau_i$, is the approximation made from statistical point of view. μ_i is called the population mean for the ith treatment. The normal assumption in testing the above statistical model

(equation 9) is that the treatment means are equal (in the present study it means that all the operating parameters under consideration and their combinations are equally contributing to influence the mean spout diameter).

One hypothesis the experimenter may wish to test is

$$H_o: \mu_1 = \mu_2 = \mu_3 = ... = \mu_a \text{ vs } H_a: \text{ at least one } \mu_i \text{ differs from the rest.}$$

This is equivalent to testing

$$H_o: \tau_1 = \tau_2 = ... = \tau_a \text{ vs } H_a: \text{ not } H_o$$

Generally, H_a is the hypothesis we wish to establish with strong evidence. It is the "new" or "against current thinking" kind of hypothesis and hence we need strong evidence before we believe it is true. H_0 on the other hand is the "old" or "status quo" hypothesis which we feel comfortable (or less costly) to believe in unless there is sufficient evidence to discard it.

The model (equation 9) above is over parameterized (i.e. has too many parameters so that no single parameter can be estimated uniquely). Thus, we enforce the restriction

$$\sum_{i=1}^{a} \tau_i = 0 \tag{10}$$

With this restriction the hypotheses for the above model becomes

$$H_o: \tau_1 = \tau_2 = ... = \tau_a = 0 \text{ vs } H_a: \text{ at least one } \tau_i \text{ is non-zero}$$

In order to test the above hypotheses, we compute the following sums of squares.

$$SS_{\text{total}} = \sum_{i=1}^{a}\sum_{j=1}^{n}\left(Y_{ij} - \bar{Y}_{\bullet\bullet}\right)^2 \tag{11}$$

$$\bar{Y}_{\bullet\bullet} = Y_{\bullet\bullet} / N, \quad Y_{\bullet\bullet} = \sum_{i=1}^{a}\sum_{j=1}^{n}Y_{ij} \tag{12}$$

$$N = na \tag{13}$$

$$SS_{\text{treatment}} = n\sum_{i=1}^{a}\left(\bar{Y}_{i\bullet} - \bar{Y}_{\bullet\bullet}\right)^2 \tag{14}$$

$$\bar{Y}_{i\bullet} = \frac{1}{n}\sum_{i=1}^{n}Y_{ij} \quad , \quad i = 1,2,...,n \tag{15}$$

$$SS_{\text{Error}} = \sum_{i=1}^{a}\sum_{j=1}^{n}\left(Y_{ij} - \bar{Y}_{i\bullet}\right)^2 \tag{16}$$

It can be shown that: $SS_{\text{Total}} = SS_{\text{Treatment}} + SS_{\text{Error}}$ (17)

Moreover, $SS_{\text{Treatment}}$ and SS_{Error} are independent and thus, under

$$H_o, \ F = MS_{\text{Treatment}} / MS_{\text{Error}} \sim F_{a-1,N-a,} \tag{18}$$

Where, $MS_{\text{Treatment}} = SS_{\text{Treatment}} / (a-1)$ and $MS_{\text{Error}} = SS_{\text{Error}} / (N-a)$ (19)

If H_0 is false, the above F statistic will have a non-central F distribution with the same degrees of freedom and hence will tend to be larger than a central F random variable. Thus, an appropriate test for testing

$$H_o: \mu_1 = \mu_2 = ... = \mu_a \text{ vs } H_a: \text{ not } H_o \tag{20}$$

Reject H_0 at significance level α if

$$F > F_\alpha,(a-1),(N-a). \tag{21}$$

The results are usually summarized in an analysis of variance table in Table 5.2.

Table 5.2. Analysis of Variance (ANOVA) table

Source of Variation	Degrees of Freedom	SS	MS	F
Treatment	a-1	$SS_{\text{Treatment}}$	$MS_{\text{Treatment}}$	$\dfrac{MS_{\text{Treatment}}}{MS_{\text{Error}}}$
Error	N-a	SS_{Error}	MS_{Error}	-
Total	N-1	SS_{Total}	MS_{Total}	

The "p" value is computed by F α, (a-1), (N-a) for any given significance value α. If the p<α, the treatment combination is significant (reject H_0) and if p>α, the treatment combination is not significant (accept H_0).

Analyzing the above factorial design in MINITAB software, the ANOVA table for the experimentation was generated. Since the experimental measurement is replicated twice, ANOVA table (Table 5.3) and the normal probability plot (Figure 5.14) can be used to determine the significant (factors which influence the spout diameter) effects. Analyzing the ANOVA table, it was observed that all five main effects (solids density, static bed height, particle diameter, superficial gas velocity and inlet diameter) were significant ($\alpha < 0.05$). The two way interactions suggested that the interaction between particle size and inlet diameter, and gas velocity and inlet diameter, were significant. The three-way, four-way and five-way interactions were found to be not significant from the ANOVA table. The effects that are negligible are normally distributed with mean equal to zero and tend to fall along a straight line (normal probability plot), while the significant effects have non-zero means and do not lie along the straight line (Montgomery, 2001). Figure 5.16 represents the normal probability plot, where factors A, B, C, D and E refer to solid density, static bed height, particle diameter, superficial gas velocity and inlet diameter, respectively. In the case of Figure 5.16, it is quite evident that except for the two-variable interaction C*E (particle diameter and inlet diameter) and D*E (gas velocity and inlet diameter) and the main effects, all of them lie along the straight line of mean equal to zero. From the normal probability plot (Figure 5.16), the particle diameter, static bed height and the interaction of particle diameter and inlet diameter, have negative

effects (point lie on the negative size of the zero mean line). This suggests that, increase of either of these parameters leads to decrease of spout diameter.
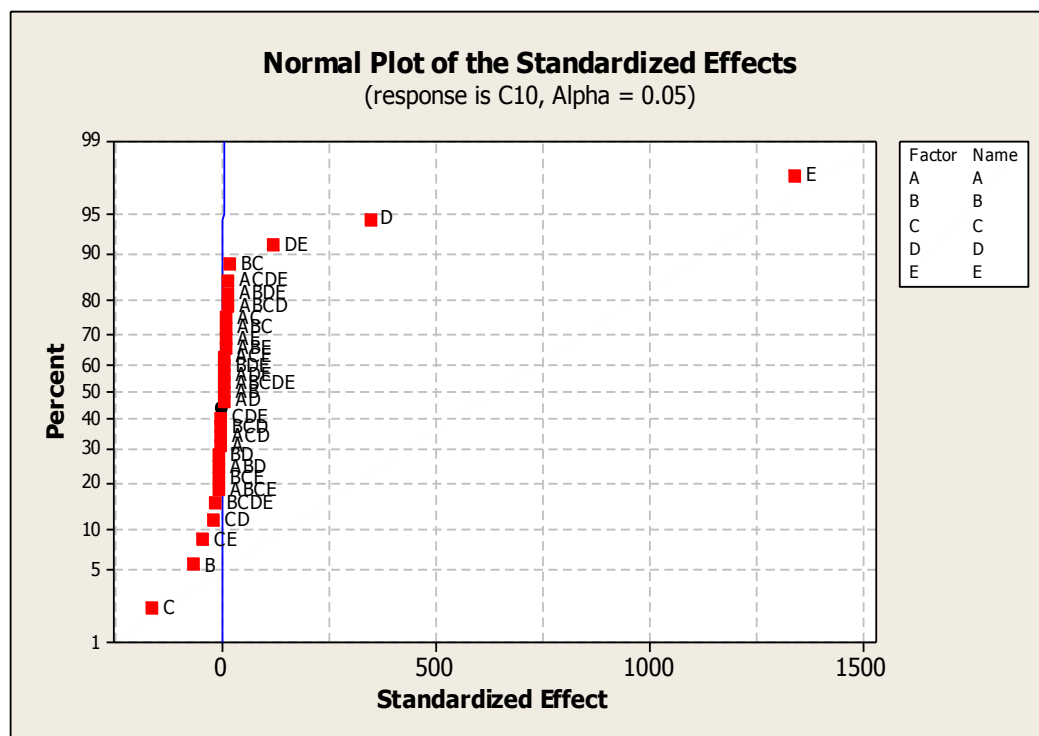
Figure 5.16. Normal plot for the parameters involved in experimentation

Table 5.3. ANOVA table for spout diameter

Source	DF	SS	MS	F	P
Main effects	5	97.0362	19.4072	55394.87	**0.0000**
Solids Density	1	0.0000	0.0000	0.4	**0.0000**
Static Bed Height	1	0.2598	0.2598	741.69	**0.0000**
Particle Diameter	1	1.4526	1.4526	4146.29	**0.0000**

Table 5.3. ANOVA table for spout diameter cont.

Source	DF	SS	MS	F	P
Superficial Gas velocity	1	5.7612	5.7612	16444.42	**0.0000**
Inlet Diameter	1	89.5626	89.5626	255642	**0.0000**
2-Way Interactions	10	0.7807	0.7807	222.84	**0.0000**
A*B	1	0.0000	0.0000	1.44	0.2495
A*C	1	0.0000	0.0000	0.66	0.4303
A*D	1	0.0000	0.0000	0.07	0.7952
A*E	1	0.0000	0.0000	0.19	0.6659
B*C	1	0.0003	0.0003	0.85	0.364
B*D	1	0.0002	0.0002	0.54	0.468
B*E	1	0.0072	0.0072	20.5	0.4611
C*D	1	0.0118	0.0118	33.76	0.5696
C*E	1	0.1446	0.1446	412.71	**0.0000**
D*E	1	0.6166	0.6166	1760.04	**0.0000**
3-Way Interactions	10	0.0220	0.0220	6.28	0.2289
4-Way Interactions	5	0.0119	0.0024	1.39	0.5062
5-Way Interactions	1	0.0325	0.0624	1.04	0.323
Residual Error	32	0.0112	0.0004		
Pure Error	32	0.0112	0.0004		
Total	63	97.8621			

A = Solid Density; B = Static Bed Height; C = Particle Diameter; D = Superficial Gas Velocity and E = Inlet Diameter.

5.2.3. Regression Analysis. Regression analysis was performed on the spout diameter data to come up with a correlation which can predict the average spout diameter

using the significant effects. In a 2^k factorial design, it is possible to represent the results of experiments in terms of a regression model. Based on the regression analysis, the following model was obtained to identify average spout diameter,

$$d_s = 4.84563 - 0.0562\rho_s - 0.05875H - 0.14563d_p + 0.487U$$
$$+1.18250D_i - 0.0644d_p * D_i + 0.0562U * D_i \tag{9}$$

Figure 5.17 shows that the regression model is able to predict the experimental average spout diameter very closely, for all the operating conditions investigated in this work. It represents exactly the experimental data due to the variable interaction that were not considered in this model are negligible. It is worth stressing that all the 64 experimental data reported in Table 5.1 are compared with predicted results from equation 9.
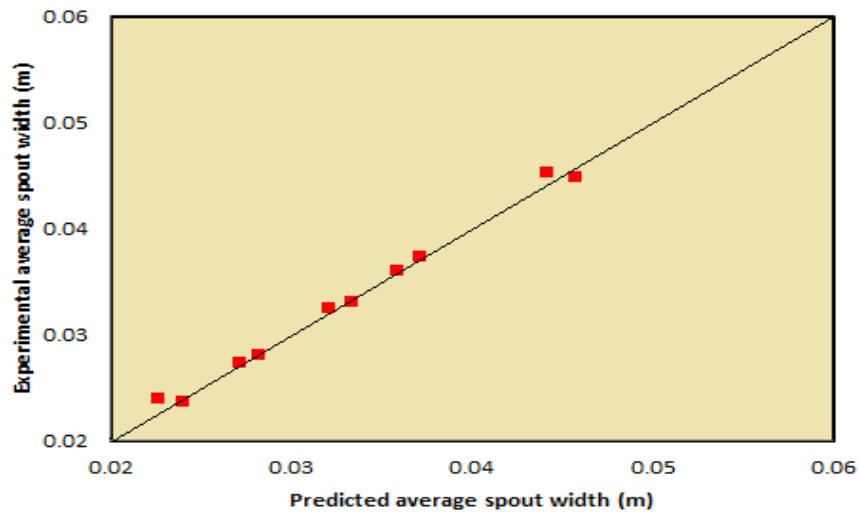
Figure 5.17. Comparison between experimental and predicted spout diameter

The average deviation from experimental and predicted results was obtained

$$\% error = \left[\sum_{i=1}^{64} \frac{d_{s,i,\exp} - \bar{d}_{s,i,pred}}{d_{s,i,\exp}} \right] * \frac{100}{64} = 2.1\%$$

(10)

The obtained results from the above correlation were compared with the correlation predictions reported in the literature (discussed in Section 2) for cone based cylindrical spouted bed. The above model was able to closely predict the values compared to literature with an absolute relative difference of 8.65%. However, the obtained correlation through the regression model is valid for spouted beds operating in stable spouting flow regime and for the configuration of spouted bed studied in this work. Once the spouted bed enters unstable spouting regime, which is characterized by swirling and pulsating of the spout, the above correlation goes void.

Table 5.4 Comparison of Spout diameter for 0.152 m spouted bed at Ug = 1.0 m/s: Regression v/s correlation prediction

	Spout Diameter by Correlation prediction	Spout Diameter by Regression Model	Error
McNab (1972)	6.08	6.61	8.4%
Bridgwater and Mathur (1972)	7.41	6.61	12.1%
Hadzisdmajlovic (1983)	7.11	6.61	7.6%

5.3 REMARKS

The vertical components of solids velocity was measured using optical probes and estimated by CFD simulation. The horizontal components of solids velocity was

estimated by CFD simulations and predicted using correlation in 0.152 m spouted bed. From the estimation of velocity vectors from CFD simulation, it was found that the spout formed in the spouted bed under study is not straight but instead forms a neck at the top part of the spout region. The preferential flow of solids from the spout-annulus interface to the spout region occurs mainly in two regions. The first is near the inlet of the bed and the second zone is near the neck of the spout. From the interpretation of CFD results, it seems that solids mainly flow into the spout region in the above mentioned zones. In regions apart from the above mentioned zones, the solids flow into the spout region from the annulus region seems to be small based on the interpretation of CFD simulations.

2^5 factorial designs of experiments were performed to identify the mean spout diameter in spouted beds. 0.152 m ID spouted bed was the only geometry studied for the above experimentation. Factorial analysis was performed in MINITAB software. From the interpretation of ANOVA results, it was found that all five main effects (solid density, static bed height, particle diameter, superficial gas velocity and inlet diameter) and the interaction between particles size and inlet diameter, and gas velocity and inlet diameter, had significant effect on the determination of spout diameter. Regression analysis was performed to obtain a correlation which could identify the average spout diameter in the current configuration of spouted beds. The obtained correlation was able to predict closely the spout diameter when compared to the correlations listed in the literature.

6. FLOW REGIME IDENTIFICATION IN SPOUTED BEDS

6.1. INTRODUCTION

As mentioned earlier, the spouted bed was initially developed by Mathur and Gishler (1974) as a means for drying wheat. Over the years, spouted bed has been used as an alternative to fluidized bed for dealing with coarse particles, since spouted beds have large advantages over the conventional fluidized beds. Spouted beds are mainly used for physical process like coating, granulation, drying etc., but recently they have been used in chemical processes as well such as coal gasification and catalytic reactions (Lopez et al., 2009). For a combination of bed geometry, solids phase and gas phase, spouting can occur over a certain range of gas velocities. Under proper conditions, the gas phase penetrates the bed of particles as a jet, creating a central spout zone, a fountain above the spout, and an annulus moving downward surrounding the spout. Particles entrained by the gas in the spout region move upward and form a fountain of particles above the bed surface that disengage from the gas and fall back to the bed surface, thus, inducing bed circulation. Hence, three distinct regions are created in the spouted bed namely: spout, annulus and fountain. There are also flow regimes in the bed that needs to be identified. Three main flow regimes are observed in spouted bed with increasing gas velocity (Epstein and Grace, 2011). They are packed bed, stable spouting regime and unstable spouting regime. Bubbling and slugging flow regimes have also been reported in the literature. Characterization of stable spouting is done by the formation of the stable spout or fountain. Unstable spouting is usually where it is observed with swirling and pulsating

of the spout with time. Identification and prediction of such flow regimes is very important in the commercial application of spouted bed.

Identification of flow regimes in different configuration of spouted beds (conical, cone based cylindrical, slot rectangular) has been reported by several researchers in the literature (Section 2). But most of these studies used techniques based on visual observation in a half column or through recording of a high speed camera in a transparent spouted bed. Recently, the use of optical fiber probes (ideal for conditions in the lab, but industrially very difficult to apply) for analyzing signal fluctuations, pressure transducer to analyze pressure fluctuations has been employed to study the flow regimes in spouted bed (Wei et al., 2004; Wang et al., 2011). Optical fiber probes is an invasive technique which would disrupt the flow dynamics in the spouted beds and pressure transducers measure the fluctuations at the wall and cannot capture completely the phenomena in the reactor. In industrial scale diameter columns which are large, sensing at the wall may not reflect well the phenomena inside. Industrial scale reactors cannot rely on techniques which deploy visual observation, techniques disrupting the flow dynamics and measurements taken at the wall, as they are opaque and operate at high temperature and pressures. Hence, there is a need to develop techniques involving non-invasive approaches. Particularly industrial scale reactors, there is a need to develop a technique for flow regime diagnosis that is non-invasive, that can be easily implemented on an industrial scale columns without disturbing the operation, and that provides reliable information. The primary objective of this section is to develop and demonstrate a non-invasive technique for online flow regime demarcation and monitoring.

6.2. EXPERIMENTAL SET-UP

Two spouted beds of 0.152 m and 0.076 m ID were used in the present study to identify the different flow regimes. The detailed dimensions and geometry of spouted bed used are discussed in Section 4. The spouted bed columns are constructed from plexiglass.

The dimensions of the spouted bed were made to satisfy the three conditions necessary for stable spouting to be achieved, which are listed below.

$$D_i/d_p < 25{\sim}30 \tag{1}$$

$$D_c/D_i > 3{\sim}12 \tag{2}$$

$$H < H_m \tag{3}$$

Where, D_i is the inlet diameter, d_p is the particle diameter, D_c is the diameter of the column, H is the static bed height and H_m is the maximum spoutable bed height. Both the spouted beds were fitted with ports at different axial heights in order to aid in measurement. Compressed air was used as the gas phase, which was supplied by industrial scale high capacity air compressor. Solids phase was glass beads of size 1mm, with a density of 2450 Kg/m^3. The measurement ports were utilized to fit the pressure transducer for experimental measurements. For the purposes of using the gamma ray densitometry system, two separate columns of 0.152 m and 0.076 m spouted beds were built without measurement ports. The measurement ports attached with secured metallic fittings were known to cause disturbances to the attenuated γ-rays received by the detector; as a result new spouted beds of same dimensions were built without ports.

6.2.1. Pressure Transducers and Optical Probes to Identify Flow Regimes. A pressure transducer/sensor measures pressure, typically of gases, liquids or solids.

Pressure is an expression of the force required to stop a fluid from expanding, and is usually stated in terms of force per unit area. A pressure transducer generates an electrical signal as a function of the pressure imposed. The pressure transducer used for the present study measures gauge pressure and is of the Model. No. PX309-002G5V purchased from Omega Dyne Inc. The pressure transducer used is a single ended pressure measurement device. The data acquisition for the pressure transducer consists of an A/D converter, which converts the pressure fluctuations into electrical signals. The time series signals obtained from the transducer are then analyzed statistically to obtain important information about different flow regimes of the multiphase systems under study. These help in understanding the flow pattern and flow dynamics of multiphase systems. Further details of pressure transducers can be found in Section 4 of this thesis.

Optical probes employ back reflection of light principle to identify the flow regions and flow patterns in spouted beds. The signal generated by the optical probes is in direct correlation with the amount of solids (particles) in front of the probe tip. The details of the working and usage of optical probes can be found in Section 3.

6.2.2. Development of Gamma Ray Densitometry (GRD). Gamma ray densitometry (GRD) consists of a sealed source (Cesium 137 of 250 mCi) in a source holder and a NaI scintillation detector in front of the source. The source holder is mounted on one side of a column, with the detector on the opposite side. A focused beam of radiation is transmitted from the source, through the column and process material, to the detector. As the density of the material in the column changes, the amount of radiation reaching the detector changes accordingly. It is generally believed that the amount of radiation that reaches the detector through the process material is reflective of

its flow behavior and properties. Figure 6.1 shows the GRD with a source and a detector in front of it. The beam of γ-rays coming from the sealed source is made such that it provides a point beam, which was custom made for the requirements of measurement by Tracer Co Company (El Paso, Texas).

GRD is used extensively in industry for such applications as level control, density measurement, and weight measurements in conveyors (P. Jackson, 2004). It is widely used in the following industries: chemicals, petrochemicals, off shore oil and gas, pharmaceuticals, cement, quarrying, solids handling, paper and food (www.vegacontrols.com). The major advantages of GRD that make it attractive in everyday industrial use are,

1. *Totally non-contact:* Because the sources and detectors are mounted externally from the column or process, they are completely unaffected by the conditions inside, however extreme, providing reliable solutions when other technologies fail. They can be easily accessed, installed or removed without the process being affected or interrupted.

2. *High integrity:* A non-invasive system mounted outside the vessel means no exposure or wear by corrosive or abrasive products, and no need for construction to resist high pressure, high temperature process conditions. This means less risk of leaks or emissions, protecting processes, people and the environment.

3. *High reliability and low maintenance:* GRD measurements offer reliability and long term performance. In addition, source checking is routine, simple and can be planned well in advance.

4.   *Low installation costs:* GRD can often be installed and commissioned without process shutdown. Also, on most applications, no alterations to the reactors or columns are needed, which means no expensive design changes for such implementation of GRD.

The radial profile of solids hold-up can be obtained with the help of GRD, which will determine the performance of the reactor (discussed in Section 4). GRD (Figure 6.2) technique is made to be flexible in order to accommodate reactors up to 1.0 m in diameter. The entire set-up is constructed on wheels, which facilitates in the 360^{0} movement of GRD. It can also be moved in horizontal and vertical positions with the help of stepper motors. Thus, measurements can be made using GRD along the diameter and height of the system under study to obtain line averaged profiles.
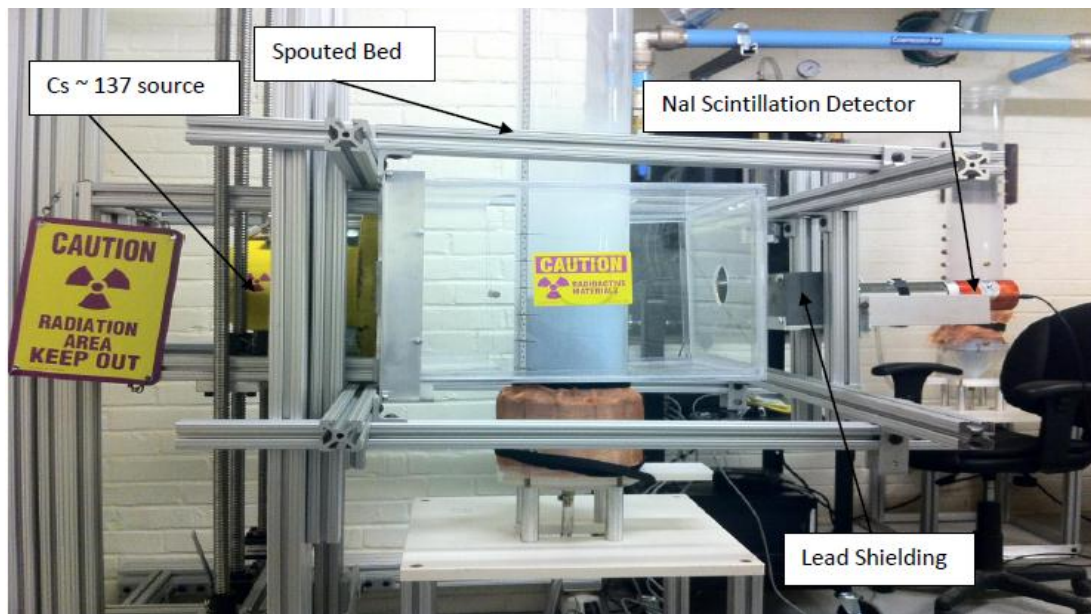
Figure 6.1. Cross sectional view of 0.152 m spouted bed used for measurement in GRD system.
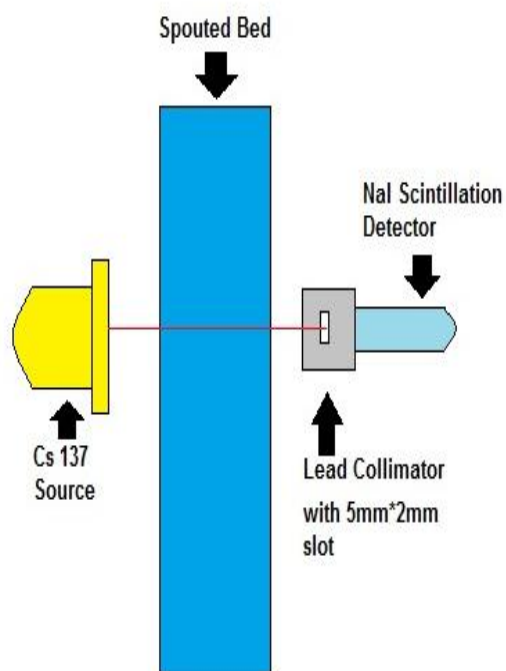
(a) (b)
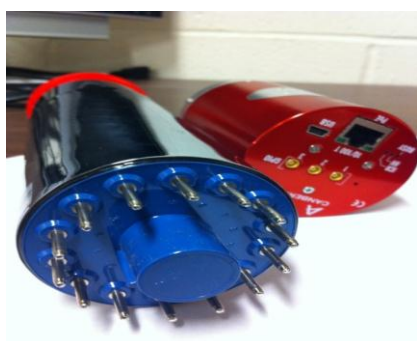
(c) (d)

Figure 6.2. Gamma Ray Densitometry system, (a) GRD technique applied to spouted bed surrounded by lead shielding; (b) Schematic representation of GRD; (c) New USB based NaI scintillation detector system and (d) Cs~137 source in a sealed source container.

6.2.3. Gamma Ray Densitometry Electronics and Data Acquisition System.

The traditional electronics system consists of detector, timing filter amplifier, cables, high voltage power supply and BIN power supply. The electronic system of GRD consists of NaI scintillating detector and Osprey USB interface. Osprey USB interface consists of all the above components in a small tube shown in Figure 6.1, thus simplifying the electronic system.

Most detectors can be represented as a capacitor into which a charge is deposited (Figure 6.3). By applying detector bias, an electric field is created which causes the charge carriers to migrate and be collected. During the charge collection small current flows, and the voltage drop across the bias resistor is the pulse voltage. The preamplifier is isolated from the high voltage by a capacitor. The rise time of the preamplifier's output pulse is related to the collection time of the charge, while the decay time of the preamplifier's output pulse is the Resistor-Capacitor (RC) time constant characteristic of the preamplifier itself. Charge-sensitive preamplifiers are commonly used for most solid state detectors. In charge-sensitive preamplifiers, an output voltage pulse is produced that is proportional to the input charge. The output voltage is essentially independent of detector capacitance. However, noise is also affected by the capacitance. Additionally, the preamplifier also serves to provide a match between the high impedance of the detector and the low impedance of coaxial cables to the amplifier, which may be located at great distances from the preamplifier. The amplifier serves to shape the pulse as well as further amplify it. The long delay time of the preamplifier pulse may not be returned to zero voltage before another pulse occurs, so it is important to shorten it and only preserve

the detector information in the pulse rise time. However, most data consists of a range of pulse heights of which only a small portion is of interest.
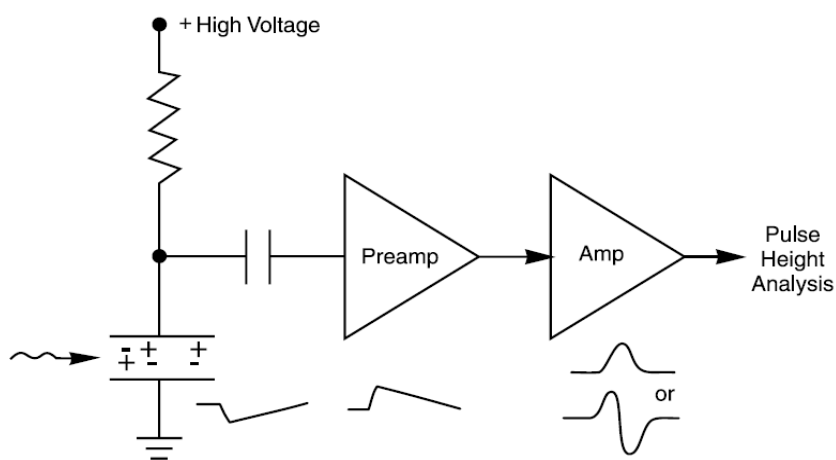
Figure 6.3. Detector and pre-amplification system

One can employ a multichannel analyzer (MCA, in GRD Osprey unit acts as an MCA) which basically consists of an analog-to-digital converter (ADC), control logic, memory and display. The multichannel analyzer collects pulses in all voltage ranges at once and displays this information in real time. An input energy pulse is checked to see if it is within the selected range, and then passed to the ADC. The ADC converts the pulse to a number proportional to the energy of the event. This number is taken to be the address of a memory location, and one count is added to the contents of that memory location. After collecting data for some period of time, the memory contains a list of numbers corresponding to the number of pulses at each discrete voltage. The memory is

accessed by a host computer which is responsible for spectrum display and analysis as well as control of the MCA. The block diagram for an MCA is shown in Figure 6.4.
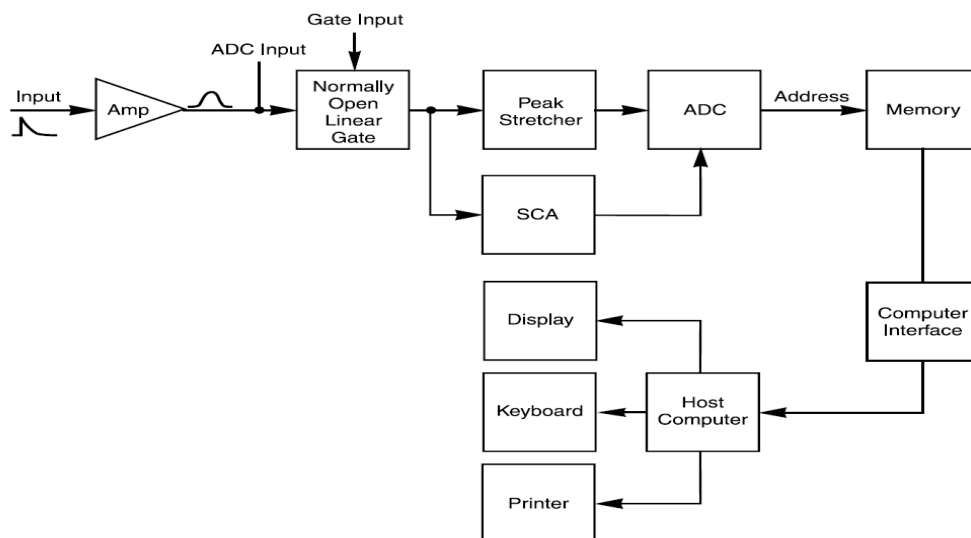
Figure 6.4. Multichannel analyzer components with analog signal processing

The need for a single-input Pulse Height Analysis system for use with a Sodium Iodide detector is served most simply by a photomultiplier tube (PMT) base MCA. The MCA includes a high voltage power supply, preamplifier, amplifier, spectrum stabilizer and ADC in addition to its MCA functions, and thus, there is no need for any NIM modules or a NIM Bin (conventional electronic system). All of this capability is provided in the Osprey unit whose enclosure is no larger than a standard tube base preamplifier, and the computer interface is via a USB port on the host computer or a USB hub (Figure 6.1). Genie Basic Spectroscopy 2000© software is used to analyze the counts received from the detector. Using these γ-ray counts, which is basically a time series is

analyzed to obtain meaningful results. The time-averaged cross sectional (along the diameter) data of the underlying detailed hydrodynamics is processed statistically for determining the flow regimes.

6.3. FLOW REGIME AND FLOW PATTERN IDENTIFICATION

6.3.1. Pressure Fluctuation Analysis. Pressure fluctuation signals were employed to recognize and characterize the flow regimes in spouted bed, i.e. packed bed (PB), stable spouting (SS) and unstable spouting (US). The statistical analysis in time domain is the simplest and the most commonly employed; it is also very fast and easily applicable. The most commonly used method in time domain is to study the amplitude of signals, expressed as a standard deviation (viz., square root of second-order statistical moment). The change in amplitude with operating conditions has been of interest to many fluidization researchers for identification of transitions between flow regimes. The pressure signals which is located at the wall, does not provide information on the flow regions (spout, annulus and fountain) or identify them. This limitation is a huge motivation for the development of non-invasive technique which can identify the flow regions.

The third-order statistical moment, skewness, which is a measure of the lack of symmetry, has also been applied by few authors as an indicator of the regime transition in fluidized beds. Lee and Kim (1988) found that the skewness of absolute pressure fluctuations shifted from negative to positive and vice versa with increasing gas velocity in fluidized beds. The zero skewness point was considered as the transition point to turbulent fluidization. However, Bi and Grace (2004) compared regime transitions based

on skewness and amplitude from time series of absolute and differential pressure transducers in 0.12 m and 0.08 m spouted beds. Their transition results differed depending on whether they used skewness or amplitude, and also depending on the type of measurement. The standard deviation and skewness have also been employed to identify flow regimes in spouted beds (Lopes et al., 2009 and Wang et al., 2011).

For a signal, xi, (i = 1,2,3,. . .,N) standard deviation is calculated by:

$$\sigma = \sqrt{\frac{\sum_{i=1}^{N}(xi - \bar{x})^2}{N-1}} \tag{4}$$

Where average is given by,

$$\bar{x} = \frac{1}{N}\sum_{i=1}^{N} xi \tag{5}$$

Skewness is represented by,

$$S_n = \frac{1}{N\sigma^3}\sum_{i=1}^{N}(xi - \bar{x})^3 \tag{6}$$

The skewness denotes the lack of symmetry about the mean value in the probability distribution, and is equal to zero for symmetric distributions, such as a normal distribution. In the present work, pressure transducer (Model. No. PX309-002G5V, Omega Dyne Inc.) was used to obtain pressure fluctuations. Air was used as a spouting gas, while glass beads (1 mm in diameter, ρ_s = 2450 Kg/m^3) were used as a solid material. The measurements were performed in two spouted beds with different diameters (0.076 m ID and 0.152 m ID) at two comparable axial positions (z) above the gas distributor: 0.19 m in the smaller column and 0.24 m in the bigger column. A mesh was installed at the tip of the transducer in order to prevent the inflow of solids and their contact with the

transducer's membrane. The static bed height of the bed in 0.152 m ID spouted bed was 0.200 m and in 0.076 m ID spouted bed was 0.140 m. The sampling time for each experimental measurement was 30 mins, which gave sufficient data points to analyze the results.

6.3.2. Pressure Transducers. The analysis of pressure fluctuation measurements by pressure transducers was performed. The magnitude of fluctuations increased, when the bed reached stable spouting regime from packed bed and then to unstable spouting regime (Figure 6.5 and 6.6). Fluctuations in stable spouting regime were more periodic in nature and when the bed transitioned into unstable spouting regime the fluctuations became more random and irregular. Bubbling and slugging regime were characterized by more chaotic nature of pressure fluctuations. This in turn implies a rapid increase in the complexity of the gas-solid dynamics with increase of gas velocity. Standard deviation and Skewness were analyzed for these time series fluctuations from 0.152 m and 0.076 m spouted bed. Standard deviation analysis from both the spouted beds increased monotonically as the gas velocity in the beds was increased. The criterion to identify regime transitions were by sudden increments of values in standard deviation compared to the previous values (Figure 6.7 and 6.8). The slope of the data points in a particular regime is different than the other regimes. This is also another parameter to identify the regime changes. Pressure transducers were attached at different axial heights of the spouted beds for measurement and to check the effect of axial height on the measurement of pressure fluctuations. It was found that the axial height did not have any drastic effect on identifying the flow regimes in the spouted beds (Figure 6.9). But the fluctuations in the conical region of the spouted bed were more magnified and the intensity of

fluctuations decreased as the axial height was increased. The gas velocity in the spout region of the conical section (which is closer to the inlet of spouted bed) is high and this will cause the intensity of the pressure fluctuations to be high. Comparison of the standard deviations at different axial heights showed that the standard deviation signals in conical region were larger than those measured at different heights (Figure 6.10). This can be attributed to the turbulent motion of the gas near the spouted bed inlet (conical region).

Skewness (third order statistical moment) was also calculated for the obtained pressure fluctuations from the spouted beds. It was observed that skewness exhibited small deviations for regime transitions as compared to standard deviation. The regime transitions were identified based on the shifting of skewness value from negative to positive and vice versa (Figure 6.10 and 6.11). There was no effect of axial height measurements on skewness (Figure 6.10).

The minimum spouting velocity was found to be 0.72 m/s and 0.58 m/s for 0.152 m and 0.076 m ID spouted beds, respectively. The transition velocity from stable spouting to unstable spouting regime was found to be 0.79 m/s and 0.66 m/s for 0.152 m and 0.076 m ID spouted beds, respectively. The obtained transition values for the flow regimes were compared with the data in the literature and were found to be in good agreement with them for both the 0.152 m and 0.076 m ID spouted beds. The standard deviation analysis was much less sensitive than the skewness. Standard deviation captured different transition velocities from stable to unstable spouting regime in 0.152 m spouted bed compared to skewness. This shows that pressure transducer measurements

cannot be fully relied on to capture important information. The measurements made at the

wall by the pressure may not fully reflect the phenomena inside the spouted beds.
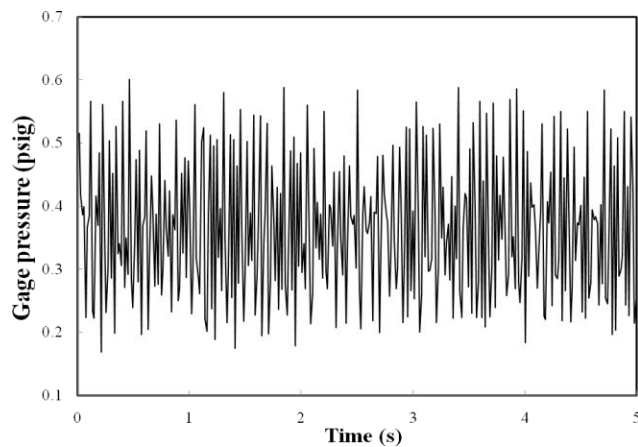
Figure 6.5. Gauge pressure fluctuations at stable spouting regime in 0.152 m ID spouted
bed at axial height of 0.183 m from the bottom of spouted bed.
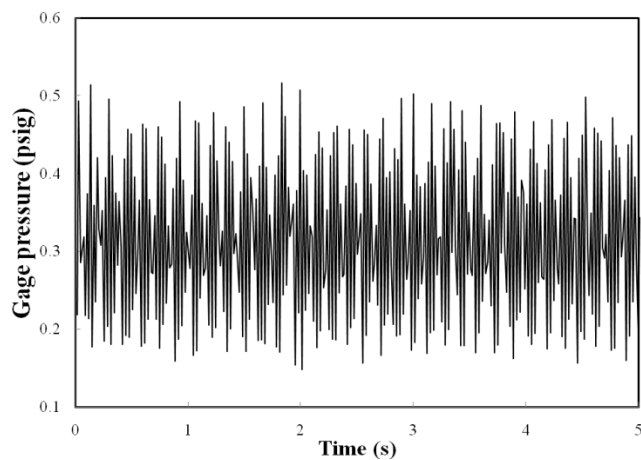
Figure 6.6. Gauge pressure fluctuations at unstable spouting regime in 0.152 m ID
spouted bed at a axial height of 0.183 m from the bottom of spouted bed.

Figure 6.7. Standard deviation analysis showing different flow regimes for 0.152 m ID spouted bed using 1mm glass beads with density of 2450 kg/m^3 (I = Packed bed; II = stable spouting regime and III = unstable spouting regime).

Figure 6.8. Skewness analysis showing different flow regimes for 0.152 m ID spouted bed using 1mm glass beads with density of 2450 kg/m^3 (I = Packed bed; II = stable spouting regime and III = unstable spouting regime).
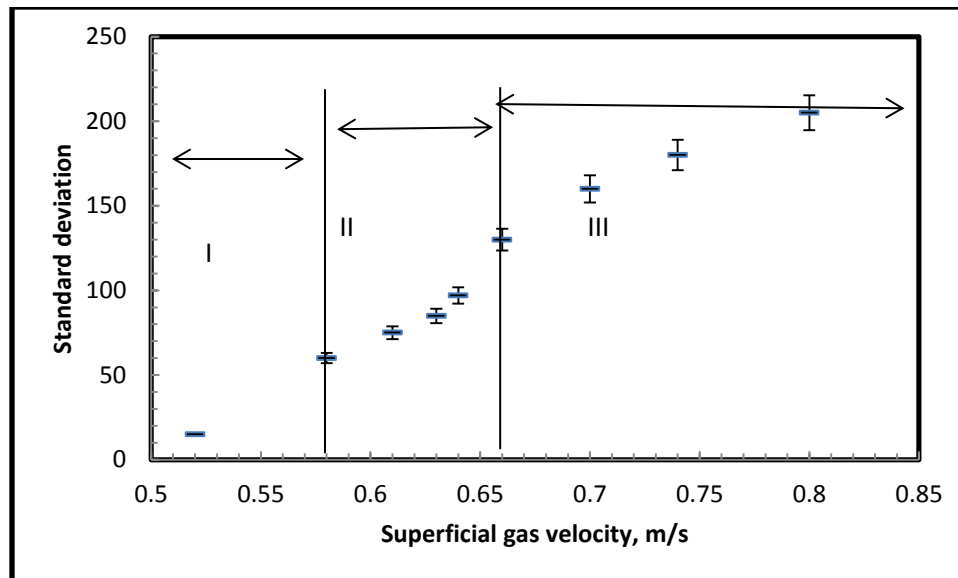
Figure 6.9. Standard deviation analysis showing different flow regimes for 0.076 m ID spouted bed using 1mm glass beads with density of 2450 kg/m^3 (I = Packed bed; II = stable spouting regime and III = unstable spouting regime).

Figure 6.10. Skewness analysis showing different flow regimes for 0.076 m ID spouted bed using 1mm glass beads with density of 2450 kg/m^3 (I = Packed bed; II = stable spouting regime and III = unstable spouting regime).
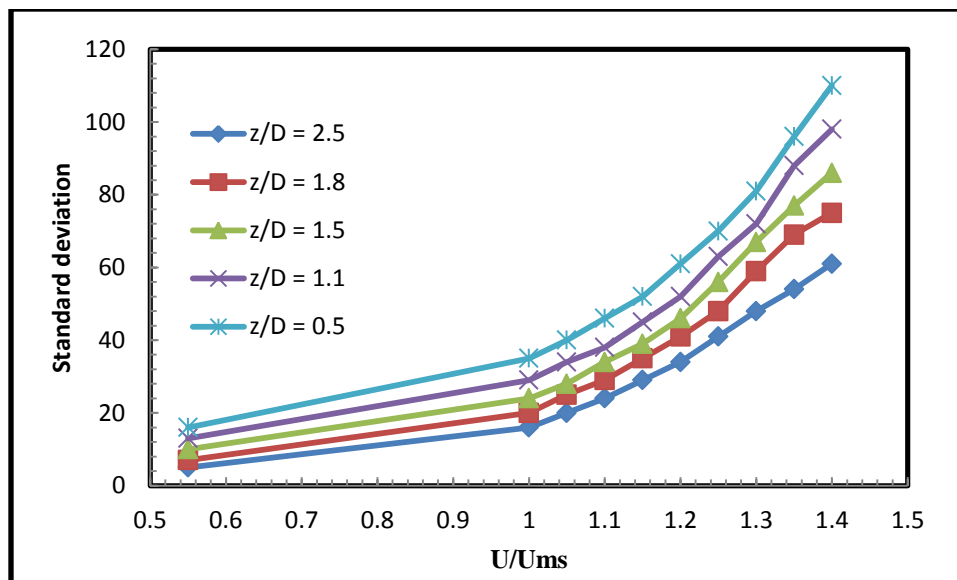
Figure 6.11. Effect of axial height measurement of pressure fluctuations on standard deviation in 0.152 m spouted bed with 1mm glass beads of density 2450 kg/m^3.
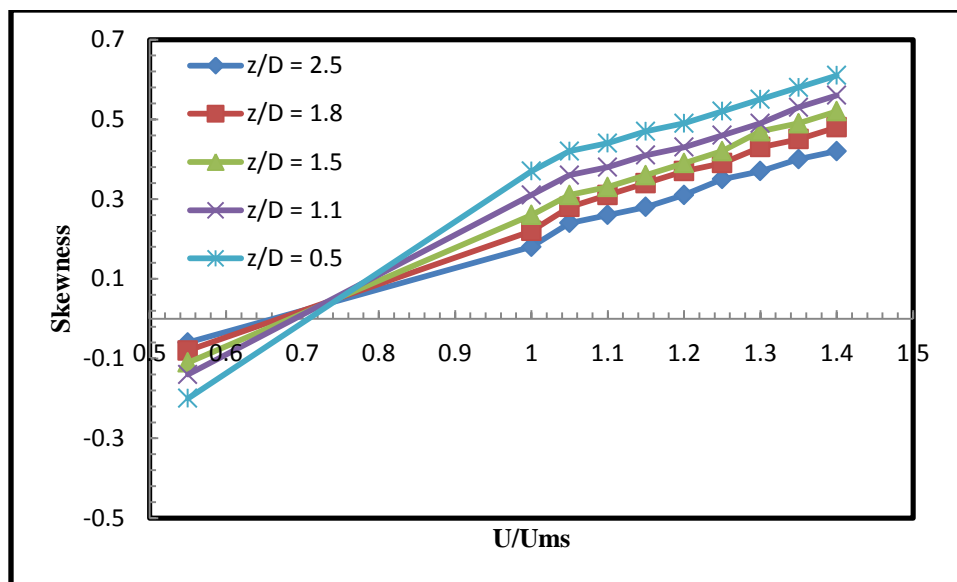
Figure 6.12. Effect of axial height measurement of pressure fluctuations on skewness in 0.152 m spouted bed with 1mm glass beads of density 2450 kg/m^3.

6.3.3. Optical Probe for Flow Regime Analysis. Optical probes are an invasive technique which works on the principle of back reflection of light. The voltage signal fluctuations measured from the optical probe are utilized to identify the flow regions and flow regimes in spouted bed. The statistical parameters used to identify flow regime was mean and variance. Optical probes were also able to distinguish between different regions of the spouted bed based on the amount of solids in each of the three different zones in the spouted bed. The spout is predominantly dominated by the gas phase and hence the number of solids in this region is less, leading to lower fluctuations of signal from the probe. The annulus region is dominated by the solids phase, which moves downward as loose moving packed bed. The voltage signal fluctuations in this region are high. The fountain region consists of solids which fall back onto the bed surface after being carried by the gas phase. The voltage signal fluctuations here are in between the spout and annulus regions. This clearly helps us in differentiating the three regions of spouted bed (discussed in Section 4).

The optical probes were placed in the spouted bed at the spout-annulus interface, as this would be the ideal location in the bed to extract significant fluctuation changes at different superficial velocities. Mean and Standard deviation were analyzed for these times series signal fluctuations from 0.152 m spouted bed. Analysis of mean from the spouted bed increased monotonically as the gas velocity in the beds was increased. The criterion to identify regime transitions was by sudden increments of mean values compared to the previous values (Figure 6.13). The slope of the data points in a particular regime is different than the other regimes. This is also another parameter to identify the regime changes. Optical probes were attached at different axial heights of the spouted

beds for measurement and to check the effect of axial height on the measurement of signal fluctuations. It was found that the axial height did not have any drastic effect on identifying the flow regimes in the spouted beds. Standard deviation was also calculated for the obtained voltage signal fluctuations from the spouted beds (Figure 6.14).

The minimum spouting velocity was found to be 0.72 m/s for 0.152 m. The transition velocity from stable spouting to unstable spouting regime was found to be 0.79 m/s for 0.152 m ID spouted bed. The obtained transition values for the flow regimes were compared with the pressure transducers and were found to be in close agreement with the 0.152 m ID spouted bed.
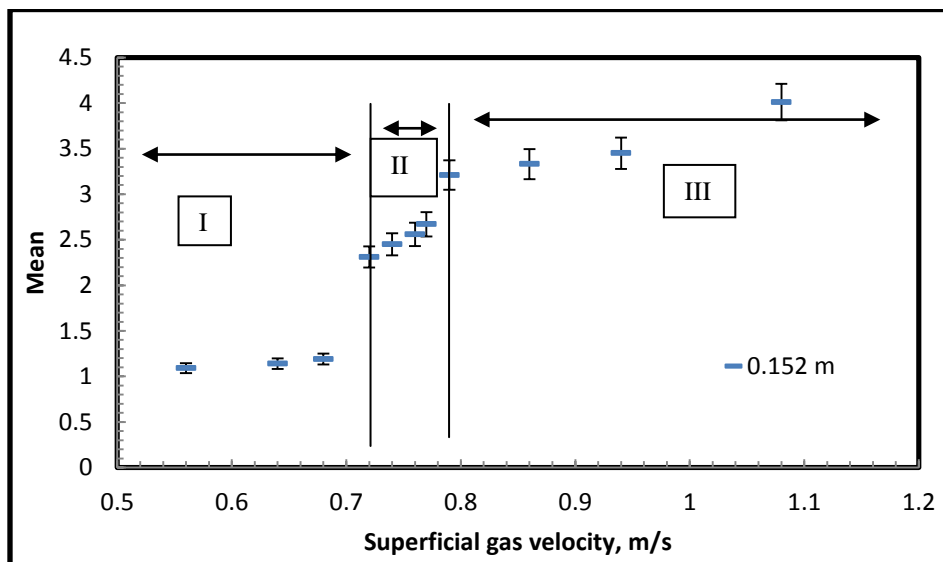
Figure 6.13. Mean versus superficial gas velocity using optical probe technique showing different flow regimes for 0.152 m ID spouted bed using 1mm glass beads with density of 2450 kg/m^3 (I = Packed bed; II = stable spouting regime and III = unstable spouting regime).
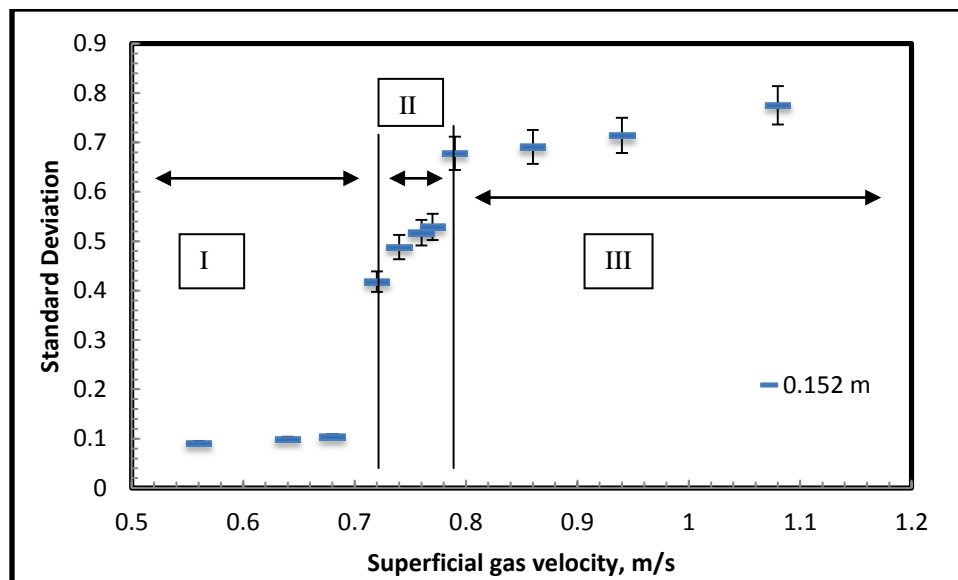
Figure 6.14. Standard deviation versus superficial gas velocity using optical probe technique showing different flow regimes for 0.152 m ID spouted bed using 1mm glass beads with density of 2450 kg/m^3 (I = Packed bed; II = stable spouting regime and III = unstable spouting regime).

6.3.4. Gamma Ray Densitometry. In the present study the time series signals of photon counts measured by the gamma ray densitometry in the gas-solid spouted bed are analyzed statistically to identify the flow regimes. The following statistical parameters are calculated

1.   Mean and variance

The mean, μ is calculated by:

$$\mu = (\sum_{i=1}^{N} Xi)/N \qquad (7)$$

Where, Xi is the collected counts at each sampling period and N are the total number of sampling points. The absolute average deviation of the measured data from the mean can be obtained by:

$$AverageDeviation = \sum_{i=1}^{N} |Xi - \mu| / (N) \tag{8}$$

The variance (σ^2) is:

$$\sigma^2 = \frac{1}{N-1} \sum_{i=1}^{N} (Xi - \mu)^2 \tag{9}$$

Where N-1 is the number of points – degree of freedom.

2.   Deviation from Poisson distribution:

The time series of gamma ray photon counts through a homogenous medium follows Poisson distribution. In a homogenous medium, (air-liquid system, Shaikh PhD thesis) the mean is equal to the variance. Hence the ratio of the variance to the mean of the time series following poisson distribution is unity. Such ratio has been used as a possible indicator to identify flow regime in bubble column (Shaikh, 2007). If the system deviates from the Poisson distribution the value of such ratio increases. Hence, the indicator, I which is called flow regime indicator (Equation 10) has the ratio of the variance and mean.

$$\text{Flow Regime Indicator (I)} = (Variance)i / Mean \tag{10}$$

Gamma ray densitometry experiments performed on bubble columns (gas-liquid system) by Shaikh, 2007, used water as the liquid medium which is a homogenous phase before gas entered the system. Therefore, the photon counts for such a homogenous phase showed mean close to variance. But the packed bed of solids, before the gas phase enters to initiate the spouting, consists of solids and voids. Hence, packed bed before spouting represents a heterogeneous medium which would not show mean close to variance of the

time series of gamma ray counts received by the detector and hence, it deviates from poisson distribution. Such deviation would change in magnitude when the spouting is initiated and flow regime changes. Hence, the analysis of regime identification of spouted bed (heterogeneous medium) depends on the percentage of deviation from the counts received from packed bed.

Figures 6.15 and 6.16 show typical photon counts received by NaI scintillation detector in packed bed, at minimum spouting velocity and at stable spouting regime, respectively for over 30 seconds of data acquisition. The flow regime transitions were identified using mean, variance and the ratio, I (percentage of deviation from packed bed), as the indicators. The main criterion for differentiating the different flow regimes were based on the large difference between the successive values of the above mentioned three parameters.

When the spouted bed was operating in the packed bed regime, there was no change in the values of mean, variance and the ratio (I). As the regime shifted from packed bed to stable spouting the values of all the three parameters increased, thus indicating the capture of flow regime transition (Figures 6.17 – 6.22). The same was observed when the flow regime shifted from stable spouting to unstable spouting regime. The onset of stable spouting regime was found to be at 0.72 m/s and 0.58 m/s for 0.152 m and 0.076 m ID spouted beds respectively. These transition velocities were in good agreement with the experimental results obtained by pressure fluctuation measurements (3.4% overall difference) and with the comparison of literature correlations (7.8% overall difference). The transition velocity for stable spouting to unstable spouting regime was found to be at 0.79 m/s and 0.66 m/s for 0.152 m and 0.076 m ID spouted beds

respectively. The close agreement in the transition velocities for the flow regimes indicates the successful demonstration of GRD technique as a means to identify different flow regimes in gas-solid systems. It was also found that the region of stable spouting regime increased from 0.076 m ID spouted bed to 0.152 m ID spouted bed.

(a)

(b)
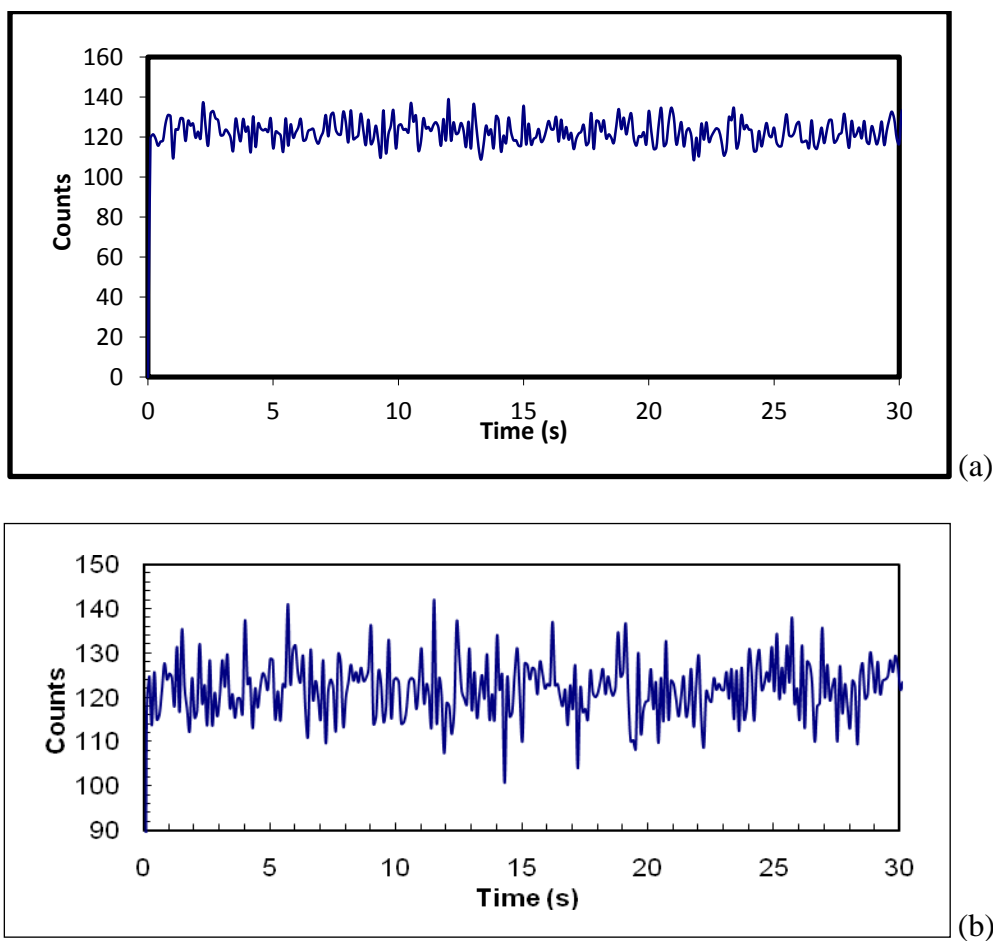
Figure 6.15. Photon counts received by NaI scintillation detector, a. Packed bed and b. At minimum spouting velocity (U_{ms}) in 0.152 m ID spouted bed at a axial height of 0.183 m at $U_g = 1.04$ m/s.
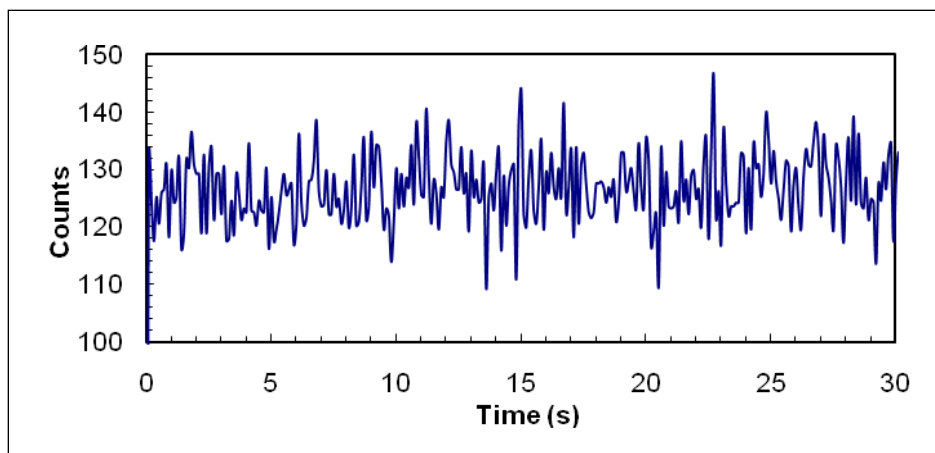
Figure 6.16. Photon counts received by NaI scintillation detector in stable spouting regime in 0.152 m ID spouted bed at a axial height of 0.183 m at U_g =1.1 m/s.
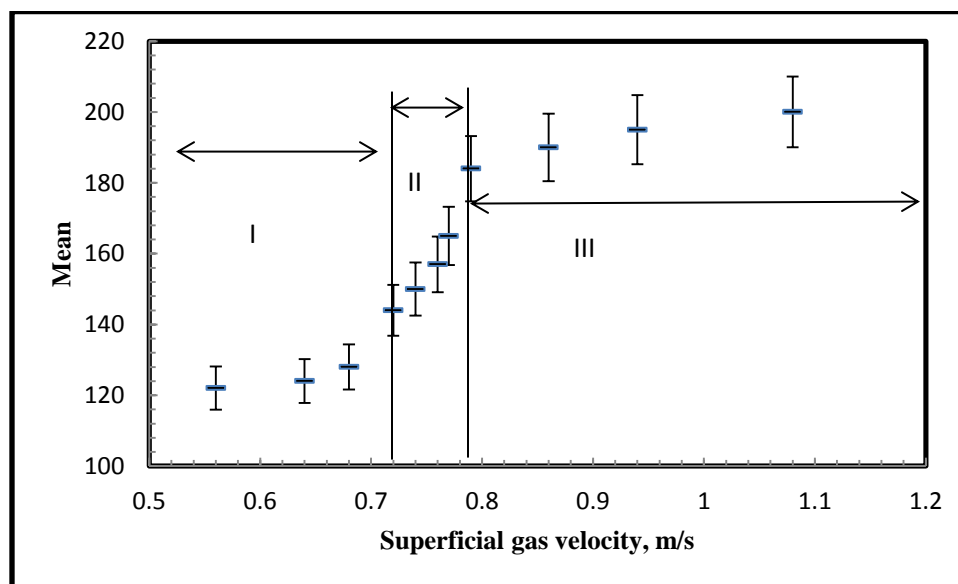
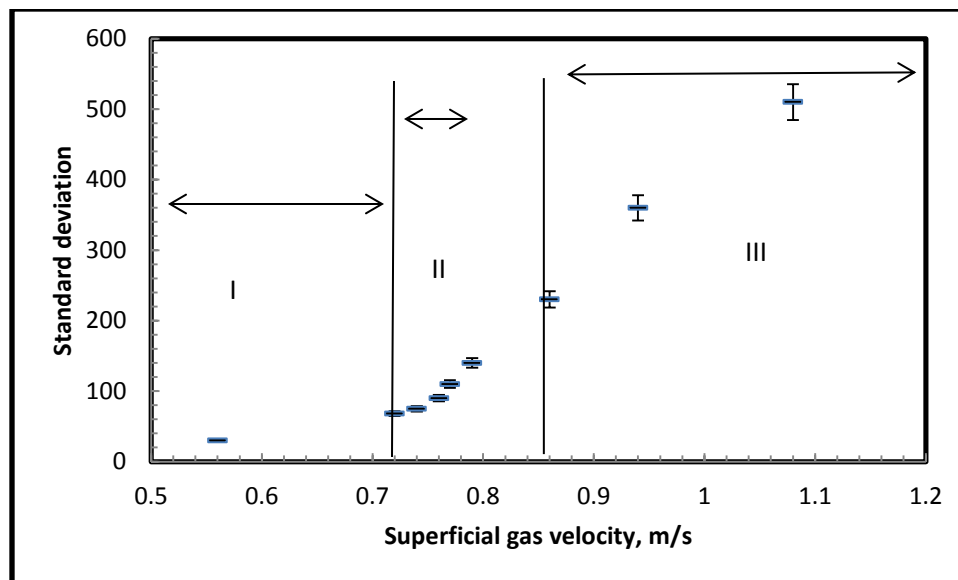Figure 6.17. Mean versus superficial gas velocity using GRD technique showing different flow regimes for 0.152 m ID spouted bed using 1mm glass beads with density of 2450 kg/m^3 (I = packed bed; II = stable spouting regime and III = unstable spouting regime)
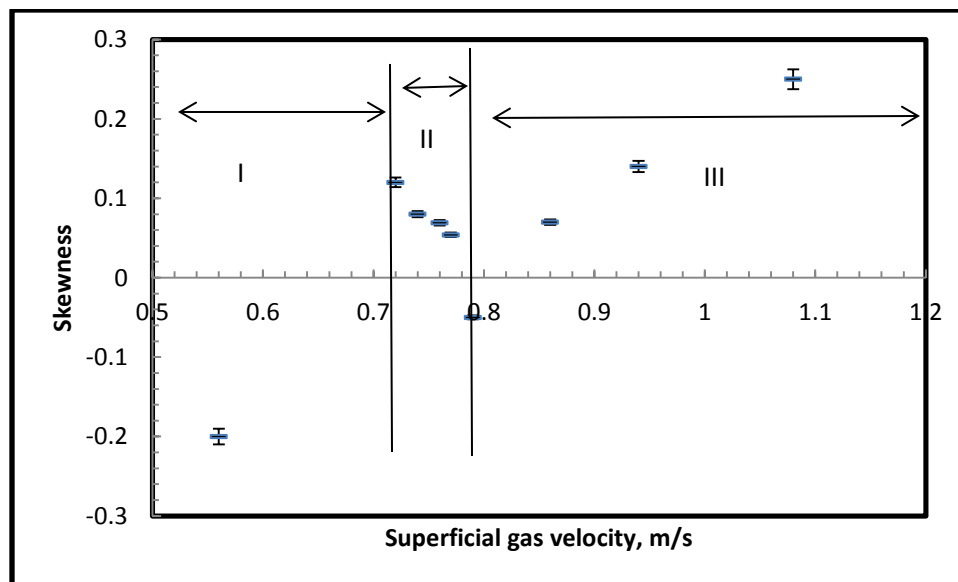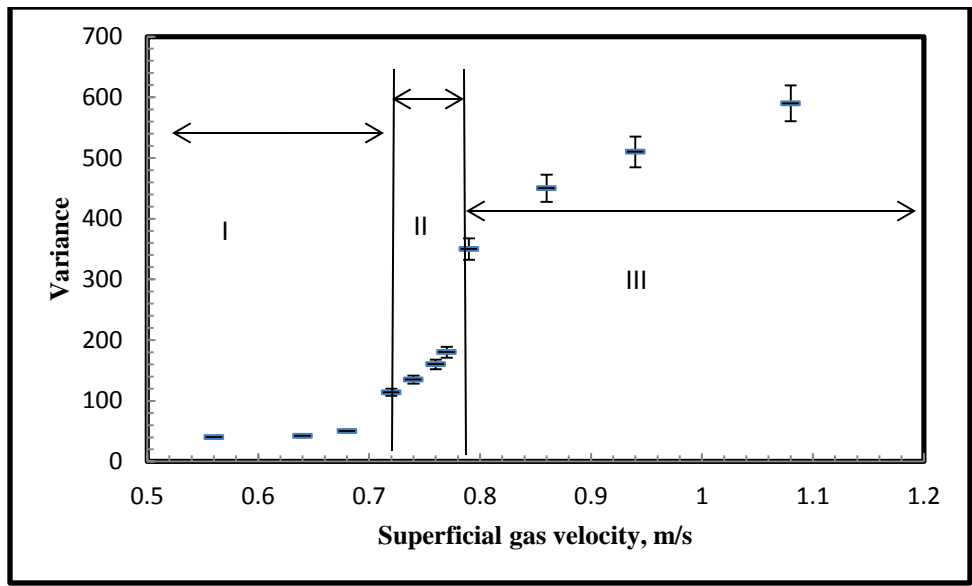
Figure 6.18. Variance versus superficial gas velocity using GRD technique showing different flow regimes for 0.152 m ID spouted bed using 1mm glass beads with density of 2450 kg/m^3 (I = packed bed; II = stable spouting regime and III = unstable spouting regime)
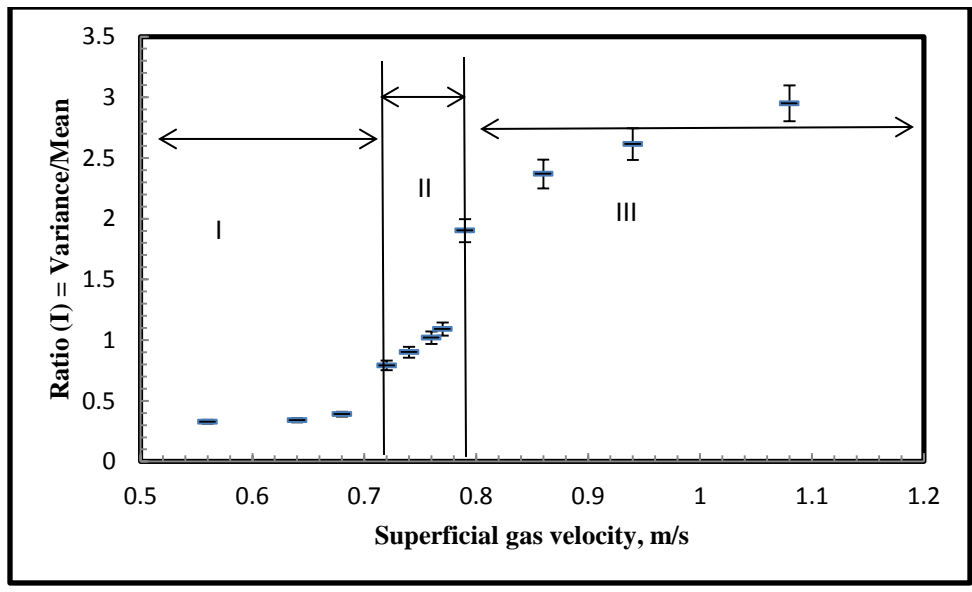

Figure 6.19. Ratio (I) = Variance/Mean versus superficial gas velocity using GRD technique showing different flow regimes for 0.152 m ID spouted bed using 1mm glass beads with density of 2450 kg/m^3 (I = packed bed; II = stable spouting regime and III = unstable spouting regime)
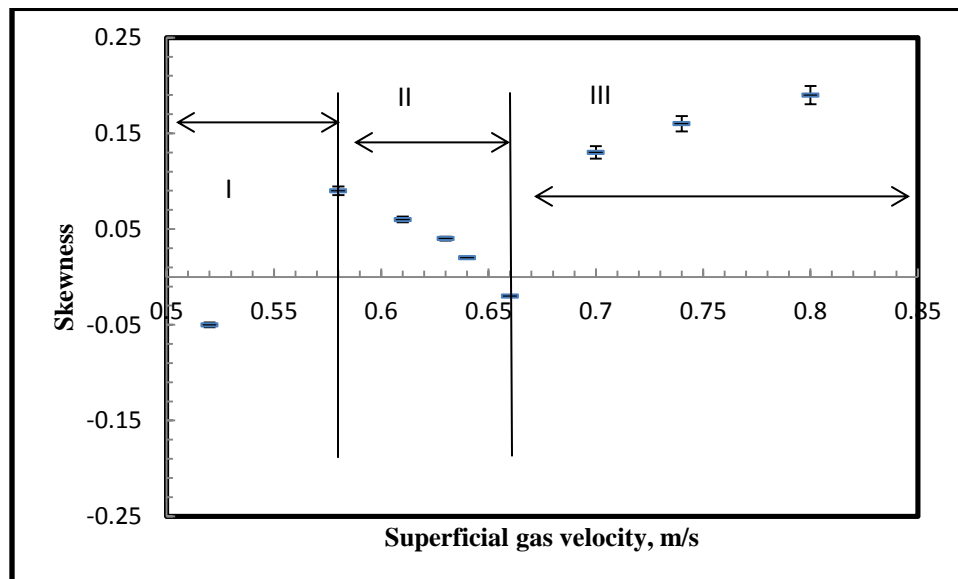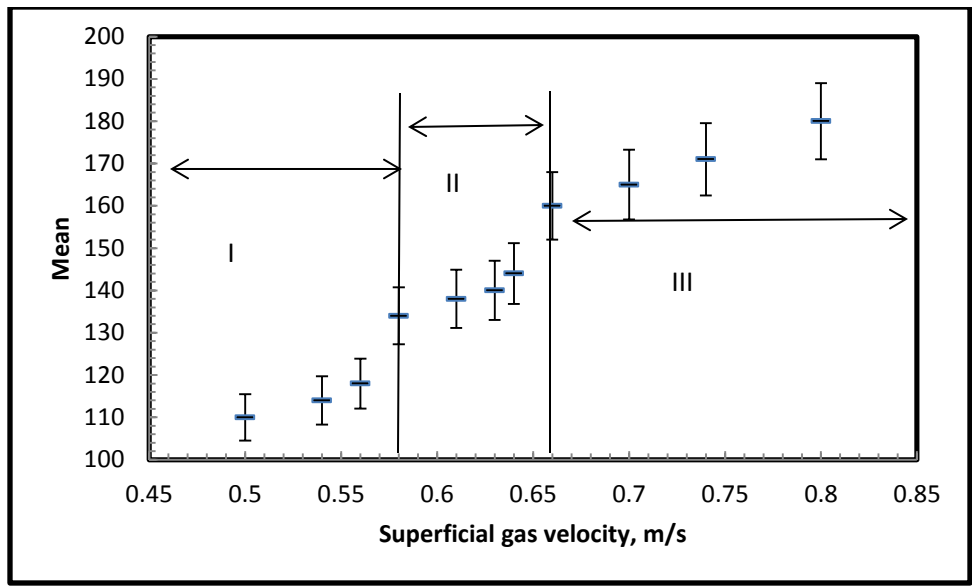
Figure 6.20. Mean versus superficial gas velocity using GRD technique showing different flow regimes for 0.076 m ID spouted bed using 1mm glass beads with density of 2450 kg/m^3 (I = packed bed; II = stable spouting regime and III = unstable spouting regime)
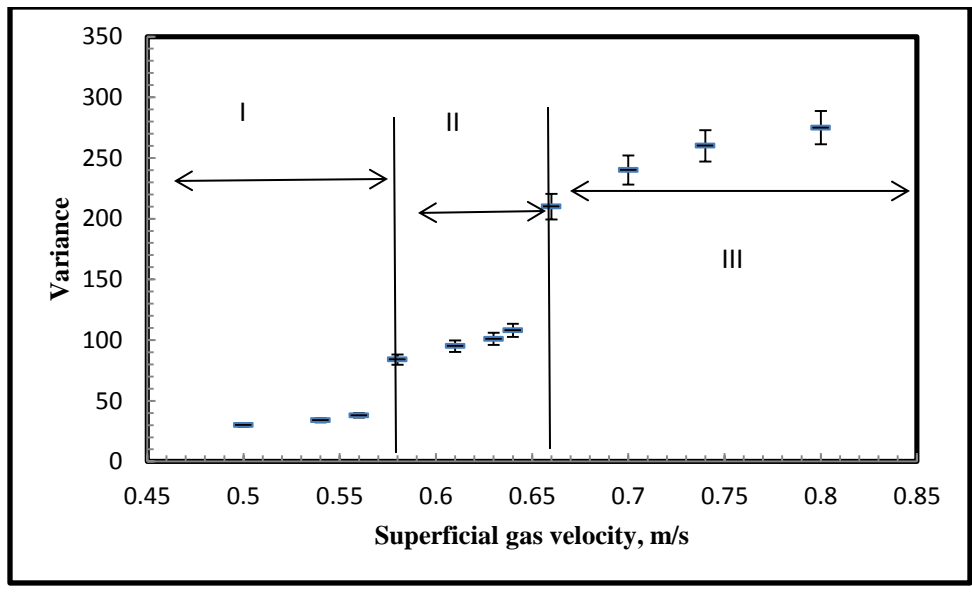
Figure 6.21. Variance versus superficial gas velocity using GRD technique showing different flow regimes for 0.076 m ID spouted bed using 1mm glass beads with density of 2450 kg/m^3 (I = packed bed; II = stable spouting regime and III = unstable spouting regime)
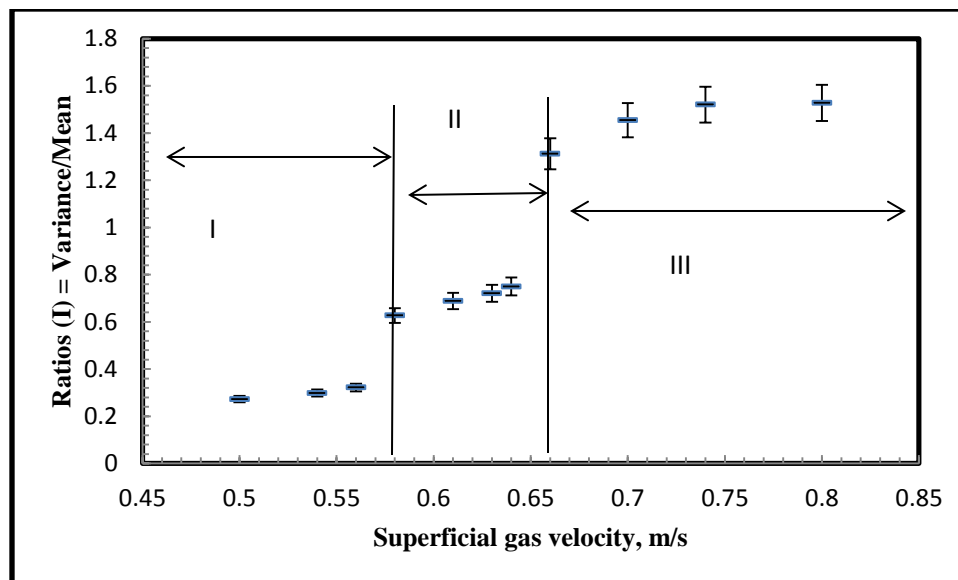
Figure 6.22. Ratio (I) = Variance/Mean versus superficial gas velocity using GRD technique showing different flow regimes for 0.076 m ID spouted bed using 1mm glass beads with density of 2450 kg/m^3 (I = packed bed; II = stable spouting regime and III = unstable spouting regime)

6.4 REMARKS

Based on the analysis of pressure fluctuation measurements from pressure transducers, signal fluctuations from optical probes and photon counts from gamma ray densitometry, flow regimes were evaluated in 0.152 m and 0.076 m ID spouted beds. The transition velocities identified by these techniques were in good agreement with the published data in the literature. The newly developed non-invasive radioisotope technique (GRD) was able to successfully identify different flow regimes and their transition velocities. GRD was also successfully able to identify radial profiles of solids volume fraction (discussed in Section 4). It was found that the region of stable spouting increased from smaller diameter bed to higher diameter bed. The implementation of such

non-invasive technique would be helpful for many industrial applications making the process reliable. Since, nuclear gauge densitometry is already available in many industries (for a level control, density measurements etc.) such applications in industry will help in better understanding of the phenomena.

**7. PERFORMING COMPUTATIONAL FLUID DYNAMICS (CFD)
SIMULATION FOR FACILITATING THE IMPLEMENTATION OF THE
NEWLY DEVELOPED SCALE-UP METHODOLOGY AND FOR
QUANTIFYING THE EFFECTS OF DESIGN AND OPERATING VARIABLES
ON THE HYDRODYNAMICS OF SPOUTED BEDS**

7.1 INTRODUCTION

The two most commonly used methods for modeling gas–solids two-phase systems are the discrete element method (DEM) and the two fluid model method (TFM). In the DEM approach, the gas phase is described by a locally averaged Navier–Stokes equation, the motion of individual particles is traced, and the two phases are coupled by interphase forces. For the TFM approach, the different phases are mathematically treated as interpenetrating continua, and the conservation equation for each of the two phases is derived to obtain a set of equations that have similar structure for each phase. Both of the two approaches are adopted in spouted bed modeling. Krzywanski et al. (1992) developed a multi-dimensional model to describe the gas and particle dynamic behavior in a spouted bed. Kawaguchi et al. (2000) proposed an Eulerian–Lagrangian approach, the three-dimensional motion of solids was discretely traced by solving Newton's equation of motion using the DEM. Huilin et al. (2001) presented a two-fluid gas–solids flow model for spouted beds, viewing spout and annulus as two interconnected regions. Huilin et al. (2004) also incorporated a kinetic-frictional constitutive model for dense assemblies of solids in the simulation of spouted beds. The model treated the kinetic and frictional stresses of particles additively.

From the point of view of computation, the TFM approach is much more feasible for practical applications to model complex multiphase flows; therefore extensive attention has been given to improving its accuracy. The success of the TFM depends on

the proper description of the solids stress and the interfacial forces. By introducing the concepts of solids "pressure" and "viscosity", the well-known granular kinetic theory has been well established and now has been widely employed for the solids stress calculation. The interfacial forces include drag force, lift force and virtual mass force, etc. In coupling the equations of the two phases, due to the large difference in their densities, those forces other than drag force are less significant, and thus can be usually neglected.

Consequently, in most reports, whenever the interfacial forces were dealt with, only drag force was considered. Some authors had noticed that the choice of drag models played a critical role in simulating gas–solids two-phase flows. Yasuna et al. (1995) showed that the solution of their model was sensitive to the values of drag coefficients. O'Brien and Syamlal (1993) suggested that the drag force correlations for fine particles should be corrected to account for the formation of clusters. Enwald et al. (1996) found that the predictions based on different drag models were in good agreements with each other for the dilute region, but obviously different for the dense region. Van Wachem et al. (2001) noticed that flow predictions were not sensitive to the use of different solids stress models or radial distribution functions, as the different approaches were very similar in dense flow regimes, but the application of different drag models significantly impacted the flow of the solids phase. More or less, these results signify that an improper choice of drag models may yield inaccurate results or even lead to incorrect descriptions of gas–solids two-phase flows. Du et al. (2006) studied the effect of different drag models on spouted bed simulation and found that Gidaspow (1994) model gives the best fits to the experimental data. Since the drag force is the only accelerating force acting on

particles, thus the selection of drag models make a difference in the CFD simulation of the spouted beds.

Two–fluid model (TFM) has been considered in the present study for the modeling of complicated gas–solid flow in spouted beds. By TFM approach, the gas–solid two phase are treated mathematically as continuous and fully interpenetrating. Generalized Navier–Stokes equations are used for the interacting continua. To close the governing equations, the constitutive relations are needed. Because the solids phase is treated as continuous, it has similar properties to a continuous fluid. By using the kinetic theory of granular flows (Ding and Gidaspow, 1990), the viscous forces and the pressure of solids phase can be described as a function of the granular temperature (Lun et al., 1984). The stress of solids phase due to frictional interactions between particles is represented by using the Schaeffer (1987) model. The governing equations and constitutive relations for spouted beds are listed in Section 7.2.

In spouted beds, the gases and particles in the spout region rise at high velocities, while particles move slowly downwards in the annulus region between the spout and the wall. In the spout region, the influence of gas turbulent fluctuations on overall gas–solid flow behavior is greatly essential. However, there has been no consistency on whether turbulent fluctuation effects should be considered and which turbulent model is the most suitable for CFD simulation of spouted beds. Du et al. (2006c) applied the dispersed turbulence model and the per-phase turbulence model, respectively, to simulate the flow in spouted beds. The results showed that the dispersed turbulence model could predict reasonable trends of spouting flow, while the per-phase turbulence model overestimated the particle turbulent fluctuations and could not predict the spouting flow trends. Hence,

in the present work, the dispersed turbulence model has been adopted, where turbulence predictions for gas phase are obtained by the standard k–ε model supplemented with extra terms that include the inter-phase turbulent momentum transfer. The equations of k–ε turbulence model are listed in Section 7.2.

As mentioned above, the gas–solid drag coefficient is critical to a successful simulation, and the Gidaspow model, a combination of the Wen and Yu model (1966) and the Ergun equation (1952), can reasonably describe the interaction of gas and solids phases in spouted beds. Lan et al. (2012) applied successfully the TFM approach to closely predict spouted bed hydrodynamics by using Gidaspow drag model. The same approach of Lan et al. (2012) has been applied in the current study to perform hydrodynamic simulations on spouted beds. The governing equations employed by Lan et al. (2012) to describe the flow dynamics in the spouted bed has been listed in Section 7.2.

7.2 GOVERNING EQUATIONS

1. Continuity equation for gas and solid phase

$$\frac{\partial}{\partial t}(\alpha_g \rho_g) + \nabla.(\alpha_g \rho_g v_g) = 0 \tag{1}$$

$$\frac{\partial}{\partial t}(\alpha_s \rho_s) + \nabla.(\alpha_s \rho_s v_s) = 0 \tag{2}$$

$$\alpha_g + \alpha_s = 1 \tag{3}$$

2. Momentum equation for gas and solid phase

$$\frac{\partial}{\partial t}(\alpha_g \rho_g v_g) + \nabla.(\alpha_g \rho_g v_g v_g) = -\alpha_g \nabla P + \nabla.\overline{\overline{\tau}}_g + \beta(v_s - v_g) + \alpha_g \rho_g g \tag{4}$$

$$\frac{\partial}{\partial t}(\alpha_s \rho_s v_s) + \nabla.(\alpha_s \rho_s v_s v_s) = -\alpha_s \nabla P_s + \nabla.\overline{\overline{\tau}}_s + \beta(v_g - v_s) + \alpha_s \rho_s g \tag{5}$$

Where,

$$\overline{\overline{\tau}}_g = \alpha_g \mu_g \left\{ \left[\nabla v_g + (\nabla v_g)^T \right] - \frac{2}{3} \nabla . v_g \overline{\overline{I}} \right\} \tag{6}$$

$$\overline{\overline{\tau}}_s = \alpha_s \mu_s \left[\nabla v_s + (\nabla v_s)^T \right] + \left(\alpha_s \lambda_s - \frac{2}{3} \alpha_s \mu_s \right) \nabla . v_s \overline{\overline{I}} \tag{7}$$

3.   Granular temperature equation (Ding and Gidaspow, 1990)

$$\frac{3}{2} \left[\frac{\partial}{\partial t} (\rho_s \alpha_s \Theta_s) + \nabla.(\alpha_s \rho_s v_s \Theta_s) \right] = \left(-\nabla P_s \overline{\overline{I}} + \overline{\overline{\tau}}_s \right) : \nabla v_s + \nabla.(\Gamma_{\Theta s} \nabla \Theta_s) - \gamma_{\Theta s} - 3\beta \Theta_s \tag{8}$$

4.   Solids pressure

$$P_s = \alpha_s \rho_s \Theta_s + 2\rho_s (1 + e_{ss}) \alpha_s^{\ 2} g_{0,ss} \Theta_s \tag{9}$$

5.   Solids shear viscosity

$$\mu_s = \mu_{s,col} + \mu_{s,kin} + \mu_{s,fr} \tag{10}$$

6.   Collisional viscosity (Gidaspow et al., 1992)

$$\mu_{s,col} = \frac{4}{5} \alpha_s^{\ 2} \rho_s d_s g_{0,ss} (1 + e_{ss}) \sqrt{\frac{\Theta_s}{\pi}} \tag{11}$$

7.   Kinetic viscosity (Gidaspow et al., 1992)

$$\mu_{s,kin} = \frac{10 \rho_s d_s \sqrt{\pi \Theta_s}}{96(1 + e_{ss}) g_{0,ss}} \left[1 + \frac{4}{5} g_{0,ss} \alpha_s (1 + e_{ss}) \right]^2 \tag{12}$$

8.   Frictional viscosity (Schaeffer, 1987)

$$\mu_{s,fr} = \frac{P_s \sin \phi}{2\sqrt{I_{2D}}} \tag{13}$$

9.   Solids bulk viscosity (Lun et al., 1984)

$$\lambda_s = \frac{4}{3} \alpha_s \rho_s d_s g_{0,ss} (1 + e_{ss}) \sqrt{\frac{\Theta_s}{\pi}} \tag{14}$$

10.   Diffusion coefficient of granular energy (Gidaspow et al., 1992)

$$\Gamma_{\Theta s} = \frac{150\rho_s d_s \sqrt{\pi\Theta_s}}{384(1+e_{ss})g_{0,ss}}\left[1+\frac{6}{5}\alpha_s g_{0,ss}(1+e_{ss})\right]^2 + 2\alpha_s^2 \rho_s d_s g_{0,ss}(1+e_{ss})\sqrt{\frac{\Theta_s}{\pi}} \quad (15)$$

11. Collisional energy dissipation (Lun et al., 1984)

$$\gamma_{\Theta s} = \frac{12(1-e_{ss}^2)g_{0,ss}}{d_s\sqrt{\pi}}\rho_s\alpha_s^2\Theta_s^{3/2} \quad (16)$$

12. Radial distribution function

$$g0,ss = \left[1-\left(\frac{\alpha_s}{\alpha_{s,max}}\right)^{\frac{1}{3}}\right]^{-1} \quad (17)$$

13. Gas viscosity

$$\mu_g = \mu_{l,g} + \mu_{t,g} \quad (18)$$

$$\mu_{t,g} = C_\mu \alpha_g \rho_g \frac{k_g^2}{\varepsilon_g} \quad (19)$$

14. Turbulent kinetic energy equation

$$\frac{\partial}{\partial t}(\alpha_g\rho_g k_g) + \nabla.(\alpha_g\rho_g v_g k_g) = \nabla.\left(\alpha_g \frac{\mu_{t,g}}{\sigma_k}k_g\right) + \alpha_g G_{k,g} - \alpha_g\rho_g\varepsilon_g + \alpha_g\rho_g\Pi_{k,g} \quad (20)$$

15. Turbulent kinetic energy dissipation rate equation

$$\frac{\partial}{\partial t}(\alpha_g\rho_g\varepsilon_g) + \nabla.((\alpha_g\rho_g v_g\varepsilon_g) = \nabla.\left(\alpha_g \frac{\mu_{t,g}}{\sigma_g}\varepsilon_g\right) + \alpha_g \frac{\varepsilon_g}{k_g}(C_{1\varepsilon}G_{k,g} - C_{2\varepsilon}\rho_g\varepsilon_g) + \alpha_g\rho_g\Pi_{\varepsilon,g}$$

$$(21)$$

Where,

$$G_{k,g} = \mu_{t,g}\left(\nabla v_g + (\nabla v_g)^T\right):\nabla v_g \quad (22)$$

$$C_\mu = 0.09, C_{1\varepsilon} = 1.44, C_{2\varepsilon} = 1.92, \sigma_k = 1 \text{ and } \sigma_\varepsilon = 1.3 \quad (23)$$

16. Gas–solid drag coefficient (Gidaspow et al., 1992)

$$\beta = 150 \frac{a_g^2 \mu_g}{a_g d_s^2} + 1.75 \frac{a_s \rho_g |v_g - v_s|}{d_s}, \alpha_g < 0.8 \tag{24}$$

$$\beta = \frac{3}{4} C_D \frac{a_s a_g \rho_g |v_g - v_s|}{d_s} a_g^{-2.65}, \alpha_g \geq 0.8 \tag{25}$$

$$C_D = \frac{24}{a_g \operatorname{Re}_s} \left(1 + 0.15(a_g \operatorname{Re}_s)^{0.687}\right), \operatorname{Re}_s < 1000 \tag{26}$$

$$C_D = 0.44, \operatorname{Re}_s \geq 1000 \tag{27}$$

$$\operatorname{Re}_s = \frac{\rho_g d_s |v_g - v_s|}{\mu_g} \tag{28}$$

7.3 NUMERICAL SIMULATION METHOD

The simulations of spouted beds have been carried out with the FLUENT 6.3 package. The set of governing equations mentioned in Section 7.2 have been solved by a finite control volume technique. The Phase Coupled SIMPLE algorithm, which is an extension of the SIMPLE algorithm for multiphase flow, has been used for the pressure-velocity coupling and correction. The momentum, volume fraction and turbulence equations have been discretized by a first-order upwind scheme. Two-dimensional and three-dimensional grids were studied and two-dimensional grid was chosen based on lesser simulation time and same accuracy of results compared to three-dimensional grids (details of the 2D and 3D simulations are discussed in APPENDIX C). Two-dimensional axial symmetry has been assumed in the simulation. The dimensions of the computational domain in radial and axial directions are the same as those of the actual spouted bed. Grids have been created in a CAD program GAMBIT 2.4 and imported into FLUENT 6.3. The geometry of spouted bed and its grids are shown in Figure 7.1. A transient

simulation has been adopted, using a very small time step of 0.0001 sec with about 20 iterations per time step. A convergence criterion of 10^{-3} for each scaled residual component has been specified for the relative error between two successive iterations. Grid convergence studies were performed on three different grids (coarse, medium and fine). Based on the simulation results, medium grid size was chosen for the present simulation studies (details of grid convergence studies are discussed in APPENDIX C).
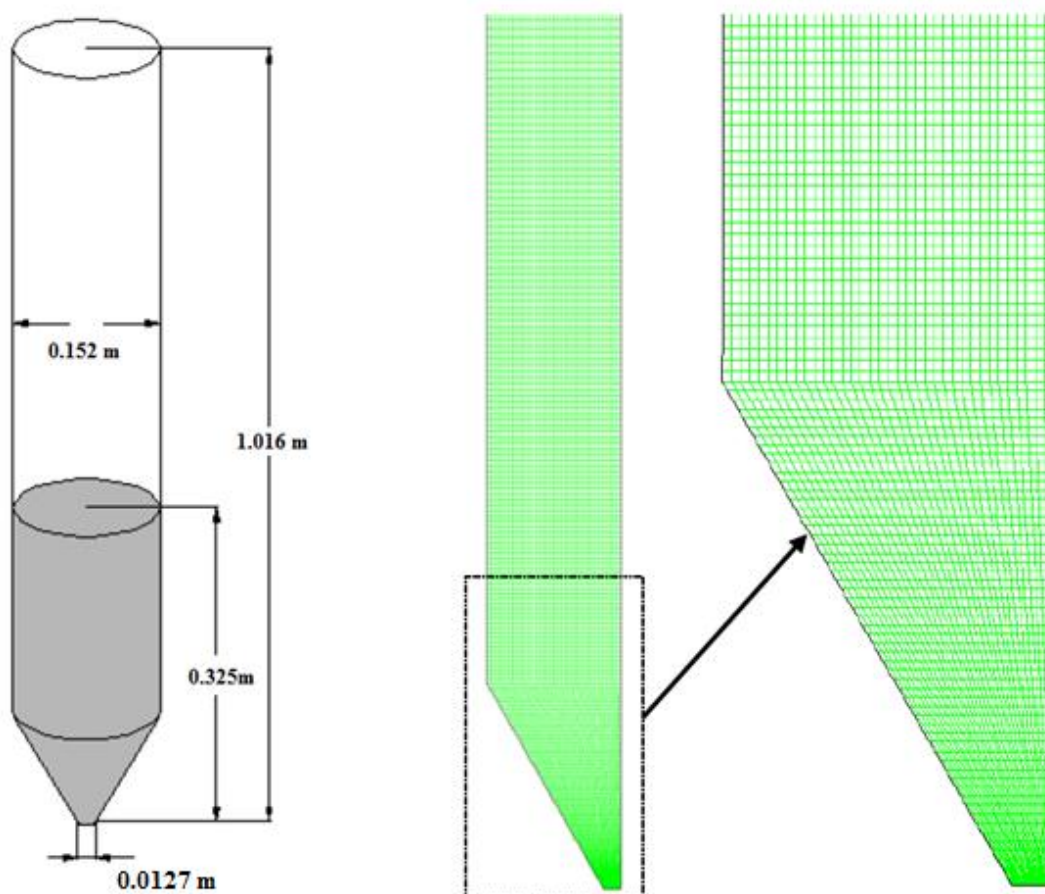
Figure 7.1. Schematic of geometry of 2D grids for spouted bed simulation

7.4 CFD VALIDATION FOR THE SELECTED MODELS

In the present work, the experimental data obtained by He et al. (1997) and the experimental work done on spouted bed in our lab was used to validate the 2D simulation results for spouted beds. He et al. (1994a; 1994b) had measured the radial profiles of particles velocity and solids holdup in spouted bed using a fiber optic probe. These experimental data were used to validate the CFD model for spouted beds by several researchers (Huilin et al., 2004; Du et al, 2006a; 2006b; Zhonghua et al. 2008; Bettega et al., 2009; Duarte et al. 2009). Hence, the available experimental data of the qualitative profiles of particles velocity and solids holdup have been used to validate the CFD model for spouted beds.

The conditions used to simulate the spouted bed are listed in Table 7.1. Figure 7.2 shows the simulated particles velocity vector and solids volume fraction of Case A, where the arrow and color of the vectors represent the motion direction and magnitude of particles velocities, respectively. The typical flow pattern of spouted beds including three regions, the spout in the center, the fountain above the bed surface, and the annulus between the spout and the wall are clearly observed. Solid particles are carried up by the gas in the spout, reach to the bed surface and form a fountain. Particles move upwards in the center of the fountain until the top, and then fall onto the annulus because of gravity. Particles move slowly in the annulus, and finally flow from the annulus to the spout at the entrance region. The particles motion in the spout, fountain and annulus regions forms a circular flow pattern in the spouted bed. The solids volume fraction is low and particle velocity is high in the spout, while the solids volume fraction is high and particle velocity is low in the annulus.

Figure 7.3 presents the simulated and experimental radial profiles of particles velocity and Figure 7.4 for gas phase holdup (voidage) at different bed heights. There is similar distributions between simulated and experimental particle velocities and gas phase holdup, although their magnitudes are not identical due to using different operating conditions. Table 7.2 shows the spout diameters and fountain heights of Case A. The simulated spout diameters and fountain heights for Case A are in agreement with the experimental results of He et al. (1997) and the work performed in our laboratory.

Table 7.1. Conditions used to simulate spouted bed hydrodynamics

Case	A
D_c (m)	0.152
D_i (m)	0.019
L (m)	1.14
H (m)	0.323
T (K)	298
P (kPa)	101
d_p (m)	0.00218
ρ_p (kg/m^3)	2400
ρ_f (kg/m^3)	1.21
μ (10^{-5}) (Pa.s)	1.81
U (m/s)	1.08
H/D_c	2.1
D_c/D_i	8
D_c/d_p	69.9
ρ_p/ρ_f	1994
ε_o	0.41
ϕ_s	1
$\rho_f d_p U/\mu$	157
U^2/gd_p	54.5
$\rho_p d_p U/\mu$	3.13
U^2/gD_c	0.78

(a)   (b)
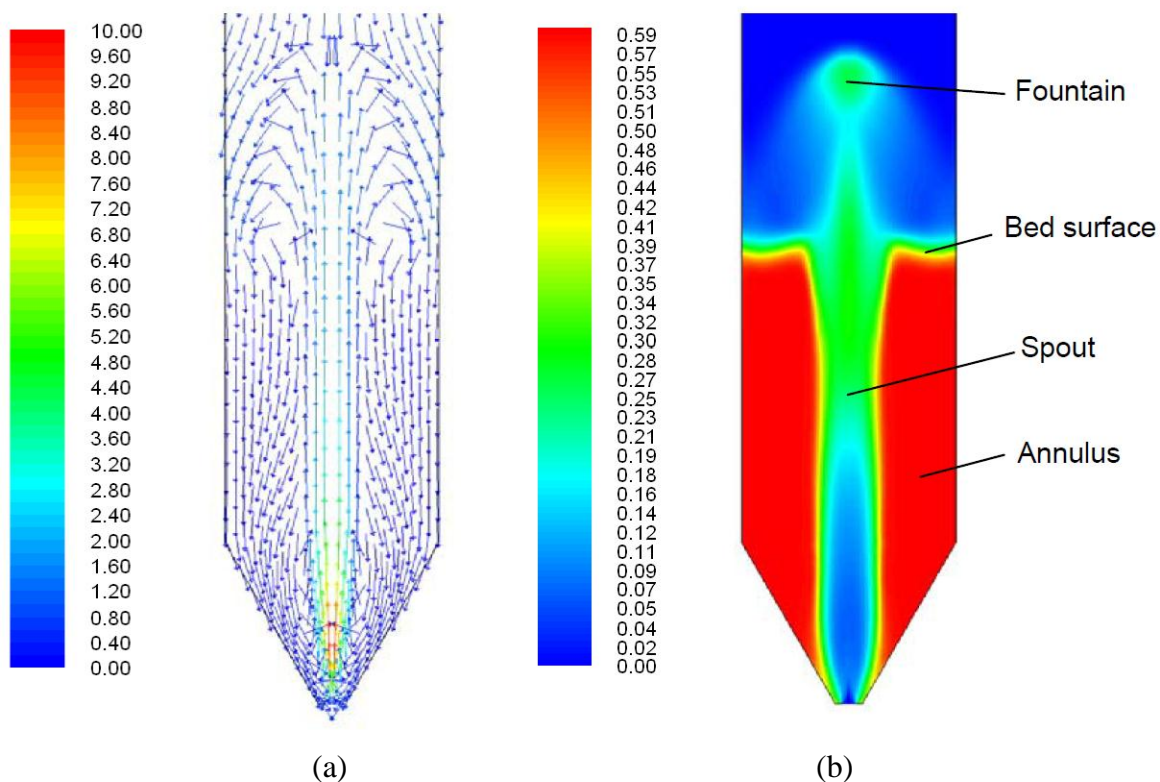
Figure 7.2. 2D CFD simulation of spouted bed, a. Predicted particle velocity vectors; b. Predicted solids volume fraction for the listed conditions in Table 7.1

Table 7.2. Experimental and simulated spout diameter and fountain heights for 0.152 m ID spouted bed

Case	A		
	Experimental (He et al., 1997)	Simulated	Experimental (Lab)
Column diameter, D_c (m)	0.152	0.152	0.152
Mean Spout diameter, D_s (m)	0.045	0.042	0.0395
Fountain Height, H_f (m)	0.135	0.138	0.131
Dimensionless Spout diameter, D_s/D_c	0.27	0.28	0.259
Dimensionless Fountain Height, H_f/D_c	0.89	0.91	0.87
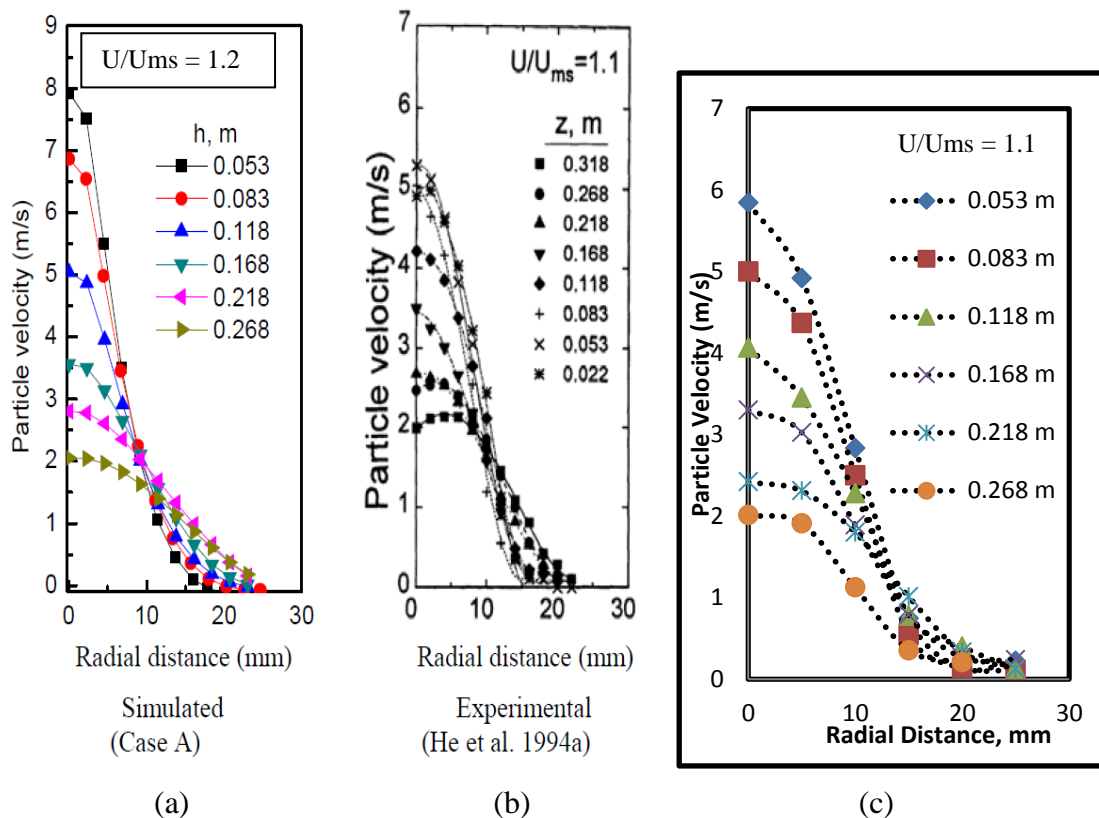
Figure 7.3. Comparison of CFD simulation and experimental results, a. Particle velocities by CFD; b. Experimental particles velocity profiles by He et al. (1997) and c. Experimental particles velocity profiles obtained in laboratory.

The quantitative comparison between experimental and simulated results and the qualitative analysis of the radial profiles of particles velocity and gas phase holdup (voidage), in addition to the similar results presented in the open literatures using similar models and the experimental work done in the laboratory for the same conditions on similar geometry of spouted bed, indicate that the CFD model used in this work is able to represent the spouted bed hydrodynamics behavior. This verified model is used for the subsequent evaluation on spouted beds scale-up.
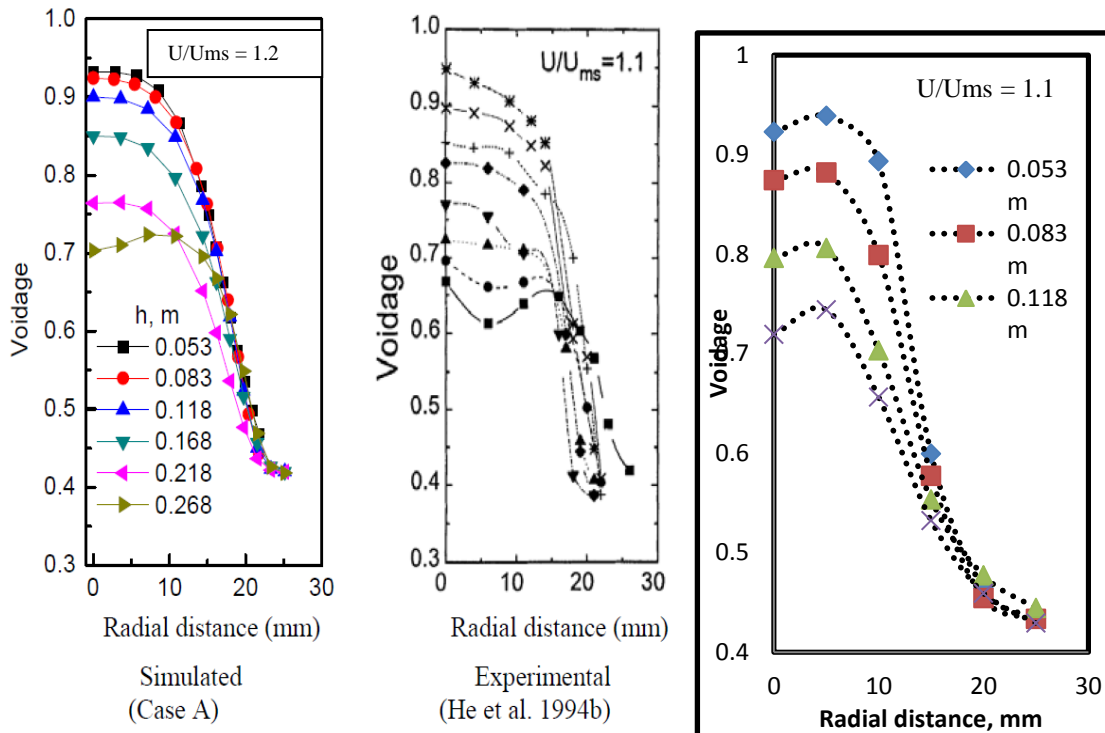
Figure 7.4. Comparison of CFD simulation and experimental results, a. Voidage profiles by CFD; b. Experimental voidage profiles by He et al. (1997) and c. Experimental voidage profiles obtained in laboratory.

7.5. SCALE-UP OF SPOUTED BEDS

7.5.1 Assessment of Dimensionless Group Approach. He et al. (1997) designed some matched (similar values of dimensionless groups in two different spouted beds) and mismatched (dissimilar values of dimensionless groups in two different spouted beds) experiments to verify their scaling parameters for spouted beds. Among their cases, Cases A and B were matched and designed to study the validity of the scaling relationships. Cases C - F were used to examine the influence of each dimensionless group on similarity, one or more groups were purposely mismatched. In the present work, Cases A - E have been chosen to assess the ability of dimensionless analysis methodology for

spouted beds scale-up using CFD approach. The parameters of Cases A - E used by He et al. (1997) in their experimental investigation are listed in Table 7.3.

Table 7.3. Conditions for matching dimensionless groups and mismatch dimensionless groups listed by He et al. (1997)

Condition	A	B	C	D	E
D_c (m)	0.152	0.076	0.076	0.076	0.076
D_i (mm)	19.1	9.5	9.5	9.5	9.5
H (m)	0.323	0.16	0.16	0.16	0.16
T (K)	298	298	298	298	298
P (kPa)	101	**312**	101	101	**312**
Particles	Glass	**Steel**	Glass	Glass	Glass
d_p (mm)	2.18	1.09	1.09	1.09	2.18
ρ_s (kg/m^3)	2450	**7400**	2450	2450	2450
ρ_f (kg/m^3)	1.21	**3.71**	1.21	1.21	3.71
$\mu(*10^5)$(Pa s)	1.81	1.81	1.81	1.81	1.81
U (m/s)	1.08	0.75	0.74	2.15	1.06
φ (^{0})	26	28	27	27	26
ε_{mf}	0.41	0.42	0.42	0.42	0.41
H/D_c	2.1	2.1	2.1	2.1	2.1
D_c/D_i	8	8	8	8	8
D_c/d_p	69.9	69.9	69.9	69.9	**35.0**
ρ_s/ρ_f	1994	1995	2029	2029	**648**
$\dfrac{\rho_f d_p U}{\mu}$	157	168	**54**	157	**474**
$\dfrac{U^2}{g d_p}$	54.5	52.6	51.2	**432**	52.5
$\dfrac{\rho_s d_p U}{\mu *10^{-3}}$	313	334	**109**	317	307
$\dfrac{U^2}{g D_c}$	0.78	0.75	0.73	**6.18**	**1.50**

Conditions for matching dimensionless groups and mismatch dimensionless groups were studied using computational fluid dynamics. The different measurement levels studied is shown in Figure 7.5. Figure 7.6 represents the solids hold-up profile and particles velocity profile in 0.152 m and 0.076 m spouted beds respectively for the conditions of matching dimensionless groups and mismatch dimensionless groups. Comparison of the profiles for all the cases clearly shows that the profiles are not similar using the conditions proposed by He et al. (1997). Figure 7.6 a, b and c; represents the solids holdup profiles. The maximum variation of solids holdup is in the spout region. This is caused by the jet of gas, which carries the particles up and then falls back onto the bed surface due to gravity. The solids movement into the spout region from the annulus varies at different heights of the spouted bed. Two zones where there is maximum inflow of solids to the spout region from the annulus are at the inlet of the spouted bed and at the neck region formed by the spout. However, there is inflow of solids from the annulus to the spout region along the height of the spouted bed. The solids volume fraction is low near the inlet of the spouted bed even though there is maximum inflow of solids from annulus to the spout region, because the solids is carried by the gas phase whose velocity is maximum at the inlet. The solids flowing into the spout region gets carried away by the incoming gas immediately. At higher regions of the spouted bed there are high volume fractions of solids as the velocity of the gas carrying the solids decreases. This explains the variation in the solids volume fraction at different heights of spouted bed. The annulus represents a slowly moving packed bed, where there is dense packing of solids. Due to this, the solids volume fraction remains almost the same at different heights of the spouted bed. When comparing the different scaled spouted beds, much attention is given

to the spout region because it dictates the spouted bed hydrodynamics. When the solid

holdup profiles are compared for the different cases of spouted bed suggested by He et al.

(1997), there is a big difference (absolute deviation = 23%) in the spout region between

the reference case A and the different match dimensionless groups (case B) and mismatch

dimensionless groups (case C, D and E) cases. Condition for matching dimensionless

group is much more important due to scaling reasons. The absolute deviation in this case

is 21%, which is considered to be large in engineering terms.
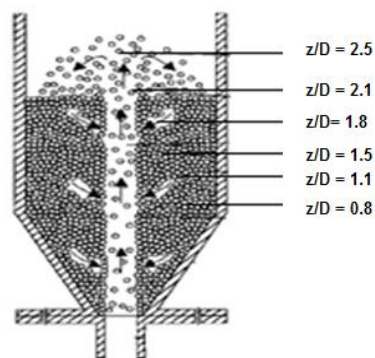
Figure 7.5. Schematic representation of different axial measurement levels performed on
spouted bed.

Particles velocity is another important parameter in the scaling process. Due to the

nature of the gas phase in the spouted bed, the particles velocity varies along the height.

The gas phase (air) enters the bed at the bottom, penetrating the solid bed of particles.

The velocity of the gas is high at the inlet and it decreases as it moves up the spouted bed.

Hence, the solids velocity is high at the inlet of spouted bed and decreases as it moves up

the spouted bed. In the annulus region, since the solids are moving down and the solids

are dense, the solids velocity is low and negative. The magnitude of the solids velocity in the annulus region is not high, but very low. Due the contrasting difference of solids velocity in these two regions, the comparison of this parameter in the spout region is important. When the solids velocity is compared in the reference case A and the cases B, C, D and E; the differences is obvious due to the nature of spouted bed. The best way to compare the velocity profiles of different conditions is by dimensionless representation of the profiles. Dividing the solids velocity by the minimum spouting velocity (U_{ms}), the velocity profiles for different cases were non-dimensionalized. The FLUENT video file was extracted for each simulation condition. With the help of the video file the time at which spouting started was noted. The velocity corresponding to the time in the video from the simulation file was taken to obtain the minimum spouting velocity (U_{ms}). Comparing the dimensionless velocity profiles (Figure 7.7), it was observed that the profiles in spout region were still significantly apart from the reference case A (absolute difference = 34%). This proves that the conditions suggested by He et al. (1997) for scaling spouted bed have significant differences when compared using solids volume fraction and dimensionless particles velocity profiles.

(a) z/D = 1.8

(b) z/D = 1.5

(c) z/D = 1.1
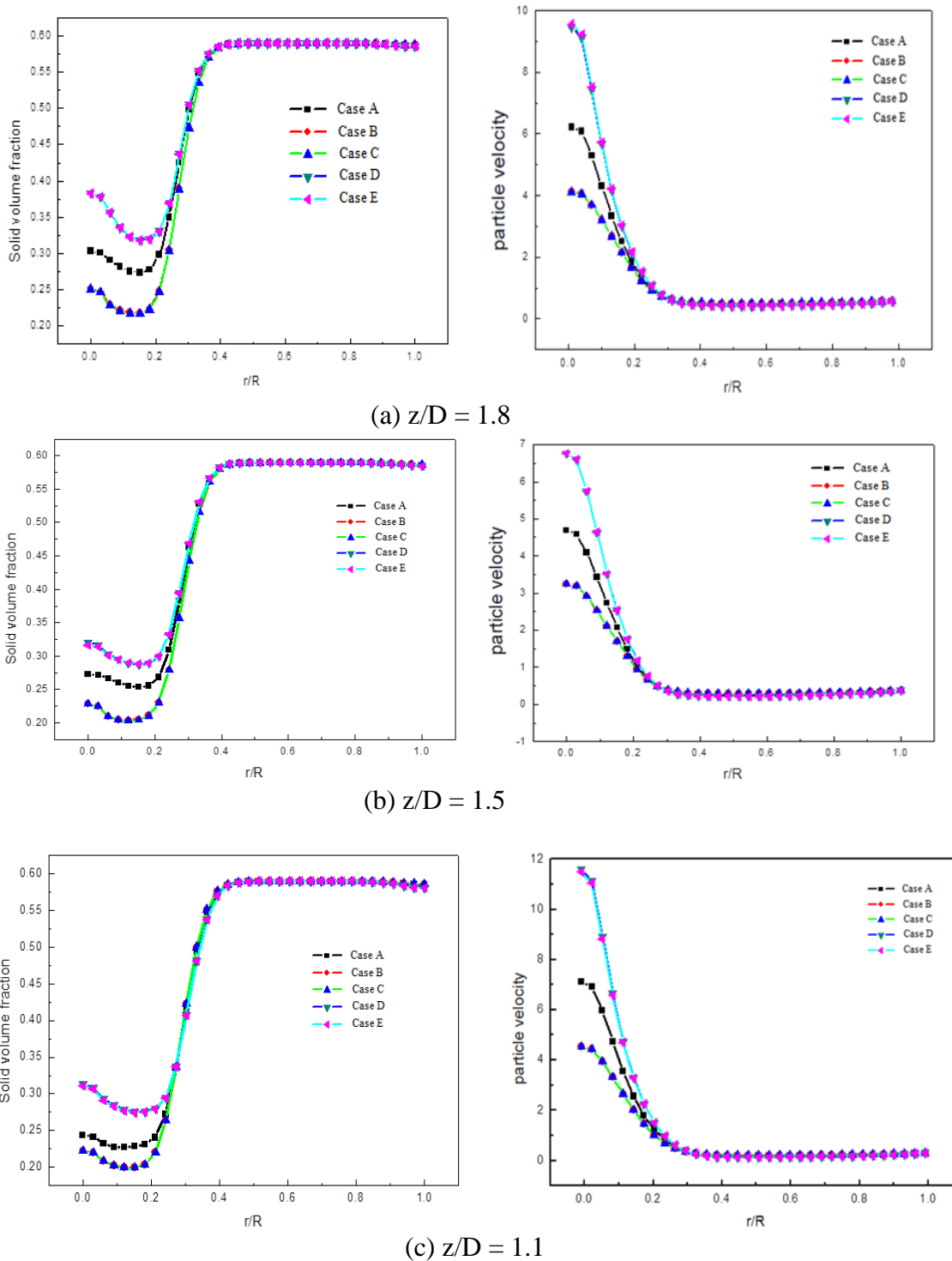
Figure 7.6. Radial profiles of solids volume fraction and particles velocity (m/s) simulated using CFD for Cases A, B, C, D and E listed in Table 7.1, at several different z/D measuring planes.

(a) z/D = 1.8

(b) z/D = 1.5

(c) z/D = 1.1
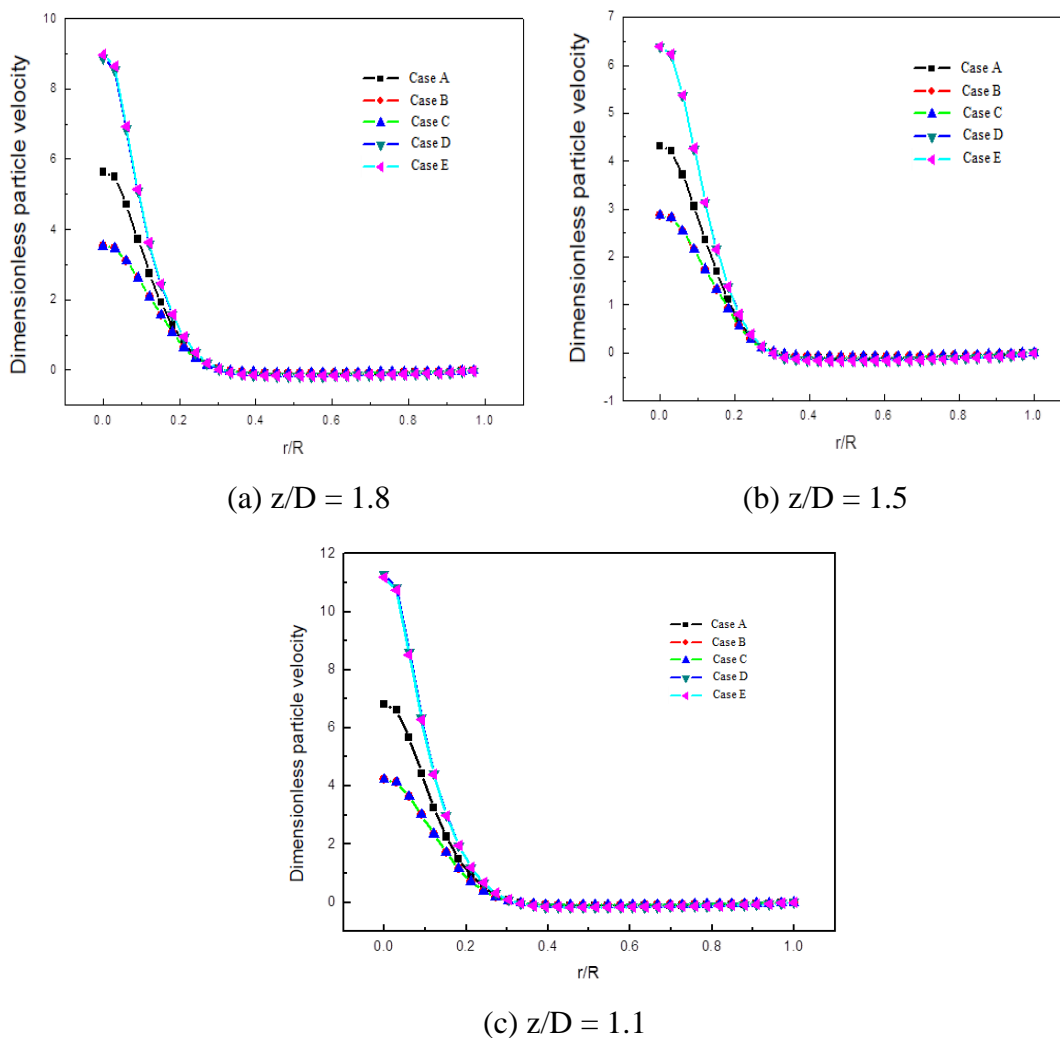
Figure 7.7. Radial profiles of dimensionless particles velocity (U/U_{ms}) simulated using CFD for Cases A, B, C, D and E listed in Table 7.1, at several different z/D measuring planes.

The comparison of the global parameters is also essential when comparing the different scale spouted beds. The dimensionless spout diameter, dimensionless fountain height and maximum spoutable bed heights for cases A-E has been shown in Table 7.4. The spout diameter and fountain heights were extracted by CFD after the simulation was completed. To find the maximum spoutable bed heights, the initial static bed height was

increased gradually for each simulation condition until there was no fountain formed in the simulation results. Each of the parameters was non-dimensionalized by dividing the parameters with corresponding spouted bed diameter. The deviations of the matching dimensionless groups (case B) and mismatch dimensionless groups (cases C, D and E) with the reference case A are shown below. This indicates that not only the local parameters (solids volume fraction and particle velocity) are significantly apart, but also the global parameters which were shown to be close in a half cylindrical spouted beds by He et al. (1997).

Table 7.4. Dimensionless spout diameters and dimensionless fountain height for different simulated cases of matching dimensionless groups and mismatch dimensionless groups

Case	A	B	C	D	E
Bed height, H (m)	0.323	0.16	0.16	0.16	0.16
D_c (m)	0.152	0.076	0.076	0.076	0.076
Spout diameter, D_s (m)	0.042	0.02	0.0205	0.0204	0.0211
Dimensionless spout diameter, D_S/D_C	0.276	0.257	0.269	0.268	0.277
Deviation (%)	-	+6.8	+3.8	+3.4	+6.5
Fountain height, H_F (m)	0.131	0.057	0.045	0.248	0.082
Dimensionless fountain height, H_F/D_C	0.87	0.75	0.52	1.54	1.21
Deviation (%)	-	-15	-46	+70	+20
Maximum spoutable bed height, H_m (m)	396	195	240	240	180
H_m/D_c	2.6	2.56	3.15	3.15	2.36
Deviation (%)	-	-1.5	+21.2	+21.2	-9.2

Comparison of all the above parameters has shown that the deviations, between the reference case (case A) and the different matching dimensionless groups and mismatch dimensionless groups cases, are significant. The matching of radial profiles is important when scaling of spouted beds is required. Based on the above-mentioned analysis of the results, the following limitations of the current dimensionless groups approach can be explained.

Limitations of the current dimensionless group scale-up approach are:

1. The deviation between the local parameter profiles is significantly large.

2. The annulus of spouted bed has similar profiles for all the cases due to the nature of the zone. Since the annulus consists of slowly moving packed bed and due to dense solids phase accumulation this result is quiet obvious.

3. The spout region has large deviations due to the variation of gas phase velocity and holdup along the height of the spouted bed. The comparison of the profiles in this region leads to large deviations among the different cases.

4. Assessment of the global parameters (spout diameter, fountain height and maximum spoutable bed height) also showed deviations when simulations were performed in a full cylindrical spouted bed.

Based on the present work, the methodology of dimensional analysis for scale-up of spouted beds should be modified to establish a reliable scale-up methodology of spouted beds. The new method should focus on maintaining similar radial profiles of gas holdup in spouted beds, which would help in achieving the desired process.

7.5.2 New Method for Scale-up. Spouted bed is a two-phase system consisting of gas and solids. The gas phase enters the spouted bed from the bottom as a jet and penetrates the bed of solid particles. As the gas phase penetrates the solids, the solids are also being carried along with the gas. The gas carrying the solids, reaches the top of the bed surface forming a fountain at the top. The solids then fall back on to the bed surface due to gravity. This nature of spouted bed creates three different zones namely: spout, annulus and the fountain. The gas phase dictates the flow dynamics of the spouted bed. Hence, if the radial profile or cross sectional distribution of gas holdup or solids holdup is maintained the same, then the two spouted beds would be similar.

We propose a new hypothesis:

"*Radial profile or cross sectional distribution of gas holdup or solids holdup should be the same or closer particularly in the spout region for two beds to be hydrodynamically similar or closer*".

Hydrodynamics similarity means either the absolute values of hydrodynamic parameters (holdup, velocity, turbulent parameters etc.) are the same or the dimensionless representations is the same. From Section 4, it was found that the later case of dimensionless representation of U/U_{ms} was found to be true. Such a scaling criterion can be used to estimate the absolute values of hydrodynamic parameters at different conditions or scales.

This work attempts to validate the hypothesis utilizing computational fluid dynamics, which is based on selecting conditions that provides similar radial profiles of gas holdup in spouted beds. This would be a difficult task as demonstrated earlier as the current dimensionless groups are not enough to predict close radial profiles of spouted

beds. CFD would help as an enabling tool in determining the conditions that would provide such matching radial profiles and hence has been selected to prove the above-mentioned hypothesis. Several trail simulations were performed using Computational fluid dynamics (CFD) as an enabling tool to identify the conditions, which would give matching radial profiles in two spouted beds. After numerous simulations following conditions were identified, which would give the desired radial profiles. The conditions are listed in Table 7.5.

Table 7.5. Conditions for new scale-up methodology

Case	Reference Case	Case A (He et al., 1997)	Conditions For Similar $(\varepsilon_g)_r$	Case B (He et al., 1997)	Conditions For Non-Similar $(\varepsilon_g)_r$
D_c (m)	0.152	0.152	0.076	0.076	0.076
D_i (m)	0.019	0.019	0.0095	0.0095	0.0095
L (m)	1.14	1.14	1.14	1.14	1.14
H (m)	0.323	0.323	0.16	0.16	0.16
T (K)	298	298	298	298	298
P (kPa)	101	101	**364**	**312**	**101**
Particle	Glass	Glass	Steel	Steel	Glass
Di (m)	0.019	0.019	0.0095	0.0095	0.0095
L (m)	1.14	1.14	1.14	1.09	1.14
H (m)	0.323	0.323	0.16	0.16	0.16
T (K)	298	298	298	298	298
ε_o	0.41	0.41	0.42	0.42	0.42
ϕ_s	1	1	1	1	1
$\rho_f d_p U/\mu$	157	157	**297**	**108**	**54**
$U^2/g d_p$	54.5	54.5	**38.3**	**52.6**	**51.2**
$\rho_p d_p U/\mu$	313	313	**139**	**334**	**109**
$U^2/g D_c$	0.78	0.78	**0.549**	**0.75**	**0.73**

The radial profiles of gas holdup and dimensionless particles velocity were evaluated for the conditions mentioned in Table 7.5. The determination of minimum spouting velocity (U_{ms}) by CFD has been explained in earlier section (Section 7.5.1). Figure 7.8 shows the gas holdup (voidage) profiles and Figure 7.9 represents the dimensionless particles velocity profiles for the two conditions at different heights of the spouted bed. The gas holdup (profiles) were expected to be same in the annulus region, because the annulus is a slow moving packed bed with dense concentration of solids. The gas volume fraction is more or less the same in this zone. Figure 7.8 reiterates the above statements showing the volume fraction in the annulus very similar in reference case and similar radial profile of gas holdup condition.
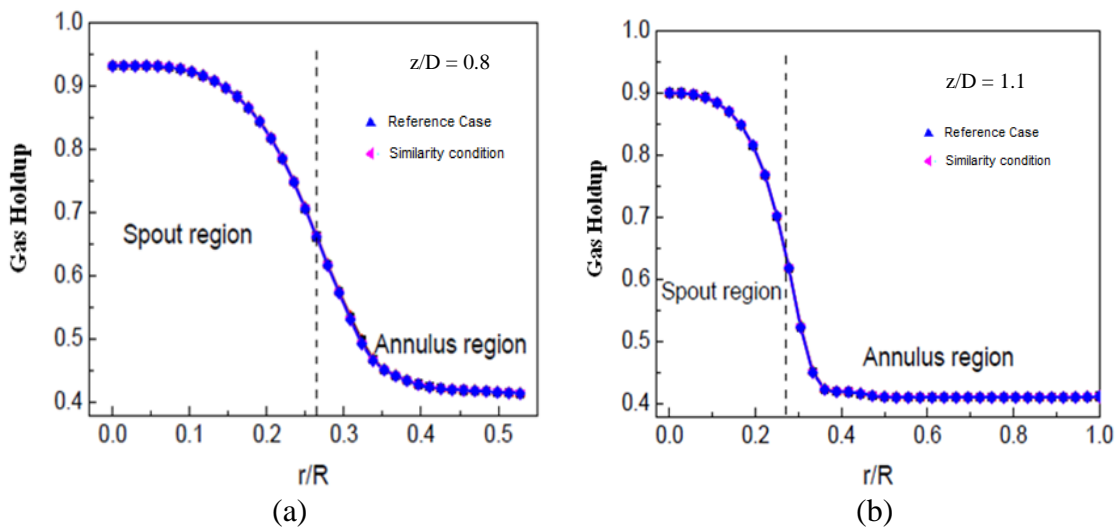
Figure 7.8. Radial profiles of voidage for 0.152 m and 0.076 m spouted bed at several different z/D levels using CFD simulation.
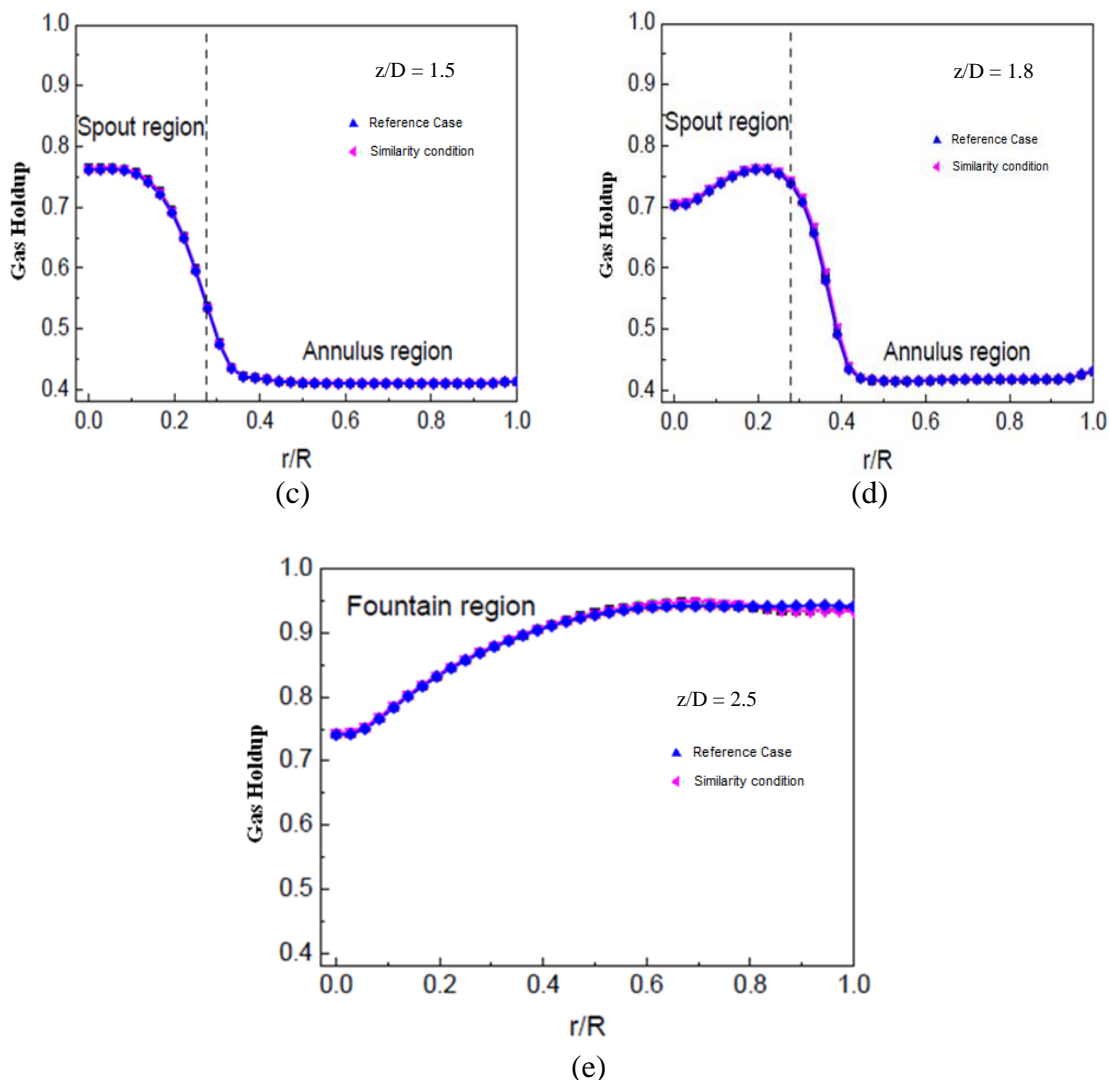
Figure 7.8. Radial profiles of voidage for 0.152 m and 0.076 m spouted bed at several different z/D levels using CFD simulation cont.

The spout region as explained in the previous section has varying degrees of volume fraction. It was demonstrated that the Cases A and B had significant difference in the radial profiles in the spout zone. With the new conditions identified the radial profiles of gas holdup in the spout region were close in the two spouted beds. Close matching of the profiles in all the three zones of the spouted bed shows the good estimation of the

condition for similar radial profile of gas holdup for scaling up. The particles velocity is another parameter, which needs close examination. Particles velocity in the annulus is very similar due to the dynamics of the zone. Spout region has different velocities at various heights of the spouted bed. The particles velocity profiles at different heights of the spouted bed are shown in Figure 7.9. When comparing two different spouted beds based on particles velocity profiles it should be first non-dimensionalized. In the present analysis the particles velocity were non-dimensionalized by dividing them by minimum spouting velocity (U_{ms}). When these profiles are compared in both the spouted beds (Figure 7.11), it was observed that the radial profiles were matching at different sections of the spouted bed. For the conditions of non-similar radial profiles of spouted bed, the dimensionless particles velocity profiles were not matching (Figure 7.12).

Table 7.6. Comparison between experimental values and CFD for U_{ms}

	Experimental	CFD
0.152 m	1.04 m/s	1.036 m/s
0.076 m	0.52 m/s	0.514 m/s
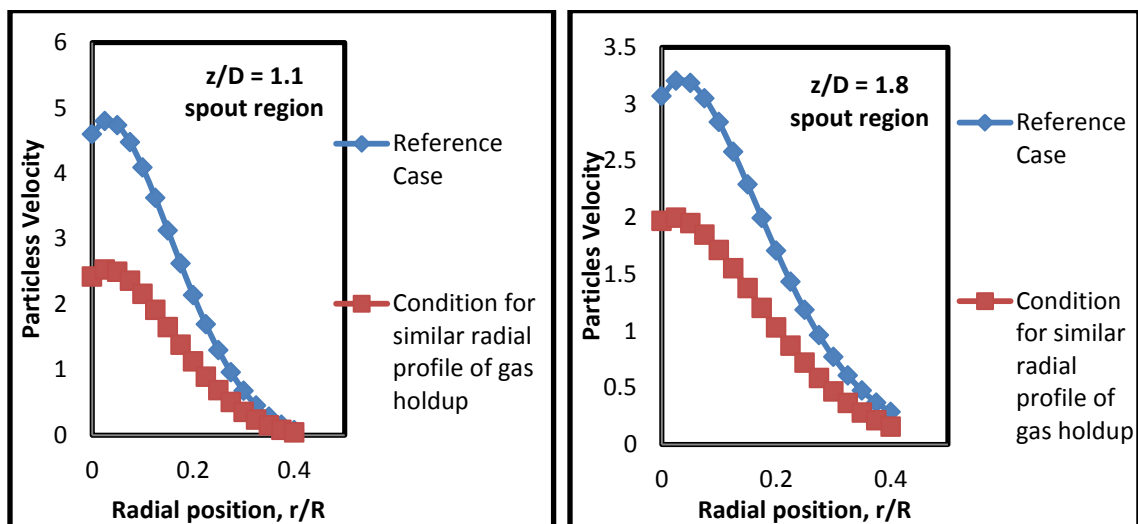
(a) z/D = 1.1

(b) z/D = 1.8
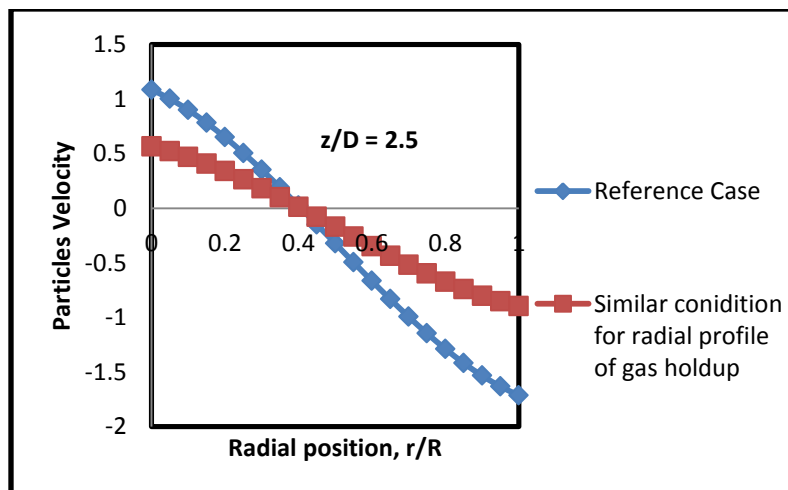
(c) z/D = 2.5

Figure 7.9. Radial profiles of particles velocity (m/s) for 0.152 m and 0.076 m spouted bed at z/D (1.1, 1.8 and 2.5) levels using CFD simulation for conditions for similar radial profiles of gas holdup.
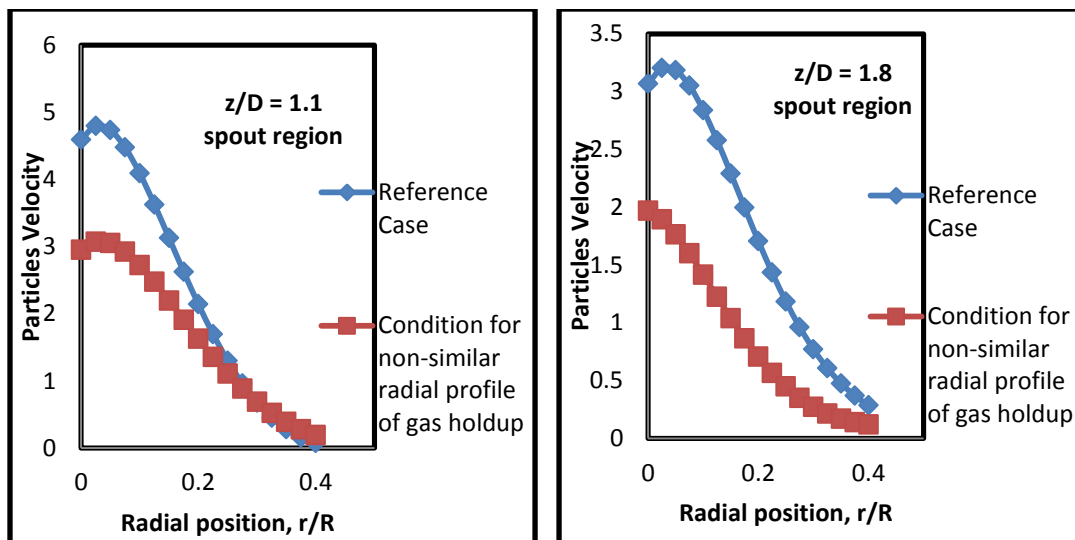
(a) z/D = 1.1

(b) z/D = 1.8
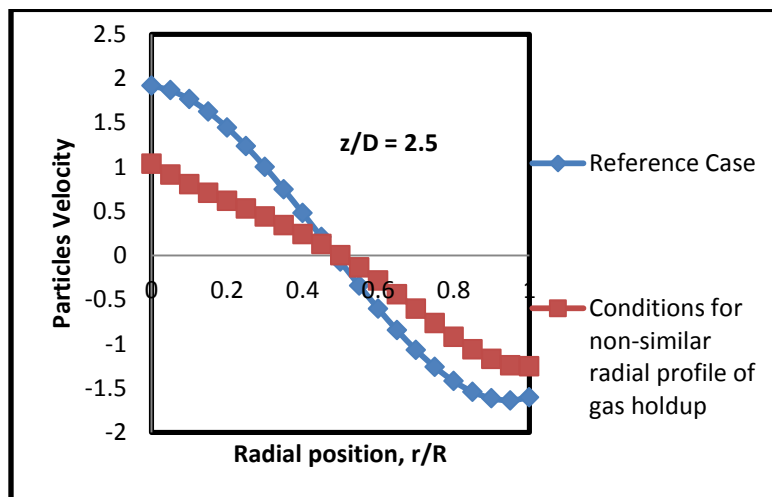
(c) z/D = 2.5

Figure 7.10. Radial profiles of particles velocity (m/s) for 0.152 m and 0.076 m spouted bed at z/D (1.1, 1.8 and 2.5) levels using CFD simulation for conditions for non-similar radial profiles of gas holdup.
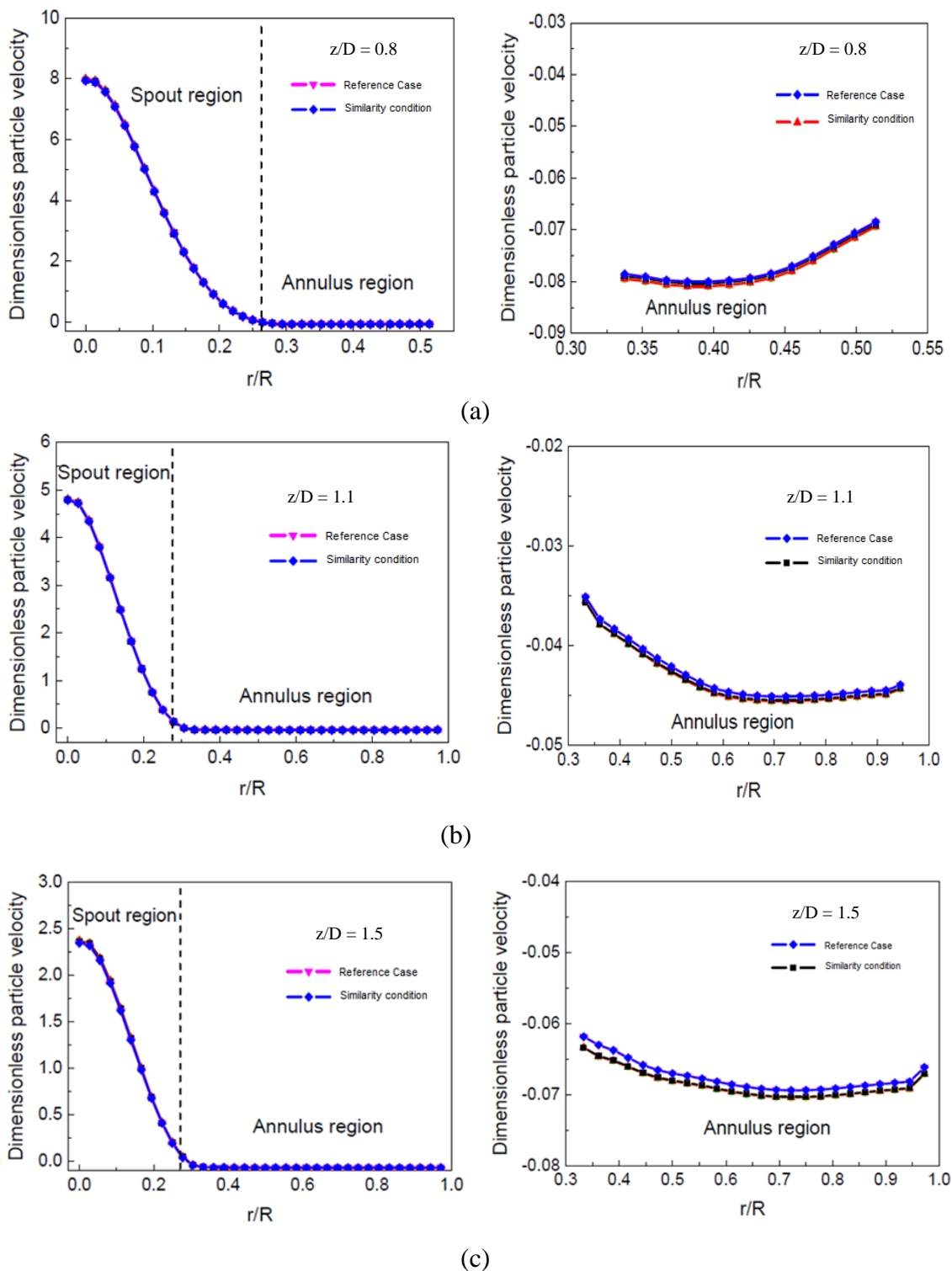
Figure 7.11. Radial profiles of dimensionless particles velocity (U/U$_{ms}$) for 0.152 m and 0.076 m spouted bed at z/D (0.8, 1.1, 1.5 and 1.8) levels using CFD simulation for conditions of similar radial profiles of gas holdup.
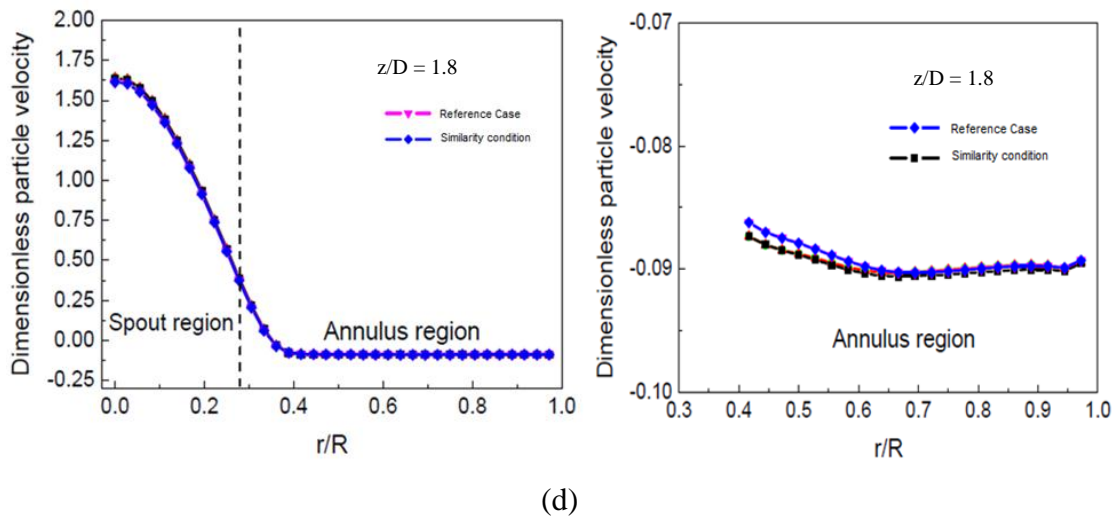
(d)

Figure 7.11. Radial profiles of dimensionless particles velocity (U/U$_{ms}$) for 0.152 m and 0.076 m spouted bed at z/D (0.8, 1.1, 1.5 and 1.8) level using CFD simulation for conditions of similar radial profiles of gas holdup cont.

(a) z/D = 1.1　　　　　　　　　(b) z/D = 1.8
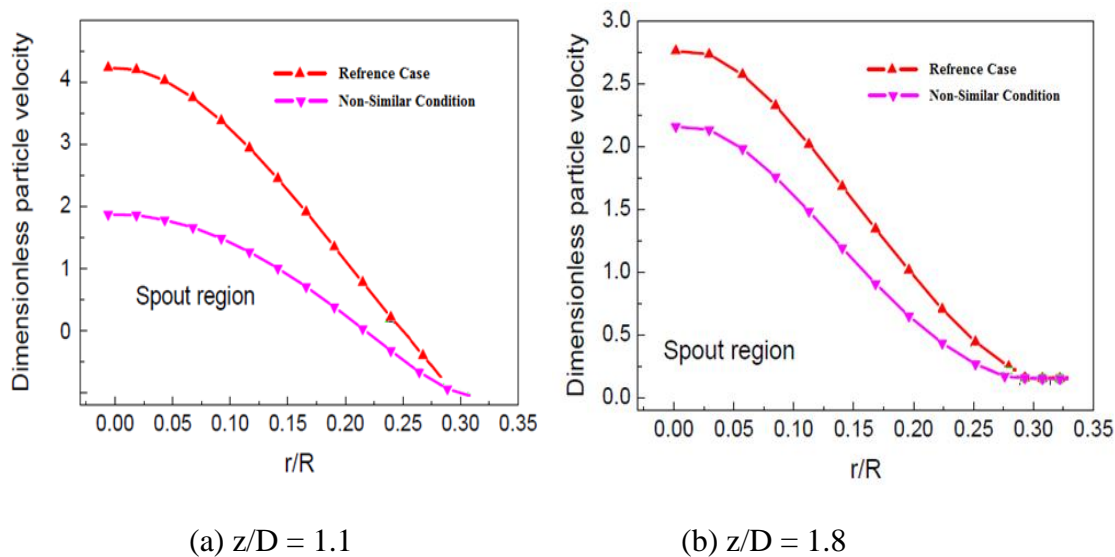
Figure 7.12. . Radial profiles of dimensionless particles velocity (U/U$_{ms}$) in the spout region for 0.152 m and 0.076 m spouted bed at z/D (1.1, 1.8 and 2.5) levels using CFD simulation for conditions of non-similar radial profiles of gas holdup.
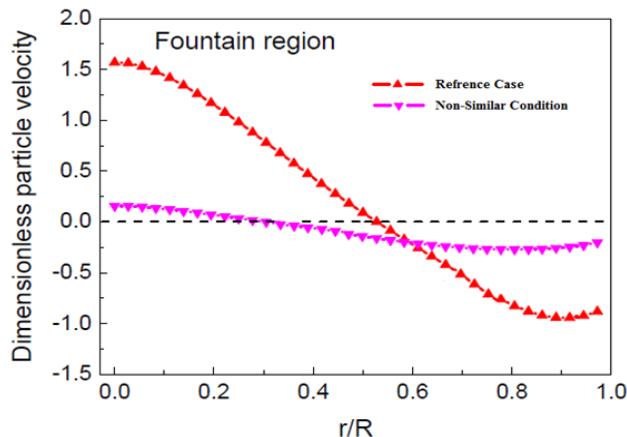
(c) z/D = 2.5

Figure 7.12. Radial profiles of dimensionless particles velocity (U/U$_{ms}$) for 0.152 m and 0.076 m spouted bed at z/D (1.1, 1.8 and 2.5) levels using CFD simulation for conditions of non-similar radial profiles of gas holdup cont.

Spout diameters and fountain height (Table 7.7) was obtained for both the cases using the newly identified conditions listed in Table 7.5. The fountain height was determined by gradually increasing in small increments the initial bed height of the spouted bed until there was no spouting obtained in the bed. This simulation results show that the two spouted beds were in close agreement with each other. The dimensionless spout diameter and dimensionless fountain height were close to the reference case.

The dimensionless pressure profiles were also simulated (Figure 7.13) for both spouted beds using the new conditions. The dimensionless pressure was obtained by dividing the pressure at that particular point by the overall bed pressure. The plot of the dimensionless pressure along the height of the spouted bed for both the beds showed a close resemblance to each other. The conditions listed by He et al. (1997), when evaluated for dimensionless pressure profiles did not show such close agreement.

Table 7.7. Dimensionless spout diameter and dimensionless fountain height for the new conditions

Case	Simulated		Deviation
	Reference	Condition for Similar $(\varepsilon_g)_r$	%
Column diameter, D_c (m)	0.152	0.076	-
Mean Spout diameter, D_s (m)	0.038	0.0196	-
Fountain Height, H_f (m)	0.129	0.058	-
Dimensionless Spout diameter, D_s/D_c	0.25	0.263	+5.2
Dimensionless Fountain Height, H_f/D_c	0.84	0.76	+9.5
Maximum Spoutable Bed Height, H_m (m)	0.398	0.198	-
H_m/D_c	2.611	2.727	+4.44
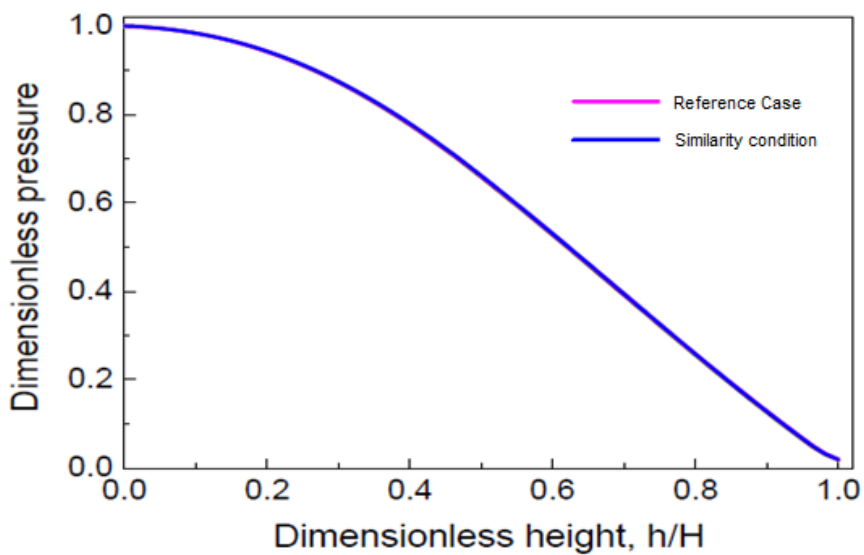
Figure 7.13. Dimensionless pressure profile for reference case and condition for similar radial profile of gas holdup using CFD simulation

The analysis of the results reiterates that the selected conditions were capable of matching the global (dimensionless spout diameter, dimensionless fountain height and pressure drop profile) and local parameters (gas holdup and dimensionless particles velocity), which showed that the profiles are close to each other in both the spouted beds. The hypothesis of similar radial profile or cross sectional distribution of gas holdup profiles yields similar hydrodynamics in two spouted beds stands true.

The analysis of the absolute particles velocity profiles for both the conditions were not similar. But when the radial profiles was dimensionally represented (U/U_{ms}) the velocity profiles were close for condition of similar radial profile of gas holdup and had large deviations for condition of non-similar radial profile of gas holdup. Based on this, U/U_{ms} ratio can be used as a scaling criterion to predict the absolute velocity profiles in different spouted beds, provided the base conditions are maintained. The dimensionless group approach of He et al. (1997) is based on maintaining the same values of different dimensionless group in the two different spouted beds, poses a practical challenge. It is very hard to match all the dimensionless groups experimentally in different spouted beds, where the U/U_{ms} criterion should be helpful. Since there are many correlations available in open literature to predict U_{ms} depending on the spouted bed geometry, the absolute particles velocity profiles can be determined using the U/U_{ms} scaling criterion and thereby predicting the spouted bed hydrodynamics.

7.6 REMARKS

Computational fluid dynamics (CFD) was used to simulate the spouted bed hydrodynamics. Various models were selected to describe the flow properties and

validated against the experimental works of He et al. (1997) and from the results performed experimentally using optical probes. The gas holdup and particles velocity profiles were in good agreement with the experimental works reported in literature, which proved the successful prediction of spouted bed hydrodynamics by CFD. CFD after validation with the experimental results was used as an enabling tool to validate the developed hypothesis of hydrodynamics similarity approach. The assessment of dimensionless group approach proposed by He et al. (1997), showed the difference in local parameters (such as solids holdup, solids velocity etc.). The new conditions identified by the CFD simulation showed that the local and global parameters were close for both the conditions, which proves the hydrodynamics similarity hypothesis, stated earlier in Section 4. CFD thus was helpful as an enabling tool to validate and capture the developed model for spouted bed.

8. SUMMARY & RECOMMENDATIONS

The main objectives set for this work are to develop a new mechanistic scale-up methodology and to investigate key hydrodynamic parameters of spouted bed reactors using techniques such as optical probes, computational fluid dynamics, pressure transducers and non-invasive radioactive technique termed as Gamma ray densitometry (GRD). With the aid of these above-mentioned state-of-the-art experimental and modeling tools, this work proposed, evaluated and developed a new methodology for similarity flow dynamics for scale-up of spouted beds. Key hydrodynamic parameters, which play an important role in spouted beds, have been studied to advance the knowledge on these beds. Present work also developed a non-invasive radioisotope based experimental technique called Gamma ray densitometry (GRD) for monitoring on-line the reactor performance by evaluating the line averaged radial profiles of solids or gas holdup for the proposed new scale-up methodology. The GRD was also demonstrated to show the capability to identify different flow regimes and flow patterns in spouted beds, in a non-invasive manner. The application of such technique has high value industrially where large diameter columns are the norm.

8.1 SUMMARY AND CONCLUSIONS

The key findings in this work are as follows

1. New technique called as optical probe based on back reflection of light was acquired from Institute of Process Engineering of the Chinese Academy of Sciences, which could measure simultaneously solids velocity, solids holdup and their times series fluctuations.

2. New calibration methodology was developed for the optical probes to convert the measured solids concentration to solids holdup. The developed methodology has been validated against non-invasive radioactive technique known as dual source computed tomography (CT) experiments, thus validating the reliability of the proposed method.

3. Based on a comprehensive review of reported scale-up procedures in literature, the current work assessed the scale-up approach based on dimensionless groups methodology proposed by He et al. (1997). The dimensionless groups approach was first assessed for local (solids and gas holdup, solids velocity and solids mass flow) and global (pressure fluctuations, spout diameters, fountain height and maximum spoutable bed height) parameters for the conditions of matching dimensionless groups and mismatch dimensionless groups reported by He et al. (1997). It was observed that the global parameters were in good agreement with each other for the studied matching dimensionless groups condition, but the local parameters were different in the two spouted beds.

4. Limitations of the dimensionless groups approach motivated the proposal of a new hypothesis based on maintaining same radial profiles or cross sectional distribution of gas holdup or solids holdup in the two spouted beds. Two conditions were identified with respect to a reference case, one which had conditions for similar radial profile of gas holdup and other having conditions for non-similar radial profile of gas holdup. The conditions for non-similar radial profile of gas holdup were identified to demonstrate the

deviation in radial profiles even if the geometric similarity is held similar in both the beds.

5. The new conditions for similar radial profile of gas holdup identified had close radial profiles of gas holdup in the two different spouted beds, which proved the hypothesis of hydrodynamic similarity proposed by maintaining similar radial profiles. The assessed global and local parameters were in close agreement with each other.

6. U/U_{ms} ratio can be used as a scaling criterion to predict the absolute velocity profiles in different spouted beds, provided the base conditions are maintained. The dimensionless group approach of He et al. (1997) is based on maintaining the same values of different dimensionless group in the two different spouted beds, poses a practical challenge. It is very hard to match all the dimensionless groups experimentally in different spouted beds, where the U/U_{ms} criterion should be helpful. Since there are many correlations available in open literature to predict U_{ms} depending on the spouted bed geometry, the absolute particles velocity profiles can be determined using the U/U_{ms} scaling criterion and thereby predicting the spouted bed hydrodynamics.

7. The above developments motivated the development of Gamma ray densitometry (GRD), a non-invasive radio-isotope based technique, to monitor on-line the radial profiles of gas holdup proved by the hypothesis. It was demonstrated that GRD had the capability to monitor on-line such profiles. Industrial reactors often vary from the laboratory scale reactors;

hence the applicability of the proposed hypothesis needs to be checked in such systems.

8. The solids velocity was studied in 0.152 m spouted bed by CFD simulations and optical probes to see the solids movement. Based on the determination of velocity vectors from CFD simulation, it was found that the spout formation is not straight, but instead forms a neck at the top part of the spout region. The preferential flow zone of solids from the annulus region to the spout region occurs in mainly two regions. The first is near the inlet of the bed and the second zone is near the neck of the spout. From the interpretation of CFD results it seems that the solids flow into the spout regions apart from the above mentioned zones is small.

9. 2^5 factorial designs of experiments were utilized to identify the average spout diameter in spouted beds. 0.152 m ID spouted bed was studied for the above experimentation with glass beads and steel shots as the solid particles. Factorial analysis was performed in MINITAB software. From the ANOVA table it was found that all five main effects (solid density, static bed height, particle diameter, superficial gas velocity and inlet diameter) and the interaction between particles size and inlet diameter, and gas velocity and inlet diameter, had significant effect on the determination of spout diameter. Regression analysis was performed to obtain a correlation which could identify the average spout diameter. The obtained correlation was able to predict closely the spout diameter when compared to the correlations listed in the literature.

10. Based on the analysis of pressure fluctuation measurements from pressure transducers, signal fluctuations from optical probes and photon counts from gamma ray densitometry, flow regimes were evaluated in 0.152 m and 0.076 m ID spouted beds. The transition velocities identified by these techniques were in close agreement with the published data in the literature. The newly developed non-invasive radioisotope technique (GRD) was able to successfully identify different flow regimes and their transition velocities. The implementation of such non-invasive technique would be helpful for many industrial applications.

11. Computational fluid dynamics (CFD) was used to simulate the spouted bed hydrodynamics. Various models were selected to describe the flow properties and validated against the experimental works of He et al. (1997) and the experimental work performed at our laboratory. The gas holdup and particles velocity profiles were in good agreement with the experimental works reported in literature, which proved the successful prediction of spouted bed hydrodynamics by CFD.

12. CFD was used as an enabling tool to validate the developed methodology based on hydrodynamics similarity approach. The assessment of dimensionless group approach proposed by He et al. (1997), showed the difference in local parameters (such as solids hold-up, solids velocity etc.). The new conditions identified by the CFD simulation showed that the local and global parameters were in close agreement for both the new conditions.

8.2 RECOMMENDATIONS

The work accomplished in the current study is, in retrospect, generic to spouted beds. Hence, it provides promising avenues to implement similar concepts in different configurations of spouted bed reactors. The few suggestions for possible extension of the work performed in different parts are listed below

1. To implement Dual Energy Computed Tomography (DECT) technique, which is a non-invasive radioisotope based technique; to further advance the knowledge on spouted beds.

2. Implement Radioactive Particle Tracking (RPT) technique to obtain detailed 3D solids flow field, velocity and turbulent parameters. The following parameters can be extracted using RPT: 3D flow pattern, 3D velocity components, 3D turbulent parameters (shear stresses, normal stresses, kinetic energy, granular temperature, eddy diffusivity), particle-particle interaction, circulation time distribution, stagnant zones, local residence time, solids flux mass balance (solids fluxes upward and downward), solids Lagrangian trajectories and solids mass circulation rate.

3. The present work for hydrodynamic similarity approach was conducted at ambient temperature conditions. More research needs to be done on spouted beds at elevated temperatures, which represent the actual TRISO manufacturing process.

4. Hydrodynamic similarity hypothesis was proved in cone-based cylindrical spouted bed. The hypothesis needs to be applied for different configurations of spouted bed (conical, slot-rectangular etc.).

5. Larger diameter spouted beds (which represent the industrial scale) need to be studied in order to improve and develop the process and product efficiency.

6. The formation of neck in the upper sections of spouted bed needs to be checked in different configurations of spouted bed to aid in knowledge of solids flow pattern for maintaining proper design and scale-up.

7. The factorial design of experiments methodology needs to be applied for systems of spouted bed operating at elevated temperatures and pressures to predict the spout diameter.

8. The present work demonstrated the use of GRD in monitoring on-line the radial profiles of holdup of spouted bed reactors. This greatly helps in design and scale-up of such multiphase systems. There is a need to also use this newly developed technique on other multiphase systems to demonstrate the universal applicability of this technique.

9. Due to the requirement of using the time-series techniques that are simpler, faster, robust, and easily used by non-experts in the plant, a basic time-series analysis was performed on photon counts history obtained using GRD. However one can use *sophisticated* time-series techniques such as chaos analysis for flow regime identification. In addition, one can apply symbolic dynamic analysis, χ^2 - analysis, and S-statistics to evaluate their feasibility for flow regime monitoring in different multiphase systems.

10.   In the spout region and the fountain region, the movement of particles is quite complex. Particles are first accelerated near the inlet region, and then decelerated in the fountain region. Currently both the spout and the fountain regions are simulated using the default fluidized bed code (k_s=1); thus, some considerations are needed to account for the acceleration and deceleration effects using improved drag models. More detailed evaluation on such parameter is required.

APPENDIX A.

OPTICAL PROBE MEASUREMENT AND ANALYSIS

A.1. Optical Probe Introduction

Optical probe is an invasive technique which has been widely used in recent years for determination of velocity and volume fraction of particles in gas-solid systems. The advantages of fast response, relatively inexpensive and reliable accuracy make it a desirable technique for many researchers. The reliability of measurements is strongly affected by the accuracy of the calibration methods. This technique is limited to the use of multiphase system components which contain reflective properties and cannot be used in highly opaque multiphase systems. Optical probes may be classified into single fiber and multi-fiber probes. The single fiber probes have only one fiber, with light being emitted and received after being reflected by particles by the same fiber. The multi-fiber type probes contain hundreds or even thousands of optical fibers arranged in precision. Some of them are light emission while others are for light reception. The new advanced multi-fiber optical probes have the advantages of measuring solids volume fraction, velocity and their fluctuations simultaneously. Their small size does not considerably disturb the overall flow structure and allows for rapid and sensitive measurement. These probes also measure from very dilute to very dense conditions. Most importantly, they are nearly free of interference by temperature, humidity, electrostatics and electromagnetic fields.

Optical probes (PV6, Figure A.1) used in the present study, which is a multi-fiber probe, has been developed in collaboration with Chinese Academy of Sciences. Optical fiber probe consists of two channels/tips of optical fibers. Each channel consists thousands of optical fibers arranged parallel to each other that can emit and reflect light. The arrangement is such that, one layer consists of light emitting fibers and the layer next

to it consists of light receiving fibers. Each fiber in the optical probe is approximately about 15μm in diameter. These probes are more precise in their measurement due to the elimination of blind region. The tips of the probe are covered with a quartz window (Figure A.5.), which eliminates the blind region (Wang et al., 2009). The old probes which had the problem of blind region (Figure A.4.) had less measuring volume leading faulty measurements. These blind zones acted as dead zones there by reducing the intensity of the reflected light and also providing a non-linear response. All these drawbacks were addressed in the new probes (PV6).

The PV6 particle velocity analyzer is an instrument for multi-phase flow measurement, which is mainly used in measurement of particle velocity in gas-solid and liquid-solid systems. The instrument has the following features:

1. Measurement of average velocity, instantaneous value and statistical distribution of particles in two-phase flow systems

2. Measurement of relative concentration (C) of moving particulate materials

3. Measurement of frequency, velocity in gas-solid two-phase flow systems

4. Judgment of moving direction of particulate materials near measuring points

The selection of probes (particle to probe ratio) for the experiment is also an important criterion. At our laboratory we have four optical probes depending on the size of particles to be used. For measurement of solids concentration, the probe size should be greater or equal to twice the size of the particle under study. Figure A.2., shows the use of different size of probes and their advantages. The particles used should have good reflective properties, should not be black or corrosive.

Figure A.1. Optical probe (PV6) system

(a)	(b)
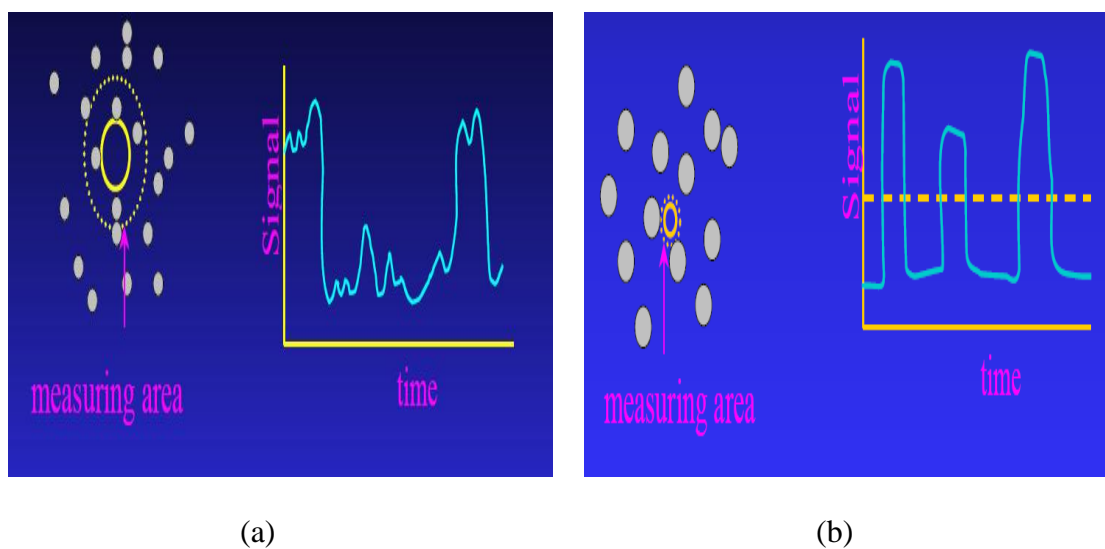
Figure A.2. (a) Probe size used for measurement of solids concentration; (b) Probe size used to measure solids velocity

A.2. Optical Probe Electronics

The particle velocity analyzer, PV6 (purchased from Chinese Academy of Sciences, Figure A.3.) consists of optical fiber probes, photoelectric converter and

amplifying circuits, signal pre-processing circuits, high-speed A/D interface card and its software PV6. Four different types of probes are available which are chosen for measurements depending on the size of particle under study. Each probe has two tips at the front face consisting of several layers of light emitting and receiving optical fibers. Two or three bundles of optical fibers with diameter of 0.2-0.3 mm are arranged at certain interval according to different sizes of particles to be measured by the optical probe. The light source is introduced into the measuring area in front of the optical fibers. The reflecting lights of particles at the end face of the optical fibers are transferred into the photoelectric detector in the instrument through the same bundle of optical fibers, and are converted into voltage signals corresponding to the concentration of particles. The A/D converter of the PV6 (software used for the optical probes) technique has two independent A/D converting paths. The maximum sampling frequency of each channel is 2000 kHz, and the maximal range of velocity measurement is no less than 25 m/s when the distance between two measuring points is 0.25 mm.

The A/D interface card of the PV6 instrument is designed for particle velocity measurement. It has the following features:

1. Synchronous and independent A/D conversion of signals from two channels without time delay

2. 60 Hz to 2 MHz sampling frequency of each channel with adjustable step

3. 32-128k x 2 data memory

4. 12-bit resolution
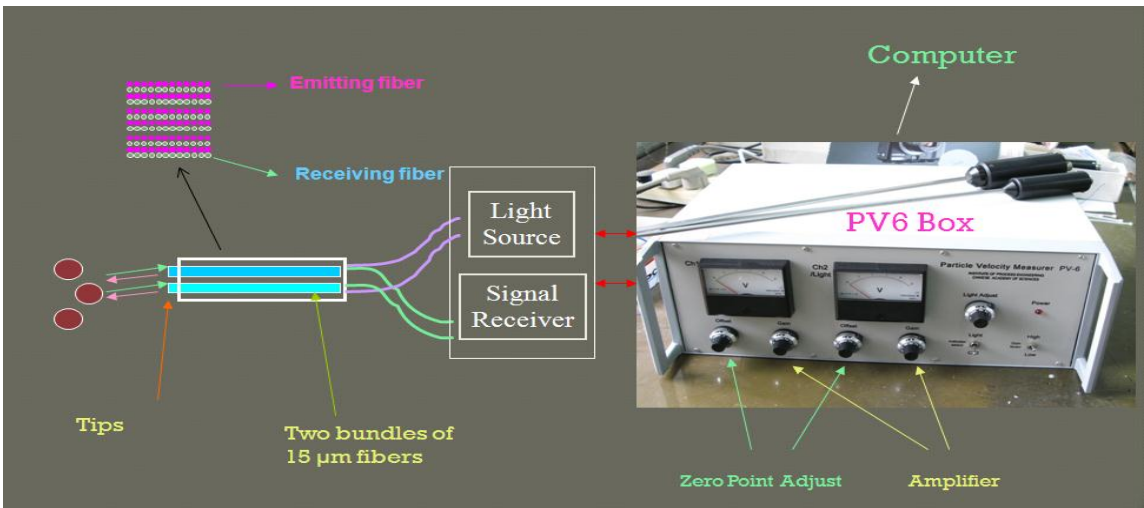
Figure A.3. Optical probe electronics set-up
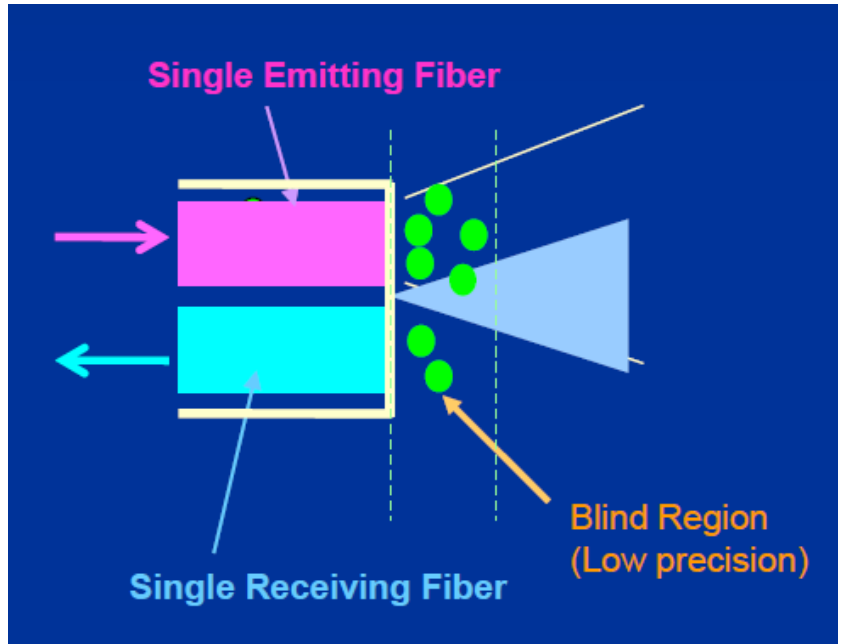
Figure A.4. Presence of blind region in old optical probes marked by poor measuring volume and low reflected light intensity
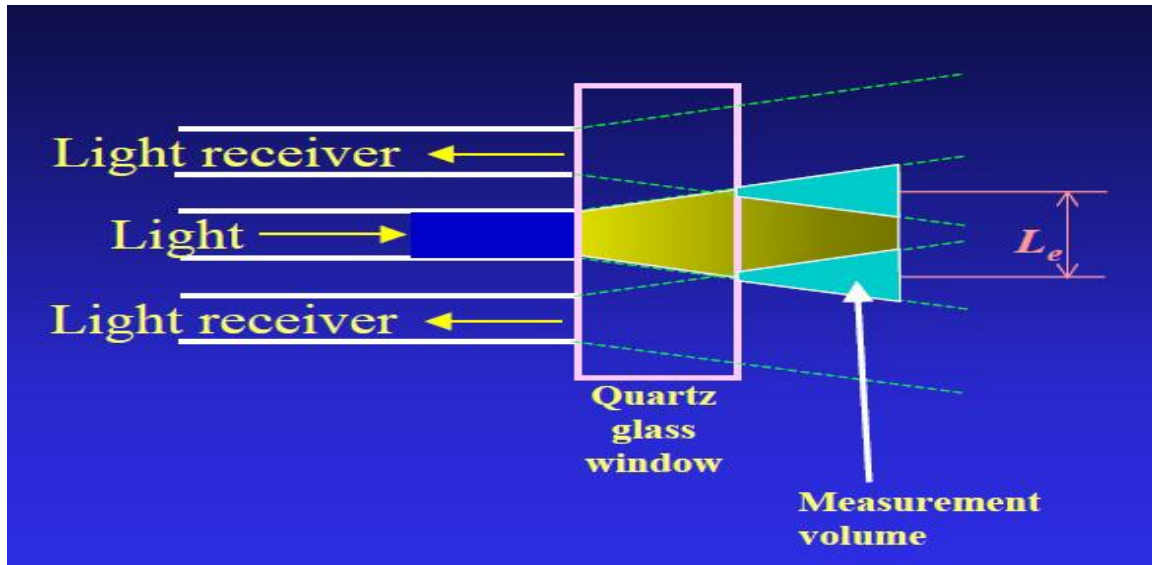
Figure A.5. New optical probe with quartz window that eliminates blind region

A.4. Solids Concentration Measurement

The probe selected for measurement of solids concentration should not greater than or equal to twice the size of the particles under study. This ensures that there is enough measuring volume to obtain accurate measurements. The probe tips illuminate a small volume in front of the probe tips. When there is a movement of particles in this measuring volume, light is reflected back, which is in turn captured by the probe. This reflected light is then converted into signals. The signal from either of the tips can be taken to process them to obtain solids concentration. Since most of the data published in the literature is in terms of solids hold-up, there is a need to convert this solids concentration into solids hold-up via a calibration equation. This calibration equation relates the measured voltage in the probe signals to the solids hold-up. The details of the calibration methodology is explained in APPENDIX B. Before the probe can be used to

measure solids concentration, boundaries should be set for the probe. The steps to follow to be given as follows,

1.   Make sure that the end face of probe is under an empty-bed state (material concentration=0), and keep the end of probe from interference of external light.

2.   Adjust the Offset potentiometer on the instrument to make the output of the instrument be 0 voltage.

3.   Place the probe under the bulk concentration state (material concentration=1), adjust the GAIN potentiometer to let the output of the instrument nearly to the full scale value (e.g., 4.5 voltage).

4.   Repeat the procedures mentioned above for 2 or 3 times until the output of the probe is 0 voltage when the material concentration is 0. And the output of the probe is close to full-scale value (e.g., 4.5 voltage) when the probe is under the state of bulk concentration. (There would be some difference in reproducibility of 0 voltage and full-scale points due to the change in bulk density of the material and contamination of the probe).

The Offset and GAIN potentiometers could not be readjusted during measurement, or otherwise the concentration measurement would be influenced. The full-scale output of the instrument can be adjusted on the basis of the maximum concentration of material to be measured, which may extend the variation scope of actual concentration of material to the full scale of the instrument. When the particle measurement mode is

selected, the magnitude of signals implies the value of relative concentration of material (0 for empty bed).
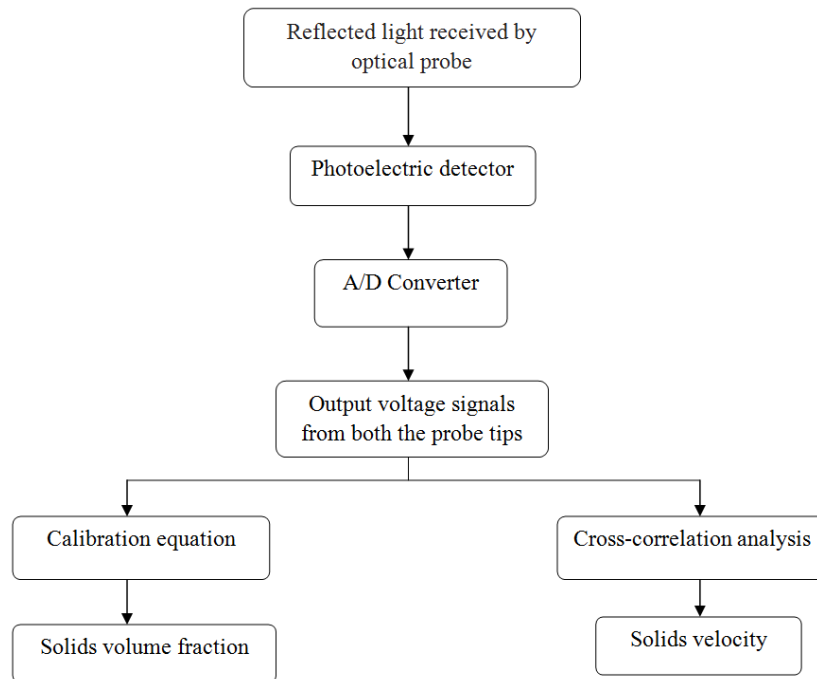
Figure A.7. Schematic representation of evaluation of different parameters using optical probes

APPENDIX B.

MATLAB PROGRAMS FOR SOLIDS VELOCITY DETERMINATION FOR GAS-
SOLID OPTICAL PROBES

B.1. Average Values of Sampled Signals

```matlab
% (Program for calculating average values of sampled signals)
%Shreekanta Aradhya, Missouri S&T, Dr. Al-Dahhan Muthanna's Research Group
%%%%%%%%%%%%%%%%%%%%%%%%%%%%%%%%%%%%%%%%%%%%%%%%%%%%%%%%%
%%%%%%%%%%%%%%%%%%%
%% %
%% Read the data from .pct and .pva files, which is the processed %
%% data of optical probe. %
%% %
%% Namestr: Data file name %
%% M : Number of groups %
%% datax : Data series of CH1 %
%% datay : Data series of CH2 %
%% datacnt: Data counts %
%% datagap: 1/Frenquency %
%% %
%%%%%%%%%%%%%%%%%%%%%%%%%%%%%%%%%%%%%%%%%%%%%%%%%%%%%%%%%
%%%%%%%%%%%%%%%%%
tic
clear
clc
Firp=1;
Nexp=136;
skip=0;
%*****************************************************%
fid1=fopen('namelist136_z5vs.txt','r');
fid2=fopen('ave_results_z5vs.dat','w');
fprintf(fid2,'%s\n',' File Name CH1(Part Average) CH2(Part Average) CH1(All Average) CH2(All
Average)');
for LL2=1:skip
skip_line=fgetl(fid1);
end
for ll=Firp:Nexp
Namestr=fgetl(fid1);
%*****************************************************%
fid=fopen(Namestr,'r');
tmp0=fscanf(fid,'%d,%f',2);
dxtoy=tmp0(2);
tt1=fgets(fid);
tmp1=fscanf(fid,'%d,%f',2);
datacnt=tmp1(1);
tmp2=fscanf(fid,'%f,%f',2);
ave_part_x=tmp2(1);
ave_part_y=tmp2(2);
for n=1:4
tt2=fgets(fid);
end
datax=fscanf(fid,'%d',datacnt);
tt3=fgets(fid);
tt4=fgets(fid);
datay=fscanf(fid,'%d',datacnt);
fclose(fid);
ave_all_x=mean(datax)/255.*5.;
ave_all_y=mean(datay)/255.*5.;
```

```matlab
%********************************************************%
Namestr1((12-length(Namestr)+1):12)=Namestr;
for jj=1:(12-length(Namestr))
Namestr1(jj)=' ';
end
fprintf(fid2,'%s %13.4f %21.4f %20.4f %21.4f\n',Namestr1,ave_part_x,ave_part_y,ave_all_x,ave_all_y);
end
fclose(fid1);
fclose(fid2);
%********************************************************%
toc
```

B.2. Plot of Data

```matlab
% Program for data plot
function plotout=plotout2(datacnt,datagap,datax,datay,tt,dt)
%Shreekanta Aradhya, Missouri S&T, Dr. Al-Dahhan Muthanna's Research Group
% Plot original signals
figure;
plot([1:datacnt]*0.001*datagap,datax/255.*5.,[1:datacnt]*0.001*datagap,datay/255.*5.+5.);
hold on;
xmax=datacnt*0.001*datagap;
xlimit1=floor(xmax);
xlimit2=floor(xmax+0.5);
if xlimit2-xlimit1>0.5
xlimit=xlimit2;
else
xlimit=xlimit1+0.5;
end
plot([0,xlimit],[5,5]);
set(gca,'XLim',[0,xlimit]);
set(gca,'YLim',[0,10]);
set(gca,'yticklabel',{'0';'1';'2';'3';'4';'0';'1';'2';'3';'4';'5'});
xlabel('Time (s)');
ylabel('Voltage Signal (v)');
% Plot original binary signals with time delay considered
figure;
plot(tt(1:datacnt),datax,'r-')
hold on
plot(tt(1:datacnt)+mean(dt),datay,'b--')
xlabel('Time (s)');
ylabel('Binary Signal');
fprintf('%s\n',' Time Delay Coefficient')
for i4=1:LTN0
fprintf('%12.4f %15.4f\n',dt(i4)*1000,coef(i4))
end
```

B.3. Time Delay Estimation

```matlab
% (Program for calculating delay time and statistical analysis)
% Shreekanta Aradhya, Missouri S&T, Dr. Al-Dahhan Muthanna's Research Group
%% %
```

```
% PROGRAMS FOR CROSS CORRELATION ANALYSIS
%%%%%%%%%%%%%%%%%%%%%%%%%%%%%%%%%%%%%%%%%%%%%%%%%
%%%%%%%%%%%%%
%%%%%%%%%%%%%%%%%%%%%%%%%%%%%%%%%%%%%%%%%%%%%%%%%%%
%%%%%%%%%%%%%%%%%
%% Read the data from .pct and .pva files, which is the processed %
%% data of optical probe. %
%% %
%% Namestr: Data file name %
%% M : Number of groups %
%% datax : Data series of CH1 %
%% datay : Data series of CH2 %
%% datacnt: Data counts %
%% datagap: 1/Frenquency %
%% %
%%%%%%%%%%%%%%%%%%%%%%%%%%%%%%%%%%%%%%%%%%%%%%%%%%
%%%%%%%%%%%%%%%%
tic
clear
clc
Firp=1;
Nexp=7;
skip=0;
%*****************************************************%
fid1=fopen('namelist7_usedP.txt','r');
fid2=fopen('dt_results_usedP.dat','w');
fprintf(fid2,'%s\n',' File Name Time Delay(Part) Time Delay(All) Time Delay(Max. Coef.) Time
Delay(Max. Freq.) Total Number');
for LL2=1:skip
skip_line=fgetl(fid1);
end
for LL=Firp:Nexp
Namestr=fgetl(fid1);
%*****************************************************%
N0=0+50.*(1:200);
LTN0=length(N0);
fid=fopen(Namestr,'r');
tmp0=fscanf(fid,'%d,%f',2);
dxtoy=tmp0(2);
tt1=fgets(fid);
tmp1=fscanf(fid,'%d,%f',2);
datacnt=tmp1(1);
datagap=tmp1(2);
tmp2=fscanf(fid,'%f,%f',2);
avex=tmp2(1);
avey=tmp2(2);
for n=1:4
tt2=fgets(fid);
end
datax=fscanf(fid,'%d',datacnt);
tt3=fgets(fid);
tt4=fgets(fid);
datay=fscanf(fid,'%d',datacnt);
fclose(fid);
ddtt=0.001*datagap;
tt=ddtt*(1:datacnt);
```

```
MM=[8 2 4 16 32 64 128];
Mmax=128;
p1=10;
p2=500;
% Find upwind or downwind
clear pmax Rxymax
[direct,Rxymax1,pmax1]=find_direct(MM,Mmax,datacnt,datax,datay,N0);
Rxymax(1)=Rxymax1;
pmax(1)=pmax1;
p1=floor(pmax1/2);
p2=floor(1.5*pmax1);
if p1<10
p1=10;
end
if p2>500
p2=500;
end
if abs(direct)>1e-3
Mmax=datacnt/(20*pmax(1));
% Find better number of groups
for ii=2:7
clear Rxy xx yy
M=MM(ii);
if M<=Mmax
N=floor(datacnt/M);
for j1=p1:1:p2
if direct>0
xx=datax(N0(1)+1:N0(1)+N);
yy=datay(j1+N0(1)+1:j1+N0(1)+N);
else
xx=datax(j1+N0(1)+1:j1+N0(1)+N);
yy=datay(N0(1)+1:N0(1)+N);
end
xave=mean(xx);
yave=mean(yy);
stdx=std(xx,1);
stdy=std(yy,1);
if stdx*stdy==0
Rxy(j1)=0;
else
Rxy(j1)=mean((xx-xave).*(yy-yave))/(stdx*stdy);
end
end
k1=find(max(Rxy)==Rxy);
Rxymax(ii)=max(Rxy);
pmax(ii)=min(k1);
Mmax=datacnt/(20*pmax(ii));
end
end
k1=find(max(Rxymax)==Rxymax);
M=MM(min(k1));
for ii=1:LTN0
clear Rxy xx yy
N=floor(datacnt/M);
for j1=p1:p2
if direct>0
```

```matlab
xx=datax(N0(ii)+1:N0(ii)+N);
yy=datay(j1+N0(ii)+1:j1+N0(ii)+N);
else
xx=datax(j1+N0(ii)+1:j1+N0(ii)+N);
yy=datay(N0(ii)+1:N0(ii)+N);
end
xave=mean(xx);
yave=mean(yy);
stdx=std(xx,1);
stdy=std(yy,1);
if stdx*stdy==0
Rxy(j1)=0;
else
Rxy(j1)=mean((xx-xave).*(yy-yave))/(stdx*stdy);
end
end
k1=find(max(Rxy)==Rxy);
coef(ii)=max(Rxy);
dt(ii)=min(k1)*ddtt;
end
% Plot original signals
% plot (datacnt,datagap,datax,datay,tt,dt,LTN0,coef)
% Preview of time delay and correlation coefficient
[tmp_coef sequ]=sort(coef);
tmp_dt=dt(sequ(floor(0.8*LTN0):LTN0))*1000;
dt_ave_part=direct*mean(tmp_dt);
dt_ave_all=direct*mean(dt)*1000;
figure
SUBPLOT(1,2,1)
plot(dt*1000,coef,'ms')
hold on
if 0.8*min(dt*1000)>1
xlow1=floor(0.8*min(dt*1000)/1)*1;
xhi1=floor(1.2*max(dt*1000)/1)*1;
else
xlow1=0.8*min(dt*1000);
xhi1=1.2*max(dt*1000);
end
if xhi1-xlow1<1e-3
axis_tmp=axis;
xlow1=axis_tmp(1);
xhi1=axis_tmp(2);
end
%%%%%%%%%%
set(gca,'YLim',[0,1]);
plot(abs(dt_ave_all)*ones(20,1),(0:1/19:1),'r-')
plot((xlow1:(xhi1-xlow1)/(LTN0-1):xhi1),0.6*ones(LTN0,1),'b--')
xlabel('Time (ms)');
ylabel('Correlation Coefficient');
dt_a=sort(dt)*1000;
m_a=1;
jj=1;
while jj<=LTN0
Y_a(m_a)=1;
X_a(m_a)=dt_a(jj);
if jj<LTN0
```

```matlab
for kk=jj+1:LTN0
if dt_a(kk)-dt_a(jj)<1e-3
Y_a(m_a)=Y_a(m_a)+1;
if kk==LTN0
jj=kk+1;
end
else
jj=kk;
break
end
end
else
jj=jj+1;
end
m_a=m_a+1;
end
% Statistical analysis----Distribution of time delay
SUBPLOT(1,2,2)
bar(X_a,Y_a)
hold on
if 0.8*min(X_a)>1
xlow2=floor(0.8*min(X_a)/1)*1;
xhi2=floor(1.2*max(X_a)/1)*1;
else
xlow2=0.8*min(X_a);
xhi2=1.2*max(X_a);
end
if xhi2-xlow2<1e-3
axis_tmp1=axis;
xlow2=axis_tmp1(1);
xhi2=axis_tmp1(2);
end
if max(Y_a)>=10
yhi=floor(1.2*max(Y_a)/10)*10;
else
yhi=10;
end
plot(abs(dt_ave_all)*ones(20,1),(0:yhi/19:yhi),'r-')
%%%%%%%%%%%%%%%%
set(gca,'YLim',[0,yhi]);
xlabel('Time (ms)');
ylabel('Distribution Number');
title(Namestr);
text(0.8*xhi2,0.95*yhi,['LL=',num2str(LL,3)],'FontSize',14);
max_index=find(max(coef)==coef);
dt_max_coef=mean(direct*dt(max_index)*1000);
max_index1=find(max(Y_a)==Y_a);
dt_max_freq=mean(direct*X_a(max_index1));
%%%%%%%%%%%%%%%%%%%%%%%%%
Namestr1((12-length(Namestr)+1):12)=Namestr;
for jj=1:(12-length(Namestr))
Namestr1(jj)=' ';
end
sum_Y_a=sum(Y_a);
fprintf(fid2,'%s %14.6f %17.6f %21.6f %24.6f %17i\n',Namestr1
,dt_ave_part,dt_ave_all,dt_max_coef,dt_max_freq,sum_Y_a);
```

```
Namestr2(1:9)=Namestr1(1:9);
Namestr2(10)='d';
Namestr2(11)='a';
Namestr2(12)='t';
fid3=fopen(Namestr2,'w');
fprintf(fid3,'%s\n',' dt(ms) Correlation Coefficient');
for jj1=1:LTN0
fprintf(fid3,'%11.6f %18.6f\n',direct*dt(jj1)*1000,coef(jj1));
end
fprintf(fid3,'%s\n','*******************************');
fprintf(fid3,'%s\n',' dt(ms) Frequency');
for jj2=1:length(X_a)
fprintf(fid3,'%11.6f %9i\n',direct*X_a(jj2),Y_a(jj2));
end
fprintf(fid3,'%s\n','*******************************');
fprintf(fid3,'%s %11.6f\n','dt_ave_part =',dt_ave_part);
fprintf(fid3,'%s %11.6f\n','dt_ave_all =',dt_ave_all);
fprintf(fid3,'%s %11.6f\n','dt_max_coef =',dt_max_coef);
fprintf(fid3,'%s %11.6f\n','max_coef =',max(coef));
fprintf(fid3,'%s %11.6f\n','dt_max_freq =',dt_max_freq);
fclose(fid3);
clear X_a Y_a dt m_a dt_a sum_Y_a coef tmp_dt;
end
end
fclose(fid1);
fclose(fid2);
%%%%%%%%%%%%%%%%%%%%%%%%%%%%%%%%
toc
```

B.4. Determination of Upward or Downward Flow

```
function [direct,Rxymax,pmax]=find_direct(MM,Mmax,datacnt,datax,datay,N0);
%Shreekanta Aradhya, Missouri S&T, Dr. Al-Dahhan Muthanna's Research Group
% Find upwind or downwind
M=MM(1);
N=floor(datacnt/M);
p1=10;
p2=500;
% Upwind( X ------> Y )
for j1=p1:1:p2
clear xx yy
xx=datax(N0(1)+1:N0(1)+N);
yy=datay(j1+N0(1)+1:j1+N0(1)+N);
xave=mean(xx);
yave=mean(yy);
stdx=std(xx,1);
stdy=std(yy,1);
if stdx*stdy==0
Rxy(j1)=0;
else
Rxy(j1)=mean((xx-xave).*(yy-yave))/(stdx*stdy);
end
end
k1=find(max(Rxy)==Rxy);
```

```matlab
Rxymax_up=max(Rxy);
pmax_up=min(k1);
clear Rxy
% Downwind( Y ------> X )
for j1=p1:1:p2
clear xx yy
xx=datax(j1+N0(1)+1:j1+N0(1)+N);
yy=datay(N0(1)+1:N0(1)+N);
xave=mean(xx);
yave=mean(yy);
stdx=std(xx,1);
stdy=std(yy,1);
if stdx*stdy==0
Rxy(j1)=0;
else
Rxy(j1)=mean((xx-xave).*(yy-yave))/(stdx*stdy);
end
end
k2=find(max(Rxy)==Rxy);
Rxymax_dn=max(Rxy);
pmax_dn=min(k2);
if Rxymax_up>0
if Rxymax_up>Rxymax_dn
direct=1.;
Rxymax=Rxymax_up;
pmax=pmax_up;
else
direct=-1.;
Rxymax=Rxymax_dn;
pmax=pmax_dn;
end
else
if Rxymax_dn>0
direct=-1;
Rxymax=Rxymax_dn;
pmax=pmax_dn;
else
direct=0;
Rxymax=0;
pmax=0;
end
end
```

APPENDIX C.

GRID CONVERGENCE STUDIES AND COMPARISON OF 3-D AND 2-D
SIMULATION FOR SPOUTED BEDS

C.1. Grid Convergence Studies

Adaptive Mesh Refinement (AMR) study is done for the spouted bed simulations in the present study. AMR is a technique for automatically refining (or de-refining) certain region of the physical domain in a finite difference calculation. For time-dependent calculations, the time step as well as the grid spacing may also be a function of the level of refinement. The hierarchical structured grid approach now known as AMR was first developed by Berger and Oliger (1984) for hyperbolic partial differential equations. The approach to adaptive gridding used here was developed for conservation laws and demonstrated to be highly successful for gas dynamics by Berger and Colella (1989) in two dimensions. Bell, Berger, Saltzman and Welcome (1991) extended the methodology to three dimensions. More recently, AMR has been extended to a variety of problems and algorithm choices, including, but not limited to, solving the variable coefficient Poisson equation, Helmholtz equation, system of hyperbolic conservation laws governing inviscid gas dynamics, compressible and incompressible Navier-Stokes equations, and the equations that govern reacting flows, such as those that occur in premixed and nonpremixed combustion.

An initial grid hierarchy is created at the start of any calculation, based on the initial data. As the simulation progresses, the grids may dynamically change to reflect the evolving solution. In both cases, the same procedures are used to create new grids. Construction of the grid hierarchy is based on error estimation criteria specified by the user to indicate where additional resolution is required. Cells requiring additional refinement at a given level are identified and tagged using these criteria. Error estimation may use Richardson extrapolation as described in Berger and Colella (1984), or it may

use some other user-supplied criteria. In the present study Richardson extrapolation criterion is used. The tagged cells are then grouped into rectangular patches using the clustering algorithm given in Berger and Rigoustsos (1991). The generated patches will, in general, contain cells that were not tagged for refinement. The grid efficiency is the fraction of the cells in a new grid that are tagged by the error estimation process. A grid efficiency criterion (typically 70%) determines the minimum grid efficiency that is acceptable. These rectangular patches are refined to form the grids at the next level. The process is repeated until either the error criteria are satisfied or a user-specified maximum level of refinement is reached. The proper nesting requirement is imposed at this stage. The geometry of Spouted bed used for our investigations on scale-up is shown in Figure C.1.

The spout diameter and fountain height are important characteristic parameters which can be used to determine how well numerical models capture the hydrodynamic behavior of spouted beds. Three different grids (Figure C.2.) which satisfy the Richardson extrapolation criterion were selected: 36*186, 42*216 and 26*135.

The predicted spout diameters for all three grid resolutions are almost the same. The predicted fountain height from medium grid resolution (36*186) is close to the height from finer grid resolution ((26*135), but higher than the height from coarse grid resolution (26*135). Radial profiles of voidage (Figure C.3.) and particle velocity (Figure C.4. and C.5.) in the spout and annulus region at H = 0.118 m and H = 0.168 m were compared to further study the grid dependence. The results do not differ vastly except for the coarse grid resolution (26*135). Nearly grid independent results can usually be obtained from medium grid resolution. Thus keeping in mind the accuracy and

computational time the simulations for spouted beds can be performed mainly using the medium grid resolution (36*186), which also satisfies the Richardson extrapolation criterion.
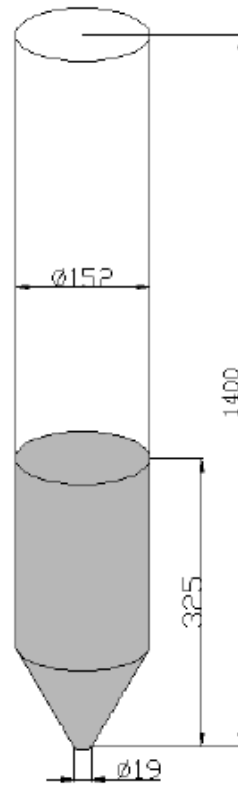
Figure C.1. Schematic of spouted bed geometry used in the present study
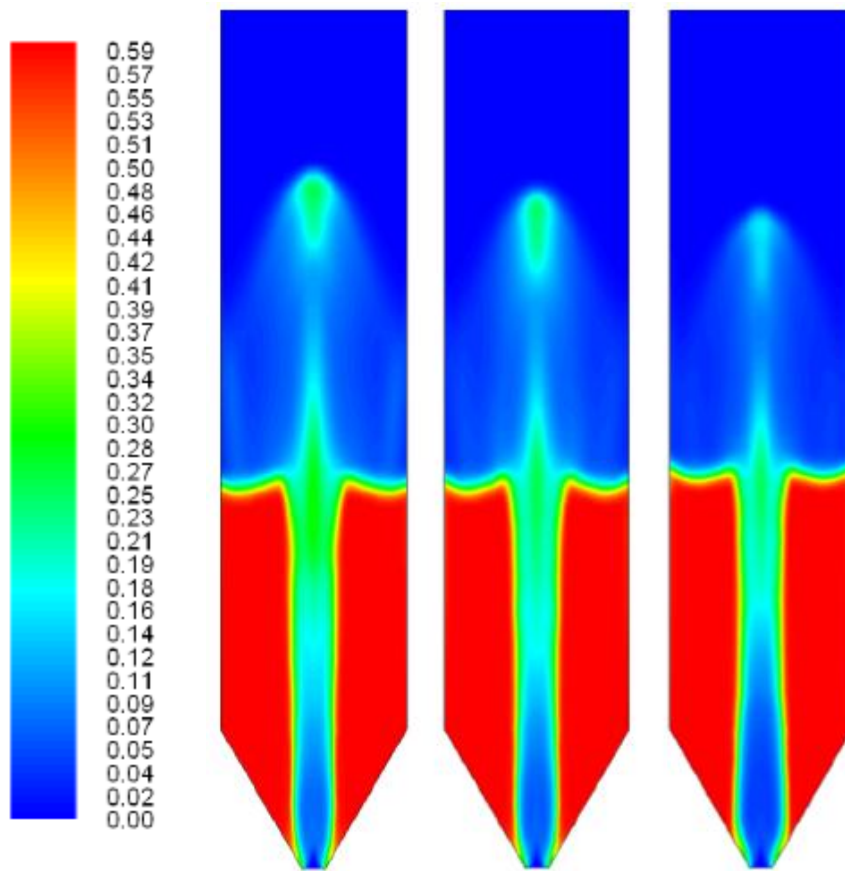
(a) 42*216   (b) 36*186   (c) 26*135

Figure C.2. Grids studied for satisfying Richardson extrapolation criterion
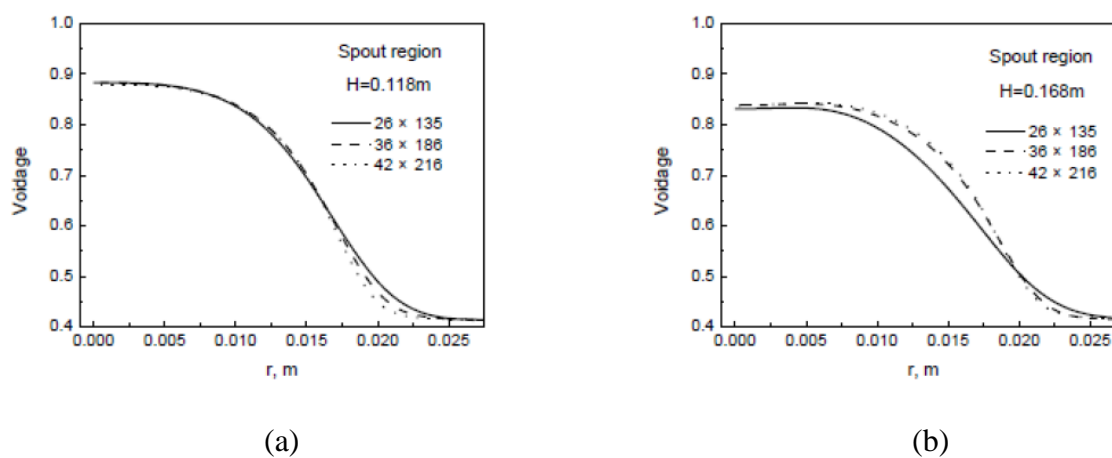
(a)   (b)

Figure C.3. Radial profiles of voidage at (a) H =0.118 m and (b) H = 0.168m
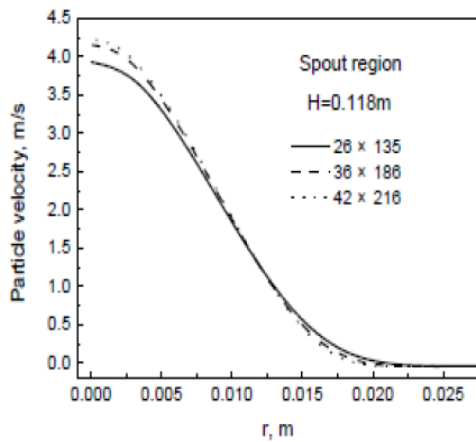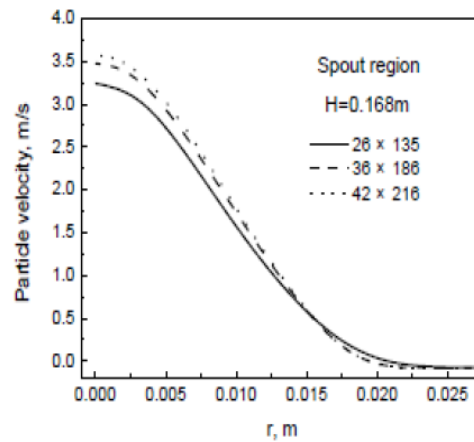
(a)   (b)

Figure C.4. Radial profiles of particle velocities in the spout region at (a) H=0.118 m and (b) 0.168m
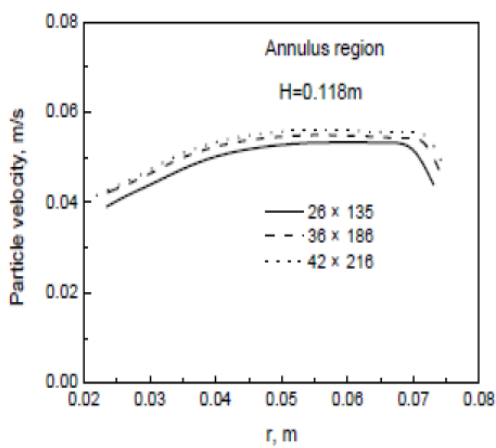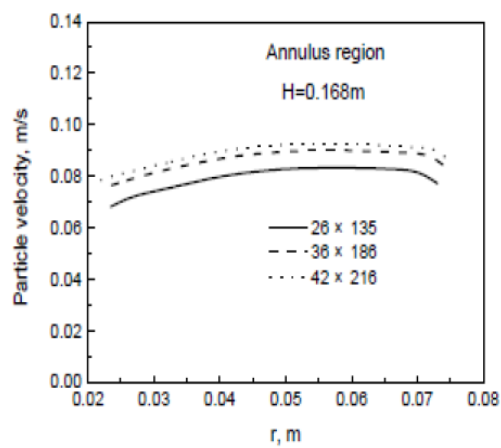
(a)   (b)

Figure C.5. Radial profiles of particle velocities in the annulus region at (a) H=0.118 m and (b) 0.168m

C.2. 3-D and 2-D Simulation Studies for Spouted Bed

The simulations for spouted bed were done for 3 dimensional (3D) models in order to compare the results with 2 dimensional (2D) models, obtained from both types of geometry. Meshes were created by the CAD program of GAMBIT 2.2.30 and exported into Fluent 6.3.26. The mesh size of 5% larger than the particle diameter was equidistant in all directions. The Phase Coupled SIMPLE algorithm was used for the pressure-velocity coupling and correction. A first-order upwind differencing scheme for momentum and volume fraction variables was used. Because of the usual instability and convergence for multiphase simulation, a very small time step (0.0001 s) with about 20 iterations per time step was used. A convergence criterion of 10-3 for each scaled residual component was specified for the relative error between two successive iterations. Meshes for 2D model incorporated axisymmetric models for convenience of simulation and also to reduce simulation time. The results for 2D and 3D simulations are presented below (Figures C.7. and C.8.).

(a)   (b)
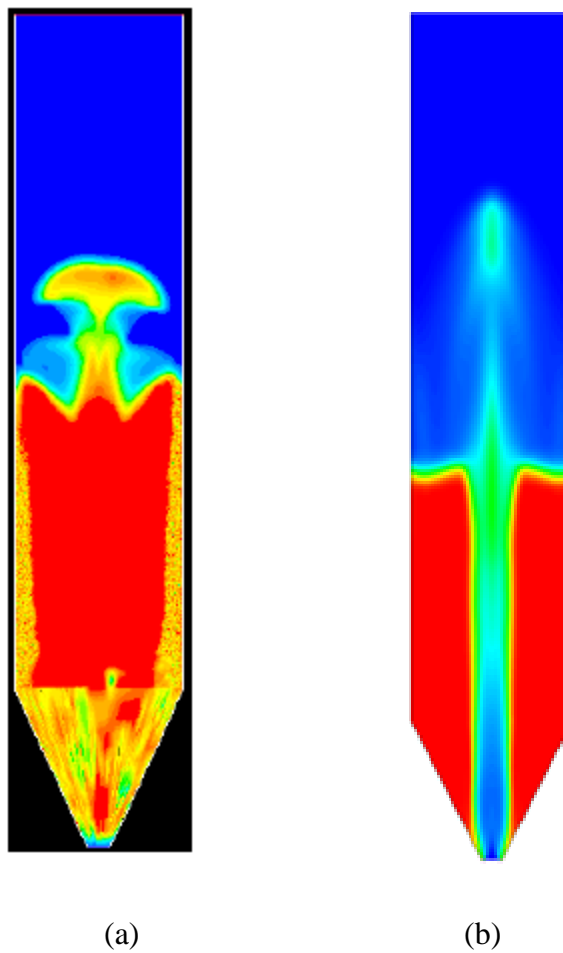
Figure C.6. (a) Contours for solid volume fraction for 3D spouted bed of 0.152 m ID obtained by CFD; (b) Contours for solid volume fraction for 2D spouted bed of 0.152 m ID obtained by CFD

(a)   (b)
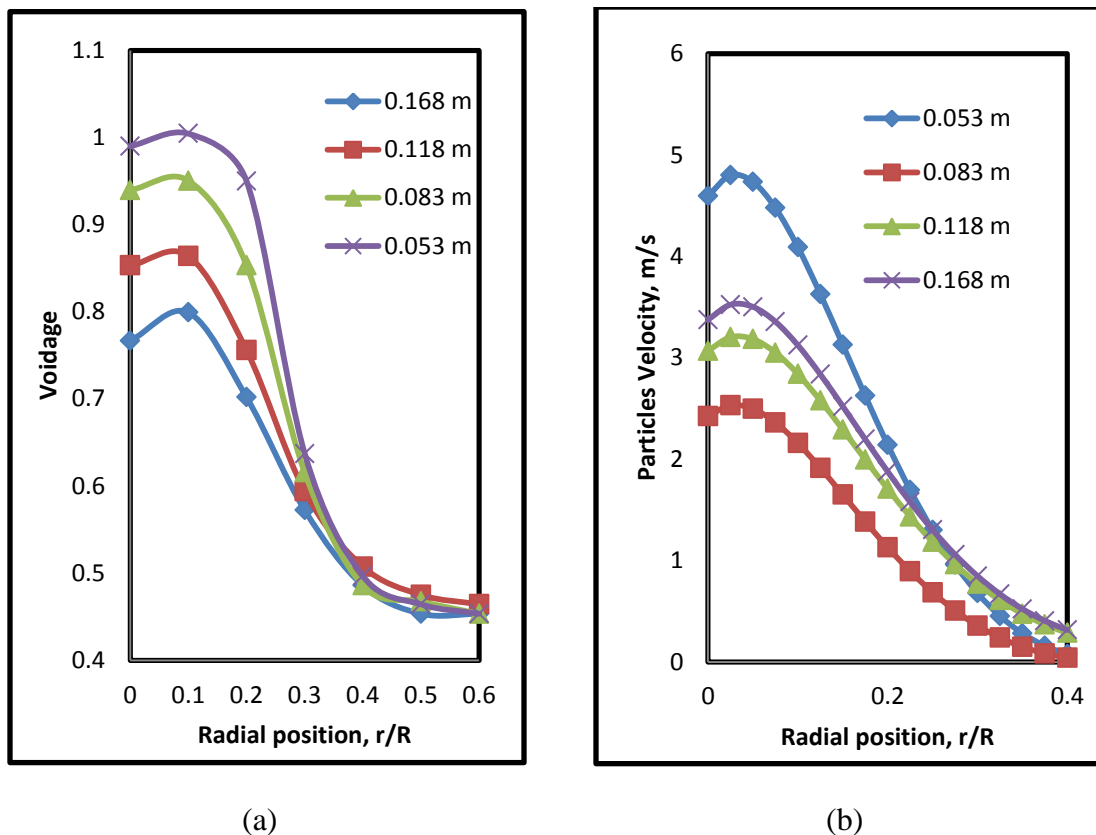
Figure C.7. (a) 3D results of voidage profile for 0.152 m spouted bed at different planes obtained by CFD; (b) 3D results for solids velocity profile for 0.152 m at different planes of the spouted bed obtained by CFD.

The simulations for 2D and 3D models for both voidage and particle velocity for the same reference case showed very slight changes. The percentage deviation of results for the 2D model from the 3D model was less than 3.5%. However, the simulation time for 3D modeling was much more than the 2D modeling. With the above observation of the results, it will be more appropriate to proceed with 2D simulations for future work taking into consideration the simulation time and accuracy. For selected key conditions then we will perform additional 3D simulation.

(a) (b)
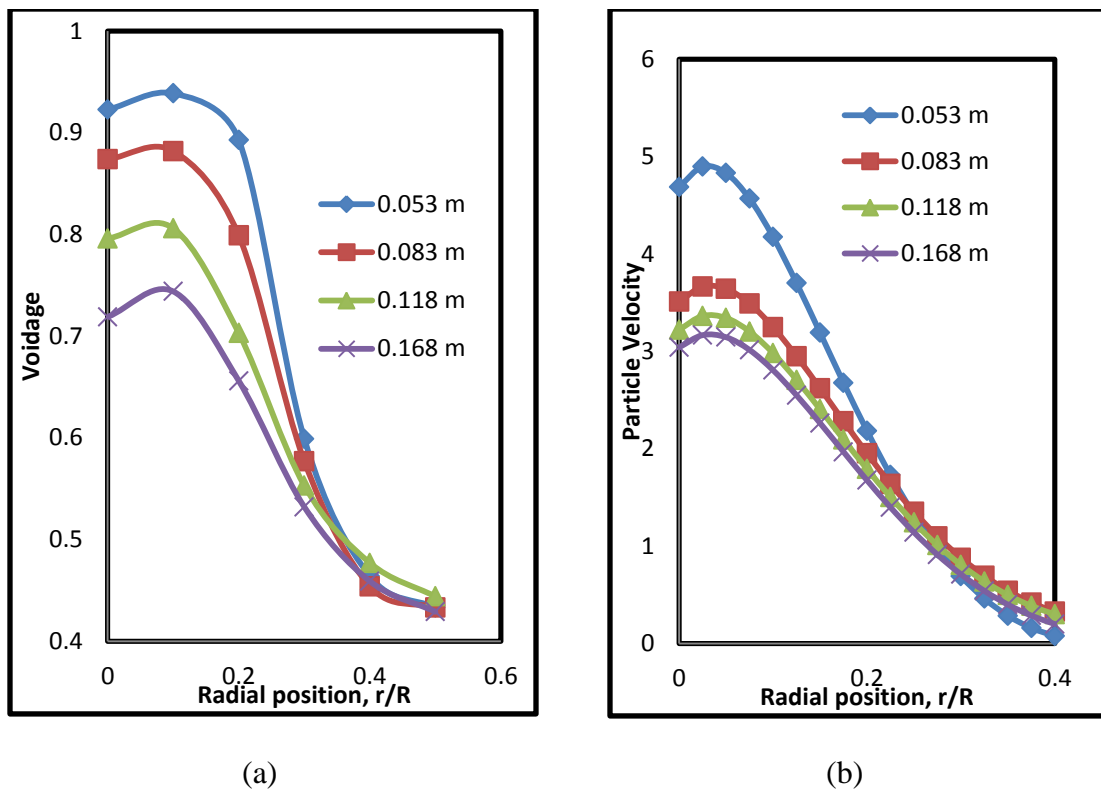
Figure C.8. (a) 2D results of voidage profile for 0.152 m spouted bed at different planes obtained by CFD; (b) 2D results for solids velocity profile for 0.152 m at different planes of the spouted bed obtained by CFD.

BIBLIOGRAPHY

A. Magnusson, R. Randqvist, A.E. Almstedt and F. Johnsson, Dual Fibre optical Probe Measurements of Solids Volume Fraction in a Circulating Fluidized Bed, Powder Technology, 151, pp. 19-26, 2005.

A. Bisio and Kabel, R, Scale-up of Chemical Processes – book, McGraw-Hill, New York, 1985.

A. G. Fane and R. A. Mitchell, Minimum spouting velocity of scaled-up beds, Canadian Journal of Chemical Engineering, Vol. 62, pp. 437–439, 1984

A. Markowski and W. Kaminski, Hydrodynamic characteristics of jet-spouted beds, Canadian Journal of Chemical Engineering, 61, pp. 377–381, 1983.

Al-Dahhan, M. and A. Shaikh, A New Methodology for Scale-up of Bubble Column Reactors, Plenary Lecture, 5th International Chemical Engineering Conference, Amman, Jordan, September 12-14, 2005.

A. Shaikh, Bubble and Slurry Bubble Column Reactors: Mixing, Flow Regime Transition and Scaleup, Doctoral Thesis, 2007, Washington University, St. Louis, Mo.

A. Cecen, Maximum spoutable bed heights of fine particles spouted with air, Can. J. Chem. Eng. 72 (1994) 792–797.

B.G.M. Van Wachem, J. C. Schouten, C. M. Van den Bleek, R. Krishna and J. L Sinclair, Comparative analysis of CFD models of dense gas–solid systems, AIChE Journal 47 (5), pp. 1035–1051, 2001.

C. Wang, Z. Zhong, R. Li and E. Jia-qiang, Recognition of the flow regimes in the spouted bed based on fuzzy c-means clustering, Powder Technology, 205, pp. 201–207, 2011.

C.J Lim and J. R Grace, Spouted bed Hydrodynamics in a 0.91m diameter vessel, Canadian Journal of Chemical Engineering, 65, pp. 366-372, 1987.

C. I. Federer, Fluidized Bed Deposition and Evaluation of Silicon Carbide Coatings on Microspheres, ORNL/TM-5152, 1977. Page 11

C. J Lim and J. R Grace, Spouted bed Hydrodynamics in a 0.91m diameter vessel, Canadian Journal of Chemical Engineering, 65, pp. 366-372, 1987.

C. R. Duarte, M. Olazar, V. V. Murata, and M. A. S. Barrozo, Numerical simulation and experimental study of fluid-particle flows in a spouted bed, Powder Technology, 188, pp. 195–205, 2009.

C. Y.Wen and Y. H. Yu, Mechanics of fluidization, Chemical Engineering Progressive Symposium Ser., 62, pp. 100–111, 1966.

D.Roy, F. Larachi, R. Legros and J. Chaouki, A study of solid behaviour in spouted beds using 3-D particle tracking, Canadian Journal of Chemical Engineering, 72, pp. 945–952, 1994.

D.C Montgomery, Design and Analysis of Experiments, John Wiley & Sons, New York, NY, 5th Edition, 2001.

D. Roy, F. Larachi, R. Legros, and J. Chaouki, A Study of Solid Behavior in Spouted Beds Using 3-D Particle Tracking, Canadian Journal of Chemical Engineering, 72, pp. 945, 1994.

D. E Hadzisdmajlovic, C. V Grabavcic, D. V Vukovic and H. Littman, The mechanics of spout-fluid beds at the minimum spout-fluid flowrate, Canadian Journal of Chemical Engineering, 61, pp. 343-347, 1983.

D. Gidaspow, R. Bezburuah, and J. Ding, Hydrodynamics of circulating fluidized beds: Kinetic theory approach, In Fluidization VII, edition: O. E. Potter and D. J. Nicklin (New York: Engineering Foundation), pp. 75–82, 1991.

D. L. Koch and R. J. Hill, Inertial effects in suspension and porous-media flows, Ann. Rev. Fluid Mechanics, 33, pp. 619–647, 2001.

D. Bai and K. Kato, Quantitative Estimation of Solids Holdups at Dense and Dilute Regions of Circulating Fluidized beds, Powder Technology, 101, pp. 183-190, 1999.

D. Rensner, J. Werther in: A. Dybbs, B. Ghorashi (Eds.), Proceedings of the Fourth International Conference on Laser Anemometric, Cleveland, OH, Vol. 2, ASME, New York, pp. 753, 1991.

E. F. Zanoelo, S. C. S. Rocha, and D. F. Rezende, Influence of Operating Parameters on the Average Spout Width in Two-Dimensional Spouted Beds, Canadian Journal of Chemical Engineering, 82, pp. 89, 2004.

E. Åbro, V.A Khoryakov, G. A. Johansen and L. Kocbach , Determination of void fraction and flow regime using a neural network trained on simulated data based on gamma-ray densitometry Measurement Science and Technology, 10, pp. 619–30, 1999.

F. Wan-Fyong, P. G. Romankov and N. B. Rashkovskaya, Research on the hydrodynamics of the spouting bed, Zh. Prikl. Khim. (Leningrad), 42, pp. 609–617, 1969.

F. Johnsson, R.C. Zijerveld, J. Schouten, C.M. van den Bleek, B. Leckner, Characterization of fluidization regimes by time-series analysis of pressure fluctuations, International Journal of Multiphase Flow 26 (4) (2000) 663– 715.

G. S. Lee, and S. D. Kim, Pressure fluctuations in turbulent fluidized beds, Journal of Chemical Engineering of Japan, 21 (5), pp. 515– 521, 1988.

G. A. Lefroy and J. F. Davidson, The mechanics of spouted beds, Transactions of the Institute of Chemical Engineers, 47, pp. T120–T128, 1969.

G. MacNab and J. Bridgwater, Spouted bed estimation of spouted pressure drop and the particle size for deepest beds, Proc. European Congress on Particle Technology, Nuremberg (1977)

G. Rovero, N. Epstein, J. R. Grace, N. Piccinini and C. M. H. Brereton, Gas phase solid catalyzed chemical reaction in spouted beds, Chemical Engineering Science, 38, pp. 557–566, 1983.

GA Technologies, HTGR Technology Program Semiannual Report (GA-A—17612, DE85 001436) Period Ending Mar. 31, 1984 - July 1984, Page 12.

GA Technologies, HTGR Technology Program Semiannual Report (HTGR-85-037) Period Ending Mar. 31, 1985 - June 1985. Page 12

G.S. McNab, J. Bridgwater, Solid mixing and segregation in spouted beds, Proceedings of the Third European Conference on Mixing BHRA Fluid Engineering (1979) 125–140.

G.C. Rovero, M.H. Brereton, N. Epstein, J.R. Grace, L. Casalegno, N. Piccinini, Gas flow distribution in conical-base spouted beds, Can. J. Chem. Eng. 61 (1983) 289–296.

H. Littman, M.H. Morgan, D.V. Vukovic, F.K. Zdanski, Z.B. Grbavcic, Prediction of the maximum spoutable height and the average spout to inlet tube diameter ratio in spouted bed of spherical particles, Can. J. Chem. Eng. 57 (1979) 684–687.

H. Littman, M.H. Morgan, D.V. Vukovic, F.K. Zdanski, Z.B. Grbavcic, Theory for prediction the maximum spoutable height in a spouted bed, Can. J. Chem. Eng. 55 (1977) 497–501.

H. A. Becker, An investigation of laws governing the spouting of coarse particles, Chemical Engineering Science, 13, pp. 245–262, 1961.

H. Littman, D.V Vukovic, F.K Zdanski and Z.B Grbavcic, Basic relations for the liquid phase spout-fluid flowrate, Fluidization Technology, Edition D.L Keairns, Hemisphere, 1, pp. 373-386, 1976.

H. Enwald, E. Peirano, A. E. Almstedt, Eulerian two-phase flow theory applied to fluidization, International Journal of Multiphase Flow, 22 (1), pp. 21–66, 1996.

H. Lu, Y. He, W. Liu, J. Ding, D. Gidaspow, and J. Bouillard, Computer simulations of gas-solid flow in spouted beds using kinetic-frictional stress model of granular flow, Chemical Engineering Science, 59, pp. 865–878, 2004.

H. Lu, Y. Song, Y. Li, Y. He, and J. Bouillard, Numerical simulations of hydrodynamic behaviour in spouted beds, Chemical Engineering Science Des., 79, pp. 593–599, 2001.

H. Jin, S. Yang and Z. Tong, Application of γ-ray attenuation for axial distribution of holdups in large-scale bubble columns with evaluated pressure, Journal of Chemical Industry and Engineering (China) 55, pp. 1523–1527, 2004b.

H. Jin, S. Yang, G. He, Z. Guo and Z. Tong, An experimental study of holdups in large-scale *p*-xylene oxidation reactors using the _-ray attenuation approach, Chemical Engineering Science, 60, pp. 5955 – 5961, 2005.

I. Pallai and J. N´emeth, Analysis of flow forms in a spouted bed apparatus by the so-called phase diagram, Third International Congress on Chemical Engineering (CHISA), Paper No. C2.4, Czechoslovak Society for Chemical Industry, Prague, 1969.

IAEA, Fuel Performance and Fission Product Behavior in Gas Cooled Reactors, IAEA-TECDOC-978, Nov. 1997. Page 12

J. Aguillon, K. Shakourzadeh and P. Guigon, A Mew Method for Local Solid Concentration Measurement in Circulating fluidized bed, Powder Technology, 86, pp. 251-255, 1996.

J. Z. Liu, J. R. Grace and X. T. Bi, Novel Multifunctional Optical-Fiber Probe: I. Development and Validation, AIChE Journal, 49 (6), pp. 1405–1420, 2003.

J-X. Zhu, H.Zhang, P.M Johnston, H.I de Lasa and M.A. Bergougnou, A Novel Calibration Procedure for a fiber Optic Solids Concentration Probe, Powder Technology, 100, pp. 260-272, 1998.

J. B. Romero and L.N Johanson, Factors affecting fluidized bed quality, Chemical Engineering Program Symposium Series, 58 (38), pp. 28-37, 1962.

J. Bridgwater and K. B. Mathur, Prediction of spout diameter in a spouted bed – a theoretical model, Powder Technology, 6, pp. 183–187, 1972.

J. Eastwood, E. J. P. Matzen, M. J. Young, and N. Epstein, Random loose porosity of packed beds, British Chemical Engineering, 14, pp. 1542–1545, 1969.

J. A. Yasuna H. R. Moyer, S. Elliott and J. L. Sinclair, Quantitative predictions of gas-particle flow in a vertical pipe with particle–particle interactions, Powder Technology, 84 (1), pp. 23–34, 1995.

J. M. Schweitzer, J. Bayle, and T. Gauthier, Local Gas Hold-up Measurements in Fluidized Bed and Slurry, Chemical Engineering Science, 56, pp. 1103, 2001.

J. Link, Development and Validation of a Discrete Particle Model of a Spout-Fluid Bed Granulator, PhD Thesis, University of Twente, The Netherlands, 2006.

J. Pina, V. Bucala, N. S. Schbib, P. Enge, and H. I. de Lasa, Modeling a Silicon CVD Spouted Bed Pilot Plant Reactor, International Journal of Chemical Reactor Engineering, 4, 2006.

J. Xu, X. Bao, W. Wei, G. Shi, S. Shen, H.T. Bi, J.R. Grace and C.J. Lim, Statistical and frequency analysis of pressure fluctuations in spouted beds, Powder Technology, 140, pp. 141– 154, 2004.

J. R. van Ommen, S. Sasic, J. van der Schaaf, S. Gheorghiu, F. Johnsson and M. O. Coppens, Time-series analysis of pressure fluctuations in gas–solid fluidized beds − A review, International Journal of Multiphase Flow, 37, pp. 403–428, 2011.

J. B. Bell, M. J. Berger, J. S. Saltzman and M. Welcome, Three Dimensional Adaptive Mesh Refinement for Hyperbolic Conservation Laws, *LLNL Report UCRL-JC-108794*, Dec. 1991.

K. A. Shollenberger, J. R. Torczynski, D. R. Adkins, Gamma densitometry tomography of gas holdup spatial distribution in industrial scale bubble columns, Chemical Engineering Science 52 (3), pp. 2037– 2048, 1997

K. B. Mathur and P. E. Gishler, A technique for contacting gases with solid particles, AIChE Journal, 1, pp. 157–164, 1955.

K. G. Santos, V. V. Murata, and M. A. S. Barrozo, Three-dimensional computational fluid dynamics modeling of spouted bed, Canadian Journal of Chemical Engineering, 87, pp. 211–219, 2009.

K. Minato, H. Kikuchi, K. Fukuda, N. Suzuki, H. Tomimoto, and N. Kitamura, Internal Flaws in the Silicon Carbide Coating of Fuel Particles for High-Temperature Gas-Cooled Reactors, Nuclear Technology, 106, 342pp, 1994.

K.B. Rao, A. Husain and Ch. D. Rao, Prediction of the maximum spoutable height in spout-fluid beds, Canadian Journal of Chemical Engineering, 63, pp. 690-692, 1985.

K.B. Mathur, N. Epstein, Spouted Bed, Academic Press, New York, 1974.

K. Oki, T. Akehata, and T. Shirai, A New Method for Evaluating the Size of Moving Particles with a Fiber Optic Probe, Powder Technology, 11, pp. 51, 1975.

K.B. Mathur, N. Epstein, Spouted Beds, Academic Press, New York, 1974.

K.B. Rao, A. Husain, C.D. Rao, Prediction of the maximum spoutable height in spout-fluid beds, Can. J. Chem. Eng. 63 (1985) 690–692.

L.A.P. Freitas, O.M. Dogan, C.J. Lim, J.R. Grace, B. Luo, Hydrodynamics and stability of slot-rectangular spouted beds, Chem. Eng. Commun. 181 (2000) 242–258 (part II: increasing bed thickness).

L. Y. He, Hydrodynamic and scale-up studies of spouted beds, Doctorial Thesis, University of British Columbia, Vancouver, Canada, 1995.

L. Schiller and A. Naumann, A drag coefficient correlation, Verein Deutscher Ingenieure, 77, pp. 318–320, 1935.

L. A. Madonnna and R.P. Lama, The derivation of an equation for predicting minimum spouting velocity, AIChe Journal, Vol. 4, No. 4, pp. 497-497, 1958.

L. A. P. Freitas, K. Mitsutani, C. Jim Lim, J. R. Grace, and W. Wei, Voidage Profiles in a Slot-Rectangular Spouted Bed, Canadian Journal of Chemical Engineering, 82, 74pp, 2004. Page 1

L. A. P. Freitas, O. M. Dogan, C. Jim Lin, J. R. Grace, and D. Bai, Identification of Flow Regimes in Slot-Rectangular Spouted Beds using Pressure Fluctuations, Canadian Journal of Chemical Engineering, 82, 60pp, Page 1, 2004.

L. Huilin, H. Yurong, L. Wentie, D. Jianmin, D. Gidaspow and J. Bouillard, Computer Simulations of Gas-Solid Flow in Spouted Beds Using Kinetic-Frictional Stress Model of Granular Flow, Chemical Engineering Science, 59(4), pp. 865-878, 2004.

L. R Glicksman, M. Hyre and K. Woloshun, Simplified Scaling Relationships for Fluidized bed, Powder Technology, 77, pp. 177-199, 1993.

L. R Glicksman, Scaling Relationships for Fluidized Beds, Chemical Engineering Science, 39, pp. 1373-1379, 1984.

L. R Glicksman, Scaling Relationships for Fluidized Beds, Chemical Engineering Science, 43, pp. 1419-1421, 1988.

L. Huilin, S. Yongli, L. Yang, H. Yurong, and J. Bouillard, Numerical simulations of hydrodynamic behavior in spouted beds, Chemical Engineering Research and Design, 79 (5), pp. 593–599, 2001.

Lu Huilin, He Yurong, Liu Wentie, Jianmin Ding, Dimitri Gidaspow, Jacques Bouillard, Computer simulations of gas–solid flow in spouted beds using kinetic–frictional stress model of granular flow, Chemical Engineering Science 59 (2004) 865 − 878

L.T. Fan, T.-C. Ho, S. Hiraoka, W.P. Walawender, Pressure fluctuations in a fluidized bed, AIChE Journal 27 (3) (1981) 388– 396.

M. J. San Jose, M. Olazar, S. Alvarez and J. Bilbao, Local Bed Voidage in Conical Spouted Beds, Industrial Engineering Chemistry, 37 (6), pp. 2553–2558, 1998b.

M. J. San Jose, M. Olazar, S. Alvarez, M. A. Izquierdo and J. Bilbao, Solid Cross-Flow Into the Spout and Particle Trajectories in Conical Spouted Beds, Chemical Engineering Science, 53 (20), pp. 3561–3570, 1998a.

M. Olazar, M. J. San Jose, M. A. Izquierdo, A. Ortiz de Salazar, and J. Bilbao, Effect of Operating Conditions on Solid Velocity in the Spout, Annulus and Fountain of Spouted Beds, Chemical Engineering Science, 56 (11), pp. 3585–3594, 2001b.

M. Olazar, M. J. San Jose, R. Llamosas, S. Alvarez and J. Bilbao, Study of Local Properties in Conical Spouted Beds Using an Optical Fiber Probe, Industrial Engineering Chemistry, 34 (11), pp. 4033–4039, 1995.

M. Olazar, M. J. San Jose, S. Alvarez, A. Morales and J. Bilbao, Measurement of Particle Velocities in Conical Spouted Beds Using an Optical Fiber Probe, Industrial Engineering Chemistry, 37 (11), pp. 4520–4527, 1998.

M. Olazar, R. Aguado, J. Bilbao and A. Barona, Pyrolysis of Sawdust in a Conical Spouted-Bed Reactor with a HZSM-5 Catalyst, AIChE Journal, 46 (5), pp. 1025–1033, 2000b.

M. Olazar, R. Aguado, M. J. San Jose, and J. Bilbao, Kinetic Study of Fast Pyrolysis of Sawdust in a Conical Spouted Bed Reactor in the Range 400–500∘C, Journal Chemical Technology, 76 (5), pp. 469–476, 2001a.

M. Olazar, R. Aguado, M. J. San Jose, and J. Bilbao, Performance of a Conical Spouted Bed in Biomass Catalytic Pyrolysis, Recents Progres en Genie des Procedes, 14 (76), pp. 499–506, 2000a.

M. J. Berger and J. Oliger, Adaptive Mesh Refinement for Hyperbolic Partial Differential Equations, *J. Comput. Phys.*, 53, pp. 484-512, 1984.

M. J. Berger and P. Colella, Local Adaptive Mesh Refinement for Shock Hydrodynamics, *J. Comput. Phys.*, 82, pp. 64-84, 1989.

M. J. Berger and I. Rigoustsos, An algorithm for point clustering and grid generation, *New York University - CIMS Report NYU-501*, 1991.

Martin Olazar, Maria J. San Jose, Ricardo LLamosas, Sonia Alvarez and Javier Bilbao, Study of Local Properties in Conical Spouted Beds using an Optical Fiber Probe, Industrial Engineering Chemistry, 34, pp. 4033-4039, 1995.

M. A. Van Der Hoef, R. Beetstra, and J. A. M. Kuipers, Lattice-Boltzmann simulations of low-Reynolds-number flow past mono- and bidisperse arrays of spheres, Journal of Fluid Mechanics, 528, pp. 233–254, 2005.

M. C Green and J. Bridgwater, An Experimental study of Spouting in large sector beds, Canadian Journal of Chemical Engineering, 61, pp. 281-288, 1983.

M. Choi and A. Meisen, Hydrodynamics of shallow conical spouted beds, Canadian Journal of Chemical Engineering, 70, pp. 916–924, 1992.

M. Horio, A. Nonaka, Y. Sawa and L. Muchi, A New Similarity Rule for Fluidized Bed Scale-up, AIChE Journal,32, pp. 1466-1482, 1986.

M. Horio, H. Ishii, Y. Kobuki and N. Yamanishi, A Sacling Law for Circulating Fluidized Beds, Journal of Chemical Engineering of Japan, 22, pp. 587-592, 1989.

M. Horio, J. Liu and I. Muchi, Direct Simulation for Predicting Bubble Distribution and Particle Circulation Pattern in Large-Scale Fluidized Beds, Kagaku Kogaku Ronbunshu, 9, pp. 176-185, 1983.

M. I. Kalwar, G. S. Raghavan, andA. S.Mujumdar, Circulation of particles in two-dimensional spouted beds with draft plates, Powder Technology, 77, pp. 233–242, 1993.

M. J. V Goldschmidt, J.A. M Kuipers, and W.P.M. van Swaaij, Hydrodynamic Modeling of Dense Gas-fluidized Beds Using the Kinetic Theory of Granular Flow: Effect of Coefficient of Restitution on Bed Dynamics, Chemical Engineering Science, 56(2), pp. 571-578, 2001.

M. Olazar, M. J. San Jos´e, A. T. Aguayo, J. M. Arandes, and J. Bilbao, Hydrodynamics of nearly flat base spouted beds, Chemical Engineering Journal, 55, pp. 27–37, 1994.

M. Olazar, M. J. San Jos´e, A. T. Aguayo, J. M. Arandes, and J. Bilbao, Design factors of conical spouted beds and jet spouted beds, Industrial and Engineering Chemistry Ressearch, 32, pp. 1245–1250, 1993.

M. Olazar, S. Alvarez, R. Aguado and M. J. San Jose, Spouted Bed Reactors, Chemical Engineering Technology 26, 845pp, 2003. Page 2

M. Syamlal and T. O'Brien, Computer simulation of bubbles in a fluidized bed, AIChE Symposium Series, 85, pp. 22–31, 1989.

M. Syamlal, W. Rogers, and T. J. O'Brien, MFIX Documentation, US Department of Energy, Federal Energy Technology Center, 1993.

M. T Nicastro and L. R Glicksman, Experimental verification of scaling relationships for fluidized bed, Chemical Engineering Science 39, pp. 1381-1391, 1984.

M. Z. Anabtawi, B. Z. Uysal, and R.Y. Jumah, Flow characteristics in a rectangular spout-fluid bed, Powder Technology, 69, pp. 205–211, 1992.

M. Cassanello, F. Larachi, R. Legros, and J. Chaouki, Solids Dynamics from experimental Trajectory Time-Series of a Single Particle Motion in Gas-Spouted Beds, Chemical Engineering Science, 54, pp. 2545, 1999.

M. Kwauk, J. Li, W.-C. Yang (Eds.), Fluidization, vol. X, Beijing United Engineering Foundation, New York, 2001, pp. 149– 156.

N.E.C. Lopes, V.A.S. Moris and O.P. Taranto, Analysis of spouted bed pressure fluctuations during particle coating, Chemical Engineering and Processing, 48, pp. 1129–1134, 2009.

N. Hilal and D. J. Gunn, Solid Hold Up in Gas fluidized Beds, Chemical Engineering and Processing, 41, pp. 373, 2001.

N. Epstein and J. R. Grace, Spouting of particulate solids. In: Fayed, M.E., Otten, L. (Eds.), Handbook of Powder Science and Technology, second ed. Chapman & Hall, New York (Section 10), 1997.

N. Epstein and G. R Grace, Spouted and Spout-fluid beds: Fundamentals and applications, book, 2011.

NUREG/CR-6844, TRISO-Coated Particle Fuel Phenomenon Identification and Ranking Tables (PIRTs) for Fission Product Transport Due to Manufacturing, Operations, and Accidents, volume 1, Page 12, 2001.

O. Gryczka, S. Heinrich, and J. Tomas, CFD-modelling of the fluid dynamics in spouted beds. In Micro-Macro-Interactions, edition: A. Bertram and J. Tomas (Berlin: Springer), pp. 265–275, 2008.

O. Gryczka, S. Heinrich, N. G. Deen, M. v. S. Annaland, J. A. M. Kuipers, and L. M˙orl, CFD modeling of a prismatic spouted bed with two adjustable gas inlets, Canadian Journal of Chemical Engineering, 87, pp. 318–328, 2009.

Organisation for Economic Co-operation and Development: INTERNATIONAL ENERGY TECHNOLOGY COLLABORATION AND CLIMATE CHANGE MITIGATION: SYNTHESIS REPORT [COM/ENV/EPOC/IEA/SLT (2005)11], Page 3.

O.M. Dogan, L.A.P. Freitas, C.J. Lim, J.R. Grace, B. Luo, Hydrodynamics and stability of slot-rectangular spouted beds, Chem. Eng. Commun. 181 (2000) 225–242 (part I: thin bed).

O.M. Dogan, B.Z. Uysal, J.R. Grace, Hydrodynamic studies in a half slot-rectangular spouted bed column, Chem. Eng. Commun. 191 (2004) 566–579.

P.P. Chandnani, N. Epstein, in: V. Fluidization, K. Ostergaard, A. Sorensen (Eds.), Spouta-bility and Spout Destabilization of Fine Particles with a Gas, Engineering Foundation, New York, 1986, pp. 233–240.

P. M. Herbert, M. E. Sc. Dissertation, University of Western Ontario, Canada, 1994.
P. A. Shirvanian, J. M. Calo, and G. Hradil, Numerical simulation of fluid-particle hydrodynamics in a rectangular spouted vessel, International Journal of Multiphase Flow, 32, pp. 739–753, 2006.

P. C. Johnson, P. Nott, and R. Jackson, Frictional-collisional equations of motion for particulate flows and their application to chutes, Journal of Fluid Mechanics, 210, pp. 501–535, 1990.

P. E. Gishler and K. B. Mathur, Method of contacting solid particles with fluids, U.S. Patent No. 2,786,280 to National Research Council of Canada, 1957.

P. Abdul Salam and S. C. Bhattacharya, A Comparative Hydrodynamic Study of Two Types of Spouted Bed Reactor Designs, Chemical Engineering Science, 61, pp. 1946, 2006.

P. Abdul Salam and S. C. Bhattacharya, A Comparative Study of Charcoal Gasification in Two Types of Spouted Bed Reactors, Energy, 31, pp. 228, 2006.

R. Mabrouk, R. Radmanesh, J. Chaouki and C. Guy, Scale Effects on Fluidized Bed Hydrodynamics. International Journal of Chemical Reactor Engineering, 3, 2005

R. B´ettega, A. R. F. de Almeida, R. G. Corrˆea, and J. T. Freire, CFD modelling of a semi-cylindrical spouted bed: Numerical simulation and experimental verification, Canadian Journal of Chemical Engineering, 87, pp. 177–184, 2009.

R. B´ettega, R. G. Corrˆea, and J. T. Freire, Scale-up study of spouted beds using computational fluid dynamics, Canadian Journal of Chemical Engineering, 87, pp. 193–203, 2009.

R. Beetstra, M. A. Van Der Hoef, and J. A. M. Kuipers, Drag force of intermediate Reynolds number flow past mono- and bidisperse arrays of spheres, AIChE Journal, 53, pp. 489–501, 2007.

R. L. Beatty, Pyrolytic Carbon Deposited from Propane in a Fluidized Bed, MS Thesis, University of Tennessee. ORNL-TM-1649, 1967. Page 11

R. S. Krzywanski, N. Epstein and B. D. Bowen, Multi-dimensional model of a spouted bed, Canadian Journal of Chemical Engineering, 70, pp. 858–872, 1992.

S. Limtrakul, A. Boonsrirat, and T. Vatanatham, DEM modeling and simulation of a catalytic gas-solid fluidized bed reactor: A spouted bed as a case study, Chemical Engineering Science, 59, pp. 5225–5231, 2004.

S. Takeuchi, S. Wang and M. Rhodes, Discrete element method simulation of three dimensional conical-base spouted beds, Powder Technology, 184, pp. 141–150, 2008.

S. Takeuchi, S.Wang, and M. Rhodes, Discrete element simulation of a flat-bottomed spouted bed in the 3-D cylindrical coordinate system, Chemical Engineering Science, 59, pp. 3495–3504, 2004.

S. Takeuchi, X. S. Wang and M. J. Rhodes, Discrete element study of particle circulation in a 3-D spouted bed, Chemical Engineering Science, 60, pp. 1267–1276, 2005.

San Jose, M. J., Olazar, M., Aguado, R., and Bilbao, J. (1996). Influence of the conical section geometry on the hydrodynamics of shallow spouted beds. Chemical Engineering Journal, 62, 113–120.

San Jose, M. J., Olazar, M., Izquierdo, M. A., and Bilbao, J. (2001). Spout geometry in shallow spouted beds. Industrial and Engineering Chemistry Research, 40, 420–426.

S.C.S. Rocha and E.F. Zanoelo, Flow Model for a Two-Dimensional Spouted Bed Including the Spout Width Variation, in "Proceedings of International Drying Symposium", Gold Coast, Australia, pp. 551–558, 1994.

S. Y.Wang, Y. R. He, H. L. Lu, J. X. Zheng, G. D. Liu, and Y. L. Ding, Numerical simulations of flow behavior of agglomerates of nano-size particles in bubbling and spouted beds with an agglomerate-based approach, Food and Bio-production Process, 85, pp. 231–240, 2007.

S. A. Tjugum, Multiphase flow regime identification by multibeam gamma-ray densitometry, Proc. 2nd World Congress on Industrial Process Tomography (Hannover, August), pp. 168–74, 2001.

S. A. Tjugum, B. T. Hjertaker and G. A. Johansen, Multiphase flow regime identification by multibeam gamma-ray densitometry, Measurement Science and Technology, 13, pp. 1319–1326, 2002.

S. B. Kumar, D. Moslemian, M. Dudukovic, Gas-holdup measurements in bubble columns using computed tomography, AIChE Journal 43, pp. 1414–1425, 2006.

Sun Dan, WangShuyan, LiuGougdong, WangShuai, LiuYongjian, WeiLixin, Simulations of flow behavior of gas and particles in a spouted bed using a second-order moment method-frictional stresses model, Chemical Engineering Science (2010), doi:10.1016/j.ces.2009.12.042

T. E. Broadhurst and H. A Becker, Proceedings of the International Symposium Fluidization Ste`, Chimie Indus., Toulouse, France, 1973.

T. Fitzgerald, D. Bushnell, S. Crane, and Y. C Shieh, Testing of cold scaled bed modeling for fluidized bed combustors, Powder Technology, 38, pp. 107-120, 1984.

T. Ishikura, H. Nagashima, and M. Ide, Behavior of Cohesive Powders in a Powder-Particle Spouted Bed, Canadian Journal of Chemical Engineering, 82, 102pp, 2004.

T. Kawaguchi, M. Sakamoto, T. Tanaka, and Y. Tsuji, Quasi-three-dimensional numerical simulation of spouted beds in cylinder, Powder Technology, 109, pp. 3–12, 2000.

T. Kawaguchi, T. Tanaka, and Y. Tsuji, Numerical simulation of two-dimensional fluidized beds using the discrete element method, Powder Technology, 96, pp. 129–138, 1998.

T. J. O'Brien and M. Syamlal, Particle cluster effects in the numerical simulation of a circulating fluidized bed, In: Avidan, A. (Ed.), Circulating Fluidized Bed Technology IV, Proceedings of the Fourth International Conference on Circulating Fluidized Beds. Somerset, PA, August 1–5, 1993.

T. Swasdisevi, W. Tanthapanichakoon, T. Charinpanitkul, T. Kawaguchi, T. Tanaka, and Y. Tsuji, Investigation of fluid and coarse-particle dynamics in a two-dimensional spouted bed, Chemical Engineering Technology, 27, pp. 971–981, 2004.

T. Djeridane, F. Larachi, D. Roy, J. Chaouki, and R. Legros, Investiagion of the Mean and Turbulent Particle Velocity Fields in a Spouted Bed Using Radioactive Particle Tracking, Canadian Journal of Chemical Engineering, 76, pp. 190, 1998.

T. H. Bi, A critical review of the complex pressure fluctuation phenomenon in gas–solids fluidized beds, Chemical Engineering Science, 62, pp. 3473–3493, 2007.

Tables (PIRTs) for Fission Product Transport Due to Manufacturing, Operations, and Accidents, volume 1, 2001. Page 12

US Department of Energy: DOE EIA 2003 *New Reactor Designs.* GIF Annual Report 2008 Page 4

V. P. Veera, Gamma ray tomography design for the measurement of hold-up profiles in two-phase bubble columns. Chemical Engineering Journal 81, pp. 251–260, 2001

V. P. Veera and J. B. Joshi, Measurement of gas holdupp rofiles in bubble column by gamma ray tomography: effect of liquid phase properties. Transaction of Institution of Chemical Engineers 78, part A, (4), pp. 425–434, 2001

W. Du, H. T. Bi, and N. Epstein, Exploring a non-dimensional varying exponent equation relating minimum spouting velocity to maximum spoutable bed depth, Canadian Journal of Chemical Engineering, 87, pp. 157–162, 2009.

W. Du, W. Wei, J. Xu, Y. Fan, and X. Bao, Computational fluid dynamics (CFD) modeling of fine particle spouting, International Journal of Chemical Reaction Engineering, 4, pp. A21, 2006.

W. Du, X. Bao, J. Xu, and W. Wei, Computational Fluid dynamics (CFD) modeling of spouted bed: Influence of Frictional Stress, Maximum Packing Limit and Restitution Coefficient of Particles, Chemical Engineering Science, 61(14), pp. 4558-4570, 2006.

W. Du, X. Bao, J. Xu, and W.Wei, Computational fluid dynamics (CFD) modeling of spouted bed: Assessment of drag coefficient correlations, Chemical Engineering Science, 61, pp. 1401–1420, 2006.

W. Zhong, Y. Xiong, Z. Yuan, and M. Zhang, DEM simulation of gas-solid flow behaviors in spout-fluid bed, Chemical Engineering Science, 61, pp. 1571–1584, 2006.

W. Zhong, X. Chen, and M. Zhang, Hydrodynamic Characteristics of Spout-Fluid Bed: Pressure Drop and Minimum Spouting/Spout-Fluidizing Velocity, Chemical Engineering Journal, 118, pp. 37, 2006.

W. Zhong, M. Zhang and B. Jin, Maximum spoutable bed height of spout-fluid bed, Chemical Engineering Journal, 124, pp. 55–62, 2006.

W. Zhong, M. Zhang, Experimental study of gas mixing in a spout-fluid bed, AIChE J. 52 (2006) 924–930.

W. Zhong, X. Chen, M. Zhang, Hydrodynamic characteristics of spoutfluid bed: pressure drop and minimum spouting/spout-fluidizing velocity,
Chem. Eng. J. 118 (2006) 37–46.

W. Zhong, M. Zhang, B. Jin, X. Chen, Flow pattern and transition of rectangular spout-fluid bed, Chem. Eng. Proc. 45 (2006) 734–746.

Wang Shuyan, Li Xiang, Lu Huilin, Yu Long, Sun Dan, He Yurong, Ding Yonglong, Numerical simulations of flow behavior of gas and particles in spouted beds using frictional-kinetic stresses model, Powder Technology 196 (2009) 184–193

X. L. Zhao, S. Q. Li, G. Q. Liu, Q. Yao, and J. S. Marshall, DEM simulation of the particle dynamics in two-dimensional spouted beds, Powder Technology, 184, pp. 205–213, 2008.

X. L. Zhao, S. Q. Li, G. Q. Liu, Q. Song, and Q. Yao, Flow patterns of solids in a two dimensional spouted bed with draft plates: PIV measurement and DEM simulations, Powder Technol., 183, pp. 79–87, 2008.

Y. He, G. Zhao, J. Bouillard, and H. Lu, Numerical simulations of the effect of conical dimension on the hydrodynamic behavior in spouted beds, Canadian Journal of Chemical Engineering, 82, pp. 20–29, 2004.

Y. L. He, C. J. Lim, and J. R. Grace, Scale-up studies of spouted beds, Chemical Engineering Science, 52, pp. 329–339, 1997.

Y. Li, C. J. Lim, and N. Epstein, Aerodynamic aspects of spouted beds at temperatures up to 580 ∘C, Journal of Serbian Chemical Society, 61:4–5, pp. 253–266, 1996.

Y. L. He, C.J. Lim, J.R. Grace, Hydrodynamics of pressurized spouted beds, Canadian Journal of Chemical Engineering, 76 (4), pp. 696– 701, 1998.

Y. Matsuno, H. Yamaguchi, T. Oka, H. Kage and K. Higashitani, Powder Technology, 36, pp. 215, 1983.
Y. L. He, C. J. Lim, and J. R. Grace, Spouted bed and spout-fluid bed behaviors in a column of diameter 0.91 m. Can. J. Chem. Eng., 70 (1992), 848–857.

Z.B. Grbavcic, D.V.Vukovic, D.E. Hadzismajlovic, R.V. Garic, H. Littman, Prediction of the maximum spoutable bed height in spout-fluid beds, Can. J. Chem. Eng. 69 (1991) 386–389.

Zhiqi Wang, Ping Chen, Haibin Li, Chuangzhi Wu and Yong Chen, Study on the Hydrodynamics of a Spouting-Moving bed, Industrial Engineering Chemistry, 40, pp. 4983-4989, 2001.

Z. B Grbavcic, D.V Vukovic, F.K Zdanski and H. Littman, Fluid flow pattern, minimum spouting velocity and pressure drop in spouted beds, Canadian Journal of Chemical Engineering, 54, pp. 33-42, 1976.

Z. G. Wang, H. T. Bi, and C. J. Lim, Numerical simulations of hydrodynamic behaviors in conical spouted beds, China Particuology, 4, pp. 194–203, 2006.

Z. H. Wu and A. S. Mujumdar, CFD modeling of the gas-particle flow behavior in spouted beds, Powder Technology, 183, pp. 260–272, 2008.

Z. Wang, P. Chen, H. Li, C. Wu and Y. Chen, Study on the hydrodynamics of a spouting moving bed, Industrial and Engineering Chemistry Research, Vol. 40, pp. 4983–4989, 2001.

Z. Wang, T. Bi. Hsiaotao and C. Jim Lim, Measurements of Local Flow Structures of Conical Spouted Beds by Optical Fibre Probes, The Canadian Journal of Chemical Engineering, 87, pp. 264-273, 2009.

VITA

Shreekanta Aradhya was born in Bangalore, Karnataka in the southern part of India. He received his Bachelor of Engineering degree in Chemical Engineering from M.S. Ramaiah Institute of Technology – Bangalore, India in May 2007. He worked with Department of Biotechnology at M.S. Ramaiah Institute of Technology – Bangalore, India as a Research Assistant from June 2007 to July 2008.

Shreekanta Aradhya entered the PhD program in Department of Chemical and Biolochemical Engineering at Missouri University of Science and Technology in the spring of 2009. His main area of research is in design and scale-up of multiphase systems, computational modeling of multiphase reactors and statistical data analysis. He received his Ph.D. in May 2013.

Mr. Shreekanta Aradhya worked as a research assistant for 4 years in the Department of Chemical and Biolochemical Engineering at the Missouri University of Science and Technology.